Analysis of the spatial and temporal variation of seasonal snow accumulation in Alpine catchments using airborne laser scanning

Basic research for the adaptation of spatially distributed hydrological models to mountain regions

DOCTORAL THESIS

in Atmospheric Sciences

Submitted to the

FACULTY OF GEO- AND ATMOSPHERIC SCIENCES

of the

UNIVERSITY OF INNSBRUCK

in Partial Fulfillment of the Requirements for the Degree of

DOCTOR RERUM NATURALIUM

by

MAG. RER. NAT. KAY HELFRICHT

Advisors

Prof. em. Dr. Michael Kuhn

Univ. Prof. Dr. Ulrich Strasser

Innsbruck, July 2014

*For all my colleagues and friends, who shared and
continue to share my enthusiasm for the cryosphere - and
not just on screen.*

Abstract

Information about the spatial distribution of snow accumulation is a prerequisite for adaptating hydro-meteorological models to achieve realistic simulations of the runoff from mountain catchments. Whereas the areal extent of the snow cover can be recorded using optical remote sensing techniques, the spatial distribution of snow depths and the total snow water equivalent (SWE) of the snow cover is difficult to measure for an entire catchment. Therefore, the spatial snow depth distribution in complex topography of ice-free terrain and glaciers was investigated using airborne laser scanning (ALS) data. This thesis presents for the first time an analysis of the persistence and the variability of the snow patterns at the end of five accumulation seasons in a comparatively large catchment. The ALS data are used to improve the performance of snow-hydrological models simulating the runoff from the mountains of the Ötztal Alps (Tyrol, Austria). The objective was first, to determine whether and where differences between ALS derived and actual snow depths on glacier surfaces reach a magnitude that means they have to be considered in snow-hydrological studies. Therefore ALS derived seasonal surface elevation changes on glaciers were compared to the actual snow depths calculated from ground penetrating radar (GPR) measurements. Areas of increased deviations caused by submergent ice flow and the densification of the firn layer were successfully delineated using Landsat images. With respect to the low glacier velocities in the investigated region, the ALS-derived snow depths on most of the glacier surface do not deviate markedly from actual snow depths. The inter-annual persistence of the snow patterns was investigated to find areas of key information for the snow cover modeling of a high Alpine basin in (Upper Rofental valley, approx. $36\,\mathrm{km}^2$). $75\,\%$ of a the total area showed low inter-annual variability of standardized snow depths at the end of five accumulation seasons. The high inter-annual variability of snow depths could be attributed to changes in the ice cover within the investigated 10-year period for much of the remaining area. Avalanches and snow sloughs continuously contribute to the accumulation on glaciers, but their share of the total snow cover volume is small. Finally, the value of ALS-derived snow maps was investigated by assimilating the ALS data in the calibration and validation of snow-hydrological

models. In general, a basin-wide SWE calculated from ALS-derived snow depths is better suited than snow covered area to constrain model parameter ranges. The assimilation of SWE maps calculated from ALS data in the adaptation of snow-hydrological models to mountain catchments improved the results not only for the but also for the simulated snow cover distribution and for the mass balance of the glaciers. The results demonstrate that ALS data are a beneficial source for extensive analysis of snow patterns and for modeling the runoff from high Alpine catchments.

Zusammenfassung

Die Kenntnis der räumlichen Verteilung der Schneedecke im Hochgebirge ist eine Voraussetzung für die realistische Modellierung des Abflussgeschehens alpiner Einzugsgebiete. Während die schneebedeckte Fläche mit Hilfe von optischen Fernerkundungsverfahren ermittelt werden kann, ist die Messung der räumlichen Verteilung von Schneehhen und damit des in der Schneedecken gespeicherten Wasservolumens für ganze Einzugsgebiete schwierig. Diese Studie präsentiert die Anwendung von luftgestützten Laserscanning Daten (Airborne Laser Scanning, ALS) zur Bestimmung der räumlichen Schneedeckenverteilung im eisfreien und vergletscherten Terrain. Die gewonnenen Informationen werden zur Steigerung der Güte von Abflussmodellierungen in den vergletscherten Einzugsgebieten der Ötztaler Alpen (Tirol, Österreich) genutzt. Zunächst wurde bestimmt, in welchen Teilflächen der Gletscher Abweichung zwischen mit ALS bestimmten Schneehöhen und tatsächlichen Schneehöhen eine Größenordnung annehmen, die es in der hydrologischen Modellierung zu berücksichtigen gilt. Dafr wurden die mit Hilfe von ALS gemessenen Oberflächenänderungen mit den von Bodenradarmessungen berechneten Schneehöhen verglichen. Unter Verwendung von Landsat Daten konnten Bereiche auf den Gletschern abgegrenzt werden, in denen Submergenz und Komprimierung der Firnschicht zu erhöhten Abweichungen beitragen. Aufgrund der geringen Firnbedeckung und den in den letzten Jahrzehnten reduzierten Eisbewegungen in den untersuchten Gebieten sind die Abweichungen auf einem Großteil der Gletscherflächen gering. Um Flächen mit einem für die Schneedeckenmodellierung hohen Informationsgehalt abzugrenzen, wurde die Persistenz der jährlichen Schneeverteilungen in einem Teileinzugsgebiet des Hinteren Rofentals (ca. $36\,\mathrm{km}^2$) bestimmt. 75 % der Gesamtfläche zeigten eine geringe zeitliche Variabilität der standardisierten Schneehöhen. Ein großer Teil der Flächen mit zeitlich hoher Variabilität der Schneehöhen ist in Gebieten zu finden, in denen sich die Eisbedeckung in dem 10-jährigen Untersuchungszeitraum geändert hat. Lawinen und Schneerutsche tragen einen stetigen Teil zur Akkumulation auf Gletschern bei, dessen zusätzliches Volumen allerdings gering ist. Der Wert der von ALS Daten abgeleiteten Schneeverteilung wurde durch die Einbindung der Daten in die Kalibrierung und Validierung

von schnee-hydrologischen Modellen untersucht. Im Allgemeinen zeigt sich, dass die von ALS berechnete Akkumulation in den Einzugsgebieten besser zur Eingrenzung von Modellparametern geeignet ist als nur die schneebedeckte Fläche. Damit konnte nicht nur die Abflusssimulation verbessert werden, sondern auch die Simulation der Schneedeckenverteilung im Hochgebirge und des Massenhaushaltes der Gletscher. Die Ergebnisse zeigen, dass ALS Daten eine nützliche Quelle für die ausgiebige Analyse von Mustern der Schneebedeckung und für die Abflussmodellierung im Hochgebirge darstellen.

Contents

Chapter 1

Introduction

1.1 Motivation

Approx. 75 % of the available freshwater on Earth is stored in ice. The Greenland and the Antarctic Ice Sheet together share 99 % of the total volume of frozen freshwater (Dyurgerov and Meier 2005; Lemke et al. 2007), whereas mountain glaciers and ice caps contain only the remaining 1 %. However, these relatively small share in volume corresponds to more than 198 000 glaciers (Pfeffer et al. 2014), which contribute to the hydrology of different mountain regions on Earth. Also, water is stored in the seasonal snow cover with different characteristics in volume and duration with respect to different climate conditions. Thus, the storage of water in the snow cover, in the multi-annual firn cover and subsequently in the ice bodies of the glaciers has a daily to multi-annual time scale (Jansson et al. 2003; Lemke et al. 2007). Whereas the inter-mediate storage of water in the snow cover affects the seasonal runoff variability, the water stored and released from the glaciers can shift runoff regimes within centuries (Fig. 1.1).

The ongoing climate change has a significant impact on the state of the cryosphere (Vaughan et al. 2013). It alters the reservoirs of snow and ice and will have a considerable impact on water regimes of snow dominated mountain regions in the future (e.g. Beniston 2003; Viviroli et al. 2007). In glacierized catchments of the Alps, the glacio-nival runoff regime is characterized by high runoff originating from melt of the seasonal snow cover in spring followed by the peak runoff caused by increased precipitation and an additional contribution of ice and snow melt from glaciers in summer (Aschwanden et al. 1986). In the last two decades, an increased contribution of glacier melt to runoff is caused by the imbalanced state of the glaciers manifested in predominantly negative mass balances in the Alps (e.g. Abermann et al. 2009, 2012; WGMS 2005, 2008, 2012). A shorter duration of the seasonal snow
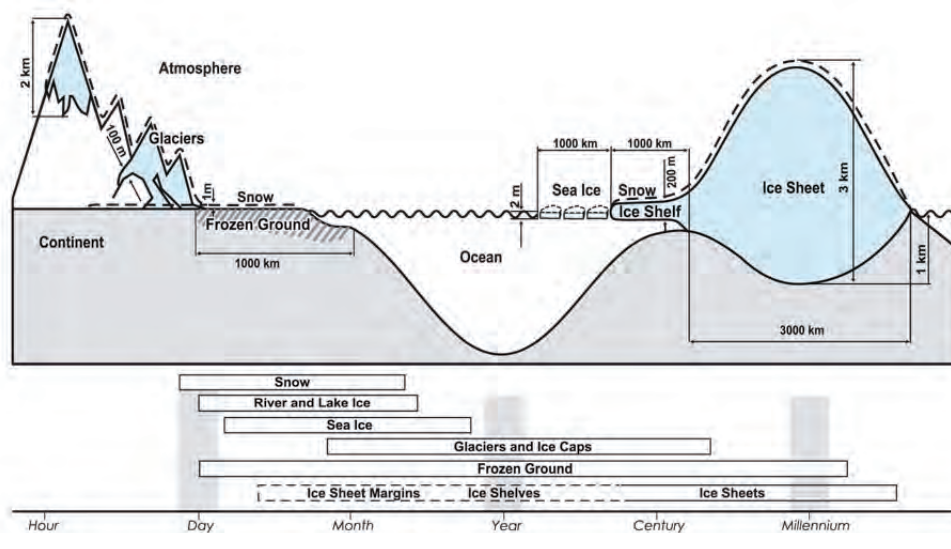
Figure 1.1: Components of the cryosphere and their typical time scales of water storage (from Lemke et al. (2007)).

cover and a decreasing glacier area will change the runoff characteristics in mountain catchments (e.g. Kuhn and Batlogg 1998; Hock 2005; Huss et al. 2008; Koboltschnig et al. 2008; Magnusson et al. 2010; Bavay et al. 2013) and downstream of mountain regions (e.g., Braun et al. 2000; Barnett et al. 2005; Kaser et al. 2010; Huss 2011). A shift of the snow melt season towards earlier time of the year and a reduction of the glacier melt contribution to the summer runoff from Alpine mountain ranges are expected.

However, the spatial distribution of the snow cover at the end of the accumulation season was found to determine spatial patterns of snow disappearance (e.g. Blöschl and Kirnbauer 1992; Anderton et al. 2004; Mott et al. 2011a; Egli et al. 2012). Thus, the spatial snow distribution has a strong influence on glacier mass balance and the seasonality of the runoff from mountain catchments (e.g. Marsh 1999; Braun et al. 2000; Lundquist and Dettinger 2005; Huss et al. 2014). Huss et al. (2014) showed that runoff projections from glacierized catchments for the 21st century are impaired with high uncertainty, which partly originates from the heterogeneous nature of the mountain snow cover:

> Knowledge about [...] the quantity of winter snow accumulation and its spatial distribution [...] is crucial for correctly capturing the future runoff response within a glacio-hydrological model. A lack of data on these variables can lead to considerable errors in predicted future runoff change. (Huss et al. 2014)

Fundamental knowledge of the spatial and temporal variability of the mountain

snow cover represents challenges for today's climatological and hydrological science. Hydro-meteorological models with a different degree of complexity in temporal and spatial resolution and different formulations of the fundamental physics are applied to simulate the runoff from mountain catchments (e.g. Kuhn 2000; Hock 2005; Lehning et al. 2006; Huss et al. 2008; Strasser 2008). For adapting these hydrological simulations to remote mountain areas, point measurements of snow depth, snow water equivalent or the precipitation are extra- and interpolated, but information on the total water volume stored in entire mountain catchments is rare (e.g. Jonas et al. 2009). In general, measurements of solid precipitation - the most important model input - are impaired with errors (e.g. Sevruk 1985; Goodison et al. 1998) and the representativeness of single accumulation measurements for entire mountain catchments is uncertain (e.g. Jansson and Pettersson 2007; Grünewald and Lehning 2011). Optical remote sensing data from space enables to compare model results for snow covered area, but not for snow depth and hence the total accumulation (e.g. Lundberg et al. 2010; Nolin 2011). Complementary measurements or inverse modeling are required to determine relations between snow covered area and snow depths using oblique aerial photographs (e.g. Blöschl and Kirnbauer 1992; Huss et al. 2013).

In recent years, the spatial snow depth distribution in mountain regions was analyzed using high resolution lidar (light detection and ranging) measurements (Deems et al. 2013). While terrestrial laser scanning (TLS) was applied to areas on the slope scale (e.g. Prokop et al. 2008; Grünewald et al. 2010; Schirmer et al. 2011), snow accumulation was determined using airborne laser scanning (ALS) measurements at small mountain test sides (Hopkinson et al. 2001, 2004; Deems et al. 2006, 2008; DeBeer and Pomeroy 2010) and in partly glacierized catchments at the end of the accumulation season (e.g. Geist and Stötter 2007; Dadic et al. 2010a; Grünewald et al. 2013; Sold et al. 2013). However, often only two years of peak snow accumulation derived from lidar data in mountain catchments exist (e.g. Deems et al. 2008; Schirmer et al. 2011; Schirmer and Lehning 2011; Grünewald et al. 2013). Thus, little is known about the multi-annual persistence of the spatial snow depth distribution in partly glacierized mountain terrain at the end of the accumulation season. Additionally, glacier dynamics and firn densification have to be considered using lidar to derive snow depths on glacier surfaces (e.g. Sold et al. 2013). With respect to the high demand on data of spatially distributed snow depths for adapting hydro-meteorological models to mountain regions, this thesis aims to investigate the applicability and the value of ALS-derived snow patterns in partly glacierized catchments in more detail.

1.2   State of Research

1.2.1   Spatial and temporal snow cover variability

The spatial and temporal variability of the mountain snow cover is of interest in cryospheric science for issues like modeling the mass balance of glaciers (e.g. Machguth et al. 2006b; Huss et al. 2008; Dadic et al. 2010a), determining the snow cover duration for ecological investigations (e.g. Tappeiner et al. 2001) and permafrost simulations (e.g. Gruber and Hoelzle 2001), identifying risks of natural hazards (e.g. Schweizer et al. 2008) and simulating the runoff from mountain catchments (e.g. Hock 2005; Lundquist and Dettinger 2005; Schöber et al. 2010; Huss 2011; Bavay et al. 2013). In complex mountain terrain, the spatial snow distribution is caused by preferential deposition of snow caused by wind-induced snow transport from exposed to sheltered areas (e.g. Winstral et al. 2002; Kuhn 2003; Lehning et al. 2008; Dadic et al. 2010a; Mott et al. 2010; Warscher et al. 2013) and the subsequent gravitational snow transport from steep slopes and sheer rock walls (e.g. Machguth et al. 2006b; Bernhardt and Schulz 2010). Lehning et al. (2011) reported that in rough terrain less snow is stored compared to snow amounts in smoother terrain. Once the snow is deposited, the locally differing energy balance of the surface increases spatial heterogeneity of the snow cover (e.g. Cline et al. 1998; Pomeroy et al. 1998; Hock 2005; Mott et al. 2011a; Grünewald et al. 2010).

The spatial variability of snow depth is a challenging characteristic, especially regarding scaling issues for the spatial design of snow depth measurements and the spatial resolution of hydro-meteorological models. Geostatistical analyses were used in cryospheric sciences to analyze scaling issues in snow hydrology by e.g. Shook and Gray (1996) and Blöschl (1999), to investigate topographic and wind control on snow depth distributions (e.g. Lehning et al. 2011; Mott et al. 2011b) and to analyze fractal dimensions and scale breaks of spatial snow depth variability (e.g. Deems et al. 2006, 2008; Trujillo et al. 2007; Schirmer and Lehning 2011). Typical breaks in the spatial autocorrelation of snow depths in mountain terrain were observed between meters and a few tens of meters, both for manually taken snow samples (e.g. Shook and Gray 1996) and snow depths derived from lidar data (e.g. Mott et al. 2011b; Deems et al. 2008; Schirmer and Lehning 2011). In general, snow depth variability decreases with increasing aggregation of snow samples (Clark et al. 2011), which was confirmed by the studies of e.g. Grünewald et al. (2013) and Melvold and Skaugen (2013).

Complex relations exist between the snow accumulation and the formation of glaciers and vice versa (Cuffey and Paterson 2010). Firn, which remains several melt seasons, is a prerequisite for the formation and existence of a glacier. In turn, the formation

of the seasonal snow layer is encouraged on glaciers due to the homogeneous surface and the reduced ground heat flux caused by ice surface temperature at 0° C.

Summarizing all processes, exposed mountain crests and steep slopes of alpine mountains mostly remain snow free towards the end of the accumulation season, whereas high snow depths can be expected in wind sheltered areas, in surface depressions, at the foot of steep slopes or rock walls and more generally on glacier surfaces.

The temporal variability of the seasonal snow cover in Alpine catchments is influenced by the regional variability of precipitation in the Alps (e.g. Fliri 1975; Frei and Schär 1998). Results of four decades of mass balance monitoring on Vernagtferner and Hintereisferner presented in Escher-Vetter et al. (2009) give an insight on interannual variability of winter accumulation on glaciers in the Ötztal Alps. Up to now, long-term observations of spatially distributed snow depths in mountain regions have been based on manually taken snow depth samples (e.g. Hoinkes 1970; Jansson and Pettersson 2007; Escher-Vetter et al. 2009; Sturm and Wagner 2010; Jepsen et al. 2012; Winstral and Marks 2014). Sturm and Wagner (2010) showed climatological patterns of standardized snow depths derived from multi-annually measured snow depth distributions , that are suitable for simulating the spatial snow distribution. Jansson and Pettersson (2007) calculated seasonal winter mass balances based on 100 snow depth samples per kilometer square on Storglaciären (Sweden). They showed that the temporal variability of the spatial snow distribution is mainly caused by wind erosion. Annual point measurements were not consistently representative of the corresponding average snow depth on this glacier. Winstral and Marks (2014) related higher spatial variability of the snow pattern measured at the peak of 11 accumulation seasons to higher wind speeds and higher melt rates. Based on a total number of 5300 snow depth measurements taken at the end of 12 accumulation seasons, Jepsen et al. (2012) found that the spatial coefficient of variation of snow depths ranged considerably from 0.73 to 1.09 in a continental Alpine watershed. Schirmer and Lehning (2011) and Melvold and Skaugen (2013) indicate an interannually consistency of the snow pattern at different spatial scales at the end of the accumulation season. Schirmer et al. (2011) found snow patterns to be more similar at the end of two accumulation seasons than snow depth distributions recorded by terrestrial laser scanning after individual storms.

1.2.2   Modeling of the mountain snow cover

Hydrological models with different complexity of required input data and different spatial and temporal resolution are used to model the seasonal snow cover in mountain catchments.

The topography of mountain environments fundamentally influences the spatial snow distribution (e.g. McKay and Gray 1981; Blöschl and Kirnbauer 1992). Empirical models were developed to reproduce the observed snow depth distributions in relation to topographic parameters such as elevation, slope, aspect, curvature, viewshed and terrain roughness. Binary regression trees were applied successfully with various topographic parameters as explanatory variables (e.g. Elder et al. 1998; Anderton et al. 2004; Molotch et al. 2005; López-Moreno and Nogués-Bravo 2006; Revuelto et al. 2014). Multiple regressions were developed using similar topographic parameters by e.g. Elder et al. (1991); Chang and Li (2000); Pomeroy et al. (2002); Marchand and Killingtveit (2005); Grünewald et al. (2010); Lehning et al. (2011); Grünewald et al. (2013). Using various spatial resolutions and differently sampled snow cover data, up to 90 % of the observed snow cover variability could be explained from the application of such statistical approaches. However, Grünewald et al. (2013), showed that statistical relations between snow depth and topography are site-specific and performance decreases considerably when applying calibrated regression formulas to snow depth distributions of different catchments.

Conceptual models use spatially aggregated areas with similar hydrological response. These Hydrological Response Units (HRU) are mostly determined due to the soil type, ice cover, land use, vegetation type, altitude and to the topographic parameters such as slope and aspect. The advantage of models implementing HRUs is the fast computational time. However, the spatial snow depth variability is limited to the number and size of different HRUs. An increase of precipitation with increasing altitude was found in Alpine catchments (e.g. Hoinkes and Steinacker 1975; Lehning et al. 2011; Grünewald and Lehning 2011) and is implemented in semi-distributed hydrological models like e.g. OEZ (Kuhn 2000, 2003), HQsim (Kleindienst 1996; Achleitner et al. 2012), HBV (Bergström 1992) or PREVAH (Viviroli et al. 2009). In addition, corrections are applied accounting for the undercatch of solid precipitation measurements using a factor related to the temperature and wind at the time of the precipitation measurements (e.g. Sevruk 1985; Goodison et al. 1998). Kuhn (2003) used constant redistribution factors to simulate the transport of solid precipitation from unglacierized areas to glacier surfaces. In most of these models, melt of snow and ice is related to the temperature above a melt-threshold using degree-day (or temperature-index) methods (e.g. Hoinkes and Steinacker 1975; Braithwaite and Olesen 1989; Ohmura 2001; Hock 2003). With respect to the lack of spatial resolution in conceptual models, snow covered area (SCA) and accumulation gradients provide useful information to validate modeled snow cover.

More sophisticated simulations of the spatial variability of the mountain snow cover are achieved with spatially distributed hydrological models such as SES (Blöschl et al. 1991a; Asztalos et al. 2006; Kirnbauer et al. 2009), AMUNDSEN (Strasser

2008), WaSIM-ETH (Schulla and Jasper 2007) or GERM (Huss et al. 2008). Similar to conceptual models, precipitation increase with elevation is considered using precipitation gradients and has to be corrected with respect to the undercatch of the solid share. More complex degree-day approaches including spatially differing solar radiation (e.g. Hock 1999; Pellicciotti et al. 2005) or parameterizations of the surface energy balance are used to simulate snow melt. In contrast to lumped models, spatial variability of the snow accumulation is related to e.g. slope and curvature of the terrain (e.g. Blöschl et al. 1991a; Farinotti et al. 2010; Schöber et al. 2014). E.g. Winstral et al. (2002), Schirmer et al. (2011) and Warscher et al. (2013) presented the successful parameterization of spatial snow depth variability using a parameterization including wind direction, wind speed and viewshed. Grid sizes of $100\,\text{m}$ or less were shown to be appropriate for spatially distributed hydro-meteorological models to simulate the spatial snow cover in the complex topography of mountain terrain (e.g. Blöschl et al. 1991b; Strasser 2008). However, information on snow depths in the similar spatial resolution of the model are required to validate the model results. But often only remote sensing data of SCA, snow depth profiles along transects or scattered snow depth measurements exist.

More complex snow cover models, which solve physical properties of a multi-layer snowpack (e.g. SNOWPACK (Bartelt and Lehning 2002; Lehning et al. 2002), ALPINE3D (Lehning et al. 2006) or SnowDrift3D Schneiderbauer and Prokop (2011)), have large requirements of meteorological input data and high computational effort. Alpine3D is the application of multi-layer model SNOWPACK on a regular grid (Lehning et al. 2006). It was successfully tested in a partly glacierized catchment (Michlmayr et al. 2008) and completed using wind fields by Mott et al. (2010). Liston et al. (2007) and Bernhardt et al. (2010) also modeled snow cover heterogeneity using simulated wind fields. (Dadic et al. 2010a) studied the wind influence over glaciers and found that accumulation patterns are related to uplift and downward air flow. A model intercomparison of Essery et al. (2013) turned out that the storage and refreezing of liquid water have to be considered in snowpack modeling. Prognostic representations of snow density and albedo lead to the most consistent results. However, they found no clear link between model complexity and model performance in runoff simulations.

1.2.3 Measuring snow distribution

Hydro-meteorological models simulating the mountain snow cover with a high spatial and temporal resolution require spatially distributed information on snow patterns for calibration and validation. Especially for the application in partly glacierized mountain catchments, simulation results should not only be validated for runoff, but

also for spatial and temporal snow cover distribution(e.g. Blöschl et al. 1991b; Huss et al. 2014).

However, snow cover properties are measured with different temporal and spatial resolution (e.g. Corps of Engineers 1956; Gray and Male 1981; WMO 1992; Lundberg et al. 2010). While point information on snow depth and snow water equivalent (SWE) can be obtained in sub-hourly time steps (e.g. Corps of Engineers 1956; WMO 1992), spatially distributed snow data are recorded with gaps of several days (e.g. König et al. 2001; Hall et al. 2002; Nolin 2011), in event-based time steps (e.g. Sturm and Wagner 2010; Schirmer et al. 2011) or at the end of the accumulation season (e.g. Kaser et al. 2003; Winstral and Marks 2014).

On the point scale, snow depth, snow density and the corresponding SWE can be measured at automatic weather stations and by manual measurements WMO (1992). Mostly, more extensive snow surveys including manually taken snow probes and snow pits are performed to derive the SWE of the seasonal snow cover for mass balance studies on glaciers (e.g. Hoinkes 1970; Kaser et al. 2003; Jansson and Pettersson 2007; Escher-Vetter et al. 2009), to evaluate remotely sensed snow data (e.g. Schaffhauser et al. 2008; Prokop et al. 2008) or to analyze the inter-annual persistence of snow patterns (e.g. Sturm and Wagner 2010; Winstral and Marks 2014). These point information are used to inter- and extrapolate the mountain snow cover to the catchment scale using different techniques (e.g. Erxleben et al. 2002; Anderton et al. 2004). However, the spatial representativeness of these individual measurements for the surrounding terrain is uncertain (e.g. Grünewald and Lehning 2011).

Another possibility to measure snow depths is ground-penetrating radar (GPR). Depending on the measurement design and operation modes, GPR is suitable to measure quasi-continuous profiles of snow depth, of snow cover stratigraphy (e.g. Heilig et al. 2009) and of multi-annual snow layers (e.g. Eisen et al. 2003) and to determine signal propagation velocity, snow density or dielectric properties of the snow cover(e.g. Daniels 2005; Lundberg et al. 2010). Machguth et al. (2006a) and Sold et al. (2013) showed the successful application of helicopter-based GPR measurements for snow cover studies in glacierized mountain terrain. However, the accuracy of GPR measurements is very sensitive to liquid water in the snow (e.g. Frolov and Macheret 1999; Lundberg et al. 2006; Sundström et al. 2012) and, thus, a good timing of the GPR-surveys is a prerequisite for successful data acquisitions of snow depths at the end of the accumulation season.

In general, in-situ measurements of the spatial snow distribution in high mountain environments are a dangerous and partly not feasible task due to objective risks (e.g. avalanches, crevasses on glaciers) and missing infrastructure. In these inacces-

sible, remote sensing enables to measure physical properties and the spatial snow distribution (e.g. König et al. 2001; Rees 2006; Nolin 2011). Optical Remote Sensing techniques from satellite are used to examine the snow covered area (SCA) (e.g. Dozier 1989; Hall et al. 2002; Rittger et al. 2013), fractional snow cover (e.g. Salomonson and Appel 2004) and snowpack properties such as grain size and albedo (e.g. Painter et al. 2009). Remotely sensed data of SCA were assimilated in hydrological simulations of mountain regions (e.g. Martinec 1987; Nagler et al. 2008). Passive (e.g. Chang et al. 1987) and active (e.g. Rott et al. 2010) microwave radiometers were used to determine SWE of the snow cover. In the course of the years, the spatial resolution and accuracy of satellite data have been increased, but remote sensing of snow depth and SWE from satellite had still limited success (Nolin 2011).

Snow cover products from aerial or terrestrial photogrammetry are useful to map spatial extent and optical properties of the snow surface (e.g. Corripio et al. 2004; Farinotti et al. 2010). However, photogrammetric calculation of snow depths within an appropriate vertical accuracy often failed due to the lack of surface structures in scenes with almost total snow coverage.

Over the last decade, lidar (light detection and ranging) technique was successfully used to measure snow depth changes between elevations of a reference surface and surface elevations measured at a second survey (Deems et al. 2013). Therefore, spatial variations in snow accumulation before and after the precipitation events (e.g. Schirmer et al. 2011), mass budgets of avalanches (e.g. Prokop et al. 2008; Prokop 2008; Schaffhauser et al. 2008; Sailer et al. 2008), seasonal snow accumulation (e.g. Hopkinson et al. 2004; Trujillo et al. 2007; Dadic et al. 2008; Grünewald et al. 2010, 2013; Lehning et al. 2011; Mott et al. 2011b; Melvold and Skaugen 2013) and the subsequent spatially differing melt of the snow cover (e.g. Grünewald et al. 2010; Mott et al. 2011a; Egli et al. 2012) were investigated.

Whereas terrestrial laser scanning (TLS) achieved high vertical accuracy of 0.01 to 0.1 m compared to manual probing (Prokop et al. 2008), airborne laser scanning (ALS) has been successfully applied to mountain regions with a vertical accuracy of 0.1 to 0.15 m at gently inclined slopes (e.g. Bollmann et al. 2011; Joerg et al. 2012; Deems et al. 2013). However, whereas lidar data were used to investigate the spatial variability of the snow cover and its causing processes, only Melvold and Skaugen (2013) used ALS derived snow depths to validate snow distributions which were simulated with a hydrological model in a large catchment.

1.2.4   Lidar principles

Lidar (light detection and ranging, also called laser scanning) is an active remote sensing technology (Baltsavias 1999a; Wehr and Lohr 1999; Kraus 2004). A laser signal is emitted and the travel time of the reflected signal is recorded. Thus, by knowing the propagation velocity of the signal, the distance between the emitting sensor and the illuminated surface on ground can be calculated. Adding the information on the exact shot position, the shot direction and the shot angle, enables the 3D location of the reflecting surface. Beside the 3D geometrical information, the backscattered energy of the reflected laser signal can be recorded (e.g. Wehr and Lohr 1999) and be related to surface characteristics (e.g. Höfle and Pfeifer 2007).
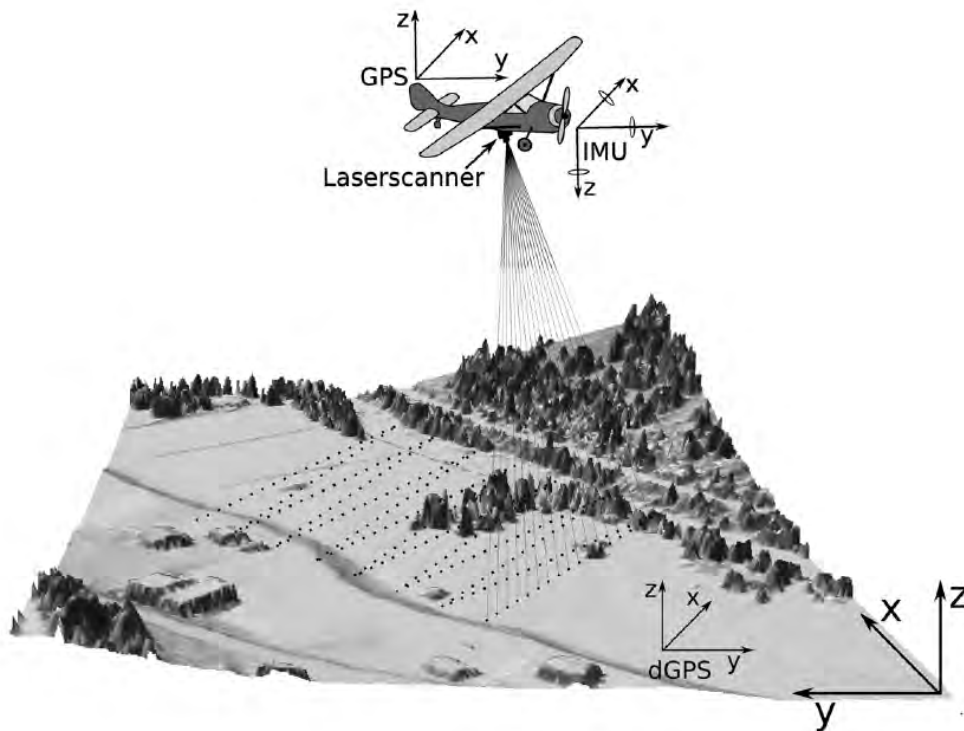

Figure 1.2: Principle components of an airborne laser scanning system: the aircraft carrying the laser scanner, the Global Positioning System GPS and the Inertial measurement Unit IMU (from Vetter (2013) p.14).

Airborne Laser Scanning (ALS) enables covering whole catchments within one survey using scanning devices mounted on an aerial platform like an aircraft or helicopter (Baltsavias 1999b). Besides the laser scanner itself, a high accuracy differential Global Positioning System (dGPS) is required to determine the location of the moving scanner system. A nearby base station is beneficial for a high accuracy processing of the dGPS data. An Internal Measurements Unit (IMU) measures roll, pitch and yaw of the aircraft to calculate the orientation of the laser scanner

(Fig. 1.2).

The dGPS measurements have to be synchronized to the IMU measurements with respect to inconsistent timing with a higher temporal frequency of the IMU data (Favey 2001). Accuracy of the 3D location of the reflecting surface is affected by the accuracy of the dGPS and the IMU and by the footprint of the laser signal. Typically diameters of the laser footprint are in the magnitude of several centimeters depending on the beam divergence, the distance between scanner system and the surface, the incidence angle as well as the shape of the illuminated surface (Baltsavias 1999a). In theory, a laser beam emitted in nadir direction in combination with a horizontal plane results in a circular footprint of the signal. However, in nature the illuminated area varies in slope, orientation and roughness and, thus, the emitted conical footprint of the laser beam is modified (Fig. 1.3).

Multiple echos can originate from objects, which split the laser beam. Thus, multiple signal echos can be related to different elevated surfaces, whereas the last echo (pulse) is related to the bare ground. (Kodde et al. 2007) showed that a large footprint and multiple pulses result from crevasses on glaciers, where the laser beam is reflected at the edge of the crevasse, but partly continues into it. The intensity of the backscattered signal depends on the incidence angle and surface properties of the illuminated surface. Höfle and Pfeifer (2007) showed that ice, firn and snow surfaces could be distinguished from intensity maps corrected for spherical loss and topographic and atmospheric effects. A further development was the full wave laser scanning (Wagner et al. 2006). The power of the received signal is recorded as a function of time, so that information is gained on the vertical distribution of the illuminated objects and on surface properties (Fig. 1.3). The distribution of data points along a flight path is controlled by the combination of flight speed and the deflection of the laser beam from the oscillating mirror (Fig. 1.2). Thus, point densities are affected by the laser repetition rate, flight speed of the aircraft, the height above ground, surface characteristics, the relief of the topography and the deflection angle of the laser beam (Baltsavias 1999a).

Horizontal and vertical accuracy of the 3D point location depend on the size and the modification of the laser footprint. The size of the laser footprint increases with increasing distance between the laser system and the illuminated surface. It is smaller for an incidence angle of 90° compared to illumination at a low angle. In general, the vertical accuracy of ALS derived lidar points is a function of the slope of the scanned surface (Kraus 2004; Bollmann et al. 2011). In steep terrain, small horizontal errors cause large vertical offsets from actual surface elevations. Carefully planned flight paths are therefore the basis for recording a high number of laser points with a high accuracy in complex mountain terrain (Deems et al. 2013). Joerg
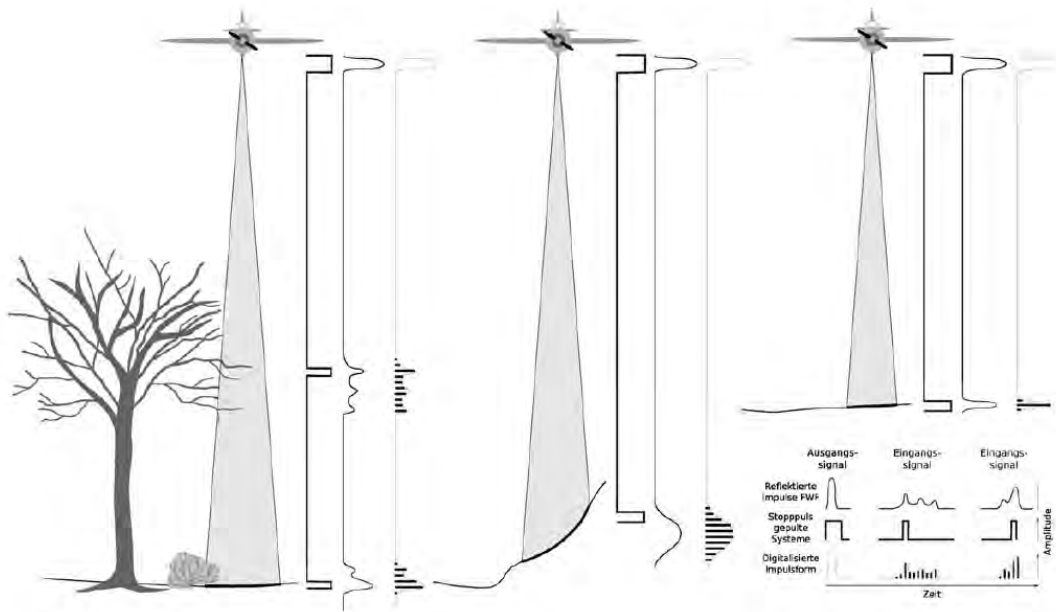
Figure 1.3: Modification of the laser signal by topography and differences in recorded waveform (from Vetter (2013) p.15).

et al. (2012) showed for ALS acquisitions at Findelengletscher in Switzerland that systematic uncertainties of the ALS measurement have to be considered, whereas stochastic uncertainties are not significant for the analysis of the glacier surface elevation changes. Bollmann et al. (2011) estimated a mean absolute vertical error of ALS point data of ± 0.05 m at slope angles of less than 40° with an exponential increase of up to ± 1.0 m at slopes of 80°.

1.2.5 Digital elevation models from lidar data

The reflections recorded at a lidar survey are stored with their coordinates x,y,z and their attributes of e.g. intensity in a so called point cloud. To derive Digital Elevation Models (DEM), this point cloud has to be filtered (Sithole and Vosselman 2004; Lui 2008). Whereas Digital Surface Models (DSM) typically include all reflections next to the scanning system, Digital Terrain Models (DTM) aim to reproduce the Earth surface without vegetation and are calculated with the last pulses of the laser echos. The quality of a DEM depends on the point density of the filtered point cloud. Higher point densities can be achieved by overlapping scan stripes. They enable to produce DEMs by simple interpolation schemes or aggregation of adjacent sample points with a small cell size and, thus, a high spatial resolution (McCullagh 1988; Lui 2008; Deems et al. 2013). The adequate number of grid cells in the DEM should be similar to the number of available 3D points, i.e. point densities of more than 1 point per square meter enable to produce DEMs with spatial resolution of

1 m.

Bollmann et al. (2011) found a cumulative vertical error of 3D point accuracy and DTM generation of $\pm\,0.12\,\text{m}$ in 40° steep and rough terrain and concluded a total vertical error of less than $\pm\,0.15\,\text{m}$ to $\pm\,0.20\,\text{m}$ for major parts of the investigated catchment. Geist et al. (2005) compared dGPS measurements and corresponding grid values of a DTM calculated from ALS data at Engabreen (Norway) and found minimal mean deviations of 0.10 m and a standard deviation of 0.10 m.

Since lidar became an appropriate method in earth system sciences, several studies have successfully applied ALS data to derive spatial snow depth distributions by subtracting the DTMs of two surveys (e.g. Hopkinson et al. 2001, 2004; Deems et al. 2006, 2008; Trujillo et al. 2007; Dadic et al. 2010a; Grünewald et al. 2010, 2013). A comprehensive review on lidar measurements of snow depths can be found in Deems et al. (2013).

1.3   Framework of the thesis

1.3.1   Study site and data

This thesis was developed in the frame of the alpS-project MUSICALS (*MU*ltiscale *S*now/*IC*e melt simulation into *AL*pine reservoir*S*). This project investigated the hydrology of approx. 560 km^2 partly glacierized mountain catchments in the Ötztal Alps (Tyrol, Austria). This area includes catchments which directly or by diversion supply water to the Gepatsch reservoir (46°57'N, 10°44'30"E, Fig. 1.4) and catchments, which are planned to contribute to the reservoir inflow. These catchments are the headwaters of the valleys Ötztal, Pitztal and Kaunertal. Due to the touristic and economic development of this region, a variety of weather stations and discharge measurements ensure an extensive basis of meteorological and hydrological data.
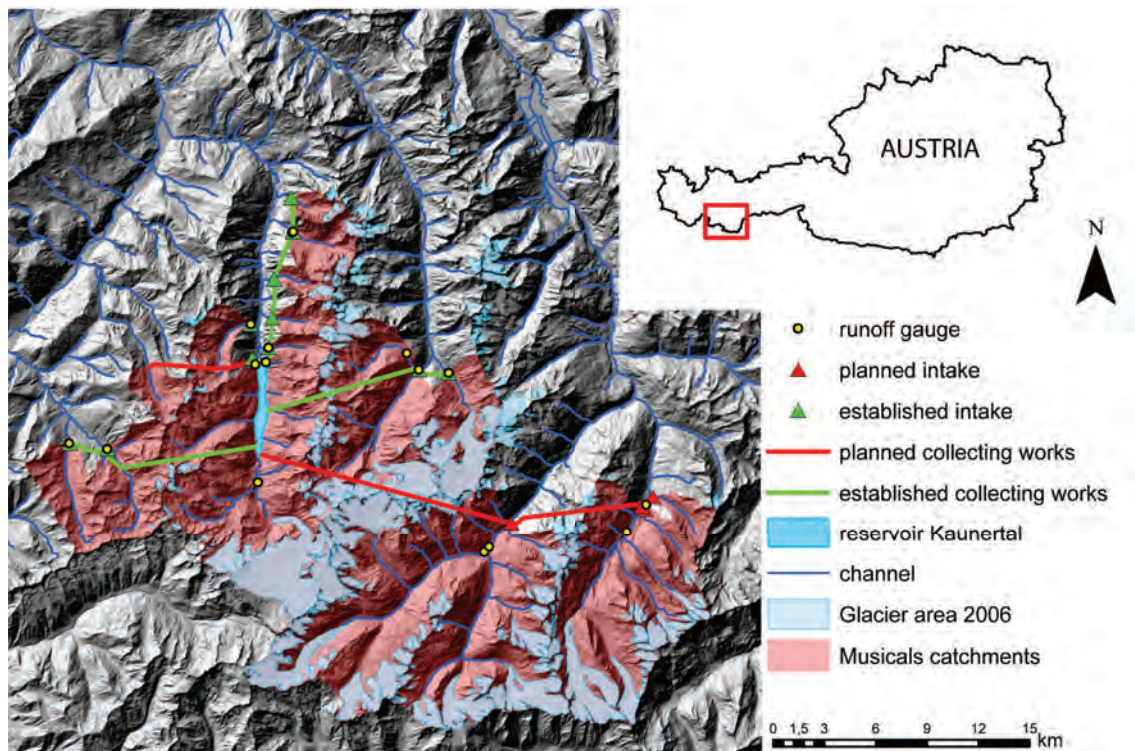

Figure 1.4: Map of investigated area showing meteo-hydrological measurement locations and the reservoir infrastructure.

The Ötztal mountains possess an outstanding role in Austrian and international cryospheric research. Multi-temporal glacier inventories (Lambrecht and Kuhn 2007; Abermann et al. 2009, 2012) and one of the world's longest glacier mass balance series at Hintereisferner (Zemp et al. 2009; Fischer 2010) enable to study the relation between glaciers and climate. With a total ice cover of 116 km^2 the Ötztal Alps are the most glacierized mountain region of the Eastern Alps accounting for almost one

third of the glacier area in Austria. Since 2001 annual and seasonal lidar surveys were conducted in a subcatchment of the Upper Rofental (46° 48' N, 10° 46' E) of approx. 36 km² (e.g. Geist and Stötter 2007; Bollmann et al. 2011; Sailer et al. 2012). Whereas Geist and Stötter (2007); Fischer (2011) analyzed these data with respect to volume changes of the glaciers, seasonal snow depth distributions were not investigated in detail. Within the time of the project, the data set of ALS derived elevation changes of the accumulation seasons 2002, 2003 and 2009 was completed by lidar surveys in 2010, 2011 and 2012 (Tab. 1.1). The ALS surveys in fall 2010 and spring 2011 were performed for the entire mountain range of the Ötztal Alps. Almost no forest and only scattered trees exist in the investigated, high elevated catchments. The mean point densities of the data set allowed us to calculate DEMs with a cell size of 1 m (Tab. 1.1).

Table 1.1: Overview of the ALS flight campaigns investigated in this thesis. Note that all scanner systems are Optech devices. The maximum scan angel α_{max}, the laser repetition rate rr, scan frequency f and mean point densities pd are given. The vertical accuracy a_z is calculated from deviations between ALS surface elevations and elevations of a known reference surface. Mean flight altitude was between 1000 m and 1200 m above ground.

accumulation season	time	date	laser system	α_{max} (°)	rr $(10^3\mathrm{s}^{-1})$	f (s^{-1})	pd (m^{-2})	a_z (m) mean	σ
2002	t1	10 Oct 2001	ALTM 1225	20	25	28	1.1	na	na
	t2	07 May 2002	ALTM 1225	20	25	28	1.2	−0.040	0.110
2003	t1	18 Sep 2002	ALTM 2050	20	50	40	1.0	−0.030	0.098
	t2	04 May 2003	ALTM 2050	20	50	40	0.8	−0.020	0.092
2009	t1	09 Sep 2008	ALTM 3100	20	70	40	2.2	0.002	0.057
	t2	07 May 2009	ALTM 3100	20	70	38	2.4	0.040	0.054
2011	t1	08 Oct 2010	ALTM Gemini	25	70	36	3.6	0.076	0.047
	t2	20 Apr 2011	ALTM Gemini	25	70	36	3.8	−0.007	0.041
2012	t1	04 Oct 2011	ALTM 3100	20	70	40	2.9	0.001	0.042
	t2	11 May 2012	ALTM 3100	20	70	40	2.8	0.005	0.057

1.3.2 Goals and outline

With respect to the high demand on data of spatially distributed snow depths for adapting hydro-meteorological models to mountain regions, this thesis aims to investigate the applicability and the value of ALS-derived snow patterns in partly glacierized catchments in more detail. Therefor following questions were addressed:

1. Are there differences between ALS derived and actual snow depths on glacier surfaces of such a magnitude that they have to be considered in hydrological studies, and if so, for what reason?

2. To which degree is the pattern of the seasonal snow cover persistent in space and time? Which processes cause the inter-annual variability of the snow pattern in glacierized mountain catchments?

3. What are the the benefits of ALS-derived snow distributions for improving the model performance of runoff simulations?

Based on existing ALS data of three accumulation seasons, the spatial and temporal snow distribution in the Upper Rofental catchment was investigated in the **Paper 1: Snow accumulation of a high alpine catchment derived from lidar measurements** (Chap. 2). Seasonal accumulation gradients were determined and a first comparison of ALS derived snow depths with snow samples on Hintereisferner showed that ALS derived snow depths locally deviate from actual snow depths on glacier surfaces. For that reason field measurements were performed contemporally to the ALS surveys of two accumulation seasons. **The Paper 2: Lidar snow cover studies on glaciers in the Ötztal Alps (Austria): comparison with snow depths calculated from GPR measurements** presents the contribution of ice dynamics and firn densification to ALS surface elevation changes within the accumulation season (Chap. 3). Inter-annual persistence of the mountain snow cover is a prerequisite for using simple parameterizations to simulate spatial snow cover variability. Based on the complete data set of five seasonal snow depth distributions, the inter-annual persistence of snow patterns was analyzed in **Paper 3: Inter-annual persistence of the seasonal snow cover in a glacierized catchment** (Chap. 4). The spatial and temporal variability of gravitational snow transport and its contribution to seasonal snow cover volume on glaciers is investigated in more detail in Chap. 5. Chapter 6 presents the successful application of the ALS derived snow distributions in the calibration and validation process of two hydro-meteorological models. Finally, the conclusions are summarized with respect to the research questions in Chap. 7.

Chapter 2

Paper I - Snow accumulation of a high alpine catchment

Advances in Geosciences

Snow accumulation of a high alpine catchment derived from LiDAR measurements

K. Helfricht[1,2], **J. Schöber**[1,3], **B. Seiser**[1,4], **A. Fischer**[2,4], **J. Stötter**[1,3], **and M. Kuhn**[2]

[1]alpS – Centre for Climate Change Adaptation Technologies, Innsbruck, Austria
[2]Institute of Meteorology and Geophysics, University of Innsbruck, Austria
[3]Institute of Geography, University of Innsbruck, Austria
[4]Institute of Mountain Research: Man and Environment, Austrian Academy of Sciences, Innsbruck, Austria

Correspondence to: K. Helfricht (helfricht@alps-gmbh.com)

Abstract. The spatial distribution of snow accumulation substantially affects the seasonal course of water storage and runoff generation in high mountain catchments. Whereas the areal extent of snow cover can be recorded by satellite data, spatial distribution of snow depth and hence snow water equivalent (SWE) is difficult to measure on catchment scale. In this study we present the application of airborne LiDAR (Light Detecting And Ranging) data to extract snow depths and accumulation distribution in an alpine catchment.

Airborne LiDAR measurements were performed in a glacierized catchment in the Ötztal Alps at the beginning and the end of three accumulation seasons. The resulting digital elevation models (DEMs) were used to calculate surface elevation changes throughout the winter season. These surface elevation changes were primarily referred to as snow depths and are discussed concerning measured precipitation and the spatial characteristics of the accumulation distribution in glacierized and unglacierized areas. To determine the redistribution of catchment precipitation, snow depths were converted into SWE using a simple regression model. Snow accumulation gradients and snow redistribution were evaluated for 100 m elevation bands.

Mean surface elevation changes of the whole catchment ranges from 1.97 m to 2.65 m within the analyzed accumulation seasons. By analyzing the distribution of the snow depths, elevation dependent patterns were obtained as a function of the topography in terms of aspect and slope. The high resolution DEMs show clearly the higher variation of snow depths in rough unglacierized areas compared to snow depths on smooth glacier surfaces. Mean snow depths in glacierized areas are higher than in unglacierized areas. Maximum mean

snow depths of 100 m elevation bands are found between 2900 m and 3000 m a.s.l. in unglacierized areas and between 2800 m and 2900 m a.s.l. in glacierized areas, respectively. Calculated accumulation gradients range from 8 % to 13 % per 100 m elevation band in the observed catchment. Elevation distribution of accumulation calculated by applying these seasonal gradients in comparison to elevation distribution of SWE obtained from airborne laser scanning (ALS) data show the total redistribution of snow from higher to lower elevation bands.

Revealing both, information about the spatial distribution of snow depths and hence the volume of the snow pack, ALS data are an important source for extensive snow accumulation measurements in high alpine catchments. These information about the spatial characteristics of snow distribution are crucial for calibrating hydrological models in order to realistically compute temporal runoff generation by snow melt.

1 Introduction

In alpine head watersheds the storage of water as snow and ice has a major impact on catchment discharge. Both, the snow cover and the ice cover, have a distinct spatial distribution storing solid precipitation and affecting melt water runoff. The water reservoir ice in its manifestations as permafrost and glaciers delivers an annual runoff contribution mainly in the summer months. Changes on extent of these reservoirs act on a timescale of years to decades (Jóhannesson et al., 1989). Temporal flow retardation due to seasonal snow cover has a magnitude of hours to months

(Braun et al., 2000; Kuhn, 2003). Areal extent of snow cover, spatial distribution of snow depth and hence SWE define seasonality and amount of runoff contribution by snow melt (Skaugen, 2007).

The catchment investigated in this study is located in the Upper Rofen valley (Tirol, Austria, 46.80° N, 10.78° E, Fig. 1) and has a size of about 26.3 km². It was covered by glaciers of 48.8 % in 2008 and its elevation ranges from 2304 m a.s.l. to 3739 m a.s.l. This implicates a glacio-nival runoff regime characterized by large amounts of glacier melt-water runoff in summer, solid precipitation stored in a snow pack covering up to almost 100 % of the area in winter and runoff generation by snow melt in spring. Two intensively studied glaciers, namely Hintereisferner and Kesselwandferner, are located in this investigation area. Data of mass balance measurements in terms of snow depth distribution and ice ablation (Kuhn et al., 1999; Escher-Vetter et al., 2009; Fischer, 2010) as well as multi-annual volume changes (Abermann et al., 2009) are the basis for hydrological modelling in this region (Kuhn and Batlogg, 1998; Braun et al., 2000).

The total amount and the spatial distribution of accumulation of solid precipitation is the key for realistic spatio-temporal modeling of meltwater runoff in alpine catchments, both from snow melt and from ice ablation. Hydro-meteorological models are constructed to simulate the total amount of winter precipitation and the spatial distribution of snow accumulation. To evaluate the distribution of SWE calculated by these models, only insufficient data are available. First of all, precipitation measurements in high alpine catchments are affected by measuring errors, especially for solid precipitation in the winter season (Sevruk, 1985; Sevruk and Mieglitz, 2002). These errors can sum up to 50 % of total precipitation. To account for higher precipitation rates in mountain areas, elevation gradients for precipitation are applied in hydrological modeling (Bergström, 1992; Kuhn, 2000), with the consequence, that highest precipitation rates occur at the highest elevations of the model region. In terms of solid precipitation, these additional precipitation amounts are redistributed from wind exposed ridges and steep slopes to sheltered and flatter regions, which has to be considered in snow cover modeling (Strasser, 2008). To date only the modeled area of snow cover can be evaluated extensively. This can be done using optical space-borne remote sensing techniques that deliver information in spatial resolutions up to 50 m (Nolin, 2011). Information on spatial distribution of snow depths and SWE is scarce. Besides snow depth measurements at several weather stations, point measurements of snow accumulation at glacierized areas exist in terms of snow probings and snow pits for calculating glacier winter mass balance (Escher-Vetter et al., 2009). Due to limited spatial coverage, these data are not applicable for the whole glacier area in a simple way.

A more favorable alternative to measure snow depths is based on application of LiDAR (Light Detecting And
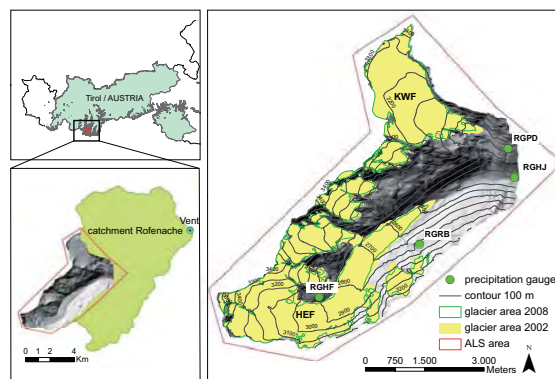

Fig. 1. Map of the investigated catchment. The village Vent, where the automatic weather station is located, the cumulative rain gauges Hochjochhospiz (RGHJ), Proviantdepot (RGPD), Rofenberg (RGRB) and Hintereisferner (RGHF) are marked. The two glaciers Hintereisferner (HEF) and Kesselwandferner (KWF) are labeled.

Ranging) technique. LiDAR, also called laser scanning, is an active remote sensing technology, producing 3-D point data representing the observed surface in a geometrical information with a high point density and accuracy. While terrestrial laser scan measurements are spatially limited due to the maximum signal distance and topographic shading, airborne laser scanning (ALS) can be applied to larger areas (Baltsavias, 1999; Wehr and Lohr, 1999; Geist, 2005). ALS can be used in remote mountain areas, because this technique requires no external light source. For georeferencing the data no ground control points are necessary. It only needs a GPS reference station in vicinity. Relatively high costs of ALS acquisitions are compensated by the comprehensive amount of data. The investigation area can be predetermined exactly with the aim of cost reduction. Based on the 3-D point data, the so-called point cloud, digital elevation models (DEM) can be produced using interpolation algorithms (Lui, 2008). These DEMs deliver a variety of topographic parameters like slope and aspect, which are useful for hydrological modeling (Hollaus et al., 2005). Multi-temporal laser scan measurements provide the possibility to detect surface elevation changes caused by mass movements, mass loss or mass gain even in terrain that is difficult to access. Many studies analyzed the potential of these multi-temporal laser scan acquisitions in high mountain catchments investigating changes of the alpine cryosphere in terms of glacier changes (e.g. Geist and Stötter, 2007; Abermann et al., 2010; Geist and Stötter, 2009; Fischer et al., 2011). Studies about the spatial distribution of the alpine snow cover based on LiDAR measurements are mainly available for restricted areas covering only a part of mountain hillsides (e.g. Grünewald et al., 2010; Mott et al., 2010; Lehning et al., 2011).

K. Helfricht et al.: Snow accumulation of a high alpine catchment derived from LiDAR measurements   **33**

In this paper a set of multi-temporal ALS-measurements of the whole catchment of about $26.3\,km^2$ is presented. The analyses were performed to answer the questions:

  i. Is it possible to investigate characteristics of snow cover heterogeneity by means of ALS data?

 ii. How crucial is the delimitation of unglacierized and glacierized areas?

iii. Which parameters can be extracted from snow accumulation distribution to improve hydrological modelling?

In Sect. 2 the ALS data set, additional data sources and the principles to convert snow depths into SWE are described. Section 3 highlights the results of the statistical analyses to describe some fundamental characteristics of the snow pack in the basin. Further, accumulation gradients of solid precipitation are presented and differences of ALS derived snow depths and measured snow depth at Hintereisferner are shown. The discussion (Sect. 4) will be addressed to the particularities of glacierized catchments in terms of surface elevation changes. Within the same section, the conclusions will state the importance of extensive information about the spatial distribution of seasonal water storage in the snow cover.

2 Data and methods

2.1 ALS Data

Laser scan flights are performed in the Upper Rofen valley, Ötztal Alps, Austria (Fig. 1) at the end of glacier ablation season since 2001 (Geist and Stötter, 2007; Fischer et al., 2011). Several flights were carried out between the annual measurements to record snow accumulation and snow ablation (Geist and Stötter, 2007; Spross, 2011). Within the airborne laser scan data series of the last 10 yr, currently three winter seasons (2001/2002, 2002/2003 and 2008/2009) are covered by laser scan flights. Dates of acquisitions, the corresponding identifier of the database and the point densities of the flight campaigns are shown in Table 1.

The pre-processed data were used to produce high resolution raster digital elevation models (DEM, cell size 1 m) (Bollmann et al., 2011). The accuracy of the raster DEM depends on the point density and the accuracy of the laser scan point measurements. The comparison of DEM elevations from ALS data and ground control points in the Hintereisferner area shows that the vertical accuracy of the DEMs is better than 0.3 m (Fischer et al., 2011). The accuracy of laser measurements is influenced by the angle of the scanned slopes (Kraus, 2004). Bollmann et al. (2011) found that vertical errors increase from ±0.04 m at slopes smaller than 35° up to ±1 m at slopes of 80° and assumed an overall vertical accuracy of the DEMs of ±0.15 m to ±0.20 m for application of multi-temporal ALS data in alpine catchments with

Table 1. ID-number, aquisition dates and point densities of the used ALS data. Year of accumulation season, which is used later on, and the mean surface elevation change Δz between the respective DEMs of the whole catchment are shown.

ID	Date	Mean point density per m^2	Accumulation period	Δz in m
hef01	11 Oct 2001	1.1	2002	2.10
hef03	7 May 2002	1.2		
hef07	18 Sep 2002	1.0	2003	1.97
hef08	4 May 2003	0.8		
hef16	9 Sep 2008	2.2	2009	2.65
hef17	7 May 2009	2.4		

slopes smaller than 70°. For that assumption differences between differential Global Navigation Satellite System measurements and airborne laser data of about 0.07 m with a standard deviation of ±0.07 m were combined with errors from ALS point to raster aggregation. The latter tends to be small on the relatively flat glacier areas without crevasses (±0.04 m). Regarding the highly glacierized investigation area with slopes mostly smaller than 35° (see Fig. 4) it is assumed here, that the vertical error of the DEM data is below ±0.15 m. While airborne laser scan data are available for an area of about $36\,km^2$, this study uses the hydrological catchment, which was determined by a GIS watershed procedure applied on a 10 m grid size of the DEM corresponding to the hef16 flight (Table 1). The catchment has a size of about $26.3\,km^2$, of which 48.8 % are covered by glaciers in 2008. Elevation ranges from 2304 m a.s.l. to 3739 m a.s.l. The area-elevation distribution of catchment area and glacier area in 100 m elevation bands are shown in Fig. 2.

Because significant glacier area loss occurred between 2002 and 2008, two glacier boundaries were produced using the procedure presented by Abermann et al. (2010). The glacierized area of this catchment was reduced by 8.7 % between 2002 ($14.1\,km^2$) and 2008 ($12.8\,km^2$). To extract surface elevation changes, the DEMs corresponding to one accumulation season were subtracted in the order spring minus autumn. Later on dates of these DEM-differences are referred to as 2002, 2003 and 2009 (Table 1).

2.2 Additional data

Precipitation and temperature data are available from an automatic weather station located in Vent (46.858° N, 10.013° E, 1890 m a.s.l.) and are shown for the analyzed accumulation seasons in Fig. 3. Four precipitation gauges located within the test site (Fig. 1) deliver a seasonal total of measured precipitation. Elevation of the precipitation gauges and measured precipitation sum of the three accumulation seasons are listed in Table 2. Whereas the weather station in Vent delivers hourly data, readings of the cumulative precipitation gauges took place coincidentally with the end of

Table 2. Elevation and precipitation sums of the weather station Vent and the four cumulative precipitation gauges Hochjochhospiz (RGHJ), Proviantdepot (RGPD), Rofenberg (RGRB) and Hintereisferner (RGHF) of the accumulation seasons ranging from the 1st of September to the 30 April.

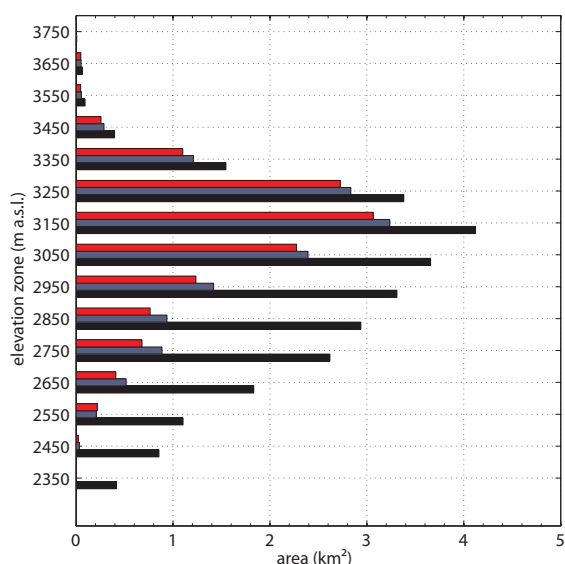|		Cumulative precipitation gauges				
Year	Vent 1890	RGHJ 2360	RGPD 2737	RGRB 2827	RGHF 2970	m a.s.l.
2002	379	411	480	619	748	mm
2003	423	468	467	593	623	mm
2009	464	460	674	853	1079	mm

Fig. 2. Area-elevation distribution of the investigated catchment. Catchment area (black), glacier area in 2002 (gray) and glacier area in 2008 (red) are shown in steps of 100 m elevation bands.

accumulation season close to 30 April. These precipitation sums are the basis for further remarks on catchment precipitation in Sect. 3.

An influence of glacier dynamic processes on ALS derived snow depths at glacier surfaces can be assumed. In the investigated area annual measurements of vertical ice flow velocities are available for Kesselwandferner (Abermann et al., 2007). Less data exist to validate snow depths derived from ALS at glacier surface. In 2009, nearly at the same date of ALS data acquisition, snow sounding measurements were performed on Hintereisferner. These snow depths can be compared to snow depths derived from ALS.
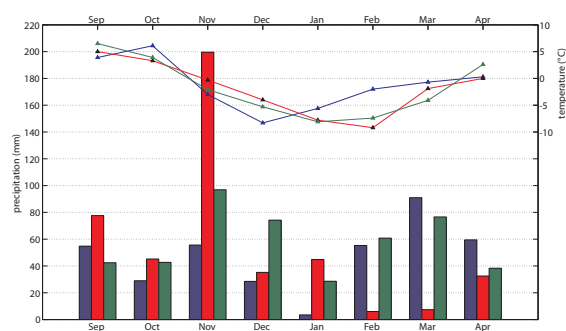

Fig. 3. Monthly precipitation sums (bars) and monthly mean temperature (lines) at the automatic weather station in Vent for the analyzed accumulation seasons 2002 (blue), 2003 (red) and 2009 (green).

2.3 Modeling snow water equivalent and accumulation gradients

Differences between the DEMs corresponding to one accumulation season deliver surface elevation changes (Δz). In a first approximation these Δz were referred to as snow depths at the end of the accumulation season. For hydrological applications snow depth has to be converted into snow water equivalent (SWE). Therefore snow density has to be known or estimated. As shown by Jonas et al. (2009), statistical relations between snow depth and snow density deliver reliable approximations. Such long time data series of snow depth and corresponding snow densities were also collected and analyzed by Schöber et al. (2012) in the Tyrolean Alps. They developed a statistical model based on one sub-dataset, which includes measurements of snow densities at the end of the accumulation season, predominantly recorded during glaciological winter mass balance measurement campaigns in the Ötztal Alps. This regression was used to calculate SWE in kg m^{-2} by multiplying snow density (ρ (kg m^{-3})) by the snow depth (h (m)) (Eq. 1).

$$\text{SWE} = \rho \cdot h \tag{1}$$

Error analysis of this statistical model show a root mean square error of $96\,\text{kg m}^{-2}$ SWE. Relative errors of modeled to measured SWE decrease with increasing snow depth, whereas absolute errors increase, respectively. For more information the reader is referred to Schöber et al. (2012). The regression model was used to convert mean surface elevation changes of the 100 m elevation bands into SWE. Error ranges for the calculated SWE and volume of the 100 m elevation bands were calculated by assuming an accuracy of ± 0.15 m from ALS data and a function taking into account snow depth dependent errors of the statistical SWE-model (Fig. 6). The volume of the snow cover of one elevation band is defined as mean SWE ($\text{SWE}_{\text{mean}(n)}$) multiplied by the area (A_n). The

sum of all elevation bands (number n, where $n = 0$ describes the lowest elevation band) gives the overall volume (V_{ALS}) of the snow cover derived by ALS data (Eq. 2).

$$V_{ALS} = \sum_0^n \left(SWE_{mean(n)} \cdot A_n \right) \qquad (2)$$

To obtain elevation gradients of snow accumulation, for each elevation band the measured precipitation sum of the cumulative rain gauge Hochjochhospiz (P_{RGHJ}) was multiplied by an accumulation gradient γ with the power of the number of the elevation band and by the area. Equation (3) shows the calculation of overall volume by adding up the snow volume of the elevation bands.

$$V_{mod} = \sum_0^n \left(P_{RGHJ} \cdot \gamma^n \cdot A_n \right) \qquad (3)$$

The accumulation gradient γ was determined iteratively with the target that the modeled volume (V_{mod}) equals the volume calculated from ALS data (V_{ALS}) in overall sum as well as in the elevation band of largest area (Eq. 4).

$$\frac{V_{mod}}{V_{ALS}} \rightarrow 1 \qquad (4)$$

3 Results

3.1 Spatial variability of surface elevation changes

Calculating the differences between the corresponding DEMs delivers a mean surface elevation change (Δz) of the whole catchment, which is presented in Table 1. Spatially distributed surface elevation changes were primarily referred to as snow depths. The mean Δz of the accumulation season 2009 is about 0.5 m larger than the mean Δz of the accumulation seasons 2002 and 2003. This signal is not obvious in the precipitation data of Vent and Hochjochhospiz, but more distinct at the higher precipitation measurement locations (Table 2). Precipitation sum measured at rain gauge Hintereisferner (RGHF) in 2009 has the highest increase relative to the previous investigated years (2002, 2003) and relative to the other rain gauges in 2009 (Table 2). Monthly distribution of precipitation and the mean monthly temperature measured at the weather station in Vent are shown in Fig. 3. It is obvious, that the largest monthly precipitation was measured in November 2002. More than twice as much precipitation was cumulated than in the other two years. A low pressure system crossing south of the alps in easterly directions caused huge amounts of orographic precipitation along the Alpine main ridge. However, the second stage of the accumulation season 2003 was very dry, which had a compensating effect at the end of winter season. In comparison to that, the accumulation season 2002 started with less precipitation, but cumulated most of the precipitation in February, March and April. The accumulation season 2009, dominated by northwesterly flow conditions, showed an almost uniform temporal distribution of precipitation with minimum precipitation in January.

Results of the statistical analyses on elevation distribution of Δz dependent on aspect and slope are shown in Fig. 4. The area-distribution dependent on aspect and elevation has its maximum on slopes exposed southeast at an elevation between 3100 m and 3200 m a.s.l. The maximum Δz occurred at easterly aspects around 3000 m a.s.l. in the accumulation seasons 2002 and 2003. At the upper elevation bands the Δz appeared two times larger on easterly to southeasterly slopes than on areas oriented west and northwest. In the accumulation season 2009 maximum Δz occurred about 200 m higher on easterly slopes. Caused by higher energy fluxes, south exposed slopes at the lowest elevation bands remain almost snow free at the end of all three accumulation seasons.

The area distribution dependent on slope and elevation showed higher fractions of area at inclined hillsides of about 25° between 2800 m and 3100 m a.s.l. Largest area fraction is located at slopes of 10° to 20° between 3100 m and 3200 m a.s.l. Maximum Δz are accumulated at nearly horizontal surfaces around 2900 m a.s.l. With increasing elevation, occurrence of maximum Δz is shifted towards steeper slopes. Also here maximum Δz in 2009 occurred at higher elevations of about 3250 m a.s.l. Like in several other studies (e.g. Blöschl and Kirnbauer, 1992; Strasser, 2008), slopes steeper than 60° show almost no snow cover.

Figure 5 shows the Δz at 100 m elevation bands of unglacierized and glacierized areas and the corresponding mean standard deviations. It is clearly visible, that smaller Δz occurred at unglacierized than at glacierized areas in all three accumulation seasons. Standard deviations of Δz for unglacierized areas are in the same order like Δz, which increase at higher elevation bands. This is caused by the rough terrain of unglacierized areas, featuring steep slopes, ridges and depressions as well as windward and sheltered areas on small scale arrays and therefore snow redistribution by wind and gravity. A much more homogeneous distribution of Δz can be deduced at glacierized areas by the relatively small standard deviations in comparison to the mean.

Differences of Δz between 2002 and 2003 occur mainly at lower elevation bands. The larger Δz in 2009 are mainly located in glacierized areas at higher elevations. Large Δz and standard deviation at highest altitudes in 2002 are caused by ALS measurement errors in steep terrain. Maximum Δz occurred between 2900 m to 3000 m a.s.l on unglacierized areas and between 2800 m to 2900 m a.s.l. on glacierized areas, respectively.

3.2 Gradients of accumulation

As described in Sect. 2.3, surface elevation changes (Δz) of the ALS data were referred to as snow depths and converted into SWE. In the left column of Fig. 6 the graph of the mean
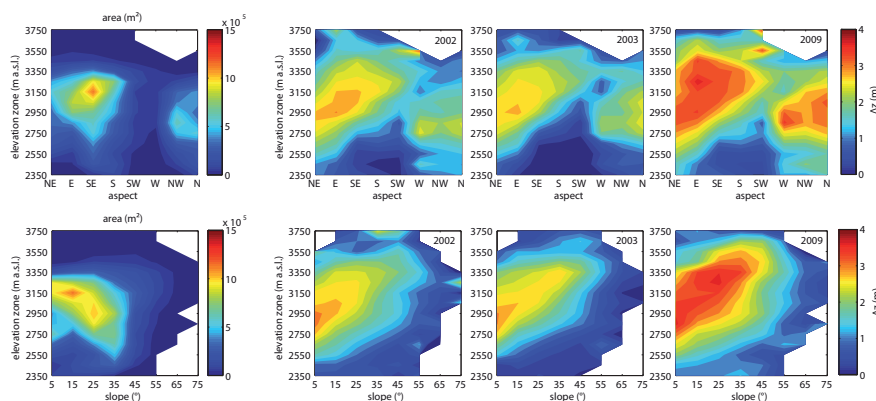
Fig. 4. Contour plots of the elevation distribution of area and surface elevation changes (Δz) dependent on aspect and slope. In the first column the area distribution is shown. Panels 2, 3 and 4 in the first row present Δz dependent on aspect for the accumulation seasons 2002, 2003 and 2009. In the second row the area and Δz dependent on slope are shown, respectively.

SWE of the 100 m elevation bands illustrates the vertical distribution of specific accumulation for the three seasons 2002, 2003 and 2009. The accumulation obtained from ALS data and the modeled accumulation, using the iteratively determined gradient, are shown. Precipitation measurements of the four gauge stations are plotted, too. The right column of Fig. 6 shows the volume of water equivalent calculated by multiplying the SWE by the area of the elevation bands. The lower and upper limit of the error range including the accuracy of the DEMs as well as the error of the SWE calculation are shown as dotted curves. In Table 3 the accumulation gradient γ and the ratios between volume by ALS and modeled volume are presented. Calculated accumulation gradients of 8 % 100 m^{-1} in 2003 and 13 % 100 m^{-1} in 2009 seem to be dependent on the overall accumulation at the end of season.

In all three seasons mean accumulation at the lowest elevation band derived from ALS data was smaller than precipitation measurement at the cumulative precipitation gauge Hochjochhospiz. Precipitation gauges located at higher altitudes show less cumulated precipitation than accumulation at the corresponding elevation bands calculated from ALS data. This can be explained by underestimation of the cumulative precipitation caused by measurement errors dependent on fraction of solid precipitation and wind speed at the high mountain precipitation measurements (Sevruk, 1985; Sevruk and Mieglitz, 2002). Evaluated by runoff measurements, this underestimation can sum up to 30 % of the total precipitation sum. In addition to local precipitation, snow can be accumulated by redistribution from wind exposed ridges and steep slopes to elevations of precipitation gauges and glacier surfaces (Kuhn, 2003; Strasser, 2008). Applying the gradient γ starting from the precipitation measurement of Hochjochhospiz results in an increase of accumulation with increasing elevation. This vertical accumulation distribution was compared to the ALS derived specific accumulation. In the lowest
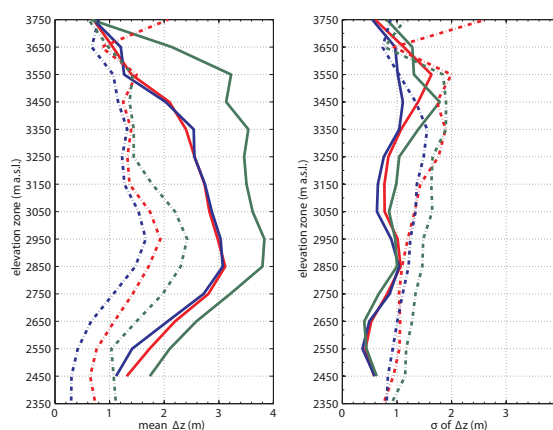

Fig. 5. Elevation distribution of the mean surface elevation change Δz and the standard deviation σ of surface elevation changes obtained from the DEM differences. data of the 2002 accumulation season are plotted in blue, data of 2003 in red and data of 2009 in green. Solid lines are the values of glacierized areas. Dotted lines show data of unglacierized areas.

elevation bands the modeled accumulation is larger than the accumulation obtained from ALS data. This is caused by significant melt and evaporation in these elevations even in the accumulation period. Further specific accumulation modeled by applying the gradient is smaller than accumulation derived from ALS, 2009 even smaller than precipitation measured at the higher located rain gauges. The condition for the second intersection is, that it is at the elevation band that has the largest area (see Sect. 2.3). Above this point the modeled specific accumulation is obviously larger than specific accumulation derived by ALS. Here snow redistribution processes in terms of wind and avalanches reduce the depth of
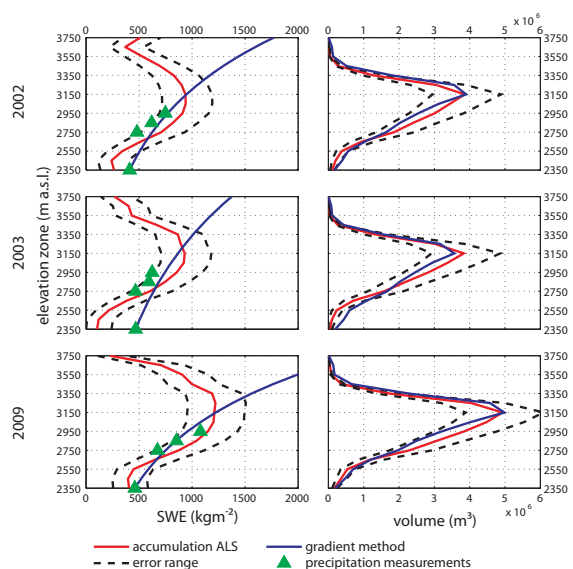
Fig. 6. Graphs of the elevation distribution of SWE in terms of specific accumulation (left column) and volume (right column) obtained from ALS data (red line), by modeling with constant gradient (blue line) and precipitation measurements (green triangle). Values are shown for the state at the end of the accumulation seasons. The black dotted curves show the upper and lower limit of error range.

Table 3. Accumulation gradients and ratios between modeled volume and volume derived from ALS measurements for catchment sum (index all) and elevation band of largest area (index max).

Accumulation period	Accumulation gradient		$\frac{V_{mod}}{V_{ALS\,all}}$	$\frac{V_{mod}}{V_{ALS\,max}}$
	γ	%/100 m		
2002	1.11	11	1.06	1.01
2003	1.08	8	1.03	0.93
2009	1.13	13	1.02	1.01

the snow cover and lead to snow accumulation in lower elevations. Considering the area elevation distribution and hence plotting the volume of the snow pack (Fig. 6, second column), it is obvious, that the specific errors at elevations with less area are not as important as realistic modeling of SWE in the altitude of largest area.

However, error range resulting from ALS measurement, DEM generation and the statistical SWE-model is largest at the elevation bands with largest area (Fig. 6). Assuming a constant error of ALS measurement, the relative error increases with decreasing snow depth. It can be assumed, that small snow depths at lowest and highest elevation bands are represented well by the ALS measurements. Higher snow depths at the elevation bands of largest area are more uncertain, but more important for the volume of the snow cover.
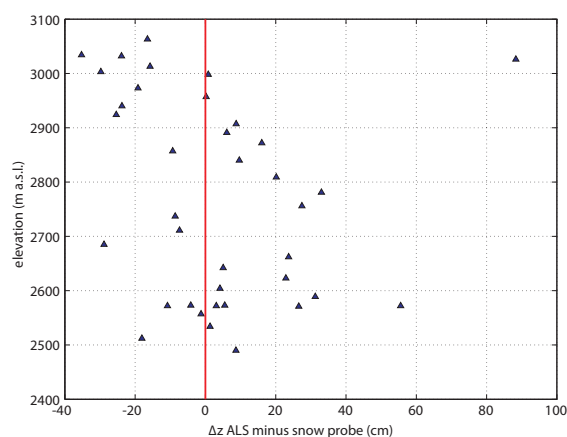

Fig. 7. Difference between ALS elevation change Δz and measured snow depth from snow probing on Hintereisferner (HEF) at the end of accumulation season 2009.

3.3   Estimates on vertical ice flow velocities

Surface elevation changes derived from ALS measurements of glacier surfaces imply dynamical processes beyond the surface mass balance (Fischer et al., 2011). The vertical component of ice flow and internal subsidence of the firn layer has to be considered in studies of geodetic surface surveys in glacierized areas. Deceleration of ice flow at Kesselwandferner within the last decades lead to maximum annual vertical ice flow velocities of about 1 m per year (Abermann et al., 2007). Assuming that vertical ice flow velocities in the accumulation season are in the order of one third of their annual magnitude, the estimated maximum submergence and emergence velocities are about 0.35 m within one accumulation season. These maximum values are substantiated by comparison of ALS differences and snow soundings on Hintereisferner in May 2009 (Fig. 7). The comparison of ALS derived snow depths and snow soundings at Hintereisferner shows differences of ±0.4 m. In the upper part of the glacier ALS snow depths are lower than snow soundings, which can be explained by submergence processes. Differences at the middle elevation zones of Hintereisferner are in the same order but have reverse sign. At the glacier tongue differences are distributed around zero.

4   Discussion and conclusions

In this study ALS data of three accumulation seasons were used to obtain catchment characteristics in terms of spatial distribution of the snow cover and its total volume. Surface elevation changes between two corresponding DEMs at the beginning and at the end of accumulation season were interpreted as snow depths and analyzed depending on slope, aspect and elevation. Characteristically snow

cover distributions were found in the investigated catchment. Whereas preferential snow accumulation areas are similar, snow depths were varying between the analyzed accumulation seasons. It has been shown that significant differences of snow depths exist between unglacierized and glacierized areas. This can be explained by redistribution of solid precipitation from slopes adjacent the glacier to the glacier surface. In hydrological modeling this process is important to compute glacier mass balance realistically (Kuhn, 2003). While standard deviations of snow depths at unglacierized areas are large in comparison to absolute snow depths, elevation changes at glacier surfaces are not only larger, but also more homogeneous. Discrete approaches for both areas, unglacierized and glacierized, in terms of snow cover variability are necessary in hydrological modeling.

Influence of vertical ice flow and compaction of firn layer at glacier surface are locally larger than ALS accuracy. The sign of differences between measured snow depths at Hintereisferner from snow probing and ALS derived snow depths could be explained by these processes at the upper part of the glacier. At the glacier tongue no interpretation of differences is feasible. Nevertheless, considering the overall volume of snow cover, errors by glacier dynamics must be balanced and are therefore negligible. Also vertical velocities are measured at the central flow lines and can be assumed to be getting smaller and approaching zero towards the ice.

As shown by Schöber et al. (2012) a simple regression method between snow depth and snow density leads to reasonable SWE data. Hence maps of SWE can be calculated from ALS elevation changes. These maps are like a big cumulative precipitation gauge on catchment scale, implying loss in terms of evaporation and melt water runoff. Of course, even in high alpine catchments snow melt and evaporation can occur during the accumulation season, which leads to a reduced volume of the snow cover. That means above all, that cumulative precipitation simulated by hydro-meteorological models should be at least as high as the SWE that is obtained from the ALS data at end of winter season. As a second step the snow, cumulated by continuous accumulation gradients at highest elevations of the alpine catchments, should be redistributed to lower elevation bands (Strasser, 2008). This would lead to more melt generation in the middle ablation period and would prevent too much snow accumulation at the top of the mountain ridges. Therefore the ALS data can not provide precipitation gradients, but accumulation gradients. From our experience the elevation of maximum accumulation is near 2900 m a.s.l. on the glaciers treated here. Due to the fact that accumulation is nearly zero at the ridges, accumulation gradients switch at elevations of maximum accumulation, which is near to 3100 m a.s.l. considering the whole catchment.

Catchment specific characteristics like the elevation of maximum specific accumulation, the aspect of largest accumulation and the relation between slope and snow depths can be determined by the shown method of spatial analyses of surface elevation changes obtained from ALS data. These characteristics and parameters like accumulation gradients can be used to calibrate and validate hydrological models for high mountain catchments. ALS at alpine catchments is a reliable technique to obtain volume and spatial distribution of solid precipitation on catchment scale within one accumulation season. As stated in Sect. 1, the application to large areas is limited by the costs of the ALS technique. So ALS measurements of the snow cover are more realizable in mountain catchments and highly complex terrain with heterogeneous snow distribution. Especially on glacier surfaces, future field surveys should be done simultaneously with the ALS flights to increase the knowledge about the accuracy of this method and to quantify potential processes influencing the interpretation of the surface elevation changes. The application of the presented method to other alpine catchments could improve calibration and validation processes in hydrological modeling to get a more realistic distribution of sources for runoff generation. This might have an impact on flood forecasting as well as future runoff scenarios. Long time monitoring of SWE stored in the snow cover of alpine catchments can lead to valuable conclusions about interannual variability and possible trends in volume and duration of snow cover as an impact of climate change.

References

Abermann, J., Schneider, H., and Lambrecht, A.: Analysis of surface elevation changes on Kesselwand glacier – comparison of different methods, Zeitschrift für Gletscherkunde und Glazialgeologie, 41, 147–167, 2007.

Abermann, J., Lambrecht, A., Fischer, A., and Kuhn, M.: Quantifying changes and trends in glacier area and volume in the Austrian Ötztal Alps (1969-1997-2006), The Cryosphere, 3, 205–215, doi:10.5194/tc-3-205-2009, 2009.

Abermann, J., Fischer, A., Lambrecht, A., and Geist, T.: On the potential of very high-resolution repeat DEMs in glacial

and periglacial environments, The Cryosphere, 4, 53–65, doi:10.5194/tc-4-53-2010, 2010.

Baltsavias, E.: Airborne laser scanning: basic relations and formulas, ISPRS J. Photogramm., 54, 199–214, doi:10.1016/S0924-2716(99)00015-5, 1999.

Bergström, S.: The HBV-model – its structure and applications, Tech. Rep. SMHI Hydrology Report No. 4, Swedish Meteorological and Hydrological Institute Narrkoping, Sweden, 1992.

Blöschl, G. and Kirnbauer, R.: An analysis of snow cover patterns in a small alpine catchment, Hydrol. Process., 6, 99–109, doi:10.1002/hyp.3360060109, 1992.

Bollmann, E., Sailer, R., Briese, C., Stötter, J., and Fritzmann, P.: Potential of airborne laser scanning for geomorphologic feature and process detection and quantifications in high alpine mountains, Z. Geomorph., Supplementary Issues, 55, 83–104, doi:10.1127/0372-8854/2011/0055S2-0047, 2011.

Braun, L., Weber, M., and Schulz, M.: Consequences of climate change for runoff from Alpine regions, Ann. Glaciol., 31, 19–25, doi:10.3189/172756400781820165, 2000.

Escher-Vetter, H., Kuhn, M., and Weber, M.: Four decades of winter mass balance of Vernagtferner and Hintereisferner, Austria: methodology and results, Ann. Glaciol., 50, 87–95, doi:10.3189/172756409787769672, 2009.

Fischer, A.: Glaciers and climate change: Interpretation of 50 years of direct mass balance of Hintereisferner, Global Planet. Change, 71, 13–26, doi:10.1016/j.gloplacha.2009.11.014, 2010.

Fischer, A., Schneider, H., Merkel, G., and Sailer, R.: Comparison of direct and geodetic mass balances on an annual time scale, The Cryosphere Discuss., 5, 565–604, doi:10.5194/tcd-5-565-2011, 2011.

Geist, T.: Application of airborne laser scanning technology in glacier research, Ph.D. thesis, Institute of Geography, University of Innsbruck, Austria, 2005.

Geist, T. and Stötter, J.: Documentation of glacier surface elevation change with multi-temporal airborne laser scanner data – case study: Hintereisferner and Kesselwandferner, Tyrol, Austria, Zeitschrift für Gletscherkunde und Glazialgeologie, 41, 77–106, 2007.

Geist, T. and Stötter, J.: Remote Sensing of Glaciers. Techniques for topographic, spatial and thematic mapping of glaciers, Chap. Airborne laser scanning in glacier studies, 179–194, Taylor and Francis, London, 2009.

Grünewald, T., Schirmer, M., Mott, R., and Lehning, M.: Spatial and temporal variability of snow depth and ablation rates in a small mountain catchment, The Cryosphere, 4, 215–225, doi:10.5194/tc-4-215-2010, 2010.

Hollaus, M., Wagner, W., and Kraus, K.: Airborne laser scanning and usefulness for hydrological models, Adv. Geosci., 5, 57–63, doi:10.5194/adgeo-5-57-2005, 2005.

Johannesson, T., Raymond, C., and Waddington, E.: Time-scale for adjustment of glaciers to changes in mass balance, J. Glaciol., 35, 355–369, 1989.

Jonas, T., Marty, C., and Magnusson, J.: Estimating the snow water equivalent from snow depth measurements in the Swiss Alps, J. Hydrol., 378, 161–167, doi:10.1016/j.jhydrol.2009.09.021, 2009.

Kraus, K.: Geometrische Informationen aus Photographien und Laserscanaufnahmen, Band 1, Walter de Gruyter, Berlin – New York, 2004.

Kuhn, M.: Verification of a hydrometeorological model of glacierized basins, Ann. Glaciol., 31, 15–18, doi:10.3189/172756400781820228, 2000.

Kuhn, M.: Redistribution of snow and glacier mass balance from a hydrometeorological model, J. Hydrol., 282, 95–103, doi:10.1016/S0022-1694(03)00256-7, 2003.

Kuhn, M. and Batlogg, N.: Glacier runoff in Alpine headwaters in a changing climate, Hydrology, Water Resources and Ecology in Headwaters (Proceedings of the HeadWater'98 Conference held at Meran/Merano, Italy, April 1998), IAHS P., 248, 79–88, 1998.

Kuhn, M., Dreiseitl, E., Hofinger, S., Markl, G., Span, N., and Kaser, G.: Measurements and Models of the Mass Balance of Hintereisferner, Geogr. Ann. A, 81, 659–670, 1999.

Lehning, M., Grünewald, T., and Schirmer, M.: Mountain snow distribution governed by an altitudinal gradient and terrain roughness, Geophys. Res. Lett., 38, L19504, doi:10.1029/2011GL048927, 2011.

Lui, X.: Airborne LiDAR for DEM generation: some critical issues, Prog. Phys. Geog., 32, 31–49, doi:10.1177/0309133308089496, 2008.

Mott, R., Schirmer, M., Bavay, M., Grünewald, T., and Lehning, M.: Understanding snow-transport processes shaping the mountain snow-cover, The Cryosphere, 4, 545–559, doi:10.5194/tc-4-545-2010, 2010.

Nolin, A. W.: Recent advances in remote sensing of seasonal snow, J. Glaciol., 56, 1141–1150, doi:10.3189/002214311796406077, 2011.

Schöber, J., Achleithner, S., Bellinger, J., Schneider, K., Kirnbauer, R., and Schöberl, F.: Spatial and temporal characteristics of the alpine snow cover: 1. Empirical basis for regional and watershed scale applications, J. Hydrol., submitted, 2012.

Sevruk, B.: Correction of precipitation measurements: Swiss experience, WMO/TD, 104, 187–196, 1985.

Sevruk, B. and Mieglitz, K.: The effect of topography, season and weather situation on daily precipitation gradients in 60 swiss valleys, Water Sci. Technol., 45, 41–48, 2002.

Skaugen, T.: Modelling the spatial variability of snow water equivalent at the catchment scale, Hydrol. Earth Syst. Sci., 11, 1543–1550, doi:10.5194/hess-11-1543-2007, 2007.

Spross, M.: Die Kryosphäre Tirols im Wandel. Geostatistische Analysen zur Quantifzierung klimabedingter Veränderungen auf der Basis multitemporaler ALS-Daten, Master's thesis, Institute of Geography, University of Innsbruck, 2011.

Strasser, U.: Modelling of the mountain snow cover in the Berchtesgaden National Park, Berchtegaden National Park research report, Nr. 55, 2008.

Wehr, A. and Lohr, U.: Airborne laser scanning – an introduction and overview, ISPRS J. Photogramm., 54, 68–82, doi:10.1016/S0924-2716(99)00011-8, 1999.

Chapter 3

Paper II - Comparison of lidar-derived snow depths with GPR measurements

The Cryosphere

Open Access

Lidar snow cover studies on glaciers in the Ötztal Alps (Austria): comparison with snow depths calculated from GPR measurements

K. Helfricht[1,2]**, M. Kuhn**[2]**, M. Keuschnig**[1,3]**, and A. Heilig**[4,5]

[1]alpS – Centre for Climate Change Adaptation, Grabenweg 68, 6020 Innsbruck, Austria
[2]Institute of Meteorology and Geophysics, University of Innsbruck, Innrain 52, 6020 Innsbruck, Austria
[3]Department of Geography and Geology, University of Salzburg, Hellbrunnerstrasse 34, 5020 Salzburg, Austria
[4]Commission for Geodesy and Glaciology, Bavarian Academy of Sciences and Humanities, Alfons-Goppel-Str. 11, 80539 Munich, Germany
[5]Institute of Environmental Physics, University of Heidelberg, Im Neuenheimer Feld 229, 69120 Heidelberg, Germany

Correspondence to: K. Helfricht (helfricht@alps-gmbh.com)

Abstract. The storage of water within the seasonal snow cover is a substantial source of runoff in high mountain catchments. Information about the spatial distribution of snow accumulation is necessary for calibration and validation of hydro-meteorological models. Generally, only a small number of precipitation measurements deliver precipitation input for modelling in mountain areas. The spatial interpolation and extrapolation of measurements of precipitation is still difficult. Multi-temporal application of lidar techniques from aircraft, so-called airborne laser scanning (ALS), provides surface elevations changes even in inaccessible terrain. These ALS surface elevation changes can be used to derive changes in snow depths of the mountain snow cover for seasonal or subseasonal time periods. However, since glacier surfaces are not static over time, ablation, densification of snow, densification of firn and ice flow contribute to surface elevation changes. ALS-derived surface elevation changes were compared to snow depths derived from 35.4 km of ground penetrating radar (GPR) profiles on four glaciers. With this combination of two different data acquisitions, it is possible to evaluate the effect of the summation of these processes on ALS-derived snow depth maps in the high alpine region of the Ötztal Alps (Austria). A Landsat 5 Thematic Mapper image was used to distinguish between snow covered area and bare ice areas of the glaciers at the end of the ablation season. In typical accumulation areas, ALS surface elevation changes differ from snow depths calculated from GPR measurements by -0.4 m on average with a mean standard deviation of 0.34 m. Differences between ALS surface elevation changes and GPR derived snow depths are small along the profiles conducted in areas of bare ice. In these areas, the mean absolute difference of ALS surface elevation changes and GPR snow depths is 0.004 m with a standard deviation of 0.27 m. This study presents a systematic approach to analyze deviations from ALS generated snow depth maps to ground truth measurements on four different glaciers. We could show that ALS can be an important and reliable data source for the spatial distribution of snow depths for most parts of the here investigated glaciers. However, within accumulation areas, just utilizing ALS data may lead to systematic underestimation of total snow depth distribution.

1 Introduction

In alpine catchments, the so-called glacio–nival runoff regime is caused by the storage of water in the seasonal snow cover and in glaciers (Aschwanden et al., 1986; Kuhn and Batlogg, 1998; Kuhn, 2000). High flow rates caused by snow- and ice melt in spring and summer are of interest in terms of water resources management for reservoirs and flood forecasting (e.g. Weingartner et al., 2003; Kirnbauer et al., 2009; Schöber et al., 2010).

For calculating reliable runoff amounts in these mountain catchments, precipitation data in high elevations are needed and the heterogeneous distribution of the snow cover has to

be considered in hydro-meteorological models (e.g. Kuhn, 2003; Huss et al., 2008). However, measurements of solid precipitation are known to be affected by considerable errors (e.g. Sevruk, 1985; Lundberg et al., 2010) and only insufficient data are available for model calibration and validation of the snow depth distribution on the catchment scale. Thereby the spatial representativeness of individual measurements of snow depths and snow densities derived from direct measurements in terms of snow probings and snow pits (Fierz et al., 2009) and from automatic measurement systems (Lundberg et al., 2010) has to be questioned (Grünewald and Lehning, 2011).

Whereas various hydro-meteorological models have been tested versus snow cover extent from satellite remote sensing data of MODIS (Moderate Resolution Imaging Spectroradiometer) or Landsat scenes (e.g. Rott and Markl, 1989; Hall et al., 2002; Schöber et al., 2010), to date no snow depth or SWE can be obtained from satellite data in a high spatial resolution of at least 100 m (Lundberg et al., 2010; Nolin, 2011), which is required to capture the spatial variability of the mountain snow cover (Blöschl, 1999). In contrast, laser altimetry was recognized to be useful to derive small scale snow depth distributions in mountain areas (Deems et al., 2013). Several snow cover studies based on the application of lidar from aircraft (airborne laser scanning – ALS) have been performed in mountain areas, mostly in unglacierized terrain (e.g. Deems et al., 2008; Melvold and Skaugen, 2013), but also in glacierized catchments (e.g. Dadic et al., 2010; Helfricht et al., 2012; Sold et al., 2013). Since 2001, ALS surveys of annual and seasonal surface elevation changes (Δz_{ALS}) were performed in glacierized catchment of the Ötztal Alps (Austria, 46°50′ N, 10°50′ E) (Geist and Stötter, 2007; Helfricht et al., 2012). In 2010/11 an ALS survey of the whole mountain range of the Ötztal Alps was conducted to estimate seasonal snow depths.

In this study Δz_{ALS} are investigated for the accumulation season ranging roughly from the beginning of October (t_1) to the end of April respective the beginning of May (t_2). Figure 1 illustrates the processes causing surface elevation changes on glaciers in this period. The elevation z_1' at the time t_2 corresponds to the primary surface z_1 at the time t_1. The elevation z_2 corresponds to the actual surface at the time t_2. Δz_{ALS} is the result of changes in snow depth (Δz_{HS}), densification of snow and firn (Δz_{DSF}), ablation (Δz_{ABL}) and vertical ice flow (Δz_{ICE})

$$\Delta z_{\mathrm{ALS}} = \Delta z_{\mathrm{HS}} + \Delta z_{\mathrm{DSF}} + \Delta z_{\mathrm{ABL}} + \Delta z_{\mathrm{ICE}} = z_2 - z_1, \quad (1)$$

whereas Δz_{HS} at the time t_2 is defined as the elevation difference between z_2 and z_1'

$$\Delta z_{\mathrm{HS}} = z_2 - z_1', \quad (2)$$

and the summation of densification, ablation and vertical ice flow is the elevation difference between $z_{1'}$ and z_1

$$\Delta z_{\mathrm{DSF}} + \Delta z_{\mathrm{ABL}} + \Delta z_{\mathrm{ICE}} = z_1' - z_1. \quad (3)$$
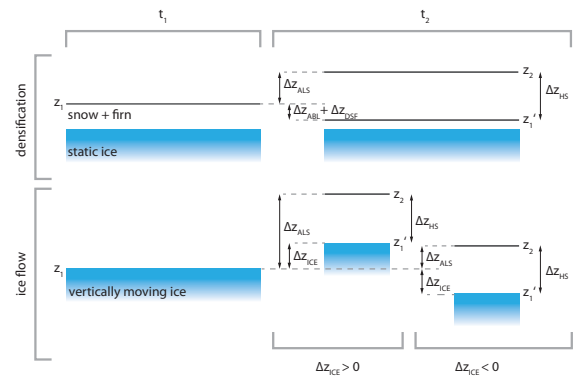
Fig. 1. Changes in surface elevation due to snow depth (Δz_{HS}), ablation (Δz_{ABL}) and densification of snow and LSC (Δz_{DSF}) resulting in ALS surface elevation changes Δz_{ALS} between the two ALS flights (t_1) and (t_2). Upper part: firn and snow on top of static ice. Lower part: firn and snow on top of a vertically moving ice surface (Δz_{ICE}).

The densification of snow and firn layers existing at t_1 leads to an underestimation of Δz_{HS} in the case of snow and firn layers on a static ice body at t_2. Changes of the reference elevation due to vertical ice flow can have both, negative and positive values. Submergence ice flow ($\Delta z_{\mathrm{ICE}} < 0$) leads to an underestimation of Δz_{HS} by Δz_{ALS}. Emergent ice flow ($\Delta z_{\mathrm{ICE}} > 0$) causes overestimation of Δz_{HS} by Δz_{ALS}. Hence, "ground truth" data are necessary to evaluate Δz_{ALS} for snow cover and mass balance studies on glacier surfaces (e.g. Huss et al., 2009; Koblet et al., 2010; Fischer, 2011).

The aim of the present study is to show the consequence of differences between Δz_{ALS} and actual snow depths on the application of multi-temporal ALS to derive seasonal snow depths on the investigated glaciers. The questions is whether and where differences between Δz_{ALS} and actual snow depths on glacier surfaces are of magnitude, such that they have to be considered in snow-hydrological studies based on ALS surveys. Therefore, we compared Δz_{ALS} to snow depths calculated from ground penetrating radar (GPR) measurements and analyzed differences larger than the combined uncertainties of ALS and GPR measurements. The presented results will support the application of ALS surveys for snow cover studies on glaciers in this mountain area and in Alpine catchments with comparable glacier behaviour in terms of ice flow velocities and accumulation area extent. Systematic underestimation or overestimation of snow depths by Δz_{ALS} can be attributed to specific areas for all here investigated glaciers.

After the introduction an overview of methods and data used to process, the GPR and lidar data is given in Sect. 2. Conditions on the glaciers during ALS surveys are treated in more detail in Sect. 3. In Sect. 4 the results are presented followed by the discussion in Sect. 5. Finally, conclusions are

made about the applicability of surface elevation changes derived from ALS for snow cover studies in glacierized catchments.

2 Data and methods

2.1 Study sites

The study sites are located next to the Alpine main ridge in the Ötztal Alps (46°48′ N, 10°46′ E; Fig. 2). Four of the largest glaciers in this mountain range, namely Hintereisferner, Kesselwandferner, Gepatschferner and Vernagtferner were chosen to evaluate Δz_{ALS} on glacier surface for snow cover studies. All of these glaciers have been subject to scientific research for decades: Hintereisferner (HEF, 46°48′ N, 10°46′ E) has one of the world's longest mass balance series starting in 1952 (Hoinkes, 1970; Fischer, 2010; Fischer et al., 2012). Based on these data sets, a variety of models with different complexity were developed to compute glacier surface mass balance (Kuhn et al., 1999; Escher-Vetter et al., 2009). Ice thickness was measured by Span et al. (2005). Since 2001 a series of ALS surveys enabled the comparison of geodetic and direct glaciological measurements of mass balance on Hintereisferner (Geist and Stötter, 2007; Fischer, 2011). However, since the last acceleration of ice flow on Hintereisferner in the 1970s, horizontal velocities have slowed down dramatically to less than $10\,\mathrm{m\,a^{-1}}$ (Span et al., 1997; Span and Kuhn, 2003). They found that emergence velocities measured on the glacier tongue of Hintereisferner decreased to about $1\,\mathrm{m\,a^{-1}}$ at the beginning of the 1990s. Haberkorn (2011) observed a depression of the ice surface for a certain area along the tongue of Hintereisferner. Measured horizontal velocities at ablation stakes were $4.6\,\mathrm{m\,a^{-1}}$ at most. Vertical velocities could not be derived due to small absolute values with changing signs. In 2010/2011 ablation stakes along the flow line on the glacier tongue of Hintereisferner were georeferenced with DGPS (H. Schneider, personal communication, 2013). In combination with the ablation measurements at these positions, vertical velocities were calculated. The mean annual vertical velocities increased from zero in the area of the GPR profile H3 (Fig. 8) to $0.55\,\mathrm{m\,a^{-1}}$ of annual emergence velocity at about $2\,\mathrm{km}$ from the terminus. Annual vertical ice flow measured at an ablation stake in the central flow line near the GPR profile H5 (Fig. 8) was $0.85\,\mathrm{m\,a^{-1}}$ in 2010/2011.

Kesselwandferner (KWF, 46°50′ N, 10°48′ E) was subject to scientific studies investigating density profiles and deformation of firn layers (Ambach and Eisner, 1966). Mass balance measurements from Kesselwandferner using the direct glaciological method started in the hydrological year 1952/53 (Fischer et al., 2011) and geodetic mass balances are available since 1964. In Abermann et al. (2007) annual vertical and horizontal velocities at several stake locations along the central flow line are presented. After the
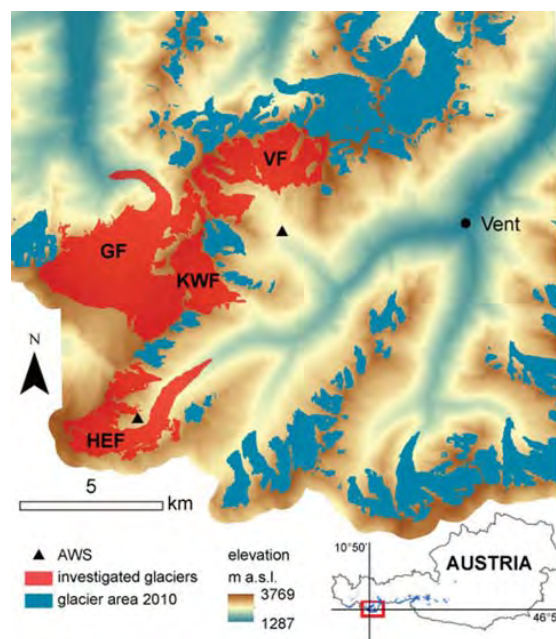

Fig. 2. Map of the investigation area next to Vent in the Ötztal Alps showing the locations of the glaciers Hintereisferner (HEF), Gepatschferner (GF), Kesselwandferner (KWF) and Vernagtferner (VF) and the automatic weather-stations (triangles).

glacier's advance in the 1980s, vertical velocities decreased to $1.5\,\mathrm{m\,a^{-1}}$ at most, both for submergence and emergent flow. Since the measurements of Abermann et al. (2007), annual surveys of the ablation stakes and the accumulation stakes have been continued. For the last 5 yr, mean annual vertical velocities along the flow line remained similar at up to $1\,\mathrm{m\,a^{-1}}$ (H. Schneider, personal communication, 2013).

Gepatschferner (GF, 46°51′ N, 10°45′ E) is the largest glacier in this region. Gepatschferner is the only glacier with an area of more than $10\,\mathrm{km}^2$ in the Ötztal Alps. Its changes in volume and area in the last decades are summarized by Abermann et al. (2009) and ice thickness was measured by Fischer et al. (2007). Glacier velocities have not been investigated on Gepatschferner. Recently a network of ablation stakes was set up to investigate the dynamical behaviour of the glacier tongue. Highest velocities are expected to occur at the crevassed area before the inflow to the glacier tongue. First results show maximum horizontal velocities of up to $50\,\mathrm{m\,a^{-1}}$ with a vertical ice flow of approx. $5\,\mathrm{m\,a^{-1}}$ measured below the ice fall. Velocities decrease towards the glacier tongue, which itself decays very rapidly. No velocity data exist from the large plateau of the accumulation area.

Since 1964 the mass balance of Vernagtferner (VF, 46°52′ N, 10°49′ E) is measured with the direct glaciological method by the Commission for Glaciology, Bavarian

Fig. 3. Mean daily air temperature measured at the automatic weather station (AWS, Fig. 2) Hintereisferner (3027 m a.s.l.; green curve) and the AWS Vernagtferner (2640 m a.s.l.; red curve) for the accumulation season 2010/2011. Cumulative precipitation is shown for the AWS Vernagtferner (blue curve). Dates of ALS surveys are marked as dotted lines.
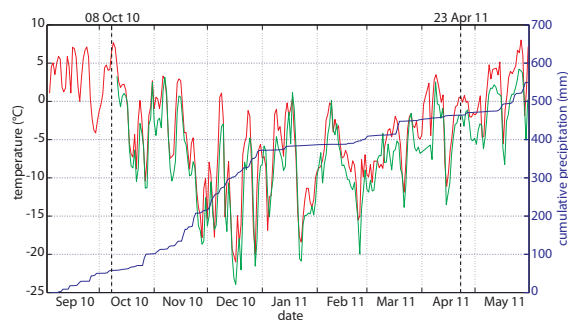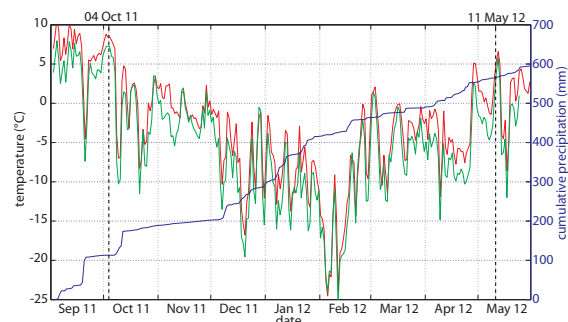

Fig. 4. Mean daily air temperature measured at the automatic weather station (AWS, Fig. 2) Hintereisferner (3027 m a.s.l.; green curve) and the AWS Vernagtferner (2640 m a.s.l.; red curve) for the accumulation season 2011/2012. Cumulative precipitation is shown for the AWS Vernagtferner (blue curve). Dates of ALS surveys are marked as dotted lines.

Academy of Sciences and Humanities, Munich. In combination with a runoff gauge in front of the glacier tongue, a series of hydro-meteorological models were calibrated for energy balance and hydrological studies (Escher-Vetter et al., 2009). Mayer et al. (2013) showed that the glacier slowed down dramatically.

Apart from the long time series of mass balance and ice flow velocity measurements on these glaciers, no measurements of ice flow in the accumulation season exist. With respect to recently observed slow ice velocities in this region, the influence of ice flow on seasonal surface elevation changes can be assumed to be small. However, even 1 m of submergence would have an enormous effect for the interpretation of Δz_{ALS} in terms of snow depth without applying corrections for ice dynamics.

For this study, glacier outlines of the four investigated glaciers derived from the Austrian glacier inventory of 2006
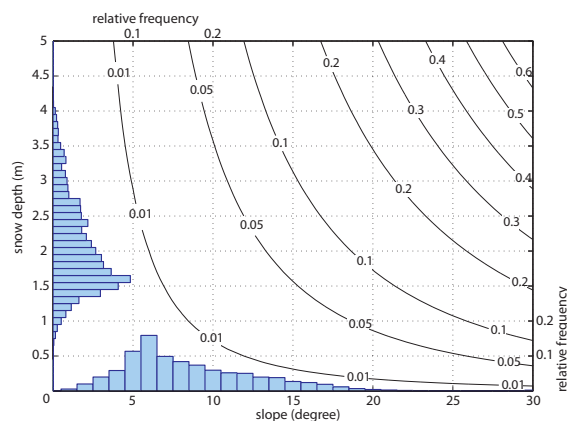

Fig. 5. Contour lines of the correction of GPR snow depth as a function of slope and snow depth. The relative frequency distribution of GPR snow depths h_v and the frequency distribution of the occurring slopes are presented in horizontal and vertical bars, respectively.

(Abermann et al., 2009) were updated based on ALS data of 2010 according to Abermann et al. (2010).

2.2 Ground penetrating radar

Ground penetrating radar (GPR) is an active sensing technique to locate targets or internal layers within ground, ice and snow (Daniels, 2004). A transmitted electromagnetic wave is partly reflected at boundaries between two layers with different relative dielectric permittivities (ϵ_r'). To convert measured two-way-travel times (TWT) of the GPR signal to depth of the reflecting layer transition, the velocity of propagation of the wave has to be determined.

In cryospheric sciences, GPR is used to detect permafrost within rocky ground (e.g. Hinkel et al., 2001; Otto et al., 2012), to determine ice thickness (e.g. Span et al., 2005; Fischer et al., 2007), ice and firn layering (e.g. Spikes et al., 2004) as well as subglacial structures and liquid water content of snow and ice (e.g. Murray et al., 1997; Lundberg et al., 2000). The spatial variability in snow depth and the temporal evolution in snowpack stratigraphy have been analyzed utilizing GPR technology as well (e.g. Machguth et al., 2006; Heilig et al., 2009; Mitterer et al., 2011).

2.2.1 Field campaigns

Three GPR campaigns were conducted close to the respective date of ALS surveys. Dates and snow pit information are displayed in Table 1.

At the end of accumulation season 2010/2011, GPR data were recorded on Vernagtferner by the Commission of Glaciology, Bavarian Academy of Sciences and Humanities (Munich, Germany). A RIS One GPR instrument from IDS (Pisa, Italy) with shielded 600 MHz antennas was used. The

Table 1. Attributes of the field measurements in spring. Number of snow depth probings and snow pits shown in brackets indicate measurements not directly located at the GPR profiles. The GPR signal velocities derived from snow depths of the reflecting snow layer in the snow pits (v_p) and GPR signal velocities calculated from measured snow densities (v_k) using Eqs. (7) and (8) with the corresponding coefficient of variation (CV, Eq. 6).

ID	Date	GPR profile length (10^3 m)	Mean trace distance (m)	Snow depth probings	Snow pits	Signal velocity (m ns^{-1})			
						v_p	CV$_p$	v_k	CV$_k$
VF	28–29 Apr 2011	15.32	0.35	102	1(6)	–	–	0.2254	0.04
GF	28 Apr 2011	5.39	0.30	33	3(1)	0.2270	0.02	0.2263	0.01
KWF	28 Apr 2011	1.84	0.45	0(17)	2				
HEF	9 May 2012	7.66	0.25	49	5	0.2254	0.96	0.2254	0.77
KWF	8 May 2012	5.19	0.18	31	2				

GPR was pulled by a snowmobile. At the first and the last point of the sections snow depths were measured by snow depth probing and coordinates were recorded with a hand-held GPS. Between these points the GPR data were continuously received while driving the snowmobile at uniform speed, which, however, differ between single sections due to topography. In total more than 15 km of GPR profiles were conducted, divided into four longitudinal profiles, three additional shorter profiles in the accumulation zone and one cross profile (Fig. 6). Snow densities were measured at six locations.

A GPR measurement campaign was conducted on Gepatschferner and Kesselwandferner in 2011. GPR data were recorded with a 3-D system from MALÅ (Malå, Sweden) with shielded 500 MHz antennas along a cross profile in the accumulation zone of Gepatschferner and a longitudinal profile on Kesselwandferner (Fig. 7). In total more than seven kilometres of profiles, divided into 33 sections, were investigated on skis. First and last points of the individual sections were georeferenced by DGPS (Fig. 7 – black dots). Three snow pits were dug on Gepatschferner and one on the tongue of Kesselwandferner. While snow depth probings were performed along the GPR sections on Gepatschferner, snow depth probings and GPR data do not spatially coincide on Kesselwandferner. Sample spacing is larger on Kesselwandferner than on Gepatschferner, due to greater velocities while skiing downhill the glacier (Table 1).

At the end of the accumulation season 2011/2012, a GPR campaign was conducted to measure snow depths along longitudinal sections and cross sections on Hintereisferner and Kesselwandferner (Figs. 8 and 9). Skis were used to pull another IDS RIS One system with shielded 400 MHz antennas. In total over 12 km of GPR data were recorded. Snow depth probings were conducted at every first and last point of the individual sections and seven snow pits were dug. All data points were georeferenced by DGPS.

For reflectors being located at a distance of half the wavelength in the respective medium, constructive and destructive interferences will occur (Daniels, 2004). The applied GPR systems with a centre frequency of 400–600 MHz, hence are

capable of distinguishing various reflectors in a vertical distance of more than 0.19 m (600 MHz) to 0.28 m (400 MHz) (Trabant, 1984). All GPR campaigns were conducted in time mode. The trace spacing for each transect was chosen such that 2 consecutive traces are always separated less than 0.5 m. So quasi-continuous information could be tracked along the profiles based on known reflector depths from snow depth probing and from snow pits.

2.2.2 Processing

GPR raw data were processed applying the ReflexW software from Sandmeier Scientific Software (Karlsruhe, Germany). Coordinates for each trace were calculated at equal distances. The surface signal reflection was set to time zero. Low frequency parts and noise in the spectrum were filtered applying a dewow and bandpass filter. In a next step temporally consistent signals were eliminated utilising a background removal. To compensate for spherical divergence losses, we applied gain functions. No migration was used due to the spatial homogeneity and the low reflector depth relative to the high density of GPR measurements. The boundaries of the snow layers were picked and corrected to the zero phase change. The picks were exported with the attribute of the two-way-travel time. Finally, we merged individual sections to continuous longitudinal and cross profiles.

Snow depth probing and snow pits were used to identify the depth of the seasonal snow layer according to the guidelines for measuring glacier mass balance (Kaser et al., 2003). GPR signal velocities were calculated from measured reflector depths and snow densities at the snow pits only. Assuming that the snow surface and the ice surface are parallel, the slope of the surface has to be considered. The recorded GPR signal corresponds to the snow depths perpendicular to the surface, but snow depths derived from snow probings and snow pits (h_m) are measured vertically. We corrected vertically measured snow depths h_m by

$$h_{cor} = h_m \cdot \cos(\alpha) \tag{4}$$

in accordance to the respective slope angle α. Signal velocities (v) for GPR measurements on Gepatschferner and

Fig. 6. Spatial distribution of ALS-derived surface elevation changes for for 10 October 2010 to 23 April 2011. Snow depths calculated from GPR measurements along the profiles at Vernagtferner plotted in the same colour-scale. Black dots indicate locations of snow depth probing. Locations of snow pits are shown as white squares. Snow covered areas derived from Landsat image of 31 August 2009 (LSC) are striped.
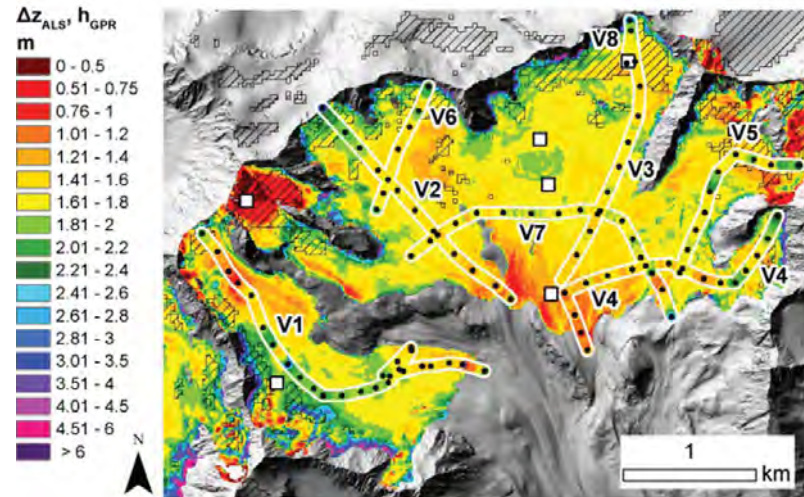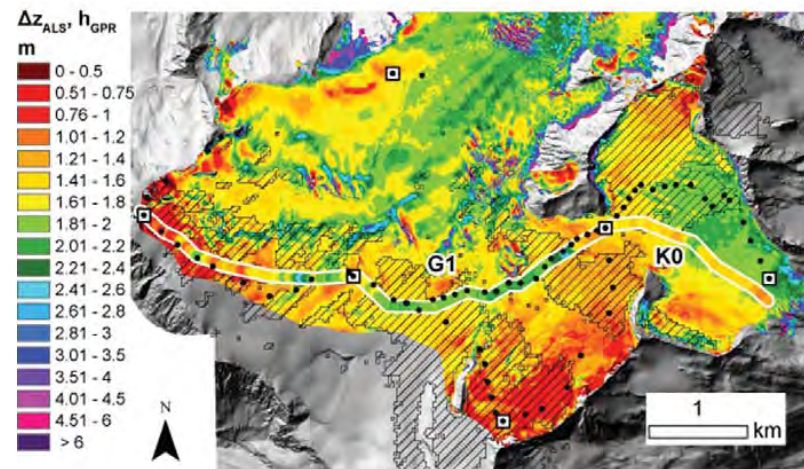

Fig. 7. Spatial distribution of ALS-derived surface elevation changes for 10 October 2010 to 23 April 2011. Snow depths calculated from GPR measurements along the profiles at Gepatschferner and Kesselwandferner shown in the same colour-scale. Black dots indicate locations of snow depth probing. Locations of snow pits are shown as white squares. Snow covered areas derived from Landsat image of 31 August 2009 (LSC) are striped.

Kesselwandferner in 2011 and GPR measurements on Hintereisferner and Kesselwandferner in 2012 were calculated following Daniels (2004):

$$v = \frac{2 \cdot h_{cor}}{\tau} \tag{5}$$

using h_{cor} and the TWT (τ) at the snow pit locations. A mean signal velocity ($\overline{v}$) was calculated for each measurement campaign individually (Table 1). The variation of the signal velocities (CV) is given by

$$CV = \frac{v_{max} - v_{min}}{\overline{v}} \tag{6}$$

as the ratio of the range between the derived maximum velocity v_{max} and minimum velocity v_{min} to the mean velocity $\overline{v}$. According to Kovacs et al. (1995), we calculated ϵ'_r of the snow cover

$$\epsilon'_r = (1 + 0.845 \cdot \rho_s)^2, \tag{7}$$

Fig. 8. Spatial distribution of ALS-derived surface elevation changes from 4 October 2011 to 11 May 2012. Snow depths calculated from GPR measurements along the profiles at Hintereisferner shown in the same colour-scale. Black dots indicate locations of snow depth probing. Locations of snow pits are shown as white squares. Snow covered areas derived from Landsat image of 31 August 2009 (LSC) are striped.
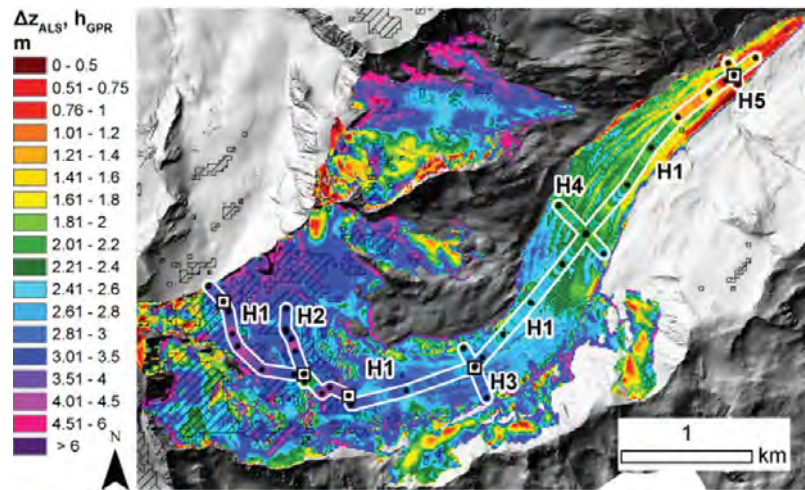
where ρ_s is the snow density in $\mathrm{g\,cm}^{-1}$. Based on ϵ_r' GPR signal velocities v were calculated

$$v = \frac{c}{\sqrt{\epsilon_r'}}, \tag{8}$$

where c is the velocity of propagation of the electromagnetic wave in a vacuum of approx. $0.3\,\mathrm{m\,ns}^{-1}$.

On Vernagtferner snow pits were not located along the GPR profiles. Therefore GPR signal velocities were calculated from measured snow densities only following Eqs. (7) and (8). Signal velocities derived from measured snow depths in the snow pits (Eq. 5) on Hintereisferner and Kesselwandferner were validated with signal velocities calculated from snow densities (Eq. 8) (Table 1). The CV of the signal velocities is larger for 2012 data due to higher variations in snow densities measured in the snow pits. Snow depth probings performed along the GPR profiles were used to validate the respective calculated wave speed. All exported TWT τ were converted into snow depths (h_v)

$$h_v = \frac{\tau \cdot \overline{v}}{2} \tag{9}$$

using the mean velocities $\overline{v}$ for each measurement campaign. Again to account for vertically measured Δz_{ALS}, GPR-determined h_v had to be corrected for the prevailing slope α resulting in the final snow depth h_{GPR}

$$h_{\mathrm{GPR}} = \frac{h_v}{\cos(\alpha)}. \tag{10}$$

Figure 5 shows the magnitude of corrections which have to be applied to h_v as a function of snow depth and slope. In the

same figure the frequency distribution of snow depths measured with GPR and the frequency distribution of the occurring slopes are shown. The most frequent snow depths were between 1.55 m and 1.65 m. The most frequent slopes were between 5° and 7°. Corrections, which therefore had to be applied, were mainly of the order of 0.01 m.

2.3 Lidar

Lidar is an active remote sensing technology (Baltsavias, 1999; Wehr and Lohr, 1999; Kraus, 2004). Airborne laser scanning (ALS) can be applied in mountain areas on the catchment scale, because it is hardly affected by topographic shading and travel distance of the signal can be controlled by flight height (e.g. Deems et al., 2013). The DGPS referenced data provide 3-D information of the reflecting surface with a high point density and accuracy. Based on these 3-D point data (the so-called point cloud) digital elevation models (DEMs) can be produced (Lui, 2008), while high point densities allow simple interpolation schemes (Deems et al., 2013). Surface elevation changes can be detected from the difference of the DEMs of multi-temporal laser scan surveys.

Accuracy of the 3-D location of each point is affected by the accuracy of the recording of the position of the scanning platform and its orientation (e.g. Joerg et al., 2012; Deems et al., 2013). Accuracy of the resulting DEMs depends on point density, the adjustment of overlapping areas of the stripes and the interpolation algorithm used (e.g. Deems et al., 2013). For DEMs derived from ALS data of the Hintereisferner region, Bollmann et al. (2011) showed that for slopes below 35° a vertical accuracy of $\pm 0.15\,\mathrm{m}$ can be assumed.
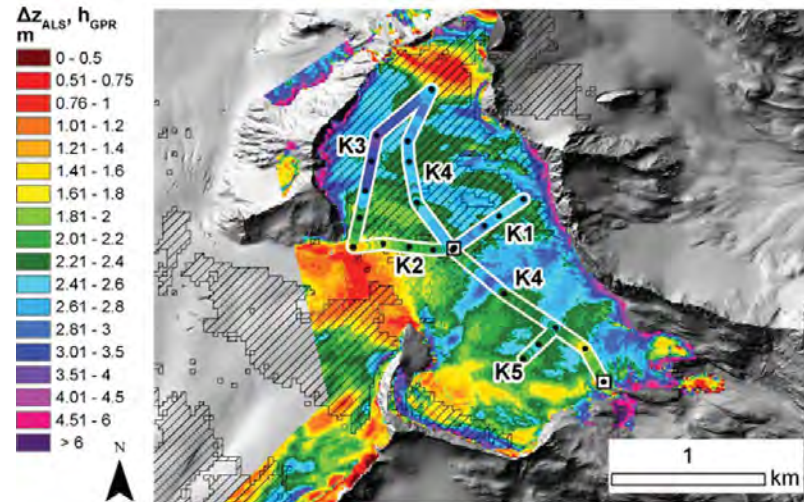
Fig. 9. Spatial distribution of ALS-derived surface elevation changes from 4 October 2011 to 11 May 2012. Snow depths calculated from GPR measurements along the profiles at Kesselwandferner shown in the same colour-scale. Black dots indicate locations of snow depth probing. Locations of snow pits are shown as white squares. Snow covered areas derived from Landsat image of 31 August 2009 (LSC) are striped.

2.3.1   Data and processing

In this study four laser scan surveys were used. They were conducted by TopScan using Optech devices mounted on Cesna aircrafts. Technical details and the accuracy measured at a reference surface are listed in Table 2. The last pulses of all ALS points within one pixel of the resulting DEMs were averaged to a grid size of 1 m. Data were analyzed on generally homogeneous glacier surfaces, which, except for very small areas, have a slope of less than 20° along the investigated profiles (Fig. 5). Surface elevation changes (Δz_{ALS}) were calculated by subtracting a DEM of an almost snow-free ALS survey in fall (t_1) from a DEM of an ALS survey at the end of accumulation season in spring (t_2), respectively, following Eq. (1), with $z_1 = z_{t1}$ and $z_2 = z_{t2}$ (Fig. 1).

2.4   Calculation of differences and uncertainties

Absolute differences (Δh_{abs}) were calculated between ALS surface elevation changes (Δz_{ALS}) and snow depths calculated from GPR (h_{GPR}) by

$$\Delta h_{\mathrm{abs}} = \Delta z_{\mathrm{ALS}} - h_{\mathrm{GPR}}. \tag{11}$$

A moving window approach was used to perform a statistical Mann–Whitney–Wilcoxon test with a number of 300 samples of Δh_{abs} around each single data point of GPR measurements. According to the mean trace distances shown in Table 1, the number of 300 samples corresponds to a distance of approx. 100 m, which is an adequate spatial scale for differences analyzed here. The null hypothesis was tested, if

the median of the two samples (Δz_{ALS} and h_{GPR}) is equal with a significance level of $p = 0.05$. If the null hypothesis is rejected, the medians of the two data sets differ from each other. Additionally the mean value of Δh_{abs} of the 300 samples was compared to an assessment of absolute uncertainty U_{abs} calculated as follows

$$U_{\mathrm{abs}} = \sqrt{2 \cdot U_{\mathrm{ALS}}^2 + (U_{\mathrm{v}} \cdot h_{\mathrm{GPR}})^2}. \tag{12}$$

Uncertainties of gridded lidar data ($U_{\mathrm{ALS}} = \pm 0.15\,\mathrm{m}$) have to be considered twice, because two elevation models are used to investigate surface elevation changes. Uncertainties caused by the calculated GPR signal velocities (U_{v}) correspond to half of maximum CV (Eq. 6, Table 1), which is ± 0.05. U_{abs} are also a function of snow depths (h_{GPR}). The results of the statistical analysis show where Δz_{ALS} and h_{GPR} differ significantly. Furthermore it was calculated where Δh_{abs} exceed U_{abs} along the profiles. In these areas, Δz_{ALS} is increasingly influenced by processes more than only snow depth uncertainties (see Sect. 1).

2.5   Accumulation areas from Landsat

The densification of firn is supposed to be one source of differences of Δz_{ALS} from actual snow depths (Sect. 1). Also submergence ice flow is very likely in the central parts of typical accumulation areas. Hence, typical accumulation areas on glaciers were expected to show larger differences since both vertical ice flow and densification work vertically in the same direction. Snow covered areas of glaciers can be delineated by application of spaceborne optical data for

Table 2. Overview of the ALS flight campaigns investigated in this study. The vertical accuracy is obtained from differences between ALS surface elevations and elevations of a known reference surface. The vertical accuracy is shown in terms of a mean offset (mean) and the standard deviation (σ).

Timestamp	Date	Laser system	Mean Flight speed (m s^{-1})	flight altitude above ground (m)	Maximum scan angle (°)	Laser repetition rate (10^3 s^{-1})	Scan frequency (s^{-1})	Mean point density (m^{-2})	Vertical accuracy (m) mean	σ
t_1	7–10 Oct 2010	ALTM Gemini	65	1000	25	70	36	3.6	0.071	0.047
t_2	20–23 Apr 2011	ALTM Gemini	65	1000	25	70	36	3.8	−0.007	0.041
t_1	4 Oct 2011	ALTM 3100	70	1200	20	70	40	2.9	0.001	0.042
t_2	11 May 2012	ALTM 3100	65	1200	20	70	40	2.8	0.005	0.057

whole catchments (Hall et al., 1987; Nolin, 2011). Landsat satellite images are available in a spatial resolution of 30 m (http://glovis.usgs.gov). A Landsat 5 Thematic Mapper (TM) image of the Ötztal Alps on the 31 August 2009 was retrieved from USGS. Snow covered areas on glacier surfaces were delineated by applying the Normalized Difference Snow Index (NDSI, Hall et al., 1987). The application of Landsat imagery is limited by the discrepancy of the date of surveys to the date of interest and the occurrence of clouds masking the surface information. The conditions of this scene fulfill all requirements in terms of no clouds, recent new-snow precipitation on the glaciers and an advanced state of snow ablation in late summer. The low accumulation area ratios (AAR, Cogley et al., 2011) derived using the NDSI for separation of snow and bare ice are comparable to those observed within the annual mass balance measurements on the glaciers in recent years. Hence the delineated snow covered areas were assumed to indicate recent accumulation areas on the investigated glaciers and are referred to as Landsat snow cover (LSC) hereafter.

3   Prevailing local conditions during lidar surveys

Surface elevation changes between field campaigns and the dates of ALS surveys (t_1, t_2) contribute to uncertainties in Δh_{abs}. Snow accumulation before the ALS surveys in the higher elevated glacier areas in fall has to be considered when identifying the snow layers in the GPR analysis. Photographs and measurements of snow depths and snow densities taken during annual glacier mass balance field campaigns on Hintereisferner, Kesselwandferner and Vernagtferner were included for data analysis. Information on the weather conditions before the ALS surveys, between the ALS surveys and the field campaigns as well as on the weather conditions during the accumulation seasons were obtained from two automatic weather stations located next to Hintereisferner (46°47′55″ N, 10°45′37″ E; 3027 m a.s.l.) and next to Vernagtferner (46°51′23″ N, 10°49′43″ E, 2640 m a.s.l., Fig. 2). The course of daily mean temperatures and cumulative precipitation at the two automatic weather stations is presented in Figs. 3 and 4.

On 12 October 2010 snow depths and snow densities of a snow layer covering the 2010 firn layer on Gepatschferner and Kesselwandferner was measured by 43 snow depth prob-

ings and three snow pits. This snow layer was accumulated in September 2010. In a warm period before the ALS survey (Fig. 3), this layer was transformed into a snowpack with a high bulk density and a melt-freeze crust at the surface. This snow layer could be identified in the stratigraphies of spring snow pits and in the snow layering derived from GPR data in 2011. Snow depths of the same snow layer were recorded by 34 snow probings within the annual mass balance measurements at Vernagtferner. Between the ALS survey in spring 2011 and the corresponding GPR field campaigns a shallow snow cover of about 0.1 m with a low density was accumulated.

In September 2011 glacier tongues and steep southerly exposed parts on Hintereisferner and Kesselwandferner appeared to be snow free on photographs taken alongside the annual mass balance measurements on 1 October 2011. Only a shallow snow layer was covering the typical accumulation areas (A. Fischer, personal communication, 2012). Shortly after the ALS survey in October 2011 a snowfall event preserved the surface recorded by ALS from melt.

4   Results

The spatial distribution of Δz_{ALS} and snow depths calculated from GPR measurements (h_{GPR}) along the profiles are illustrated in Figs. 6–9. Locations of snow pits and snow depth probings of the spring field campaigns are included. Data corresponding to the individual profiles are listed in Table 3.

Figure 10 shows the total number of analyzed data points for LSC areas and bare ice areas (Sect. 2.5) from the profiles and the statistical distribution of all absolute differences (Δh_{abs}, Eq. 11) in terms of the median (red line), the scatter (25 % and 75 % percentiles, blue box), the range of extreme values (1.5 times the interquartile range added to the 25 % percentile and to the 75 % percentile, black whiskers) and the outliers (red crosses).

The profiles H1 (Fig. 11) and K4 (Fig. 12) along the central flow lines of the glaciers show distinct negative Δh_{abs} (Eq. 11) in the LSC areas. Δh_{abs} are constantly small along most of the glacier tongue of Hintereisferner. At the very front of the glacier tongue, Δh_{abs} increases towards positive values. Along the profile K4 on KWF distinctly less h_{GPR} match with the corresponding Δz_{ALS}. Towards the tongue of the glacier, Δh_{abs} is constantly positive for about 500 m in

Table 3. Properties of the GPR profiles in terms of ID, profile length, number of sections, the mean section length ($\overline{l_S}$), minimum elevation and maximum elevation. Mean value of the surface elevation changes derived from ALS data $\overline{\Delta z}_{ALS}$ (Eq. 1) and the mean absolute difference of this value from mean GPR snow depth $\overline{\Delta h}_{abs}$ (Eq. 11) are shown for LSC areas and ice areas of each profile.

Profile ID	Length (m)	Sections n	$\overline{l_S}$ (m)	Elevation (m a.s.l.) max	Elevation (m a.s.l.) min	Ice areas (m) $\overline{\Delta z}_{ALS}$	Ice areas (m) $\overline{\Delta h}_{abs}$	LSC areas (m) $\overline{\Delta z}_{ALS}$	LSC areas (m) $\overline{\Delta h}_{abs}$
H1	5788	25	232	3364	2532	2.32	−0.01	3.10	−0.50
H2	586	5	117	3159	3096	3.00	0.31	2.95	−0.38
H3	414	2	207	2905	2895	2.73	0.02	2.46	−0.47
H4	498	2	249	2754	2736	2.27	0.10	–	–
H5	176	2	88	2565	2557	1.33	0.07	–	–
K1	550	3	183	3175	3164	–	–	2.26	−0.32
K2	6576	4	164	3210	3174	1.72	−0.19	1.94	−0.15
K3	1207	5	241	3293	3210	–	–	2.23	−0.60
K4	2485	8	311	3293	3019	2.43	0.23	2.32	−0.26
K5	291	2	146	3087	3072	2.33	0.02	–	–
G1	5391	26	207	3484	3154	1.38	−0.28	1.23	−0.49
K0	1844	7	263	3212	3035	1.76	0.29	1.52	0.04
V1	3458	25	138	3370	2803	1.61	−0.01	1.25	−0.35
V2	2022	11	184	3303	2892	1.54	0.00	1.79	−0.23
V3	2093	9	233	3307	2961	1.56	0.02	1.55	−0.10
V4	2412	17	142	3327	2864	1.47	0.01	1.48	−0.22
V5	1488	9	165	3355	3091	1.67	−0.08	1.36	−0.28
V6	1007	6	168	3264	3131	1.54	−0.05	1.66	−0.03
V7	2526	14	180	3060	3020	1.62	0.01	1.50	−0.05
V8	314	1	314	3303	3255	–	–	1.57	−0.22

distance of the profile. For most parts of the profiles from Vernagtferner, Δh_{abs} do not exceed the uncertainty range (Sect. 2.4).

The profiles H2 on Hintereisferner, K1, K2, K3 on Kesselwandferner, V8 on Vernagtferner and G1 on Gepatschferner are mostly located in the accumulation area of the glaciers. Only very few parts of the respective profiles cover bare ice areas. For each of those profiles, the median of Δh_{abs} is distinctly negative. The cross profiles H3, H4, H5, K5 and V7, located in areas with bare ice at the surface, show up with a median of Δh_{abs}, which is close to 0. The interquartile ranges of these profiles are comparably small in contrast to most LSC areas (Fig. 10).

Figure 13 shows the comparison of Δh_{abs} to calculated uncertainties U_{abs} (Eq. 12) in combination with the results of the Mann–Whitney–Wilcoxon test (Sect. 2.4). Δh_{abs} calculated for LSC areas of several profiles exceed U_{abs}, which is ± 0.24 m for a mean snow depth of 2 m (Table 3). Along most parts of the profiles located in ice areas on the investigated glaciers, differences between Δz_{ALS} and h_{GPR} are significant ($p = 0.05$) but within the range of the calculated uncertainties (Eq. 12). Distinct positive Δh_{abs} were found on the very front of the glacier tongue of Hintereisferner and on the tongue of Kesselwandferner. Small areas of positive Δh_{abs} were found in crevassed zones located in the higher elevated parts of the glaciers.

Table 3 highlights the increased negative values of Δh_{abs} calculated for ALS measurements in LSC areas compared to Δh_{abs} for ice areas. Figure 10 shows that only a small number of Δh_{abs} values in ice areas are as negative as the majority of Δh_{abs} determined in LSC areas. In these LSC areas mean Δh_{abs} is -0.40 m with a standard deviation of 0.34 m, which is approximately 20 % of the mean value of h_{GPR} with a standard deviation of 17 %.

Very locally, absolute differences are in the magnitude of about 1 m, which corresponds to relative differences of up to -40 % or more. For the ice areas of the profiles, the mean absolute difference is 0.004 m with a standard deviation of 0.27 m, in relative values -0.002 % with a standard deviation of 14.4 %. Depending on the location of the profiles, negative Δh_{abs} were also found for ice areas (e.g. K2, G1; Table 3) or increased positive Δh_{abs} of up to 1 m (K0, K4; Fig. 12) were calculated.

5 Discussion

5.1 Differences in accumulation areas

The Landsat image of snow covered areas from 31 August 2009 cannot give direct proof for the general distinction between areas, where Δz_{ALS} is considerably influenced by snow densification and vertical ice flow, and areas with only small Δh_{abs}. In addition, only the areal extent of the snow
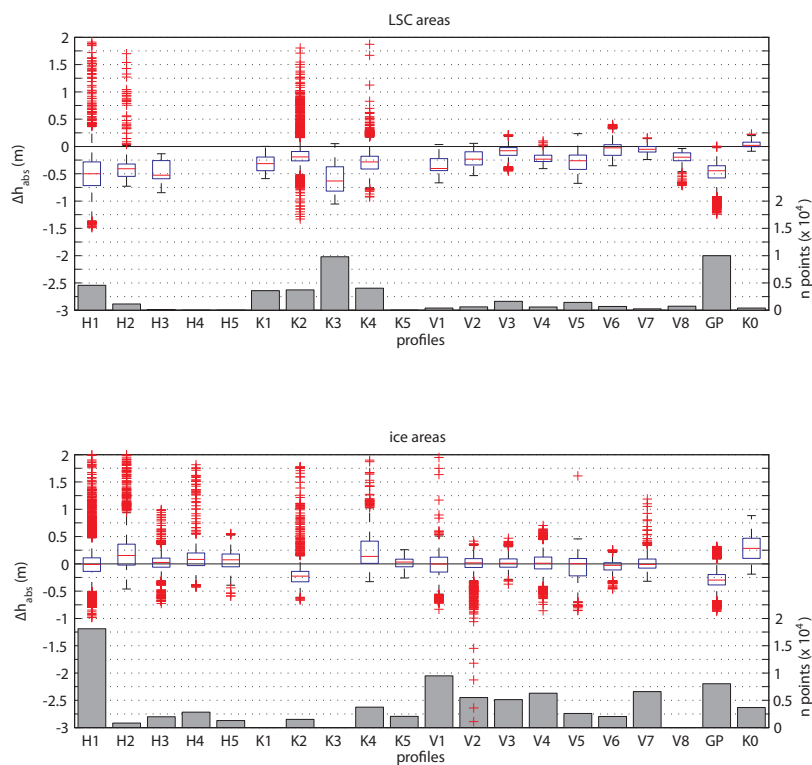
Fig. 10. Box plots of the absolute differences Δh_{abs} at the profiles for snow covered areas derived from Landsat (LSC, upper plot) and ice areas (lower plot) separately. Statistical distribution is shown in terms of the median (red line), the scatter (25 % and 75 % percentiles, blue box), the range of values within 1.5 times the interquartile range added to the 25 % percentile and to the 75 % percentile (black whiskers) and the outliers (red crosses). The number of points included in the statistics are plotted as grey bars (right scale).

cover (LSC) can be derived from Landsat imagery (30 m pixel resolution). No information on snow depths and, hence, spatial distribution of densification is provided by this data source. It does, however, give a broad picture of the distribution of typical firn areas and ice in the period of investigation. Areal snow cover extent on 31 August 2009 is generally in good agreement with the small firn areas observed for the last decade, which caused low accumulation area ratios (AAR) on these Alpine glaciers (e.g. http://www.glaziologie.de/) LSC area probably do not display the total zone of submergence ice flow, because flow dynamics are controlled by a variety of properties and usually adapt to mass changes within decades. Superimposed ice zones, which are part of the accumulation zone, are likely not visible to Landsat either. Furthermore, the applicability of Landsat scenes to distinguish typical accumulation areas on glaciers has to be proved carefully in terms of the state of seasonal ablation and the presence of new snow at the date of survey.

However, LSC areas at the end of ablation season used here show consistently higher Δh_{abs} compared to ice areas (Table 3, Fig. 13), since, as mentioned in Sect. 2.5, both

vertical ice flow and densification of firn work in the same direction in typical accumulation areas of the glaciers. On Vernagtferner firn areas detected from Landsat data are very small. Even for these small firn areas the distinctly negative Δh_{abs} are evident. The total profile on Gepatschferner shows negative differences for subtracting h_{GPR} from Δz_{ALS}. This can be attributed to the location of the profile in the accumulation zone of the glacier. However, even in this accumulation zone different magnitudes of Δh_{abs} calculated for ice areas and Δh_{abs} calculated for LSC areas could be detected (Table 3).

Ambach and Eisner (1966) measured snow densities in a firn pit of 20 m depth on Kesselwandferner at an elevation of 3200 m a.s.l. Firn densities increased roughly linear from $630\,kg\,m^{-3}$ in the uppermost layer to $836\,kg\,m^{-3}$ in a layer at the age of 10 yr. The firn compression rate of 3 % per year in this 10 yr firn cover lead to a vertical compression of 16 m firn depth by approx. 0.5 m per year. Similar rates of densification are presented in a density profile of upper Seward Glacier (Yukon, Canada) in Cuffey and Paterson (2010) (page 17, Fig. 2.3). However, percolating meltwater
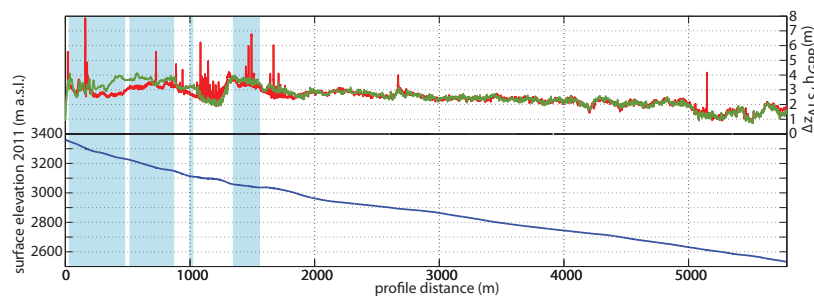
Fig. 11. Elevation of the surface in fall 2011 (blue curve), ALS surface elevation change Δz_{ALS} (red curve) and GPR snow depth h_{GPR} (green curve) along the longitudinal profile H1 at Hintereisferner. Snow covered areas derived from Landsat image of 31 August 2009 (LSC) are shaded in blue.

may contribute to annual densification of firn on Alpine glaciers. Because Δh_{abs} were investigated for the comparatively shorter accumulation season, the contribution of densification of firn to Δh_{abs} is assumed to be less than 0.5 m.

5.2 Comparison to measured ice flow velocities

Our data comparison does not allow to assess the quantitative proportion of the particular processes contributing to differences of Δz_{ALS} from actual snow depths (Fig. 1). However, the four investigated glaciers show different dynamical behaviour, which is also the case for annual ice flow velocities presented in Sect. 2.1.

In the uppermost parts of Hintereisferner negative Δh_{abs} (Eq. 11) occur in between the crevassed areas (Fig. 11). These Δh_{abs} exceed the uncertainties of the applied methods (Eq. 12). However, no measurements of vertical ice flow exist for this area. Positive Δh_{abs} could be detected only at the very front of the glacier tongue of Hintereisferner. These results coincide with the findings that mean annual vertical ice flow velocities are around $0.5\,\mathrm{m\,s^{-1}}$ and less apart from the front of the glacier tongue (Sect. 2.1) .

Distinct positive and negative Δh_{abs} are evident on Kesselwandferner (Fig. 12). Maximum Δh_{abs} in the LSC areas are within the magnitude of the measured annual vertical ice flow velocity (Sect. 2.1). Δh_{abs} of the profile K3 of 0.6 m (Table 3) is slightly more than half of the measured annual vertical ice flow velocities. Locally, derived Δh_{abs} are larger than half of the observed annual emergence of the ice surface which is about 1 m at the glacier tongue of Kesselwandferner (Sect. 2.1 and Fig. 9). For the accumulation zone of Gepatschferner no measurements of ice flow velocities exists. On this glacier Δh_{abs} are comparable to Δh_{abs} of the uppermost profiles on Hintereisferner (H1) and Kesselwandferner (K3). Differences between Δz_{ALS} and h_{GPR} are within the uncertainty range of the measurements for most parts of Vernagtferner. This coincides with the decreased ice flow of the glacier observed by Mayer et al. (2013).

5.3 Influence of prevailing conditions

In glacierized mountain catchments, it is generally difficult to coordinate the dates of maximum ablation in fall and maximum accumulation in spring with the ALS surveys. In this study, both the temporal offsets between GPR and ALS measurements and the dates of ALS surveys in relation to the weather conditions are in good accordance to the required accuracy based on the previous assumptions for this study (Sect. 3, Figs. 3 and 4).

Due to the short delay between ALS surveys and GPR campaigns, simple assumptions were made for processes causing surface elevation changes within this time period. The thin layer of new snow in spring 2011 was neglected, because this layer was moved aside when pulling the GPR antenna over the snow surface on Gepatschferner and Kesselwandferner. On Vernagtferner this new-snow layer was assumed to be depleted by the snowmobile. In 2012 the GPR campaign took place before the ALS survey. The snow depth reduction due to melt conditions is assumed to be in the magnitude of the immersion of the GPR antenna into the uppermost snow layer during the measurements.

To account for the densification of snow accumulated before the ALS survey in fall 2010, measurements of this snow layer can give a rough estimate. From snow depth and density measurements in fall 2010 and spring 2011, a compaction of approx. 0.07 m of a corresponding snow depth at ALS (t_1) of 1 m was calculated. However, measured snow depths at time of ALS(t_1) in 2010 was considerably less with mean values of 0.64 m on Gepatschferner and Kesselwandferner and 0.38 m on Vernagtferner.

5.4 Uncertainties

U_{abs} was calculated accounting for stochastic uncertainties of the combination of the applied measurement methods (Eq. 12). Further sources for systematic errors and uncertainties have to be mentioned: data were analyzed in the spatial resolution of 1 m for DEM data and for each GPR trace
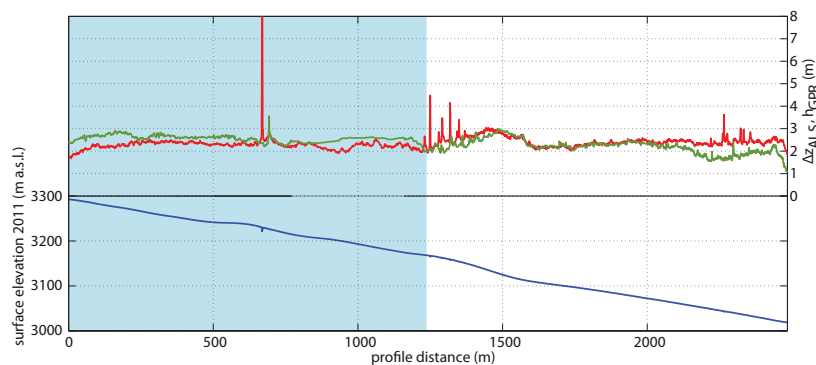
Fig. 12. Elevation of the surface in fall 2011 (blue curve), ALS surface elevation change Δz_{ALS} (red curve) and GPR snow depth h_{GPR} (green curve) along the longitudinal profile K4 at Kesselwandferner. Snow covered areas derived from Landsat image of 31 August 2009 (LSC) are shaded in blue.

separated by the trace distance (Table 1). Both, in ALS and in GPR data, surface heterogeneities (e.g. crevasses) in the scale of 1 m are mapped. Horizontal ice flow shifts surface heterogeneities along the flow direction within one accumulation season. Hence, location of crevasses in fall are included in the data of Δz_{ALS}, whereas GPR data show the location of the crevasse in spring (e.g. Fig. 12 at a profile distance of 700 m). In the analysis of Δh_{abs} the horizontal shift is not considered, because ALS data are validated with respect to all processes contributing to surface elevation change. Resulting maximum differences are displayed as outliers in the Fig. 10.

As shown by Joerg et al. (2012), stochastic uncertainties of ALS-derived surface elevations are strongly reduced on less inclined, homogeneous glacier surfaces. Mean systematic offset of each ALS survey was calculated based on a reference surface (Table 2). However, this systematic offset is not identical with a systematic offset of the ALS data at the investigated glaciers. Due to the fact that the systematic offsets are smaller than the assumed vertical uncertainty of the DEMs of ± 0.15 m, no corrections have been applied to ALS data.

The quality of the GPR data analysis depends strongly on the amount of additional information. While stochastic uncertainties are due to the vertical resolution of the used GPR frequency, systematic errors and stochastic uncertainties result from velocity assumptions and the non-automated analysis of the GPR data. In a snowpack, ϵ_r' is a function of the mixing ratio between ice, air and liquid water (e.g. Lundberg et al., 2006). However, the proportion of liquid water in a wet snowpack can alter ϵ_r' and hence the signal velocity in a significant way (Frolov and Macheret, 1999; Sundström et al., 2012). Snow depths calculated from GPR data (h_v, Eq. 9) and slope corrected snow depths (h_{cor}, Eq. 4) from snow probings were compared to validate the used GPR velocities. On Vernagtferner 95 snow probings show a mean

offset of $+0.08$ m with a standard deviation of 0.13 m, accounting for lower snow depths calculated from GPR data. This can be related to the usage of a snowmobile for GPR measurements. While GPR data were recorded in the track of the snowmobile, snow depth probings were performed beside the snowmobile in the undisturbed snow. On Hintereisferner and Kesselwandferner in 2012, the comparison of snow depths calculated from GPR measurements and snow depth probings show a mean difference of 0.01 m with a standard deviation of 0.13 m.

5.5 Consequence for ALS snow cover studies on glaciers

For most of the ice areas of the four investigated glaciers differences between Δz_{ALS} and observed "ground truth" snow depths are less than the assumed uncertainties of the applied methods. The corresponding relative differences are less than 15 % for a mean snow depth of 1.5 m, decreasing with increasing snow depths. This is considerably less than the relative errors of measurements of solid precipitation, which may be up to 50 % when using rain gauges in high mountain catchments (Sevruk, 1985). In contrast, rain gauge measurements have the advantage of a high temporal resolution in comparison to ALS surveys. Hence the combination of both, ALS data for total volume and spatial distribution of the snow cover and rain gauge data for the timing of precipitation events, ensure a high potential for simulating the seasonal hydrology of mountain catchments more realistically.

Typical accumulation areas have to be considered when relating Δz_{ALS} to snow depth. For these areas, Δz_{ALS} has to be considered as a minimum snow depth value, as deviations to h_{GPR} appear to be systematic. However, at the end of ablation seasons, recent firn areas cover considerably smaller parts of the investigated glaciers than bare ice areas. Accumulation-area ratios (AAR) derived from LSC are 0.14 for Vernagtferner, 0.15 for Hintereisferner and 0.41 for Kesselwandferner. Mean Δh_{abs} of -0.4 m on average corresponds to a
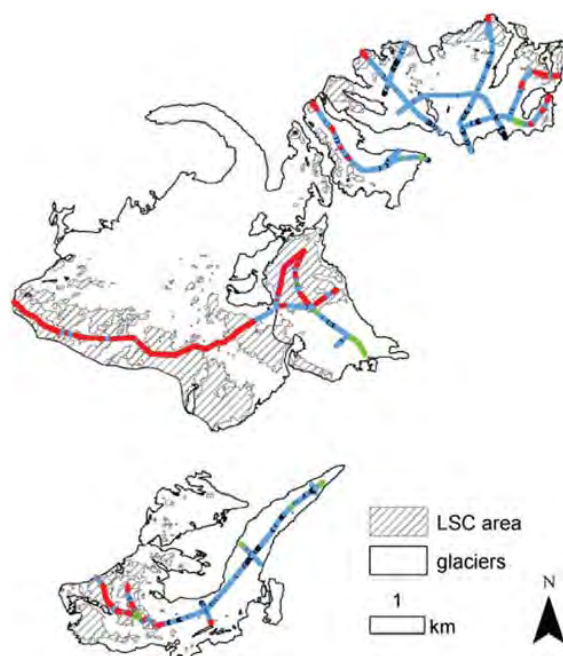
Fig. 13. Results of similarity between Δz_{ALS} and h_{GPR} applying a Mann–Whitney–Wilcoxon test (level of significance $p = 0.05$) and the comparison of Δh_{abs} (Eq. 11) to uncertainties of the two methods: ALS and GPR (Eq. 12) are given. Each midpoint of a window including $n = 300$ samples is coloured indicating not significant Δh_{abs} (black), significant Δh_{abs} (blue), significant and negative Δh_{abs} larger than uncertainty (red) and significant and positive Δh_{abs} larger than uncertainty (green). The outlines of the investigated glaciers (black) and the snow cover derived from Landsat image of 31 August 2009 (LSC, striped) are shown.

mean relative underestimation of approx. 20 % for the investigated LSC areas. Regarding the whole investigated glacierized areas, this systematic underestimation results in a mean relative error of 3 to 7 % for the respective glaciers. Hence, the information on snow depths from Δz_{ALS} is supposed to be a more reliable measurement not only of the spatial distribution of snow depths, but also for total volume of the snow cover in the investigated glacierized region at the time of the snow-on ALS survey (t_2).

In addition ablation in fall or already prevailing seasonal accumulation before the ALS survey at t_1 influence the accuracy of the derived ALS-derived snow depths on glacier surfaces. Furthermore, in contrast to non-glaciated areas, the ALS survey for t_1 has to be repeated annually, because glacier surface elevation varies annually. To calculate SWE from Δz_{ALS}, additional assumptions on the relation of snow density on snow depth (e.g. Jonas et al., 2009) or a spatially uniform snow density (e.g. Lehning et al., 2011) have to be made. This results in additional uncertainties of the derived

accumulation based on the conversion used and the prevailing conditions of the snowpack.

The data presented in this study were analyzed for differences between Δz_{ALS} and actual snow depths, because recently an increased number of research projects using ALS data to investigate the spatial and temporal variability of the cryosphere are conducted in the mountain range of Ötztal Alps. The results may be transferable in the study region and to Alpine glaciers of similar size and with similar mass turnover. Nevertheless, various process parameters contributing to Δz_{ALS} (Sect. 1) have to be considered, for example, on larger or steeper glaciers, on glaciers with faster ice flow, on glaciers gaining more accumulation or on glaciers with a less distinctive seasonal cycle of ablation and accumulation period.

In difficult mountain terrain, the acquisition of actual snow depths by GPR along profiles delivers less information on spatial snow distribution compared to ALS surveys covering total mountain catchments. However, systematic differences between Δz_{ALS} and actual snow depths have to be analyzed separately for individual glaciers when using ALS for recording snow depths even in glacierized catchments. This study demonstrated that the usage of ALS data and GPR measurements appears to be a promising combination of methods to identify differences of Δz_{ALS} from actual snow depths and corresponding uncertainties not only for single points, but along profiles on glacier surfaces worldwide.

6   Conclusions

The study presented here was accomplished to evaluate surface elevation changes derived from airborne laser scanning (Δz_{ALS}) on glacier surfaces for snow cover studies in the Ötztal Alps. Therefore, differences of Δz_{ALS} from snow depths calculated from more than 35 km of GPR profiles (h_{GPR}) on the four glaciers Hintereisferner, Kesselwandferner, Vernagtferner and Gepatschferner were analyzed. It is shown that GPR can be applied to validate Δz_{ALS} regarding snow depths and be used to analyze systematic differences. The sum of all processes contributing to Δz_{ALS} in addition to seasonal snow depths on glacier surfaces could be detected by combining ALS and GPR data. A more extensive measurement set-up would be necessary for detailed analysis of the partitioning and magnitude of the individual processes causing these differences. The delineation of snow covered areas at the end of ablation season from Landsat imagery highlights areas of increased differences between Δz_{ALS} and "ground truth" snow depth derived from h_{GPR}, snow pits and snow probing. This study shows that on four different glaciers systematic differences between Δz_{ALS} and h_{GPR} greater than calculated uncertainties of the applied techniques were observable almost exclusively within the respective accumulation areas. Most of ice areas on the investigated glaciers do not show differences between Δz_{ALS} and

K. Helfricht et al.: Comparison of lidar and GPR on Alpine glacier surface   **55**

actual snow depths larger than the uncertainty of the used combination of measurements. Distinct overestimation of actual snow depths by Δz_{ALS} could be detected at the very front of the glacier tongues. In summary, relative differences of Δz_{ALS} from actual snow depths are small for analysis of the mountain snow cover in the study area and comparable glacierized catchments. Hence, spatial distributed snow depths derived from Δz_{ALS} at glacier surface provide an information on minimum snow depths which must be simulated by hydro-meteorological models, particularly in the higher elevated parts of the glaciers in this region.

References

Abermann, J., Schneider, H., and Lambrecht, A.: Analysis of surface elevation changes on Kesselwand glacier – comparison of different methods, Z. Gletsch.kd. Glazialgeol., 41, 147–167, 2007.

Abermann, J., Lambrecht, A., Fischer, A., and Kuhn, M.: Quantifying changes and trends in glacier area and volume in the Austrian Ötztal Alps (1969–1997–2006), The Cryosphere, 3, 205–215, doi:10.5194/tc-3-205-2009, 2009.

Abermann, J., Fischer, A., Lambrecht, A., and Geist, T.: On the potential of very high-resolution repeat DEMs in glacial and periglacial environments, The Cryosphere, 4, 53–65, doi:10.5194/tc-4-53-2010, 2010.

Ambach, W. and Eisner, H.: Analysis of a 20 m firn pit on the Kesselwandferner (Ötztal Alps), J. Glaciol., 6, 223–231, 1966.

Aschwanden, H., Weingartner, R., and Leibundgut, C.: Zur regionalen Übertragung von Mittelwerten des Abflusses – Teil 1: Raumtypisierung der Abflussregime der Schweiz, Dtsch. gewässerkdl. Mitt. , 30, 52–61, 1986.

Baltsavias, E.: Airborne laser scanning: basic relations and formulas, ISPRS J. Photogramm. and Remote Sens., 54, 199–214, doi:10.1016/S0924-2716(99)00015-5, 1999.

Blöschl, G.: Scaling issues in snow hydrology, Hydrol. Process., 13, 2149–2175, doi:10.1002/(SICI)1099-1085(199910)13:14/15<2149::AID-HYP847>3.0.CO;2-8, 1999.

Bollmann, E., Sailer, R., Briese, C., Stötter, J., and Fritzmann, P.: Potential of airborne laser scanning for geomorphologic feature and process detection and quantifications in high alpine mountains, Z. Geomorphol. Supp., 55, 83–104, doi:10.1127/0372-8854/2011/0055S2-0047, 2011.

Cogley, J., Hock, R., Rasmussen, L., Arendt, A., Bauder, A., Braithwaite, R., Jansson, P., Kaser, G., Möller, M., Nicholson, L., and Zemp, M.: Glossary of Glacier Mass Balance and Related Terms, Tech. Rep., IHP-VII Technical Documents in Hydrology No. 86, IACS Contribution No. 2, UNESCO-IHP, Paris, 2011.

Cuffey, K. and Paterson, W.: The Physics of Glaciers, Academic Press, 4th Ed., 2010.

Dadic, R., Mott, R., Lehning, M., and Burlando, P.: Wind influence on snow depth distribution and accumulation over glaciers, J. Geophys. Res., 115, F01012, doi:10.1029/2009JF001261, 2010.

Daniels, D.: Ground Penetrating Radar, The Institution of Electrical Engineers, London, UK, 2nd Ed., 2004.

Deems, J., Paintner, T., and Finnegan, D.: Lidar measurement of snow depth: a review, J. Glaciol., 59, 467–479, doi:10.3189/2013JoG12J154, 2013.

Deems, J. S., Fassnacht, S. R., and Elder, K. J.: Interannual consistency in fractal snow depth patterns at two Colorado mountain sites, J. Hydrometeorol., 9, 977–988, doi:10.1175/2008JHM901.1, 2008.

Escher-Vetter, H., Kuhn, M., and Weber, M.: Four decades of winter mass balance of Vernagtferner and Hintereisferner, Austria: methodology and results, Ann. Glaciol., 50, 87–95, doi:10.3189/172756409787769672, 2009.

Fierz, C., Armstrong, R., Durand, Y., Etchevers, P., Greene, E., McClung, D., Nishimura, K., Satyawali, P., and Sokratov, S.: The International Classification for Seasonal Snow on the Ground, Tech. Rep., IHP-VII Technical Documents in Hydrology No. 83, IACS Contribution No. 1, UNESCO-IHP, Paris, 2009.

Fischer, A.: Glaciers and climate change: Interpretation of 50 years of direct mass balance of Hintereisferner, Global Planet. Change, 71, 13–26, doi:10.1016/j.gloplacha.2009.11.014, 2010.

Fischer, A.: Comparison of direct and geodetic mass balances on a multi-annual time scale, The Cryosphere, 5, 107–124, doi:10.5194/tc-5-107-2011, 2011.

Fischer, A., Span, N., Fischer, A., Kuhn, M., Massimo, M., and Butschek, M.: Radarmessungen der Eisdicke Österreichischer Gletscher. Band II: Messungen 1999 bis 2006, Österreichische Beiträge zu Meteorologie und Geophysik, 39, 142 pp., 2007.

Fischer, A., Markl, G., Kuhn, M., Schneider, H., and Abermann, J.: Glacier Mass Balance of Kesselwandferner, Ötztal Alps, Austria, from 1952/53–2009/11, World Data Center for Climate, doi:10.1594/WDCC/MB_KWF_1953-2011, 2011.

Fischer, A., Markl, G., and Kuhn, M.: Glacier Mass Balance of Hintereisferner, Ötztal Alps, Austria, from 1952/53–2010/11, doi:10.1594/WDCC/MB_HEF_1953-2011, 2012.

Frolov, A. D. and Macheret, Y. Y.: On dielectric properties of dry and wet snow, Hydrol. Process., 13, 1755–1760, doi:10.1002/(SICI)1099-1085(199909)13:12/13<1755::AID-HYP854>3.0.CO;2-T, 1999.

Geist, T. and Stötter, J.: Documentation of glacier surface elevation change with multi-temporal airborne laser scanner data – case study: Hintereisferner and Kesselwandferner, Tyrol, Austria, Z. Gletsch.kd. Glazialgeol., 41, 77 – 106, 2007.

Grünewald, T. and Lehning, M.: Altitudinal dependency of snow amounts in two small alpine catchments: can catchment-wide snow amounts be estimated via single snow or precipitation stations?, Ann. Glaciol., 52, 153–158, doi:10.3189/172756411797252248, 2011.

Haberkorn, A.: Assessing the contribution of basal melt processes to the local mass balance at the tongue of Hintereisferner, Ötztal, Austria, Master's thesis, Institute of Meteorology and Geophysics, University of Innsbruck, http://imgi.uibk.ac.at/sites/default/files/migration/thesisAnnaHaberkorn.pdf, 2011.

Hall, D. K., Ormsby, J. P., Bindschadler, R. A., and Siddalingaiah, H.: Characterization of snow and ice reflectance zones on glaciers using Landsat thematic mapper data, Ann. Glaciol., 9, 104–108, 1987.

Hall, D. K., Riggs, G. A., Salomonson, V. V., DiGirolamo, N. E., and Bayr, K. J.: MODIS snow-cover products, Remote Sens. Environ., 83, 181–194, doi:10.1016/S0034-4257(02)00095-0, 2002.

Heilig, A., Schneebeli, M., and Eisen, O.: Upward-looking ground-penetrating radar for monitoring snowpack stratigraphy, Cold Reg. Sci. Technol., 59, 152–162, doi:10.1016/j.coldregions.2009.07.008, 2009.

Helfricht, K., Schöber, J., Seiser, B., Fischer, A., Stötter, J., and Kuhn, M.: Snow accumulation of a high alpine catchment derived from LiDAR measurements, Adv. Geosci., 32, 31–39, doi:10.5194/adgeo-32-31-2012, 2012.

Hinkel, K. M., Doolittle, J. A., Bockheim, J. G., Nelson, F. E., Paetzold, R., Kimble, J. M., and Travis, R.: Detection of subsurface permafrost features with ground-penetrating radar, Barrow, Alaska, Permafrost Periglac., 12, 179–190, doi:10.1002/ppp.369, 2001.

Hoinkes, H.: Methoden und Möglichkeiten von Massenhaushaltsstudien auf Gletschern, Z. Gletsch.kd. Glazialgeol., 6, 37–90, 1970.

Huss, M., Farinotti, D., Bauder, A., and Funk, M.: Modelling runoff from highly glacierized alpine drainage basins in a changing climate, Hydrol. Process., 22, 3888–3902, doi:10.1002/hyp.7055, 2008.

Huss, M., Bauder, A., and Funk, M.: Homogenization of long-term mass-balance time series, Ann. Glaciol., 50, 198–206, doi:10.3189/172756409787769627, 2009.

Joerg, P. C., Morsdorf, F., and Zemp, M.: Uncertainty assessment of multi-temporal airborne laser scanning data: A case study on an Alpine glacier, Remote Sens. Environ., 127, 118–129, doi:10.1016/j.rse.2012.08.012, 2012.

Jonas, T., Marty, C., and Magnusson, J.: Estimating the snow water equivalent from snow depth measurements in the Swiss Alps, J. Hydrol., 378, 161–167, doi:10.1016/j.jhydrol.2009.09.021, 2009.

Kaser, G., Fountain, A., and Jansson, P.: A manual for monitoring the mass balance of mountain glaciers, International Hydrological Programme (IHP-VI. Technical Documents in Hydrology 59), UNESCO, Paris, 2003.

Kirnbauer, R., Achleitner, S., Schöber, J., Asztalos, J., and Schönlaub, H.: Hochwasservorhersage Inn: Modellierung der Gletscherabflüsse, Mitteilungsblatt des Hydrographischen Dienstes in Österreich, Nr. 86, 109–130, 2009.

Koblet, T., Gärtner-Roer, I., Zemp, M., Jansson, P., Thee, P., Haeberli, W., and Holmlund, P.: Reanalysis of multi-temporal aerial images of Storglaciären, Sweden (1959–99) – Part 1: Determination of length, area, and volume changes, The Cryosphere, 4, 333–343, doi:10.5194/tc-4-333-2010, 2010.

Kovacs, A., Gow, A. J., and Morey, R. M.: The in-situ dielectric constant of polar firn revisited, Cold Reg. Sci. Technol., 23, 245–256, doi:10.1016/0165-232X(94)00016-Q, 1995.

Kraus, K.: Geometrische Informationen aus Photographien und Laserscanaufnahmen, Band 1, Walter de Gruyter, Berlin – New York, 2004.

Kuhn, M.: Verification of a hydrometeorological model of glacierized basins, Ann. Glaciol., 31, 15–18, doi:10.3189/172756400781820228, 2000.

Kuhn, M.: Redistribution of snow and glacier mass balance from a hydrometeorological model, J. Hydrol., 282, 95–103, doi:10.1016/S0022-1694(03)00256-7, 2003.

Kuhn, M. and Batlogg, N.: Glacier runoff in Alpine headwaters in a changing climate, Hydrology, Water Resources and Ecology in Headwaters (Proceedings of the HeadWater'98 Conference held at Meran/Merano, Italy, April 1998), IAHS Publication, 248, 79–88, 1998.

Kuhn, M., Dreiseitl, E., Hofinger, S., Markl, G., Span, N., and Kaser, G.: Measurements and models of the mass balance of Hintereisferner, Geogr. Ann. A, 81, 659–670, doi:10.1111/1468-0459.00094, 1999.

Lehning, M., Grünewald, T., and Schirmer, M.: Mountain snow distribution governed by an altitudinal gradient and terrain roughness, Geophys. Res. Lett., 38, L19504, doi:10.1029/2011GL048927, 2011.

Lui, X.: Airborne LiDAR for DEM generation: some critical issues, Prog. Phys. Geog., 32, 31–49, doi:10.1177/0309133308089496, 2008.

Lundberg, A., Thunehed, H., and Bergström, J.: Impulse Radar Snow Surveys – Influence of Snow Density, Nord. Hydrol., 3, 1–14, 2000.

Lundberg, A., Richardson-Näslund, C., and Andersson, C.: Snow density variations: consequences for ground-penetrating radar, Hydrol. Process., 20, 1483–1495, doi:10.1002/hyp.5944, 2006.

Lundberg, A., Granlund, N., and Gustafsson, D.: Towards automated "Ground truth" snow measurements: a review of operational and new measurement methods for Sweden, Norway, and Finland, Hydrol. Process., 24, 1955–1970, doi:10.1002/hyp.7658, 2010.

Machguth, H., Eisen, O., Paul, F., and Hoelzle, M.: Strong spatial variability of accumulation observed with helicopter-borne GPR on two adjacent Alpine glaciers, Geophys. Res. Lett., 33, L13503, doi:10.1029/2006GL026576, 2006.

Mayer, C., Lambrecht, A., Blumthaler, U., and Eisen, O.: Vermessung und Eisdynamik des Vernagtferners, Ötztaler Alpen, Z. Gletsch.kd. Glazialgeol., 45–46, 259–280, 2013.

Melvold, K. and Skaugen, T.: Multiscale spatial variability of lidar-derived and modeled snow depth on Hardangervidda, Norway, Ann. Glaciol., 54, 273–281, doi:10.3189/2013AoG62A161, 2013.

Mitterer, C., Heilig, A., Schweizer, J., and Eisen, O.: Upward-looking ground-penetrating radar for measuring wet-snow properties, Cold Reg. Sci. Technol., 69, 129–138, doi:10.1016/j.coldregions.2011.06.003, 2011.

Murray, T., Gooch, D., and Stuart, G.: Structures within the surge front at Bakaninbreen, Svalbard, using ground-penetrating radar, Ann. Glaciol. 24, 122–129, 1997.

Nolin, A. W.: Recent advances in remote sensing of seasonal snow, J. Glaciol., 56, 1141–1150, doi:10.3189/002214311796406077, 2011.

Otto, J.-C., Keuschnig, M., Götz, J., Marbach, M., and Schrott, L.: Detection of mountain permafrost by combining high resolution surface and subsurface information: an example from the Glatzbach Catchment, Austrian Alps, Geogr. Ann. A, 94, 43–57, doi:10.1111/j.1468-0459.2012.00455.x, 2012.

Rott, H. and Markl, G.: Improved snow and glacier monitoring by Landsat Thematic Mapper, in: Proceedings of Workshop on Earthnet Pilot Projects on Landsat Thematic Mapper Applications, 3–12, ESA SP-1102, 1989.

Schöber, J., Achleitner, S., Kirnbauer, R., Schöberl, F., and Schönlaub, H.: Hydrological modelling of glacierized catchments focussing on the validation of simulated snow patterns – applications within the flood forecasting system of the Tyrolean river Inn, Adv. Geosci., 27, 99–109, doi:10.5194/adgeo-27-99-2010, 2010.

Sevruk, B.: Correction of precipitation measurements: Swiss experience, WMO/TD, 104, 187–196, 1985.

Sold, L., Huss, M., Hoelzle, M., Andereggen, H., Joerg, P. C., and Zemp, M.: Methodological approaches to infer end-of-winter snow distribution on alpine glaciers, J. Glaciol., 59, 1047–1059, doi:10.3189/2013JoG13J015, 2013.

Span, N. and Kuhn, M.: Simulating annual glacier flow with a linear reservoir model, J. Geophys. Res.-Atmos., 108, 4313, doi:10.1029/2002JD002828, 2003.

Span, N., Kuhn, M., and Schneider, H.: 100 years of ice dynamics of Hintereisferner, Central Alps, Austria, 1894–1994, Ann. Glaciol., 24, 297–302, 1997.

Span, N., Fischer, A., Kuhn, M., Massimo, M., and Butschek, M.: Radarmessungen der Eisdicke Österreichischer Gletscher. Band I: Messungen 1995 bis 1998, Österreichische Beiträge zu Meteorologie und Geophysik, 33, 145 pp., 2005.

Spikes, V. B., Hamilton, G. S., Arcone, S. A., Kaspari, S., and Mayewski, P. A.: Variability in accumulation rates from GPR profiling on the West Antarctic plateau, Ann. Glaciol., 39, 238–244, doi:10.3189/172756404781814393, 2004.

Sundström, N., Kruglyak, A., and Friborg, J.: Modeling and simulation of GPR wave propagation through wet snowpacks: Testing the sensitivity of a method for snow water equivalent estimation, Cold Reg. Sci. Technol., 74–5, 11–20, doi:10.1016/j.coldregions.2012.01.006, 2012.

Trabant, P.: Applied high resolution geophysical methods: Offshore geoengineering hazards, IHRDC Press, Boston, MA, IHRDC Press, 137 Newbury Street, Boston, MA 02116, 1984.

Wehr, A. and Lohr, U.: Airborne laser scanning – an introduction and overview, ISPRS J. Photogramm. Remote Sens., 54, 68–82, doi:10.1016/S0924-2716(99)00011-8, 1999.

Weingartner, R., Barben, M., and Spreafico, M.: Floods in mountain areas – an overview based on examples from Switzerland, J. Hydrol., 282, 10–24, doi:10.1016/S0022-1694(03)00249-X, 2003.

Chapter 4

Paper III - Inter-annual persistence of the seasonal snow cover

1

Inter-annual persistence of the seasonal snow cover in a glacierized catchment

Kay HELFRICHT,[1,2] Johannes Schöber,[3] Katrin Schneider,[1] Rudolf Sailer,[1,4]
Michael Kuhn[2]

[1]*alpS - Centre for Climate Change Adaptation, Grabenweg 68, Innsbruck, Austria*
E-mail:kay.helfricht@oeaw.ac.at
[2]*Institute of Meteorology and Geophysics, University of Innsbruck, Austria*
[3]*TIWAG Tiroler Wasserkraft AG, Innsbruck, Austria*
[4]*Institute of Geography, University of Innsbruck, Austria*

ABSTRACT. Knowledge of the spatial snow distribution and its inter-annual persistence is of interest for a broad spectrum of issues in cryospheric sciences. In this study, snow depths derived from airborne laser scanning are analyzed for inter-annual persistence of the seasonal snow cover in a partly glacierized mountain area (approx. $36\,\mathrm{km}^2$). At the end of five accumulation periods, the snow-covered area varied by **16 %** of its temporal mean. Mean snow depth of the total area ranged by a factor of two from $1.31\,\mathrm{m}$ to $2.58\,\mathrm{m}$, with a standard deviation of $0.42\,\mathrm{m}$. Inter-annual correlation coefficients of snow depth distribution ranged between **0.68** and **0.84**. **75 %** of the investigated area turned out to be inter-annually persistent. The remaining area showed a variable snow cover from year-to-year caused by occasional avalanches and changes in surface topography as a result of glacier retreat. Snow cover underwent a change from homogeneous distribution on the former glacier surface to a more heterogeneous snow cover in the recently deglaciated terrain. A geostatistical analysis shows inter-annual persistence in scaling behavior of snow depth in ice-free terrain with scale break distances at $20\,\mathrm{m}$. Scale invariant behavior of snow depth is indicated over more than $100\,\mathrm{m}$ on smooth glacier surfaces.

1. INTRODUCTION

The spatial distribution of the mountain snow cover is of interest in cryospheric science for issues like modeling mass balance of glaciers (e.g., Huss and others, 2008; Dadic and others, 2010b), determining the snow cover duration for ecological investigations (e.g., Tappeiner and others, 2001), identifying risks of natural hazards (e.g., Schweizer and others, 2008) and simulating the runoff regime of mountain catchments (e.g., Lundquist and Dettinger, 2005; Schöber and others, 2010; Bavay and others, 2013). The spatial variability of snow depths is recognized as a challenging feature, especially regarding scaling issues and the simulation of the fundamental processes causing the heterogeneity of snow (e.g., Pomeroy and others, 1998; Blöschl, 1999; Deems and others, 2006, 2008; Trujillo and others, 2007; Grünewald and others, 2013). Since simulations of mountain hydrology require not only runoff measurements but also ground-truth data of the snow cover for validation (e.g., Blöschl and others, 1991; Matthias and others, 2014), snow cover distribution is measured using in-situ measurements (e.g., Elder and others, 1991; Kaser and others, 2003; Lundberg and Gustafsson, 2010) and remote sensing techniques (e.g., Nolin, 2011; Rittger and others, 2013). Point information from weather stations or snow depth measurements are used to interpolate and extrapolate the mountain snow cover to the catchment scale for snow-hydrological studies (e.g., Blöschl and others, 1991; Anderton and others, 2004). Still, the representativeness of individual measurements is uncertain (Sevruk, 1985; Grünewald and Lehning, 2011). The active remote sensing technique of lidar (light detection and ranging) (e.g., Baltsavias, 1999; Wehr and Lohr, 1999) is a useful tool to obtain spatially distributed snow depth data in a high spatial resolution from repeated surveys (Deems and others, 2013). Lidar was applied to derive snow depths in test areas (e.g., Hopkinson and others, 2001; Deems and others, 2006, 2008), on individual mountain slopes (e.g., Prokop and others, 2008; Schaffhauser and others, 2008; Sailer and others, 2008; Grünewald and others, 2010; Schirmer and others, 2011), for individual glaciers (e.g., Joerg and others, 2006; Geist and Stötter, 2007; Sold and others, 2013; Helfricht and others, 2014) and entire mountain catchments (e.g., Dadic and others, 2010b; Helfricht and others, 2012; Grünewald and others, 2013; Schöber and others, 2014). However, multi-annual data of spatial snow depth distribution,i.e. the total volume of the snow cover in entire catchments, are rare.

Inter-annual persistence of the spatial snow distribution is a prerequisite for applying simple parameterizations of snow redistribution in hydro-meteorological models simulating the snow cover of high mountain catchments (e.g., Huss and others, 2008; Strasser, 2008; Mott and others, 2010; Dadic and others, 2010a; Schöber and others, 2014). Up to now, long-term observations of spatially distributed snow depths have been based on manually taken snow depth samples (Sturm and Wagner, 2010; Jepsen and others, 2012; Winstral and Marks, 2014). Sturm and Wagner (2010) showed that climatological snow patterns derived from multi-annually measured snow depth distributions are suitable for simulating the snow depth distribution. In Alpine mountain catchments, spatial snow distribution is attributed to preferential deposition of snow and the subsequent wind-induced snow transport processes acting on various scales (e.g., Lehning and others, 2008; Dadic and others, 2010b; Mott and others, 2010). Mott and

others (2011b) suggest that still model resolution of 5 m is not sufficient to capture all processes that drive snow cover variability in areas of complex Alpine topography.

Geostatistical analyses are a basis for the spatial design of measurements of snow depth and snow cover models (Blöschl, 1999). Snow cover presents a multi-scaling behavior (e.g., Shook and Gray, 1996; Deems and others, 2008; Schirmer and Lehning, 2011) with a short-range fractal and a long range fractal separated by a scale break. Typical scale breaks of snow depths were observed between meters and tens of meter, both for manually taken snow samples (e.g., Shook and Gray, 1996) and snow depths derived from lidar data (Deems and others, 2006, 2008; Trujillo and others, 2007; Schirmer and Lehning, 2011). The fractal (Hausdorff-Besicovich) dimension was found to be useful for analyzing the irregularity of objects and surfaces (Burrough, 1993; Gao, 1996). The fractal dimension allows differentiating the influence of short-range fluctuations caused by e.g. snow surface structures, sastrugi and cornices from long range fluctuations related to topography on snow cover variability (e.g., Schirmer and Lehning, 2011). Detailed analyses of multi-annual consistency in scaling behavior based on high resolution lidar data are limited to the comparison of two accumulation seasons. Schirmer and Lehning (2011) and Deems and others (2008) indicate an inter-annual consistency of fractal dimensions and scale breaks of snow depths at the end of the accumulation season. Schirmer and Lehning (2011) showed that the scale breaks increase while short-range fractal dimensions decrease due to smoothing of the surface by snow accumulation associated with northwesterly storms towards the end of the accumulation season.

In this study, a unique multi-year data set of snow depths is introduced which is derived from airborne laser scanning (ALS) surveys of the seasonal snow cover in a partly glacierized mountain catchment of approx. 36 km^2. The detailed snow depth data allows combining the advantages of high spatial resolution and multi-annual data. The study aims to investigate the temporal and spatial inter-annual persistence of seasonal snow depths, snow patterns and scaling behavior of the snow cover.

Annual mean snow depths and their spatial variability are determined to compare the overall temporal persistence of snow accumulation in the investigated basin. Correlations coefficients between each of the annual snow depth distributions are calculated at spatial resolutions of 1 to 100 m. This allows us to differentiate between processes causing high inter-annual variability even at coarser resolutions and the increasing correlation with decreasing resolution as a result of a reduction of the spatial variability of snow depth (e.g., Blöschl, 1999; Melvold and Skaugen, 2013). Areas with persistent snow cover are distinguished from areas with variable snow cover by analyzing the temporal variability in standardized snow depths. Maps of squared errors of standardized snow depths are shown to locate processes causing inter-annual differences in snow patterns. A k-means clustering is used to detect areas of similar spatial and temporal characteristic of the residuals of snow depths from mean snow depth in their vicinity. Finally, the inter-annual variability in fractal dimensions and scale breaks of the snow depth distribution is derived from a semivariance analysis.

The results will help to emphasize the main characteristics of the snow depth distribution in this Alpine catchment and support simulations of the snow cover in this mountain region and comparable mountain basins.

2. STUDY SITE AND DATA

The investigated area is located at the main Alpine ridge in the Ötztal Alps, Austria (46°48′ N, 10°46′ E). It covers a partly glacierized catchment of the Upper Rofen valley (Fig. 1). The total area is 35.9 km^2, from which 50 % were glacierized in 2001 and 44 % in 2011. This equals a loss in glacier area of 12 % in ten years. The elevation within the study area ranges from 2234 m a.s.l. to 3738 m a.s.l. The mean elevation of the investigated area is 3005 m a.s.l.. Aspect is predominantly southeast at elevations below 2500 m a.s.l. (Fig. 1). Most slopes face southeast and northwest at elevations between 2500 and 3500 m a.s.l. Aspects from southwest to west are in general less frequent. Most of the area below 3000 m a.s.l. has a slope angle of 20 ° to 40 °. Between 3000 m a.s.l. and 3500 m a.s.l., glacier surface with a slope of less than 30 ° is most frequent. The glaciers Hintereisferner (HEF) and Kesselwandferner (KWF) are located in the investigated area. Both glaciers have been monitored for decades (Hoinkes, 1970; Kuhn and others, 1999; Fischer, 2010; Fischer and others, 2012). The upper parts of the glaciers Gepatschferner (GPF) and Langtauferer Ferner (LF) are partly included in the investigated area. Since 2001, annual ALS flights have been conducted in this mountain area, from which annual glacier volume changes (Geist and others, 2005; Bollmann, 2010) and intra-annual surface elevation changes (Geist and Stötter, 2007) were calculated. For this study, glacier outlines were derived separately for the date of ALS ($t1$) according to Abermann and others (2010). Available ALS data cover five accumulation seasons between 2001 and 2012.

Table 1 shows the dates of the ALS surveys, the devices used, maximum scan angles, laser repetition rates, used scan frequencies and assessments of the vertical accuracy since 2002. Vertical accuracy was derived by comparing ALS data to a flat and snow free reference surface down the valley nearby the study area. Mean deviation between actual altitude of the reference surface and the z-value of the lidar points had a maximum of 0.076 m and a maximum standard deviation of 0.11 m (Tab. 1). Point densities increase over time due to the improvement of the used scanner devices. Mean flight speed was between 65 m s^{-1} and 70 m s^{-1}. Mean flight altitude ranged from 1000 m to 1200 m above ground.

Point clouds were filtered to bare ground using last returns of the laser signal. All points within a grid cell were averaged to generate DEMs with a grid size of 1 m,. Grid cells without lidar point measurements were filled using inverse distance weighting. Due to the high number of measured points and the location of the investigation area above the tree line, simple interpolation schemes deliver high accuracy DEMs (Deems and others, 2013). Bollmann and others (2011) showed for DEMs produced in the Hintereisferner region that a relative vertical accuracy better than ±0.15 m for slopes below 35 ° can be estimated. The accuracy of the ALS measurements decreases considerably with increasing laser distance and decreasing illumination angle (Bollmann and others, 2011; Joerg and others, 2012). Early stage application of ALS measurements in 2002 might be influenced by higher uncertainties due to the lower point densities compared to the subsequent years (Bollmann and others, 2011; Fritzmann and others, 2011).

Two lidar surveys are required to extract seasonal snow depth from multi-temporal ALS data (e.g., Hopkinson and others, 2001; Deems and others, 2013). Data have to be recorded prior the accumulation season ('snow-off', here referred to
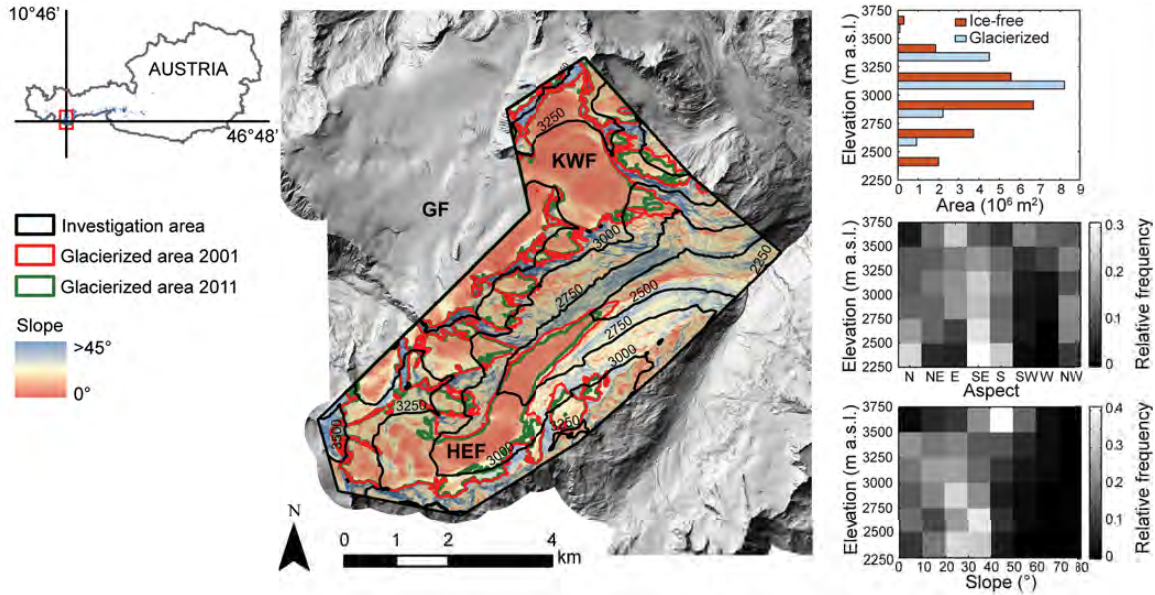
Fig. 1. Map of the investigated area including the glaciers Hintereisferner (HEF), Kesselwandferner (KWF) and the uppermost part of Gepatschferner (GF). The color scale shows the slope of the surface. Glacier outlines of the years 2001 (red) and 2011 (green) and contour-lines of elevation in 250 m steps (black) are presented. The area-elevation-distribution (upper right) and the frequency distribution of aspect (middle right) and slope (lower right) of 250 m elevation zones are shown.

date $t1$) and next to the time of the maximum of snow depth ('snow-on', here referred to date $t2$, Tab. 1). In mountain catchments with a high elevation range it is difficult to cover the date of the minimum and maximum accumulation exactly. While snow accumulates at higher elevations, ice and snow melt can occur at lower elevations simultaneously.

The densification of the fresh snow accumulated prior the ALS $(t1)$ causes underestimation of actual snow depths by lidar measurements. Snow ablation or ice ablation lower the surface between ALS $(t1)$ and the final formation of the seasonal snow cover and, thus, lead to underestimation of the actual snow depths as well. The densification of the firn cover and ice flow causes underestimation of the actual snow depths by lidar in typical accumulation areas of the glaciers (e.g., Sold and others, 2013; Helfricht and others, 2014). With respect to the glacierized study area, the dates of the ALS flights (Tab. 1) were chosen to be close to the typical dates of glacier mass balance measurements using the fixed date system according to Kaser and others (2003).

3. METEOROLOGICAL CONDITIONS

Meteorological measurements located in the investigation area do not cover the whole time period of this study. To give an overview on the weather conditions, temperature and precipitation measured at six weather stations next to investigated basin are spatially interpolated using an Inverse Distance Weighting algorithm for precipitation and a regression approach for temperature implemented in the pre-processing module of the flood forecasting system of the river Inn (Achleitner and others, 2012). The data are valid for an elevation of 2400 m a.s.l., which coincides with the lowest elevations of the investigated basin (Fig. 1). Mean daily temperatures and cumulative precipitation of all five accumulation seasons are shown in Fig. 2.

In September 2001, a snow cover was accumulated in the study area and persisted until the ALS $(t1)$ (e.g., Bollmann and others, 2011). The mean temperatures after the ALS $(t1)$ provided melt condition from the end of September to mid October. Only 30 % of the seasonal precipitation cumulated until the end of January. Snow was accumulated frequently in February and March 2002. A precipitation event caused a

Table 1. Overview of the ALS flight campaigns investigated in this study. The accuracy is obtained from deviations between ALS surface elevations and elevations of a known reference surface. Mean flight altitude was between 1000 m and 1200 m above ground.

| accumulation season	timestamp	date	laser system	maximum scan angle (°)	laser repetition rate ($10^3 s^{-1}$)	scan frequency (s^{-1})	beam divergence (mrad)	mean point density per m²	vertical accuracy (m) mean	σ
2002	t1	10 October 2001	Optech ALTM 1225	20	25	28	0.1	1.1	na	na
	t2	07 May 2002	Optech ALTM 1225	20	25	28	0.1	1.2	−0.040	0.110
2003	t1	18 September 2002	Optech ALTM 2050	20	50	40	0.2	1.0	−0.030	0.098
	t2	04 May 2003	Optech ALTM 2050	20	50	40	0.2	0.8	−0.020	0.092
2009	t1	09 September 2008	Optech ALTM 3100	20	70	40	0.3	2.2	0.002	0.057
	t2	07 May 2009	Optech ALTM 3100	20	70	38	0.3	2.4	0.040	0.054
2011	t1	08 October 2010	Optech ALTM Gemini	25	70	36	0.25	3.6	0.076	0.047
	t2	20 April 2011	Optech ALTM Gemini	25	70	36	0.25	3.8	−0.007	0.041
2012	t1	04 October 2011	Optech ALTM 3100	20	70	40	0.3	2.9	0.001	0.042
	t2	11 May 2012	Optech ALTM 3100	20	70	40	0.3	2.8	0.005	0.057
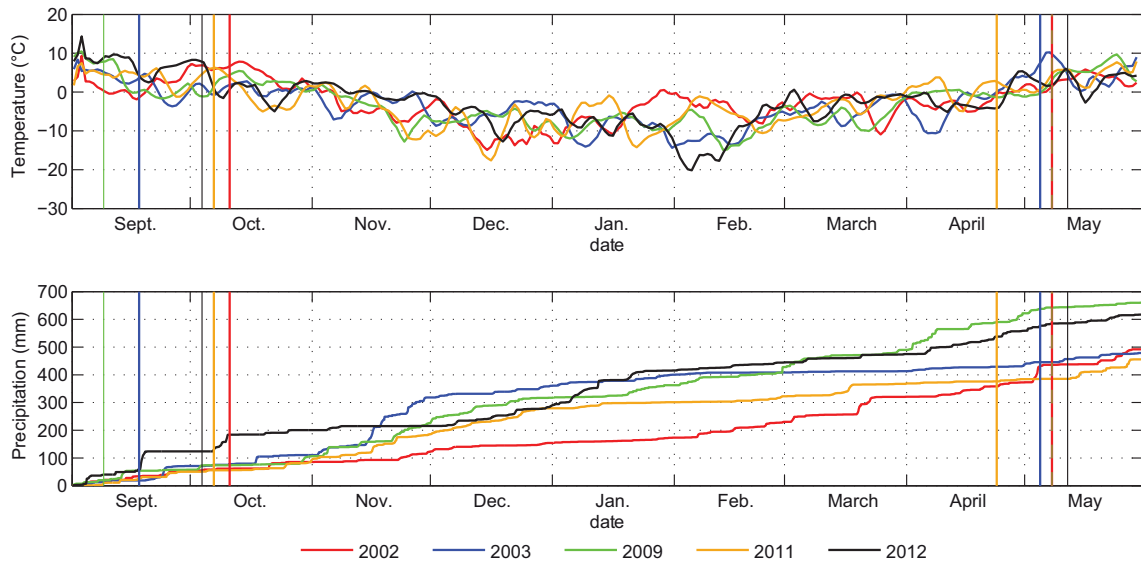
Fig. 2. Mean daily air temperatures valid for an elevation of 2400 m a.s.l. (top) and the cumulative precipitation (bottom) of the five accumulation seasons. Dates of the ALS surveys are shown as vertical lines. Note that $t2$ of 2002 and 2009 coincide on May 7.

distinct increase in snow depth a few days prior to ALS $(t2)$ 2002.

In 2002, ALS $(t1)$ was performed in mid September. Temperatures decreased to $0°$ C shortly after, indicating less melting of the ice or snow until the formation of the seasonal snow cover. While almost 50 % of the seasonal precipitation was accumulated in November, particularly the second half of this accumulation season continued with precipitation below average.

In 2008, mean daily temperatures were close to $0\,°C$ after ALS $(t1)$. In October 2008, a period of positive temperatures caused potential melt at the glacier tongues (Schöber and others, 2014). However, the highest cumulative precipitation amount of the five investigated accumulation seasons was measured in 2009 due to a steady occurrence of precipitation events preferentially in the second half of the accumulation season.

Snow was accumulated prior to ALS $(t1)$ in 2010 (Helfricht and others, 2014; Schöber and others, 2014). Until end of January 2011, cumulative precipitation amount was similar to 2009. Subsequently the accumulation season stayed dry. Positive temperatures enabled snow melt on several days prior to ALS $(t2)$ in April 2011.

Prior the ALS $(t1)$ in 2011, a snow cover was accumulated in mid September. However, this snow cover was distinctly reduced by melt until the date of ALS $(t1)$ (personal communication A. Fischer, 2012). A snow fall was recorded shortly after ALS $(t1)$ followed by almost dry conditions for two months. Higher accumulation rates were observed in December and January 2012.

Schöber and others (2014) discussed the influence of melt and sublimation during the two winter seasons 2009 and 2011 based on model simulations of the energy balance of the snow cover. Whereas melt and sublimation cumulate to 0.17 m of the surface elevation change between ALS $(t1)$ in 2008 and ALS $(t2)$ in 2009, same calculation resulted in a surface low-

ering by only 0.04 m between ALS $(t1)$ in 2010 and ALS $(t2)$ in 2011. Results for the accumulation periods 2002 and 2003 were found to be in between these values.

Table 2. Precipitation measured between 1.10. and 30.4. at the three cumulative precipitation gauges Hintereisferner (HEF), Proviantdepot (PD) and Rofenberg (RB). Winter precipitation measured in the investigated seasons are shown for each accumulation season separately. Minimum, mean and maximum values and the temporal CV are presented for the 30 year period between 1983 and 2012.

cum. gauges		HEF	RB	PD	
	elevation	2970	2827	2737	m a.s.l.
ALS	2002	627	521	396	mm
	2003	502	488	370	mm
	2009	998	793	622	mm
	2011	578	440	344	mm
	2012	696	604	441	mm
1983 - 2012	min	329	302	217	mm
	max	998	793	652	mm
	mean	632	526	410	mm
	CV	0.22	0.21	0.22	

Precipitation measured at three cumulative precipitation gauges located in the investigated catchment, namely Hintereisferner (HEF), Rofenberg (RB) and Proviantdepot (PD), allows comparing the variability in precipitation of the five investigated seasons to a climatic series. Precipitation measured at the gauges was summarized for the months October till April in the period between 1983 and 2012 (Tab. 2). The mean cumulative precipitation of the five investigated accumulation periods is slightly higher than mean cumulative precipitation of the 30 year period at all three gauges. The maximum of

winter precipitation measured in this catchment over the last 30 years in 2009 is included in the five investigated seasons. Cumulative winter precipitation was lower than the climatic mean in the season 2011, but within one standard deviation of the winter precipitation between 1983 and 2012. The temporal CV of measured winter precipitation was 0.22 for the 30 year period (Tab. 2).

4. METHODS OF SNOW COVER ANALYSES

4.1. Analysis of spatial and temporal distribution

Seasonal snow cover is analyzed based on digital elevation models (DEM) with a grid size of 1 m (Chap. 2). The surface elevation at ALS $(t1)$ is subtracted from the surface elevation at ALS $(t2)$ to calculate surface elevation changes (Δz_{ALS})

$$\Delta z_{ALS} = z_{t2} - z_{t1} \approx HS. \qquad (1)$$

Δz_{ALS} are interpreted as snow depth (HS). HS values in the range of $-10\,m \leq HS \leq 15\,m$ are used for the analysis. Negative HS which are an artifact of the measurement principle (Hopkinson and others, 2001), are not removed to maintain the original distribution of the ALS-derived information. The temporal variability of the mean annual snow depth $(\bar{HS})$ and its spatial variability in terms of the standard deviation (σ) and the corresponding coefficient of variation (CV) are analyzed. A threshold HS of 0.15 m is used to distinguish between snow-free and snow-covered area (SCA). According to the assumed relative vertical accuracy indicated by Bollmann and others (2011), this threshold accounts for the distribution of zero snow depths at $\pm 0.15\,m$, i.e. HS below 0.15 m can result from zero snow depth and an error of the DEMs. Areas of $HS < 0.15\,m$ are also assumed to feature a scattered snow cover. The inter-annual persistence of HS and SCA over altitude is analyzed in 25 m elevation zones.

Pearson correlation coefficients (r) of HS are calculated between each combination of the five HS distributions. HS are sampled to coarser grid sizes (10, 30, 50 and 100 m) using the area-weighted mean of the 1 m HS values. Variability is known to decrease with increase of spatial aggregation (e.g., Blöschl, 1999). The spatial scale of 10 m is chosen to reduce the noise of the original 1 m data without losing much information of snow cover variability. The spatial resolution of 30 m was used in studies of Sturm and Wagner (2010) and Winstral and Marks (2014), who analyzed manually sampled snow depth data. 50 m is a typical scale used for the simulation of the high mountain snow cover and mountain hydrology (e.g., Strasser, 2008; Schöber and others, 2014). Spatial scales of more than 100 m show a reduction in variability of high resolution snow depth data (e.g., Grünewald and others, 2013) and cause a distinct loss in information on spatial snow depth patterns (e.g., Melvold and Skaugen, 2013).

Spatially distributed standardized snow depths (HS_s) are calculated according to Sturm and Wagner (2010) for the inter-annual comparison of seasonal snow depths with

$$HS_s = \frac{HS - \bar{HS}}{\sigma_{HS}}, \qquad (2)$$

where σ_{HS} is the annual areal standard deviation of HS in one winter. Squared errors of HS_s (SE_s) are calculated for all possible combinations of two available snow depth distributions (*1* and *2*) with

$$SE_s = (HS_{s1} - HS_{s2})^2. \qquad (3)$$

The resulting maps of SE_s (10 in total) are used to identify regions of high inter-annual snow depth variability and areas of inter-annually persistent HS_s. Areal mean of the squared errors of standardized snow depths (MSE_s) are used as a metric of overall similarity of the snow depth distributions.

4.2. Residual analysis

Spatial snow cover variability is expressed by residuals of HS (r_{HS}) to their vicinity. We use a moving window approach to calculate the residual of each HS to the mean HS of its squared vicinity of 5 x 5 raster cells (Eq. 4)

$$r_{HS(x,y)} = HS(x,y) - \frac{\sum_{i=-2}^{2} \sum_{j=-2}^{2} HS(x+i, y+j)}{n}, \qquad (4)$$

where n is the number of cells of the window and i,j are the distances in x- and y-direction from the center. While a homogeneous snow cover is characterized by almost zero r_{HS}, a heterogeneous snow cover shows distinctly negative and positive values of r_{HS}. The magnitude of r_{HS} is controlled by spatial variations in the underlying topography and variability of the snow on its surface. r_{HS} are calculated in a raster resolution of 10 m within a 50 m square. Thus, the residual analysis covers the scale for which snow typically shows a high spatial auto-correlation (e.g., Shook and Gray, 1996; Deems and others, 2008; Schirmer and Lehning, 2011). We used a k-means clustering algorithm (Forgy, 1965; MacQueen, 1967; Hartigan and Wong, 1979) integrated in SAGA (System for Automated Geoscientific Analyses) to automatically group observations with similar characteristics in magnitude and temporal variability of r_{HS}. A set of approx. 36000 spatially distributed observations of r_{HS} is used. Each observation consists of a 5-dimensional vector representing r_{HS} values of the five years. This clustering method does not create spatial connected clusters as for example image segmentation algorithms. Rather, the high number of observations distributed over the entire basin are grouped into classes. We clustered the observations to a pre-set of 10 classes. Frequency distributions are calculated for annual r_{HS} of all observations grouped in each of the 10 classes. The advantage of the clustering of r_{HS} is the spatially distributed information on the temporal persistence of snow depths residuals to mean snow depth of their vicinity.

4.3. Geostatistical analysis

Geostatistical analyses are used in cryospheric sciences for scaling issues by e.g., Blöschl (1999); Shook and Gray (1996), to investigate topographic and wind control on spatial snow depth distribution and to analyze regional and temporal variability of fractal dimensions and typical scale breaks of the mountain snow cover (e.g., Deems and others, 2006, 2008; Trujillo and others, 2007; Lehning and others, 2011; Mott and others, 2011b; Schirmer and Lehning, 2011).

Experimental variograms are used to analyze the spatial autocorrelation of data pairs as a function of their separation distance h (Olea, 1999; Sun and others, 2006). The semivariance $\gamma(h_k)$ of HS is given for the mean lag distance h of the bin k as

$$\gamma(h_k) = \frac{1}{2n_k} \sum_{i=1}^{n_k} \{HS_i - HS_{i+h}\}^2, \qquad (5)$$

where HS are snow depth samples at locations i and $i + h$, and n_k is the number of data pairs in the bin k. The spatial characteristics of HS can be explored by the properties of the variogram - nugget, sill and range (Olea, 1999). The nugget indicates small-scale variability which has not been captured by the measurement. The sill is the overall variability ($\gamma(h_k)$) in the data set, i.e. the higher the sill, the higher is the spatial variability in the data. The distance between sampling points (range) from the increase in $\gamma(h_k)$ with increasing h changes considerably is called scale break distance L. In case of flattening of the increase in $\gamma(h_k)$ on a log-log plot, L marks the separation of the sampling points at which no more autocorrelation between data pairs exists.

The fractal (Hausdorff-Besicovich) dimension D was found to be useful to analyze the irregularity of objects and surfaces (Burrough, 1993; Gao, 1996). Nearly planar surfaces feature a D of 2, while a rugged surface filling the third dimension has a limiting D of 3.

Fractal dimensions are estimated from the slope of a power law fitted to the log-spaced data

$$\gamma(h_k) = \alpha \cdot h_k^{\beta}, \tag{6}$$

where α is the ordinal intercept and the power β is the slope of the linear fit in the log-transformed variogram. The fractal dimension D is calculated from β (Gao, 1996)

$$D = 3 - \frac{\beta}{2}. \tag{7}$$

The application and interpretation of geostatistics is strongly limited by the measurement scale and the sampling design. For example, if the spacing between the sampling points is large compared to the extent of the sampled area, the true variability in the data might not be captured. The high spatial resolution of the ALS data supports the applicability of the semivariance analysis. However, the results of L and D are highly influenced by the methods used. Sources of different estimates for scale breaks and fractal dimension are discussed in Xu and others (1993) and Sun and others (2006).

For this study, semivariance is calculated for HS in the entire ice-free terrain with respect to the largest glacier extent in 2001 (17.75 km^2), separately for HS on Hintereisferner (HEF, 6.99 km^2) and on Kesselwandferner (KWF, 3.65 km^2) and for HS on the remaining small glaciers (2.00 km^2). With respect to the results of other studies analyzing geostatistical properties of Alpine HS (e.g., Deems and others, 2008; Mott and others, 2011a; Schirmer and Lehning, 2011), scale breaks in the order of meters to tens of meters are expected. Thus, this length characteristic is considered calculating omni-directional variograms with 2 m grid spacing. The lag distance h is subdivided into 20 log-spaced bins for each power of ten. The maximum h is set to 200 m for ice-free terrain. With respect to the more homogeneous snow cover on glaciers, semivariance is calculated with a maximum h of 1000 m for small glaciers and of 3000 m for the two large glaciers HEF and KWF.

For ice-free terrain, a preliminary first break distance L_p is calculated automatically fitting an exponential function to h and using a threshold of 95% of $\gamma(h_k)$ (Webster and Margaret, 2007). This automatically fitted L is only used to separate the data of the used bins into a short-range set and a long range set. Power laws are fitted to the two data sets in the log-transformed variogram solving least squares to calculate the short-range fractal dimension D_s for $h \leq L_p$ and the long-range fractal dimension D_l for $h > L_p$. The intersection
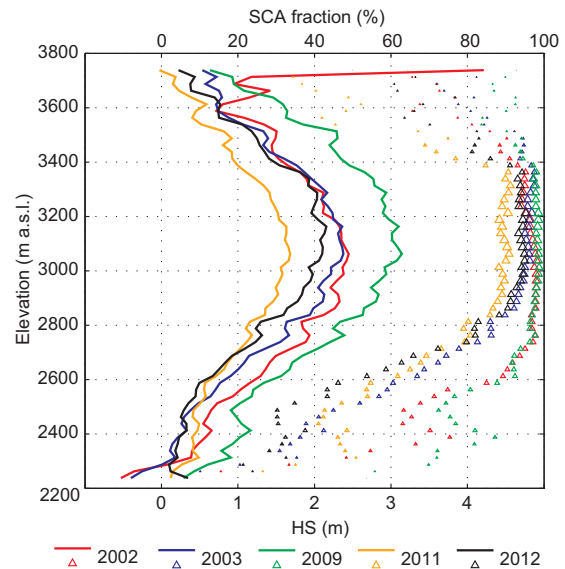

Fig. 3. Mean snow depth HS (solid lines) and SCA fraction (triangles) of 25 m elevation zones. The size of the triangles presents the area of the corresponding elevation zone scaled by the total investigation area, i.e. small triangles present only small areas with less contribution to total snow cover volume compared to the contribution of areas marked with large triangles.

of the two fitted lines present the final L, which depends on the slope of the power laws and differs from L_p. In contrast to Shook and Gray (1996), who used a fixed D_l of 3 (completely random spatial distribution), we calculated D_l also for the long-range section.

5. RESULTS

5.1. Spatial and temporal snow distribution

Mean snow depth at the end of each accumulation season ($\bar{HS}$) and its spatial and temporal variability are shown in Table 3. $\bar{HS}$ ranged from 1.31 m in 2011 to 2.58 m in 2009. This range corresponds to 68% of the temporal mean $\bar{HS}$ of 1.88 m. Whereas the temporal CV of $\bar{HS}$ and the long-term temporal CV of winter precipitation measured at cumulative gauges in the investigated catchment (Tab. 2) are similar, observed range between minimum and maximum of winter precipitation is higher than the range of $\bar{HS}$ in the five investigated years.

Snow covered area (SCA) varied inter-annually by 16% of its mean value. Temporal mean snow covered area fraction was 87% of the total area. The standard deviation of spatially distributed HS (σ_{HS}) was lowest in the year of minimum $\bar{HS}$ in 2011. σ_{HS} was similar in 2002, 2003 and 2012. In these years, the spatial CV is varying due to inter-annual variations in $\bar{HS}$. Maximum σ_{HS} occurred in 2009, whereas the spatial CV was lowest in this year of highest $\bar{HS}$. This shows the great influence of $\bar{HS}$ on the spatial CV of one year compared to the influence of σ_{HS}. Mean spatial CV of $\bar{HS}$ was 0.72. The temporal CV shows that $\bar{HS}$ was interannually more variable than σ_{HS} and the spatial CV.

Pearson correlation coefficients (r, Tab. 4) of spatial distributed HS show a high correlation of HS between all ac-

Table 3. Mean snow depths ($\bar{HS}$), the standard deviation of spatial distributed snow depth (σ_{HS}), the corresponding spatial CV and the snow covered area (SCA) for each accumulation seasons calculated from 1 m gridded snow depth data. The inter-annual mean and inter-annual variability in terms of range, σ and temporal CV are shown in the second part of the table.

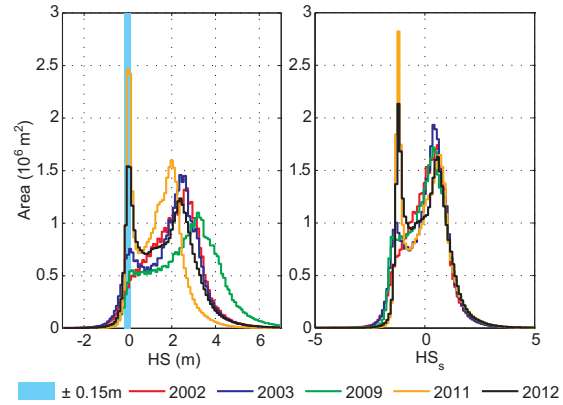| Season	$\bar{HS}$ (m)	σ_{HS} (m)	CV /	SCA 10^6 m^2
2002	1.98	1.34	0.68	32.9
2003	1.86	1.33	0.71	31.3
2009	2.58	1.61	0.62	33.6
2011	1.31	1.04	0.79	28.6
2012	1.65	1.33	0.80	29.9
mean	1.88	1.33	0.72	31.3
range	1.27	0.57	0.18	5.0
σ	0.42	0.18	0.07	1.85
CV	0.22	0.14	0.10	0.06

Fig. 4. Frequency distribution of snow depth HS and standardized snow depth HS_s (Eq. 1 and 2) for the five accumulation seasons. The uncertainty of ALS data (± 0.15 m) is shaded in blue at zero HS.

cumulation seasons. In the high spatial resolution of 1 m, r is highest for the two seasons with a high fraction of snow free area in 2011 and 2012 and second highest for the two seasons of the lowest $\bar{HS}$ in 2011 and the highest $\bar{HS}$ in 2009. The correlations are lower for combinations including the HS distributions of 2002 and 2003. Thus, no clear dependence of correlation on $\bar{HS}$ is obvious. In general, correlations of HS distributions decrease with increasing time lag between the two seasons. At a spatial resolution of 100 m, correlations between HS distribution of 2003 and later years are similar, but correlations including HS distributions of 2002 show still lower values. In general, an increase in correlation with decrease in raster resolution is obvious due to a reduction in small-scale variability by spatial aggregation as shown by e.g. Melvold and Skaugen (2013).

A high Pearson correlation ($r = 0.94$) was found between $\bar{HS}$ and SCA with lower $\bar{HS}$ indicating less SCA. This is obvious in Fig. 3, where mean HS and SCA fraction of the investigated years are shown for 25 m elevation zones. In this figure, large triangles represent elevation zones with a large

Table 4. Correlation coefficients r of spatial distributed HS calculated in raster resolutions from 1 to 100 for each possible combination of the individual accumulation seasons.

	1 m	10 m	30 m	50 m	100 m
2002/2003	0.68	0.77	0.82	0.84	0.86
2002/2009	0.64	0.72	0.76	0.78	0.81
2002/2011	0.62	0.70	0.75	0.78	0.82
2002/2012	0.64	0.73	0.78	0.81	0.85
2003/2009	0.74	0.81	0.85	0.87	0.89
2003/2011	0.74	0.81	0.85	0.87	0.90
2003/2012	0.71	0.79	0.83	0.85	0.88
2009/2011	0.82	0.87	0.89	0.90	0.92
2009/2012	0.79	0.84	0.87	0.88	0.89
2011/2012	0.84	0.87	0.89	0.90	0.91

area and, thus, a high contribution to total snow cover volume compared to elevation zones marked with small triangles. In these elevations of largest contribution to total catchment area, HS varied by a factor of two, whereas SCA fraction varied only by 11 % between 87 % in 2011 and 98 % in 2009.

In general, annual elevation distribution of HS and SCA fraction seem to run parallel (Fig. 3). HS increased to an elevation of 3100 m a.s.l. and decreased above 3200 m a.s.l. Inter-annual differences of HS and SCA fraction can be found in the lowest elevations and at the mountain ridges above 3400 m a.s.l. Differences in mean HS of up to 0.5 m occurred for inter-annually similar SCA fraction below 2800 m a.s.l.(i.e. 2002 and 2009).

The remarkable high fraction of snow-free areas in 2011 and 2012 is obvious at HS of 0 ± 0.15 m in Fig. 4. The year with lowest $\bar{HS}$ (i.e. 2011) shows a peak of most frequent HS at 2 m. In contrast, the year with highest $\bar{HS}$ (i.e. 2009) result in a peak of most frequent HS at 3.2 m. Frequency distributions of standardized snow depths (HS_s) were found to be inter-annually more consistent than frequency distributions of HS. Hence, HS_s was chosen to distinguish between areas of persistent snow cover and areas of high inter-annual snow depth variability.

The temporal mean of HS_s (Fig. 5a) represents the standard snow pattern in the investigation area with respect to the available ALS data. South-facing slopes at lower elevations showed almost no snow cover at the time of the ALS ($t2$). At higher elevations, a low snow coverage can be found at sheer rock faces and along mountain crests. In general, HS_s on the glacier surfaces was higher compared to HS_s in ice-free areas. Increased HS_s can be found at the base of steep slopes and along the glacier margins. These are the areas of a high temporal standard deviation of HS_s (σHS_s) with respect to the available ALS data.

The areas A and B in Fig. 5b emphasis examples of regions showing high σHS_s as a result of avalanche release and accumulation. Corresponding profiles of HS are shown in Fig. 6. In both areas, HS of the year 2002 is low at steep slopes and high on glacier surface in a distance of approx. 100 m from the slope base. In profile A, high HS can be found directly at the slope base in the other years. Peaks of HS at a distance between 0 and 100 m in profile A and at 200 m in profile B
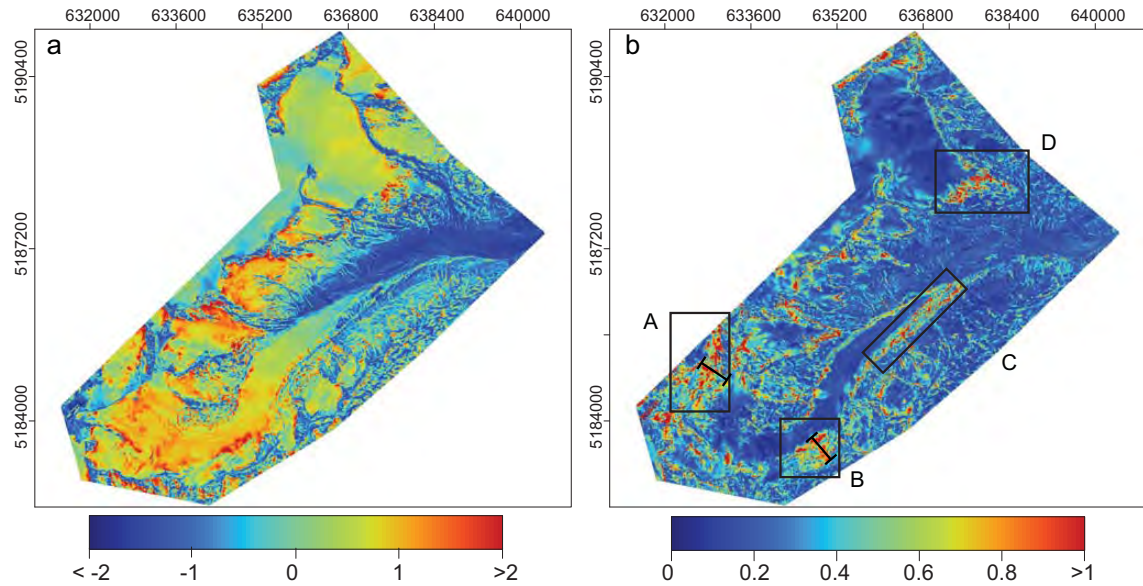
Fig. 5. Spatial distribution of a) temporal mean standardized snow depth HS_s and b) its inter-annual standard deviation σHS_s including all five accumulation seasons. The capital letters A, B, C and D mark regions of high inter-annual variation of HS_s)and are discussed in the text.
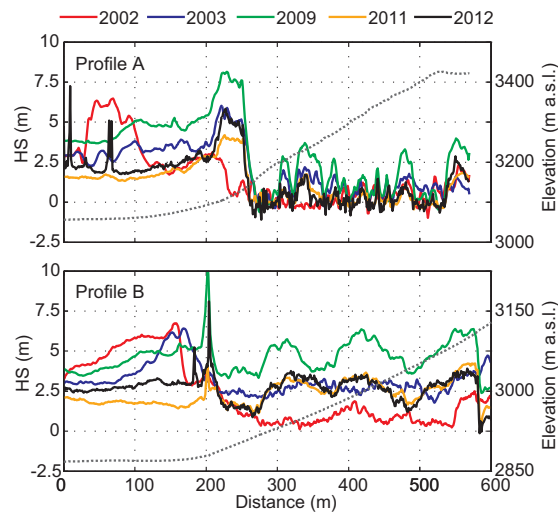

Fig. 6. Snow depth HS along the profiles A and B (Fig. 5b) for the five accumulation seasons. The dotted lines show the corresponding mean elevation of the ALS($t1$) surface (right axis).

are caused by crevasses at the ALS($t1$) reference surface. A substantial snow volume was kept on the slope in area B (6b) and not released to the glacier surface prior to ALS($t2$) in 2009. Box C highlights a typical dead ice area next to the tongue of Hintereisferner which was investigated by e.g., (Bollmann and others, 2011) and (Sailer and others, 2012). In dead ice zones, the high temporal variability of HS_s results from spatially differing surface lowering within the ten year period. The retreat of the glacier tongue of Kesselwandferner

in the 10 year period caused a high inter-annual variability of HS_s in box D (see also Chap. 5.2). In contrast to the zones A - D, large parts of the investigation area present low σHS_s, which is indicated by the dominating blue color graduation in Fig. 5b. An area fraction of 75 % corresponds to a threshold σHS_s of 0.4 (Fig. 7). This large section is characterized by inter-annually persistent HS_s. Conversely, about one fourth of the total area shows a high inter-annual variability of HS_s. These areas were found not necessarily to be located in steep terrain and are more frequent at the base of steep slopes and along glacier margins (Fig. 1 and 5).
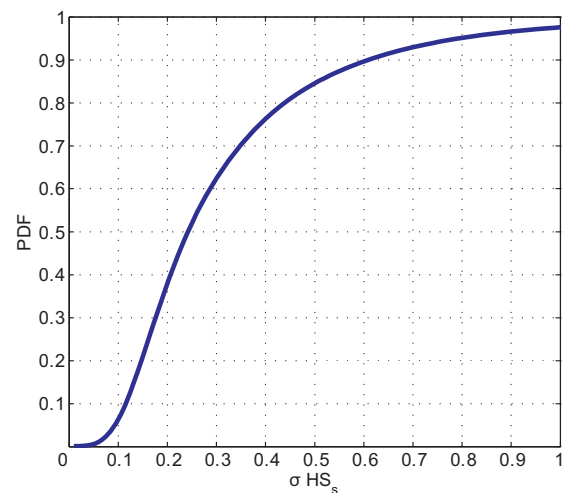

Fig. 7. Cumulative probability density function (PDF) of the temporal standard deviation of standardized snow depths σHS_s.
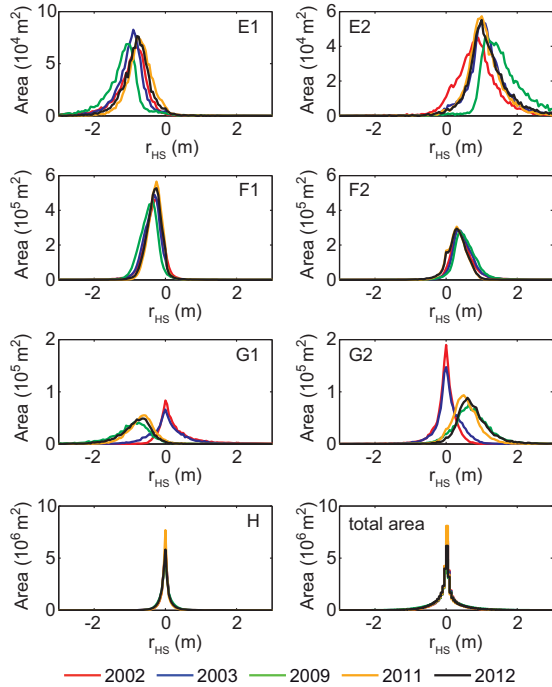
Fig. 10. Histogram of annual r_{HS} for the clusters derived by k-means clustering of snow depth residuals r_{HS}. Capital letters are similar to classes shown in Fig. 9. Note that the scales of the area vary.

The multi-annual cross-combination of squared errors of HS_s (SE_s, Eq. 3) helps to analyze the temporal frequency of the processes causing high inter-annual variability of snow depths and to explain the magnitude of spatial means of SE_s (MSE_s, Fig. 8). Most parts of the areas featuring SE_s lower than 0.5 (masked white in Fig. 8) correspond to areas of σHS_s lower than 0.4 (Fig. 5 b).

High SE_s are obvious within the areas A and B (Fig. 8, upper row), where snow variability is a result of the release and accumulation of avalanches (Fig. 6). These inter-annual differences of HS_s are pronounced especially in combinations including 2002. High SE_s between the years 2002, 2003 and the more recent surveys 2009, 2011 and 2012 are obvious for the areas C and D along the glacier margins. In these areas, high SE_s are caused by continues changes in topography due to melt of dead-ice, collapse of moraines and glacier retreat within at least 6 years between the surveys (e.g., Fischer, 2011; Sailer and others, 2012). Thus, MSE_s (Fig. 8) and correlation coefficients (r, Tab. 4) are highest for cross-combinations including 2002 and smaller for shorter time lags between the years. Even in the two-year period 2009/2011 and the three-year period 2009/2012, high SE_s can be found along the glacier margins (Fig. 5b, box C). SE_s along the glacier margins are small for the one-year periods 2002/2003 and 2011/2012, which reduces MSE_s for these cross-combinations.

5.2. Residual analysis

While high inter-annual variability was detected for areas along the glacier margins, it is not shown yet, what causes

the inter-annual variability of SE_s in these zones. The temporal clustering of the residuals of each HS value from its surrounding mean (r_{HS}, Eq. 4) is applied to show more in detail the differences in the areas highlighted in (Chap.5.1). The clustering of r_{HS} resulted in seven reasonable classes. Three of the ten initial classes are not further discussed because they originate from extreme values of individual seasons and cover a small relative fraction of 0.1 % of the total area. A map of the clusters with a zoom to the area of the tongue of KWF is shown in Fig. 9. Figure 10 shows the frequency distribution of r_{HS} within the classes E to H and for the total area. 63 % (22.5 km^2) of the investigated area is characterized by a homogeneous snow cover predominantly located on glaciers and in areas with no snow in all five years (class H). In these areas the mean r_{HS} are close to zero (maximum $\sigma = 0.18$ m) in all five accumulation seasons. The transition zone from homogeneous ($r_{HS} \cong 0$) to heterogeneous ($r_{HS} \neq 0$) snow distribution (class F1 and F2) cover 25 % of the total area. Frequency distributions of r_{HS} in F1 and F2 were similar for the individual accumulation seasons (Fig. 10). More inter-annual variability of r_{HS} is obvious in the classes E1 and E2 of distinct positive and negative r_{HS} (Fig. 10). Maximum and minimum r_{HS} were found in 2009. This shows that the spatial variability of HS increases in years of high $\bar{HS}$, i.e. HS increases in sinks and channels, whereas crests and bumps maintain snow-free. In 2002, frequency distribution of r_{HS} was shifted towards lower values in areas of positive r_{HS} (Fig. 10). This resulted from a snow cover accumulated at the mountain crests prior to ALS ($t1$). The two classes G1 and G2 are characterized by a change in r_{HS} within the five accumulation seasons. These two classes are located at the glacier margins (Fig. 9) and together share 6 % of the total area. They show a homogeneous snow cover in 2002 and 2003, but distinct positive or negative r_{HS} in 2009, 2011 and 2012 (Fig. 10). This change is a result of glacier retreat which exposes the more heterogeneous surface of the former glacier bed compared to the homogeneous glacier surface. However, differences in these two classes are not visible in the frequency distribution of r_{HS} for the total area due to the large fraction of homogeneous snow cover (class H) within the investigation area.

5.3. Geostatistical analysis

Variograms were calculated for HS in ice-free terrain, for HS on Hintereisferner (HEF) and Kesselwandferner (KWF) and for HS on the remaining small glaciers (Fig. 11). The scale break L, the corresponding sill $\gamma(h_L)$, the short range fractal Dimension D_s and the long range fractal dimension D_l were calculated for ice-free terrain (Tab. 5).

An inter-annual consistent L was found in ice-free terrain at approx. 20 m, whereas $\gamma(h_L)$ ranged considerably between the two years of lowest and highest $\bar{HS}$ (Tab. 5). The short range variability of HS is highest in 2002 (Fig. 11a). This results in a high D_s compared to the inter-annually persistent D_s of the other four years (Tab. 5). In all five years, the increase of $\gamma(h)$ with h flattens out to a consistent D_l of 2.9 for HS in ice-free terrain. $\gamma(h)$ for $h > L$ depends on the spatial mean snow depth $\bar{HS}$ of the individual years with increasing $\gamma(h)$ for increasing $\bar{HS}$.

In contrast, no distinct flattening of $\gamma(h)$ with increasing h could be found for $h > 10\,m$ on glacier surface. The overall spatial variability of HS in ice-free terrain was found to be higher compared to γh on glaciers. A break in scaling behavior of HS on glaciers is indicated at L of 10 m (Fig. 11b-d).
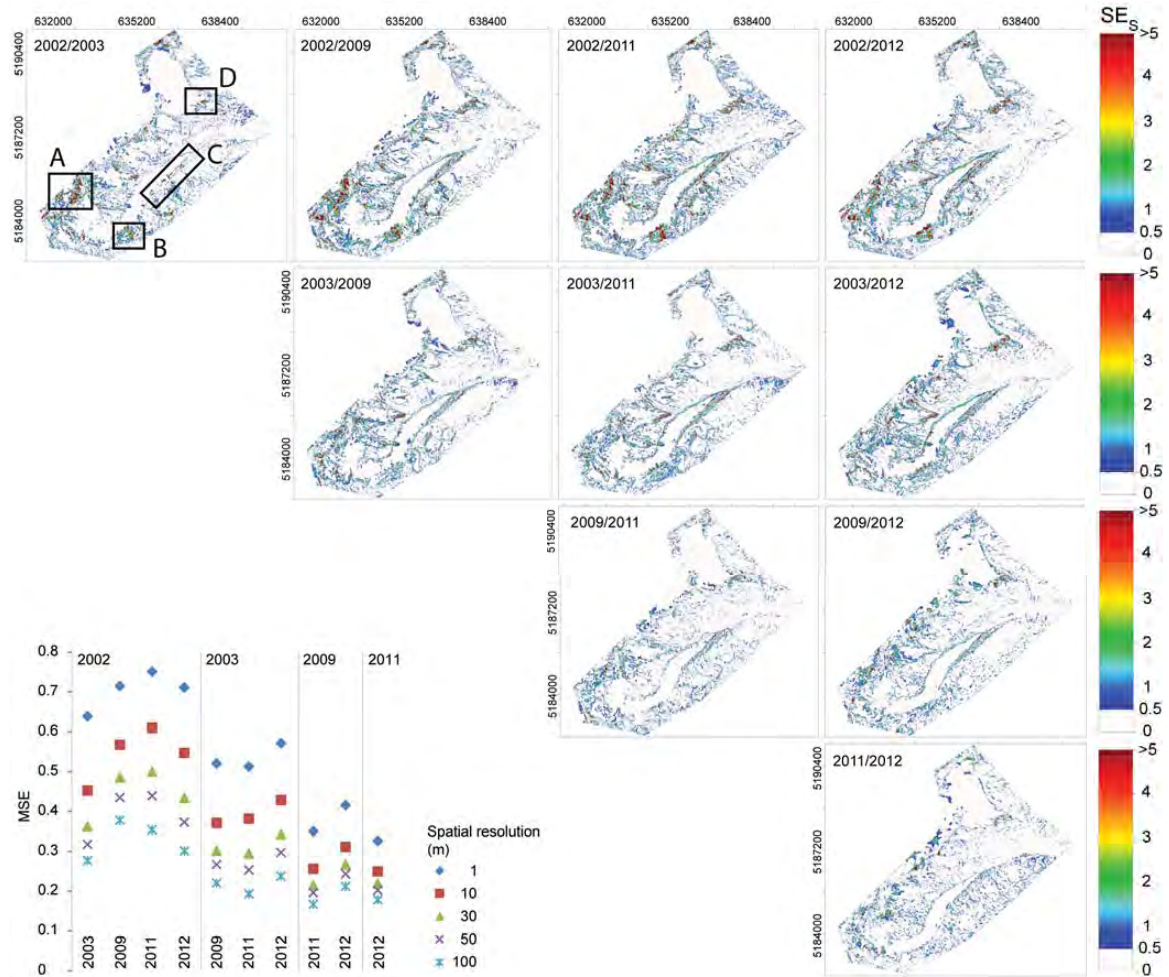
Fig. 8. Maps of squared errors of standardized snow depths SE_s (Eq. 3) between all possible combinations of the five accumulation seasons. In the lower left corner, mean squared errors MSE of the cross-combinations are shown for different spatial resolutions.

Table 5. Annual scale break L, the corresponding sill $\gamma(L)$, short range fractal dimension D_s and long range fractal dimension D_l calculated for HS in ice-free terrain.

	2002	2003	2009	2011	2012
$L\,(\mathrm{m})$	18.0	19.7	19.8	20.4	21.7
$\gamma(L)\,(\mathrm{m})$	0.92	0.75	1.27	0.54	0.64
D_s	2.66	2.45	2.44	2.34	2.43
D_l	2.93	2.93	2.92	2.92	2.91

However, $\gamma(h)$ is in the magnitude of a few centimeters to one decimeter at h of 10 m and, thus, in the range of the assumed accuracy of Δz_{ALS}. At h of 10 m, $\gamma(h)$ is slightly higher on HEF compared to $\gamma(h)$ on small glaciers and on KWF. At scales of h below 10 m, $\gamma(h)$ is highest in 2003 and 2012 on all glaciers. Whereas $\gamma(h)$ of HS is lowest in 2011, differences can be found between $\gamma(h)$ in different accumulation seasons on the glaciers. Especially HS in 2002 shows low variability

at shorter scales, but $\gamma(h)$ increases towards scales of about 100 m on small glaciers and on HEF. However, variability of HS in 2002 stays at comparatively low values on KWF. The variability of HS on KWF in 2003 does not increase for a large range of h.

6. DISCUSSION

6.1. Spatial and temporal snow distribution

The inter-annual analysis of the snow cover in this partly glacierized catchment shows a higher range of $\bar{HS}$ (68 % of its temporal mean) compared to the inter-annual range in SCA (16 % of its temporal mean, Tab. 3). Nevertheless, annual SCA and $\bar{HS}$ of the total area have a high correlation ($r = 0.94$). With respect to the total snow cover volume and hence $\bar{HS}$, elevations of the largest area present a roughly parallel shift in elevation distribution of HS and SCA (Fig. 3). But differences in SCA fraction are small in these elevations. This is a result of the large fraction of glacierized area which is totally snow covered in all years. At lower elevations, snow melt caused different HS and variable SCA due to the seasonal
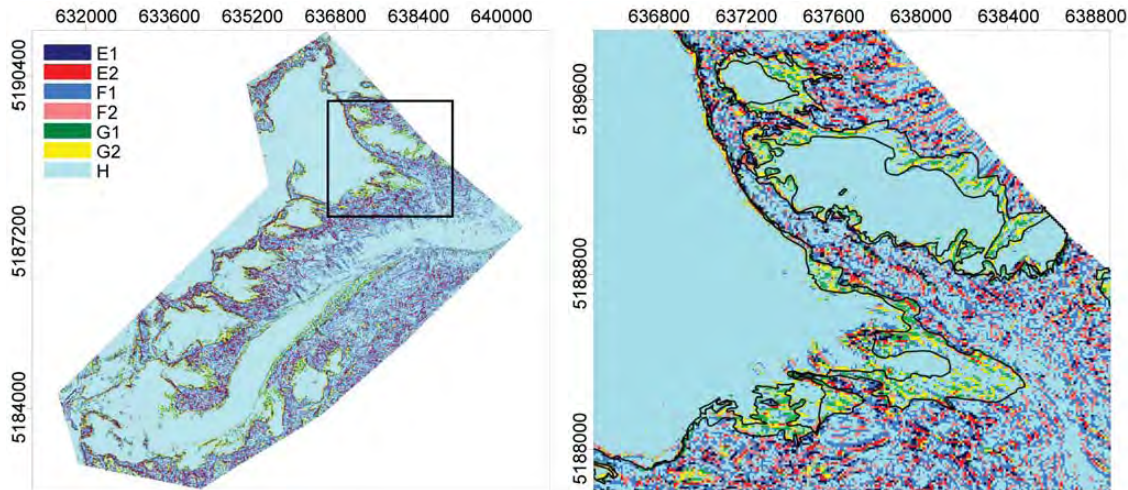
Fig. 9. Clusters derived by k-means clustering of snow depth residuals r_{HS}. The capital letters pair classes with similar temporal characteristics in magnitude of r_{HS}. The index 1 indicates negative r_{HS} and the index 2 indicates positive r_{HS}. The detailed view highlights areas of changes in snow accumulation as a result of glacier retreat (black glacier outlines) in the ten-year period between 2001 and 2011.

course of weather conditions. However, variabel HS in these elevations have less influence on $\bar{HS}$ due to their small area fraction. The small variation of SCA compared to variation of $\bar{HS}$ might be challenging for the determination of relationships between snow covered area fraction and snow depths, like used to calculate subgrid variability of snow cover products from satellite data (e.g. Swenson and Lawrence, 2012) or to model spatial variability of snow depths (e.g. Luce and others, 1999; Liston, 2004; Clark and others, 2011). At the time of peak snow accumulation, very detailed surveys of the SCA in elevations zones of largest area would be necessary to obtain mean snow depth of the partly glacierized catchment from small changes in SCA.

As a result of ice flow and densification of firn, HS can be underestimated in typical firn areas of the glaciers. This is more relevant for elevations higher than 3250 m a.s.l. Helfricht and others (2014) compared ALS data and ground penetrating radar measurements on the investigated glaciers and found a mean underestimation of HS of 0.4 m ($\sigma = 0.34$ m) by ALS data in the firn areas of the glaciers. The decrease of mean HS in glacierized areas above 3250 m a.s.l. (Fig. 3) can partly result from firn densification and ice dynamics. Areas of emergent ice flow were found to be small having no considerable influence on the interpretation of HS. However, we assumed these dynamical processes to be constant in time and thus no corrections were applied. Further, in many studies rough and steep surfaces were found to store less snow on average (Blöschl and Kirnbauer, 1992; Grünewald and Lehning, 2011; Grünewald and others, 2013; Helfricht and others, 2012; Schöber and others, 2014).

An increase in annual σ_{HS} with increasing $\bar{HS}$ was found. This finding was also indicated by Sturm and Wagner (2010), who analyzed $\bar{HS}$ derived from snow depth samples taken on a regular 30 m grid within an 1 x 1 km Arctic test area. Melvold and Skaugen (2013) also found a decreasing spatial CV with increasing HS with values between 0.86 ($\bar{HS} = 1.42$ m) and 0.62 ($\bar{HS} = 2.89$ m). Winstral and Marks (2014) discussed the variation of spatial CV when $\bar{HS}$ is changing at a faster

rate than σ. In their study, the mean spatial CV of 11 years was 0.71, with a slightly higher value for snow surveys in spring (0.81). This finding is in agreement with the variability in mean spatial CV found in our study. Winstral and Marks (2014) also indicate a high spatial CV of 0.89 for one-year ALS data. Winstral and Marks (2014) related higher spatial CV of HS to higher wind speeds and higher melt rates. To some degree this might be true for the spatial CV of HS in 2011 and 2012 where potential melt conditions appeared prior to ALS ($t2$) (Chap. 3). Marchand (2005) showed that the spatial CV ranges between 0.72 and 0.96 for open sites in Norway. Jepsen and others (2012) analyzed a total of 5300 snow depth measurements taken at the end of 12 accumulation seasons. They found that the spatial CV of the snow cover ranged from 0.73 to 1.09 in a continental Alpine watershed. In their study, the temporal variability of the spatial CV is 0.15, which is higher than the temporal variability of CV of 0.1 found here. Grünewald and others (2010) derived a spatial CV of HS between 0.6 and 2.0 from terrestrial lidar data, whereas lowest values were found at the beginning of ablation season.

In general, the temporal mean spatial CV of ALS-derived HS in this study (0.72) is at the lower end of values derived in open and high-elevation Alpine areas in previous studies. Schöber and others (2014) present a map of spatially distributed CVs of HS in 2011, which includes the investigation area of the present study showing low CVs on glaciers. Thus, with respect to the homogeneous snow cover on the glacier surface, annual and multi-annual mean spatial CVs of HS in partly glacierized catchments tend to be lower compared to CVs in ice-free terrain.

Maximum correlation between two years is 0.84 (2011/2012) for the original spatial resolution of 1 m. This is lower than inter-annual correlations found for HS by Deems and others (2008) ($r = 0.88$ - 0.92), Melvold and Skaugen (2013) ($r = 0.95$) or Schirmer and others (2011) (up to $r = 0.97$). This results from the large area and complex terrain investigated in this study. The wide range of snow depths (snow-free to HS of
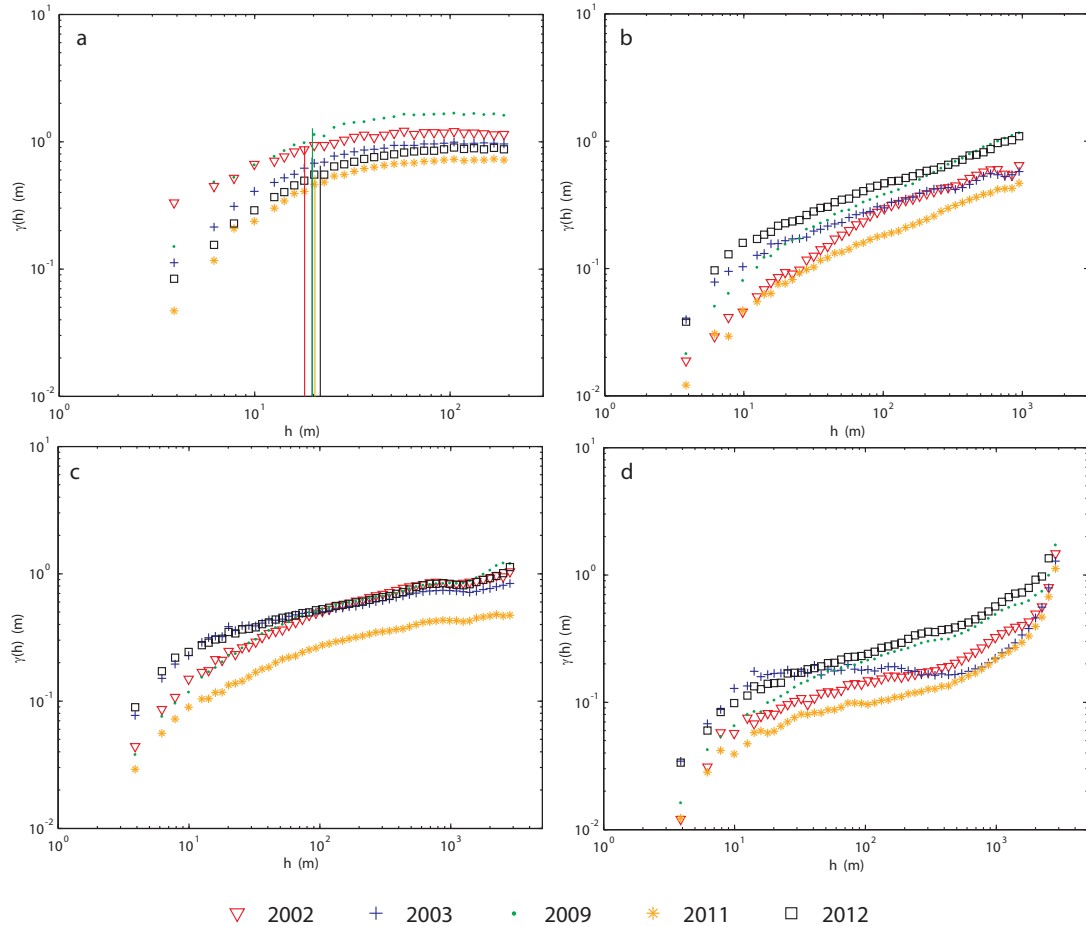
Fig. 11. Variograms for HS of the five accumulation seasons a) in ice-free terrain, b) on small glaciers, c) on Hintereisferner and d) on Kesselwandferner. Vertical lines in (a) show the location of the calculated scale breaks L.

more than 5 m in avalanche accumulation areas), the high number of different topographic features (glaciers, rock walls, slopes, mountain crests,...) and the corresponding dynamical processes (glacier retreat, rock fall, collapse of moraines,...) reduce the inter-annual correlation compared to smaller, temporally more consistent test sites.

Since HS is scaled for statistical models to simulate snow cover distribution (e.g., Sturm and Wagner, 2010; Lehning and others, 2011; Grünewald and others, 2013), different measures of snow depth have been used. We found standardized snow depth (HS_s) best suited to describe the inter-annual frequency distribution of HS of this area. Thus, we used HS_s to distinguish inter-annually persistent snow cover from areas of high inter-annual variability of HS_s. According to Sturm and Wagner (2010), we showed a climatological snow distribution pattern in terms of spatially distributed, temporal mean HS_s of the investigated snow surveys. Whereas in Sturm and Wagner (2010) inter-annually persistent areas were visually striking, they did not present a measure to differentiate between inter-annually variable HS_s and areas of persistent snow cover. Thus, we used the temporal standard deviation of HS_s (σHS_s) (Fig. 5b) and showed that 75 % of

the investigated area present inter-annually HS_s for a threshold of σHS_s of 0.4.

In general, σHS_s is low on glacier areas and at gentle slopes (Fig. 5b). Especially in these areas, lidar measurements of HS have an appropriate accuracy and most of the snow cover volume is accumulated there. Thus, ALS is suitable for recording characteristic snow depth distributions for the calibration and validation of hydro-meteorological models, as demonstrated for instance by Schöber and others (2014). High HS were found consistently on glaciers which are characterized by flat, sheltered surfaces at high elevations. The preferential accumulation in these areas is also the reason why glaciers exist where they do. For instance, Dadic and others (2010b) related the location of the glaciers to differences in the wind field. Redistribution of snow to glacier surface was already included in hydro-meteorological models adapted to the investigated catchment (Kuhn, 2003).

The reduction of MSE_s with increasing aggregation of raster resolution (Fig. 8) is distinctly higher for MSE_s including 2002 or 2003 compared to MSE_s calculated between surveys since 2009. Small-scale features of high SE_s are smoothed, especially in narrow areas along sheer rock walls and glacier

margins. Two studies calculated mean squared errors of HS_s (MSE_s) for multi-annual data. HS_s in Sturm and Wagner (2010) for snow surveys in March and April compared to one survey in March ranged from 0.31 and 1.34. Lower MSE_s were found by Winstral and Marks (2014). Based on the snow depth data of 11 years at a spatial resolution of 30 m the calculated MSE_s ranged between 0.06 and 0.6 with a mean MSE_s of 0.31. This range is comparable to mean MSE_s of the present study (0.22 to 0.5) with a mean of 0.34 for a spatial resolution of 30 m (Fig. 8).

Areas of high inter-annual snow depth variability (i.e. high σHS_s) are not restricted to mountain crests and steep slopes, where ALS data are affected by large errors. In general, 82 % of all $\sigma HS_s \geq 0.4$ were located at slopes of less than 40°. High σHS_s were detected at gently inclined slope toes and on homogeneous glacier surfaces (Fig. 7). These are typical accumulation areas of gravitational snow transport by avalanches and snow sloughs.

Geomorphological processes change the mountains surface topography continuously (Bollmann and others, 2011; Sailer and others, 2012). Thus, the variation in the reference surface at ALS($t1$) affects snow depth variability. Further, glacier retreat alters the surface relief from a more homogeneous surface to heterogeneous landforms featuring ridges and sinks, which lead to a heterogeneous snow depth distribution (Fig. 9 and 10). This coincides with the findings of Lehning and others (2011) and Schirmer and others (2011), who demonstrated that topographic roughness controls snow cover variability. The shift of the frequency distribution of r_{HS} towards more positive and negative values in the year of highest mean snow depth (i.e. 2009) shows that differences of HS between preferential accumulation areas and areas with less or no snow increase with an increasing $\bar{HS}$.

6.2. Scaling behavior of snow depths

The multi-scaling behavior of HS separated by a scale break distance L into short range fractal dimensions D_s and a long range fractal dimension D_l was assessed for HS. In ice-free terrain, L was found to be inter-annually consistent at approx. 20 m, which is comparable to L of 17.3 and 20.4 m found by Schirmer and Lehning (2011) for a cross-loaded slope (i.e. variable wind direction) in complex mountain terrain. However, L found by Deems and others (2008) for HS distribution of two seasons in a forested, moderate elevation terrain with low rolling topography (L of 15.5 and 15.9 m) and at an Alpine site above the tree line(L of 31.5 and 26.4 m) are slightly lower and slightly higher, respectively. Mott and others (2011b) showed very similar values for peak HS calculated from terrestrial laser scanning measurements in a small Alpine area ($L = 20.4$, $D_s = 2.31$) to those found in this study. Also Schirmer and Lehning (2011) showed a reduction in D_s towards values between 2.3 and 2.5 at the end of the accumulation season. D_l was found to be consistently close to 2.9 in all studies.

L determined for HS in ice-free terrain marked the beginning of a curve-like reduction in the increase of $\gamma(h)$ rather than a distinct bend in $\gamma(h)$ like for instance those found in Mott and others (2011b) or Schirmer and Lehning (2011). This is a result of the large area (approx. 14 km^2) and the high number of different surfaces types (rocks, boulders, talus,...) in a complex topography (sheer walls, gentle slopes, flat valley floors) with a different exposure to meteorological conditions (radiation, wind). Since values of L depend strongly on the bin spacing, grid resolution, area considered for the variogram

and the maximum range of h used for calculation, they give an order of magnitude (here a few tenths of meter) rather than exact values.

$\gamma(h)$ of HS at $h = 2\,m$ is highest in 2002 (0.23 m) and stays high for h lower than the scale break L (Fig. 11a). Whereas $\gamma(h)$ at $h < 4\,m$ might be influenced by the accuracy of the ALS data (Chap. 2), similarities between snow cover distribution in 2002 and 2009 can also be found in SCA and HS at lower elevations (Fig. 3). In addition, the avalanche activity in 2002 (Fig. 7) increased the small-scale variability of HS. No distinct, inter-annually persistent scale break could be detected on glaciers. Nevertheless, increase in $\gamma(h)$ appeared to be higher at scales below 10^{-1} m compared to increase in $\gamma(h)$ at larger h. Even if this variability is obvious in some years, $\gamma(h)$ below 10^{-1} m is close to the accuracy of Δz_{ALS} of $\pm 0.15\,m$ (Chap. 2). Thus, an interpretation of this scale break would be more speculative. However, years without considerably snow fall prior to ALS ($t1$) (2003, 2012) show higher $\gamma(h)$ at short scales compared to years, where snow fall occurred prior the survey in autumn (see Chap. 3). This is a result of crevasses and surface structures like melt water channels and moraines on the glacier surface which, if they are not covered by snow at ALS($t1$), increase small-scale variability.

Especially in 2011, $\gamma(h)$ of HS was reduced over the whole range of h by snow accumulation prior to ALS ($t1$), the comparatively low precipitation amount of this season and already proceeded melt at the snow surface on the glaciers prior to ALS ($t2$). The lower values of $\gamma(h)$ on glaciers in comparison with $\gamma(h)$ in ice-free terrain highlight the more homogeneous snow depth distribution on the ice surfaces.

7. CONCLUSIONS

In this paper we report a comprehensive analysis of the spatial distribution of the snow cover at the end of five accumulation seasons between 2002 and 2012 in a partly glacierized mountain catchment in Tyrol, Austria. The distribution of HS at the end of the accumulation season is of high relevance for cryospheric and hydrologic studies, such as snow melt modeling or seasonal glacier mass balances. The analysis makes evident that the snow covered area (SCA) is inter-annually much more persistent than the mean annual snow depths ($\bar{HS}$). Although a strong correlation was found between SCA and $\bar{HS}$, SCA varied only by 16 % of its temporal mean, but $\bar{HS}$ varied by a factor of two in the five years. The inter-annual variability of $\bar{HS}$ in the five accumulation seasons ($CV = 0.22$) is of similar magnitude to the climatic variability of winter precipitation in this region. Although 5 years of data do not make a climatic mean, the presented dataset - including one season of comparatively low HS and one season of extremely high HS - may provide a more reasonable base for statistical analysis and simulation of the snow depth distribution than data of one-year acquisitions. With respect to the statistical analysis, frequency distribution of standardized snow depths turned out to be more inter-annually consistent compared to frequency distribution of absolute snow depths. 75 % of the investigated area present an inter-annual standard deviation of the standardized snow depth of less than 0.4 at a spatial scale of 10 m and, thus, can be interpreted as the standard snow pattern representing highly valuable information for the snow cover modelling of this area. The high inter-annual variability in snow depth in the remaining area is attributed to occasional avalanches, wind transport and changes in the surface topography. Especially areas associated with changes in

glacierization were found to cause inter-annual snow depth variability. Ice melt in dead-ice bodies causes inter-annual variability in snow depth. A shift from homogeneous snow distribution towards a more heterogeneous snow cover was observed in areas which became ice free due to glacier retreat within the investigated 10 year period. Compared to ice-free basins, this circumstance keeps the modeling of snow challenging with regard to the expected proceeding glacier retreat. So far, these changing zones cover only a low area-fraction and still have a low impact with respect to i) the total snow volume in the basin and ii) a coarse spatial resolution of the data as typically used for modeling (e.g. 50 - 100 m). Nevertheless, areas of high inter-annual variability caused inter-annual differences in the correlation of snow depths which are even visible at a spatial resolution of 100 m. Geostatistical analysis is performed to show inter-annual persistence of the scaling behavior of the mountain snow cover. The differences between spatial autocorrelation of HS in ice-free terrain and spatial autocorrelation of HS on glaciers show the great influence of glaciers on the snow depth variability in mountain catchments. Spatial variability of snow depth turned out to depend on mean snow depth in ice-free terrain, but is influenced by the existence of a snow layer at ALSt1 on glacier surfaces. In accordance with typical scale breaks shown by other authors for HS in Alpine areas at the end of the accumulation season (e.g., Deems and others, 2006; Mott and others, 2011b; Schirmer and Lehning, 2011), inter-annually persistent scale breaks at 20 m were detected in ice-free terrain of the total investigated catchment. On smooth glacier surfaces, the short and long range fractal characteristics can not be distinguished easily indicating a scale invariant behavior of HS in such areas. However, disruptive surface structures, such as crevasses or meltwater channels, could turn the fractal parameters into length scales comparable to length scales in ice-free terrain. While our results in general confirm the fractal characteristics of HS indicated by other studies in ice-free terrain, these have so far only been shown for smaller areas. Fractal parameters calculated for irregular or smaller regular subareas may be a next step in obtaining parameters for statistical snow models (e.g., Lehning and others, 2011) or deterministic snow models working in a gridded model layout. The present study shows for the first time the persistence and variability of the snow pattern for five accumulation seasons in a comparatively large catchment with a complex topography of ice-free terrain and glaciers.

8. ACKNOWLEDGEMENTS

REFERENCES

Abermann, J., A. Fischer, A. Lambrecht and T. Geist, 2010. On the potential of very high-resolution repeat DEMs in glacial and periglacial environments, *The Cryosphere*, **4**, 53–65.

Achleitner, S., J. Schöber, M. Rinderer, G. Leonhardt, F. Schöberl, R. Kirnbauer and H. Schönlaub, 2012. Analyzing the operational performance of the hydrological models in an alpine flood forecasting system, *Journal of Hydrology*, **412/413**, 90 – 100.

Anderton, S. P., S. M. White and B. Alvera, 2004. Evaluation of spatial variability in snow water equivalent for a high mountain catchment, *Hydrological Processes*, **18**(3), 435–453.

Baltsavias, E.P., 1999. Airborne laser scanning: basic relations and formulas, *ISPRS Journal of Photogrammetry and Remote Sensing*, **54**(2-3), 199 – 214.

Bavay, M., T. Grünewald and M. Lehning, 2013. Response of snow cover and runoff to climate change in high Alpine catchments of Eastern Switzerland, *Advances in Water Resources*, **55**, 4 – 16.

Blöschl, G., 1999. Scaling issues in snow hydrology, *Hydrological Processes*, **13**(14-15), 2149–2175.

Blöschl, G., D. Gutknecht and R. Kirnbauer, 1991. Distributed Snowmelt Simulations in an Alpine Catchment: 2. Parameter Study and Model Predictions, *Water Resources Research*, **27**(12), 3181–3188.

Blöschl, G. and R. Kirnbauer, 1992. An analysis of snow cover patterns in a small alpine catchment, *Hydrological Processes*, **6**(1), 99–109.

Bollmann, E., 2010. Airborne laser scanning glacier mass balance, (Master's thesis), Institute for Geography, University of Innsbruck.

Bollmann, R., E.and Sailer, J. Briese, C.and Stötter and P. Fritzmann, 2011. Potential of airborne laser scanning for geomorphologic feature and process detection and quantifications in high alpine mountains, *Zeitschrift für Geomorphologie, Supplementary Issues*, **55**(2), 83–104.

Burrough, P., 1993. Fractals in Geography, PTR Prentice Hall, Englewood Cliffs, NJ, chap. Fractals and geostatistical methods in landscape studies, 87–121.

Clark, Martyn P., Jordy Hendrikx, Andrew G. Slater, Dmitri Kavetski, Brian Anderson, Nicolas J. Cullen, Tim Kerr, Einar rn Hreinsson and Ross A. Woods, 2011. Representing spatial variability of snow water equivalent in hydrologic and land-surface models: A review, *Water Resources Research*, **47**(7), W07539.

Dadic, R., R. Mott, M. Lehning and P. Burlando, 2010a. Parameterization for windinduced preferential deposition of snow, *Hydrological Processes*, **24**(14), 1994–2006.

Dadic, R., R. Mott, M. Lehning and P. Burlando, 2010b. Wind influence on snow depth distribution and accumulation over glaciers, *J. Geophys. Res.*, **115**, F01012.

Deems, J.S., T.H. Paintner and D.C. Finnegan, 2013. Lidar measurement of snow depth: a review, *Journal of Glaciology*, **59**(215), 467–479.

Deems, J. S., S R. Fassnacht and K. J. Elder, 2006. Fractal Distribution of Snow Depth from Lidar Data, *J. Hydrometeor*, **7**(2), 285–297.

Deems, J. S., S. R. Fassnacht and K. J. Elder, 2008. Interannual consistency in fractal snow depth patterns at two Colorado mountain sites, *J. Hydrometeor*, **9**(5), 977–988.

Elder, K., J. Dozier and J. Michaelsen, 1991. Snow accumulation and distribution in an Alpine Watershed, *Water Resour. Res.*, **27**(7), 1541–1552.

Fischer, A., 2010. Glaciers and climate change: Interpretation of 50 years of direct mass balance of Hintereisferner, *Global and Planetary Change*, **71**(1-2), 13 – 26.

Fischer, A., 2011. Comparison of direct and geodetic mass balances on a multi-annual time scale, *The Cryosphere*, **5**(1), 107–124.

Fischer, A., G. Markl and M. Kuhn, 2012. Glacier Mass Balance of Hintereisferner, Ötztal Alps, Austria, from 1952/53-2010/11.

Forgy, E.W., 1965. Cluster analysis of multivariate data: efficiency versus interpretability of classifications., *Biometrics*, **21**, 768–769.

Fritzmann, Patrick, Bernhard Höfle, Michael Vetter, Rudolf Sailer, Johann Stötter and Erik Bollmann, 2011. Surface classification based on multi-temporal airborne LiDAR intensity data in high mountain environments:A case study from Hintereisferner, Austria, *Zeitschrift für Geomorphologie, Supplementary Issues*, **55**(2), 105–126.

Gao, Z., J.and Xia, 1996. Fractals in physical geography, *Progress in Physical Geography*, **20**(2), 178–191.

Geist, T., H. Elvehoy and J. Jackson, M.and Stötter, 2005. Investigations on intra-annual elevation changes using multi-temporal airborne laser scanning data: case study Engabreen, Norway, *Annals of Glaciology*, **42**(1), 195–201.

Geist, T. and J. Stötter, 2007. Documentation of glacier surface elevation change with multi-temporal airborne laser scanner data - case study: Hintereisferner and Kesselwandferner, Tyrol, Austria, *Zeitschrift für Gletscherkunde und Glazialgeologie*, **41**, 77 – 106.

Grünewald, T. and M. Lehning, 2011. Altitudinal dependency of snow amounts in two small alpine catchments: can catchment-wide snow amounts be estimated via single snow or precipitation stations?, *Annals of Glaciology*, **52**(58), 153–158.

Grünewald, T., M. Schirmer, R. Mott and M. Lehning, 2010. Spatial and temporal variability of snow depth and ablation rates in a small mountain catchment, *The Cryosphere*, **4**(2), 215–225.

Grünewald, T., J. Stötter, J. W. Pomeroy, R. Dadic, I. Moreno Baños, J. Marturià, M. Spross, C. Hopkinson, P. Burlando and M. Lehning, 2013. Statistical modelling of the snow depth distribution in open alpine terrain, *Hydrology and Earth System Sciences*, **17**(8), 3005–3021.

Hartigan, J. A. and M. A. Wong, 1979. A K-means clustering algorithm, *Applied Statistics*, **28**, 100108.

Helfricht, K., M. Kuhn, M. Keuschnig and A. Heilig, 2014. Lidar snow cover studies on glaciers in the Ötztal Alps (Austria): comparison with snow depths calculated from GPR measurements, *The Cryosphere*, **8**(1), 41–57.

Helfricht, K., J. Schöber, B. Seiser, A. Fischer, J. Stötter and M. Kuhn, 2012. Snow accumulation of a high alpine catchment derived from LiDAR measurements., *Advances in Geoscience*, **32**, 31–39.

Hoinkes, H., 1970. Methoden und Möglichkeiten von Massenhaushaltsstudien auf Gletschern, *Zeitschrift für Gletscherkunde und Glazialgeologie*, **6**, 37 – 90.

Hopkinson, C., M. Sitar, L. Chasmer, C. Gynan, D. Agro, R. Enter, J. Foster, N. Heels, C. Hoffman, J. Nillson and R. St. Pierre, 2001. Mapping the Spatial Distribution of Snowpack Depth Beneath a Variable Forest Canopy Using Airborne Laser Altimetry, *Proccedings of the 58th Annual Eastern Snow Conference, Ottawa, Canada.*

Huss, D., M.and Farinotti, A. Bauder and M. Funk, 2008. Modelling runoff from highly glacierized alpine drainage basins in a changing climate, *Hydrological Processes*, **22**(19), 3888–3902.

Jepsen, S. M., N. P. Molotch, M. W. Williams, K. E. Rittger and J. O. Sickman, 2012. Interannual variability of snowmelt in the Sierra Nevada and Rocky Mountains, United States: Examples from two alpine watersheds, *Water Resources Research*, **48**(2), W02529.

Joerg, P., R. Fromm, R. Sailer and A. Schaffhauser, 2006. Measuring snow depth with a terrestrial laser ranging system, ISSW 2006, 452 – 460.

Joerg, P.C., F. Morsdorf and M. Zemp, 2012. Uncertainty assessment of multi-temporal airborne laser scanning data: A case study on an Alpine glacier, *Remote Sensing of Environment*, **127**(0), 118 – 129.

Kaser, G., A. Fountain and P. Jansson, 2003. A manual for monitoring the mass balance of mountain glaciers., International Hydrological Programme. (IHP-VI. Technical Documents in Hydrology 59.), UNESCO, Paris.

Kuhn, M., 2003. Redistribution of snow and glacier mass balance from a hydrometeorological model, *Journal of Hydrology*, **282**(1-4), 95 – 103.

Kuhn, M., E. Dreiseitl, S. Hofinger, G. Markl, N. Span and G. Kaser, 1999. Measurements and models of the mass balance of Hintereisferner, *Geografiska Annaler: Series A, Physical Geography*, **81**(4), 659–670.

Lehning, Michael, Thomas Grünewald and Michael Schirmer, 2011. Mountain snow distribution governed by an altitudinal gradient and terrain roughness, *Geophys. Res. Lett.*, **38**(19), L19504.

Lehning, M., H. Löwe, M. Ryser and N. Raderschall, 2008. Inhomogeneous precipitation distribution and snow transport in steep terrain, *Water Resources Research*, **44**(7), W07404.

Liston, Glen E., 2004. Representing Subgrid Snow Cover Heterogeneities in Regional and Global Models, *J. Climate*, **17**(6), 1381–1397.

Luce, Charles H., David G. Tarboton and Keith R. Cooley, 1999. Sub-grid parameterization of snow distribution for an energy and mass balance snow cover model, *Hydrological Processes*, **13**(12-13), 1921–1933.

Lundberg, N., A.and Granlund and D. Gustafsson, 2010. Towards automated "Ground truth" snow measurements: a review of operational and new measurement methods for Sweden, Norway, and Finland, *Hydrological Processes*, **24**(14), 1955–1970.

Lundquist, J. D. and M. D. Dettinger, 2005. How snowpack heterogeneity affects diurnal streamflow timing, *Water Resources Research*, **41**(5), W05007.

MacQueen, J., 1967. Some methods for classification and analysis of multivariate observations, Proceedings of the Fifth Berkeley Symposium on Mathematical Statistics and Probability, Volume 1: Statistics, University of California Press, Berkeley, Calif., 281–297.

Marchand, A., W.D.and Killingtveit, 2005. Statistical probability distribution of snow depth at the model sub-grid cell spatial scale, *Hydrological Processes*, **19**(2), 355–369.

Matthias, H., M. Zemp, P.C. Joerg and N. Salzmann, 2014. High uncertainty in 21st century runoff projections from glacierized basins, *Journal of Hydrology*, **510**(0), 35 – 48.

Melvold, K. and T. Skaugen, 2013. Multiscale spatial variability of lidar-derived and modeled snow depth on Hardangervidda, Norway, *Annals of Glaciology*, **54(62)**, 273–281.

Mott, R., L. Egli, T. Grünewald, N. Dawes, C. Manes, M. Bavay and M. Lehning, 2011a. Micrometeorological processes driving snow ablation in an Alpine catchment, *The Cryosphere*, **5**(4), 1083–1098.

Mott, R., M. Schirmer, M. Bavay, T. Grünewald and M. Lehning, 2010. Understanding snow-transport processes shaping the mountain snow-cover, *The Cryosphere*, **4**(4), 545–559.

Mott, R., M. Schirmer and M. Lehning, 2011b. Scaling properties of wind and snow depth distribution in an Alpine catchment, *Journal of Geophysical Research: Atmospheres*, **116**(D6).

Nolin, A. W., 2011. Recent advances in remote sensing of seasonal snow, *Journal of Glaciology*, **56**(200), 1141–1150.

Olea, R.A., 1999. Geostatistics for engineers and earth scientists., Kluwer Academic Publishers, Boston.

Pomeroy, J. W., D. M. Gray, K. R. Shook, B. Toth, R. L. H. Essery, A. Pietroniro and N. Hedstrom, 1998. An evaluation of snow accumulation and ablation processes for land surface modelling, *Hydrological Processes*, **12**(15), 2339–2367.

Prokop, A., M. Schirmer, M. Rub, M. Lehning and M. Stocker, 2008. A comparison of measurement methods: terrestrial laser scanning, tachymetry and snow probing for the determination of the spatial snow-depth distribution on slopes, *Annals of Glaciology*, **49**(1), 210–216.

Rittger, K., T. H. Painter and J. Dozier, 2013. Assessment of methods for mapping snow cover from MODIS, *Advances in Water Resources*, **51**(0), 367 – 380.

Sailer, R., E. Bollmann, S. Hoinkes, L. Rieg, M. Spross and J. Stötter, 2012. Quantification of geomorphodynamics in glaciated and recently deglaciated terrain based on airborne laser scanning data, *Geografiska Annaler: Series A, Physical Geography*, **94**(1), 17–32.

Sailer, R., R. Fromm, P. Joerg, A. Schaffhauser and M. Adams, 2008. Ground based remote Sensing of Snow properties and avalanche simulation, Proceedings of UNESCO Earth Conference, Lesbos, Greece.

Schaffhauser, A., M. Adams, R. Fromm, P. Jörg, G. Luzi, L. Noferini and R. Sailer, 2008. Remote sensing based retrieval of snow cover properties, *Cold Regions Science and Technology*, **54**(3), 164 – 175.

Schirmer, M. and M. Lehning, 2011. Persistence in intra-annual snow depth distribution: 2. Fractal analysis of snow depth development, *Water Resources Research*, **47**(9), W09517.

Schirmer, M., V. Wirz, A. Clifton and M. Lehning, 2011. Persistence in intra-annual snow depth distribution: 1. Measurements and topographic control, *Water Resour. Res.*, **47**(9), W09516.

Schöber, J., S. Achleitner, R. Kirnbauer, F. Schöberl and H. Schönlaub, 2010. Hydrological modelling of glacierized catchments focussing on the validation of simulated snow patterns - applications within the flood forecasting system of the Tyrolean river Inn, *Advances in Geosciences*, **27**, 99–109.

Schöber, J., K. Schneider, K. Helfricht, P. Schattan, S. Achleitner, F. Schöberl and R. Kirnbauer, 2014. Snow cover characteristics in a glacierized catchment in the Tyrolean Alps - Improved spatially distributed modelling by usage of Lidar data, *Journal of Hydrology*, **in press**, –.

Schweizer, j., K. Kronholm, J. B. Jamieson and K. W. Birkeland, 2008. Review of spatial variability of snowpack properties and its importance for avalanche formation, *Cold Regions Science and Technology*, **51**(23), 253 – 272.

Sevruk, B., 1985. Correction of precipitation measurements: Swiss experience, *WMO/TD*, **104**, 187 – 196.

Shook, K. and D. M. Gray, 1996. Small-Scale Spatial Structure of Shallow Snowcovers, *Hydrological Processes*, **10**(10), 1283–1292.

Sold, L., M. Huss, M. Hoelzle, H. Andereggen, P. C. Joerg and M. Zemp, 2013. Methodological approaches to infer end-of-winter snow distribution on alpine glaciers, *Journal of Glaciology*, **59**(218), 1047–1059.

Strasser, U., 2008. Modelling of the mountain snow cover in the Berchtesgaden National Park, *Berchtesgaden National Park research report*, **55**.

Sturm, M. and A. M. Wagner, 2010. Using repeated patterns in snow distribution modeling: An Arctic example, *Water Resources Research*, **46**(12), W12549.

Sun, W., G. Xu, P. Gong and S. Liang, 2006. Fractal analysis of remotely sensed images: A review of methods and applications, *International Journal of Remote Sensing*, **27**(22), 4963–4990.

Swenson, S. C. and D. M. Lawrence, 2012. A new fractional snow-covered area parameterization for the Community Land Model and its effect on the surface energy balance, *Journal of Geophysical Research: Atmospheres*, **117**, D21107.

Tappeiner, U., G. Tappeiner, J Aschenwald, E. Tasser and B. Ostendorf, 2001. GIS-based modelling of spatial pattern of snow cover duration in an alpine area, *Ecological Modelling*, **138**(13), 265 – 275.

Trujillo, E., J. A. Ramrez and K. J. Elder, 2007. Topographic, meteorologic, and canopy controls on the scaling characteristics of the spatial distribution of snow depth fields, *Water Resour. Res.*, **43**(7), W07409.

Webster, R. and A. O. Margaret, 2007. Geostatistics for environmental scientists, Wiley, 2. ed.

Wehr, A. and U. Lohr, 1999. Airborne laser scanning - an introduction and overview, *ISPRS Journal of Photogrammetry and Remote Sensing*, **54**(2-3), 68 – 82.

Winstral, A. and D. Marks, 2014. Long-term snow distribution observations in a mountain catchment: Assessing variability, time stability, and the representativeness of an index site, *Water Resources Research*, **50**, 293305.

Xu, T., I. D. Moore and J.C. Gallant, 1993. Fractals, fractal dimensions and landscapes: a review, *Geomorphology*, **8**(4), 245 – 262.

Chapter 5

Locally extreme snow depths on glaciers

The idea for the work presented in this chapter came up at the Davos Atmosphere and Cryosphere Assembly DACA-13 in Davos (Switzerland). Besides the evaluation of areas with inter-annually consistent accumulation, areas of extreme snow depths are of interest in terms of their contribution to the total snow cover volume on glacier surfaces.

A poster on this topic was presented at the Alpine Glaciology Meeting in Innsbruck.

Helfricht, K., Lehning, M., Sailer, R. and Kuhn, M.: The influence of gravitational snow transport on the winter mass balance of Alpine glaciers in the Ötztal Alps. Poster presentation: *Alpine Glaciology Meeting in Innsbruck (Austria)*, 27-28 February, 2014.

The corresponding manuscript is in preparation. Parts of the manuscript are presented hereafter.

5.1   Introduction and Methods

Parameterizations based on terrain characteristics were developed to simulate gravitational snow transport in hydrological models by e.g. Gruber (2007) and Bernhardt et al. (2010). Machguth et al. (2006b) found that simple parameterization of gravitational snow transport improved model performance of glacier mass balance simulations. Likewise, Dadic et al. (2008) used a the slope-dependent parameterization of gravitational transport according to Gruber (2007) to improve glacier mass-balance estimations. As shown by Strasser (2008) and Warscher et al. (2013), the same

approach turned out to be a valuable tool to simulate snow transport from steep mountain slopes to the valley floors in hydrological model setups. Gravitational transport of snow by avalanches released in ice-free areas is known to be a significant part of the accumulation on Himalayan glaciers (e.g. Bolch et al. 2011, 2012), but mass budgets of gravitational snow transport on the catchment scale do not exist from these regions. Detailed studies on avalanche conditions and the final snow deposition were carried out by e.g. Sovilla et al. (2001, 2006), Sailer et al. (2008) or Schweizer et al. (2008). However, multi-annual data of extreme snow depths in total catchments at the end of the accumulation season are rare. In general, in-situ snow depth samples are risky in typical avalanche deposition zones. Since lidar technique enables data acquisitions of surface elevation changes even in inaccessible terrain, avalanches and snow depths were studied at the slope scale using terrestrial laser scanning (e.g. Prokop et al. 2008; Schaffhauser et al. 2008; Grünewald et al. 2010; Schirmer et al. 2011; Wirz et al. 2011).

The aim of this study is to investigate the spatial and temporal variation in extreme snow depths on glaciers from ALS data and their contribution to the total snow cover volume on glaciers. Thus, the five-year dataset of ALS derived snow depths (HS_{ALS}) on 13km^2 of glacier surface in the Upper Rofental catchment (Chap. 1.3.1) and the one-year data of HS_{ALS} on approx. 125km^2 of glacier surface in the entire mountain range were used to analyze the size of areas with extreme snow depths caused by lateral snow transport and the contribution of this increased snow deposition to the total snow cover volume. Glacier outlines of previous work were used (Chap. 4) and were drawn for the entire mountain range in 2010 according to Abermann et al. (2010). The size of the areas with extreme snow accumulation and their contribution to the the total snow cover volume are investigated. Multi-annual data are analyzed with respect to the spatial and temporal variation of extreme snow depths and their location to distinguish different processes of gravitational snow transport. The findings on extreme snow depths on glaciers in the entire mountain range are related to different glacier sizes.

According to the study presented in Chap 4, relative snow depths (HS_r) and standardized snow depths (HS_s) were calculated with

$$HS_r = \frac{HS}{\mu}, \tag{5.1}$$

and

$$HS_s = \frac{HS - \mu}{\sigma}. \tag{5.2}$$

where μ is the areal mean HS on each glacier separately and σ the corresponding

standard deviation.

To determine grid cells of extreme snow depths (HS_x), thresholds T of HS_r and HS_s were used

$$HS_x = HS \ (HS_{r,s} \geq T). \tag{5.3}$$

Increased snow depths exceeding the mean snow depth μ on the individual glacier (HS_{exc}) were calculated using

$$HS_{exc} = HS_x - \mu. \tag{5.4}$$

Raster cells showing extreme snow depths were aggregated into connected patches. The number of raster cells showing extreme snow depths n_x was multiplied with the size of the raster cells of $100\,\mathrm{m}^2$ to calculate the total area of extreme snow depths (A_x) for each glacier

$$A_x = n_x \cdot 100. \tag{5.5}$$

The exceeding volume (V_{exc}) on each glacier was calculated multiplying the mean of the exceeding snow depths $\bar{HS}_{exc}$ with A_x

$$V_{exc} = \bar{HS}_{exc} \cdot A_x. \tag{5.6}$$

Finally, A_x and V_{exc} were compared to the total glacier area and snow cover volume on the individual glaciers.

For the spatial and temporal analysis of connected areas of HS_x based on the multi-annual ALS data, the mean HS, mean slope, mean slope height and the corresponding normalized slope height were calculated for each patch of HS_x with a minimum size of $1000\,\mathrm{m}^2$.

5.2 Results

5.2.1 Multi-annual analysis of extreme snow depths

A threshold has to be determined for the extraction of areas with extreme snow depths. With respect to the high inter-annual variability of mean snow depths in this region (Helfricht et al. 2014b), standardized snow depths HS_s (Eq. 5.2) and relative snow depths HS_r (Eq. 5.1) were calculated. It is shown that similar cumulative proportions of glacier area and the corresponding volume of the snow pack were derived for HS_s (Fig. 5.1a left axis) and HS_r (Fig. 5.1a right axis)
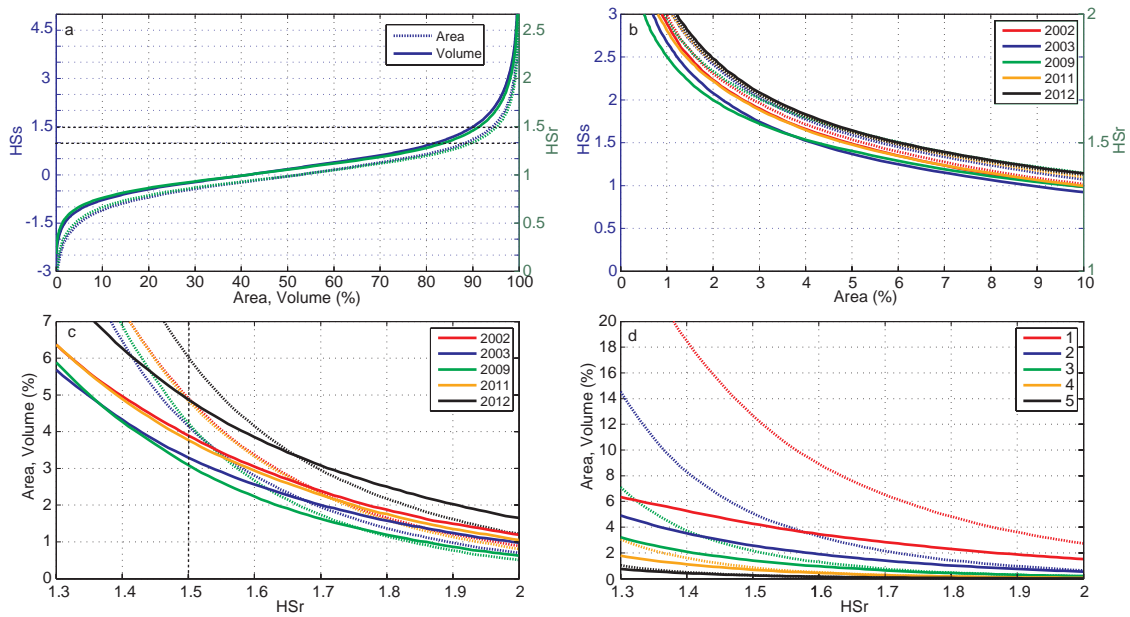
Figure 5.1: a) Cumulative proportion of the area (dotted lines) and of the volume (solid lines) for all HS corresponding to standardized snow depths (HS_s, blue) and relative snow depths (HS_r, green) less or equal than the given value. b) Percentage of the total area with values higher than the given HS_s (dotted lines) and HS_r (solid lines) separately for the five accumulation seasons. c) Percentage of the total area with HS_r higher than the given value (A_x, dotted lines) and the corresponding exceeding volume (V_{exc}) related to the total volume (solid lines) separately for the five accumulation seasons. d) Percentage of the total area with HS_r higher than the given values (A_x, dotted lines) and the corresponding exceeding volume (V_{exc}) related to the total volume (solid lines) for different years of occurrence.

of 1.5, where approx. 10 % of the total snow cover volume can be found at 5 % of the total area. HS_s of 1.5 would include 93.3 % of all HS in case of a normal distribution. Thus, inter-annually persistent A_x of 6 to 7 % of the total area could be expected. With respect to the not normal distribution, the inter-annual range of the area proportion is between 5 and 6 % for $HS_s \geq 1.5$ (Fig 5.1b). However, the inter-annual variability of the area proportion is higher for $HS_r \geq 1.5$. This range of 2 % corresponds to 50 % of the minimum area proportion of 4 % in 2003 and 2009 (Fig 5.1b). With respect to this higher inter-annual variability, we used HS_r of 1.5 as the threshold for HS_x. In general, the volume proportion of V_{exc} was about 1 % lower compared to the corresponding area proportion of A_x for HS_r of 1.5 (Fig. 5.1c).

We determined the overlapping regions for values of HS_r above a certain threshold for the five years investigated (Fig. 5.1d). Approx. 13 % of the total glacierized area turned out to show HS_x for $HS_r > 1.5$ at least one time within the five years.

The corresponding V_{exc} is less than 5 % of the total snow cover volume. A strong reduction in area affected by HS_x is obvious for locations with HS_x in at least two of the investigated years. Only a small area and volume fraction of less than 1 % shows HS_x in all of the five investigated years.

This may be seen as a surprising result given the fact that snow depth distributions have been found to be persistent at least in less extreme terrain (e.g. Schirmer et al. 2011). However, the less persistent pattern found here can be understood considering that the maximum snow depths in our terrain is at least partly caused by avalanches, which have inherently a more random probability of occurrence between the years.

Table 5.1: Ratio of area showing extreme snow depths (A_x) to the total glacier area and the corresponding fraction of exceeding volume (V_{exc}) to the total snow cover volume calculated with a threshold HS_r of 1.5 for the individual glaciers. n gives the number of years of occurrence. Glaciers are arranged with descending area of the 2011 extent. Mean area ratio and mean volume ratio for all glaciers in the catchment are shown.

	ID	Name	area (km^2)	n = 1	n = 2	n = 3	n = 4	n = 5
	1	Hintereis Ferner	6.99	0.14	0.05	0.02	0.01	0.00
	2	Kesselwand Ferner	3.65	0.08	0.04	0.02	0.01	0.00
	3	Vernaglwand Ferner Süd	0.51	0.10	0.04	0.02	0.01	0.00
	4	Mittlerer Guslar Ferner	0.43	0.05	0.02	0.01	0.00	0.00
area ratio	5	Hintereiswände	0.40	0.13	0.06	0.03	0.01	0.00
	6	Rofenberg West	0.34	0.12	0.02	0.01	0.00	0.00
	7	Vernaglwand Ferner Nord	0.22	0.09	0.05	0.04	0.01	0.00
	8	Rofenberg East	0.09	0.19	0.08	0.04	0.02	0.00
	9	Kleiner Guslar Ferner	0.01	0.03	0.02	0.00	0.00	0.00
	all		12.65	0.12	0.05	0.02	0.01	0.00
volume ratio	all		12.65	0.04	0.02	0.01	0.01	0.00

We calculated A_x and V_{exc} for each glacier in the subcatchment separately using a threshold HS_r of 1.5 (Table 5.1). Values of A_x for n = 1 range between 0.03 and 0.19 for the individual glaciers, where both limiting values were found at the two smallest glaciers.

Figure 5.2 shows the areal distribution of A_x. In general, areas of HS_x can be found along the foot of steep rock walls along the glacier margins. Only some areas of HS_x extend further onto the glacier. For instance, at the southern glacier margin of Hintereisferner (HEF), an area of HS_x is visible, for which the threshold was met more than once within the five years investigated. A_x with an occurrence of n = 5 are located very isolated at small cirques near steep rock faces. With respect to the presented spatial distribution of A_x (Fig. 5.2), areas of HS_x with $HS_r \geq 1.5$ give reasonable results for typical accumulation areas of gravitational mass transport.
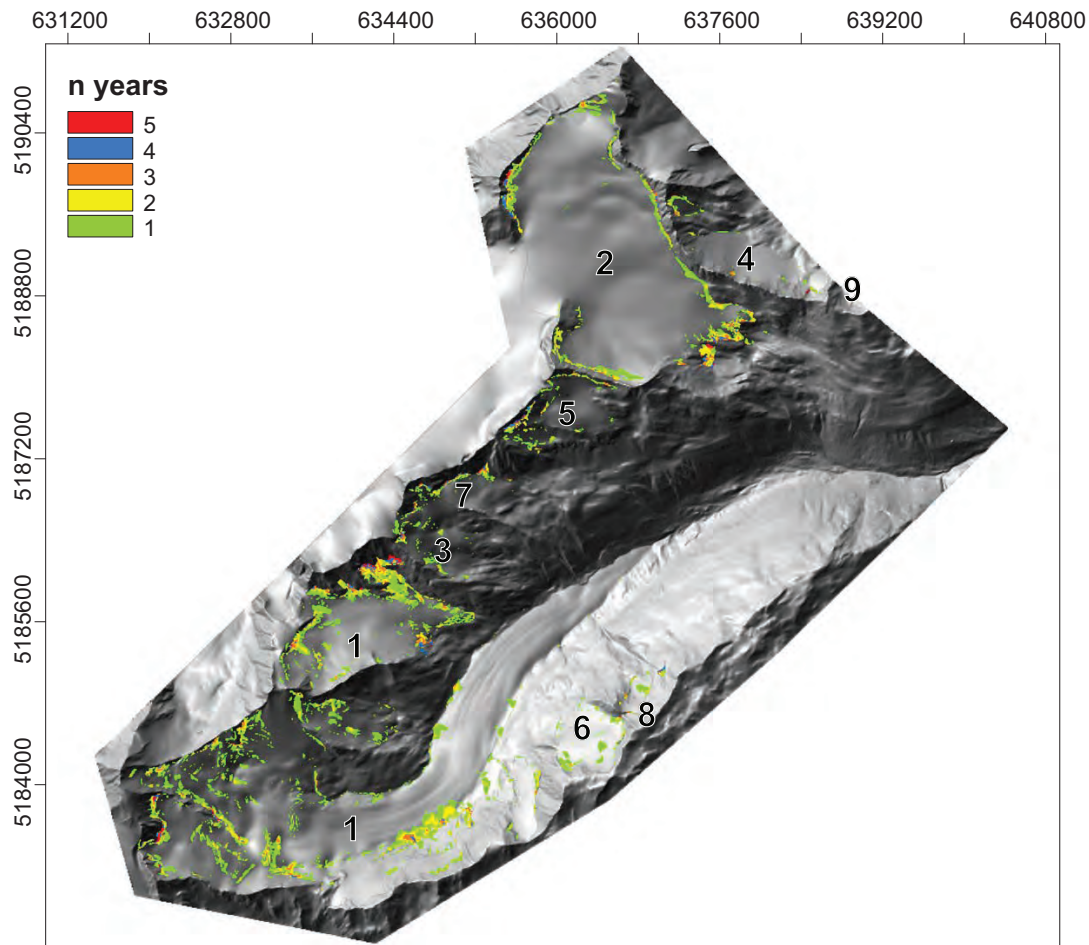
Figure 5.2: Distribution of areas affected by extreme snow depths ($HS_r \geq 1.5$) according to the number of years of occurrence. Shown IDs of the glaciers are listed in Table 5.1.

Mean slope angle, slope height and mean snow depth HS were analyzed for connected patches of extreme snow depths HS_x with $HS_r > 1.5$. Slope height is the vertical difference between the elevation of the foot of the slope and the elevation of the grid cell along the path of gravitational flow accumulation. The normalized slope height presents the position of HS_x in relation to the total vertical extend of the slope with values between 0 and 1 (equivalent to 0 and 100 %). Both parameters have lower values at the foot of the slope. Figure 5.3 presents the results for one, three and five years of occurrence.

Most of the area with extreme snow depths in at least one of the investigated years is located on slopes between 10 and 30° and at slope heights lower than 200 m (Fig. 5.3). The two largest connected patches are found on slopes between 20 and 30°, but at different absolute and normalized slope heights. Largest connected patches of HS_x with a occurrence in at least 3 of the investigated years are located at slopes between 20 and 40° and at approx. 30 to 60 % of the total slope height
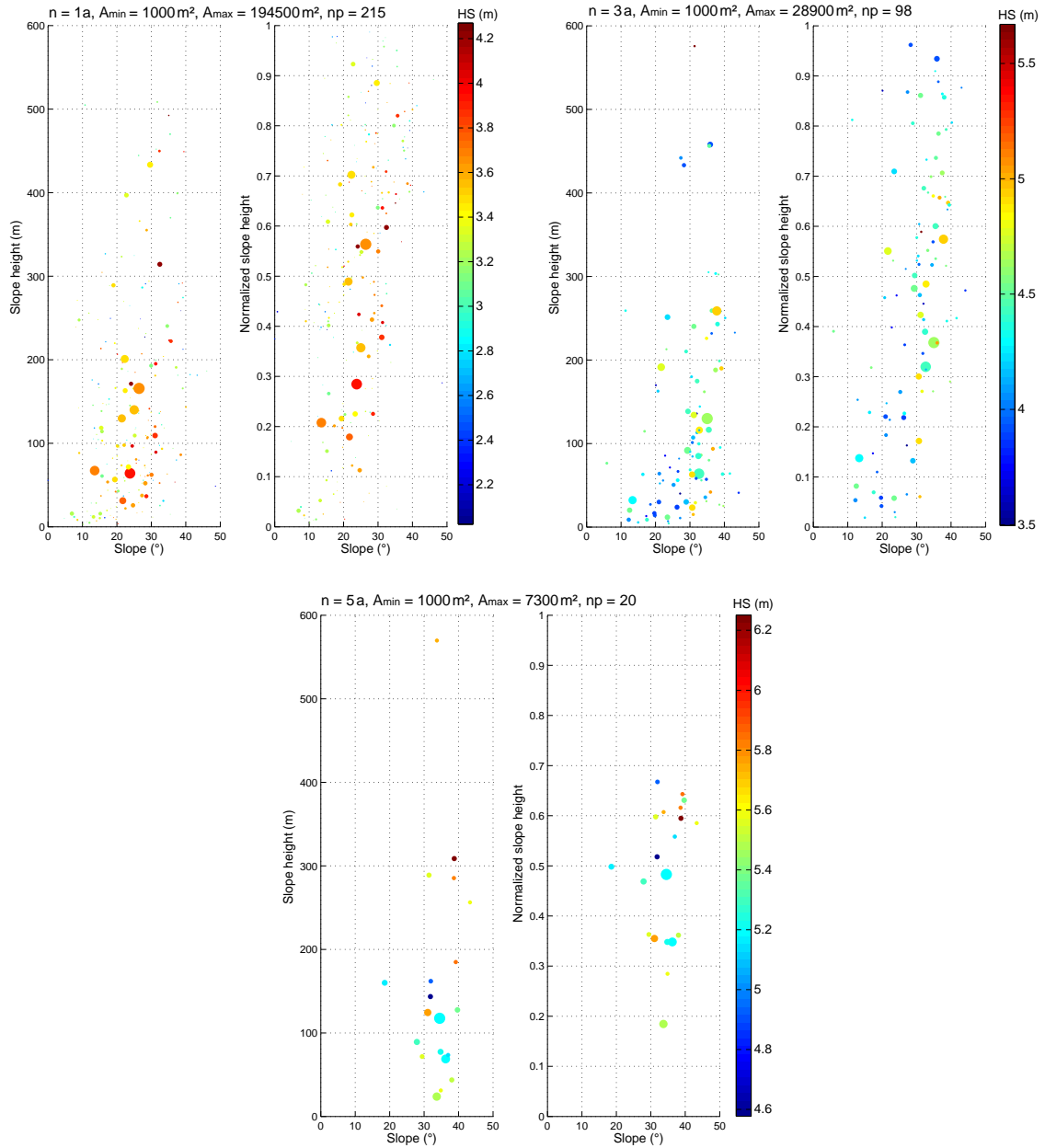
Figure 5.3: Mean slope, slope height, normalized slope height, snow depth (HS, color scale) and area (size of dots) of connected patches showing $HS_r \geq 1.5$ for different years of occurrence years (n). The number of years (n), minimum area (A_{min}) and maximum area (A_{max}) of the patches are given in the title of each subplot together with the total number of patches np. Note that the size of the dots is scaled to the corresponding A_{max}.

(Fig. 5.3). Smaller connected patches are found even in less steep areas (10 to 30 °) at the lowest 30 % of the slopes. A high number of patches were found in the upper 30 % of the slopes. In the upper 30 % of the slopes, comparatively small patches were found for an occurrance of 1 year. These patches were consistent for at least 3 years and are attributed to cornices and increased accumulation in wind sheltered areas next to the ridges. Only 20 connected patches with an area larger than $1000 \, \text{m}^2$ are identified for an occurrence of HS_x in all five investigated years (Fig. 5.3). Almost all of these patches are located at slopes between 30 and 40 °. Whereas larger patches are found in the lower half of the slopes, ten smaller patches are located between 50 and 70 % of the total slope height. In general, mean absolute snow depth HS in the patches (color scales in the subfigures of Fig. 5.3) increases with decreasing patch size and increasing annual occurrence of HS_x.

5.2.2   One-year analysis in the entire mountain range of the Ötztal Alps

A_x was determined for 188 glaciers in Ötztal Alps using a threshold HS_r of 1.5 (Fig. 5.4). Areas showing HS_x at the glacier tongues of Gepatschferner (box A) and Taschachferner (box B) are visually striking. These are the two glacier tongues with actually highest annual emergence flow of the ice in the investigated region. Thus, A_x are more likely caused by glacier dynamics than by extreme snow depths. At most of the other glaciers, HS_x can be found along the glacier margins at the foot of steep slopes and rock walls.

Table 5.2: Absolute and relative number of glaciers n and corresponding area for the given glacier size classes.

sice class (km^2)	<0.1	0.1 - 0.5	0.5 - 1	1 - 5	5 - 10	>10	Sum
n glaciers	82	69	13	16	7	1	188
n glaciers (%)	44	37	7	9	4	1	
area (km^2)	3.47	17.08	8.85	30.47	49.18	16.00	125.06
area (%)	3	14	7	24	39	13	

According to Abermann et al. (2009), results at the 188 glaciers were divided into 6 classes of glacier size (Tab. 5.2). The statistical distribution of mean snow depth μ, of HS_{exc} (Eq. 5.4) and of the ratios for A_x to the total glacier area and V_{exc} to the total snow cover volume are shown in Fig. 5.5. The high number of 82 small glaciers with a size of less than $0.1 \, \text{km}^2$ (44 % of the investigated glaciers) sum up to only 3 % of the total glacierized area (Tab. 5.2). HS_{exc}, the corresponding area A_x and V_{exc} are small at these glaciers. This can be caused by the generally higher mean
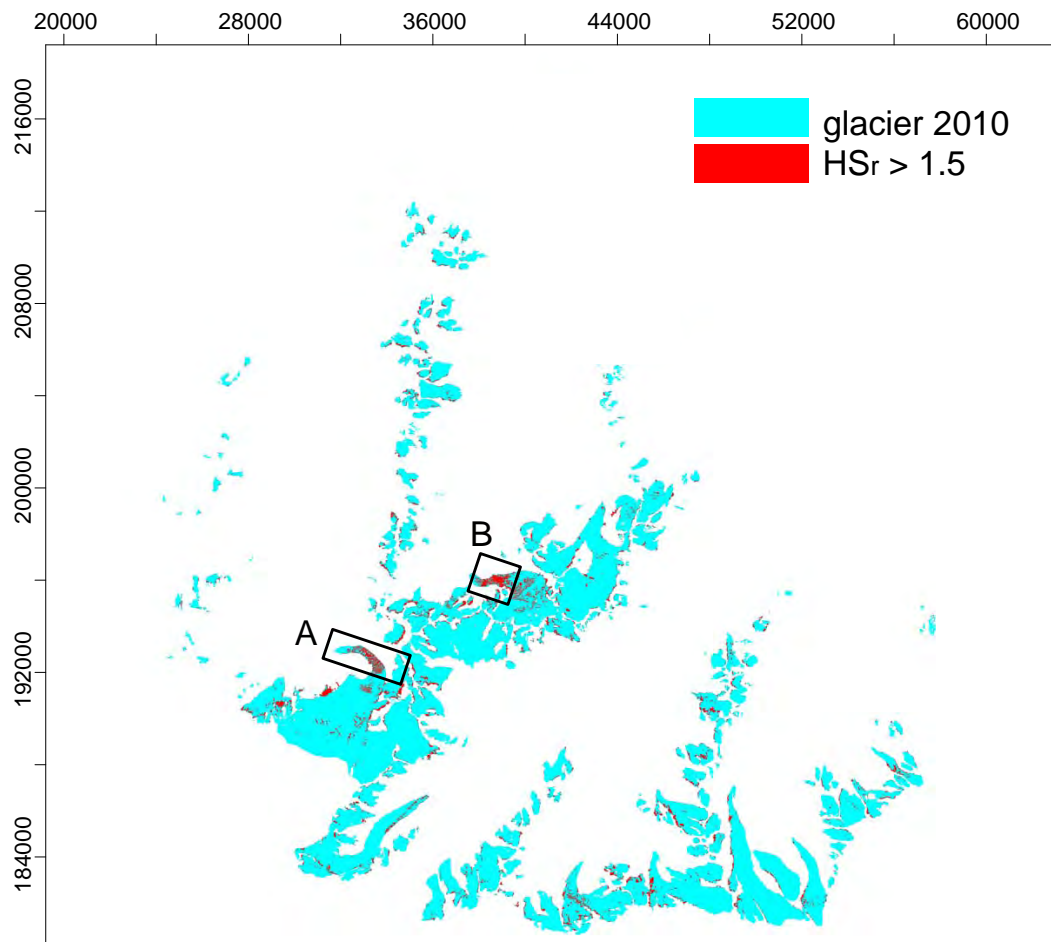
Figure 5.4: Spatial distribution of $HS_r > 1.5$ on glacier surfaces in the Ötztal Alps at the end of the accumulation season 2011. Box A and B highlight areas of HS_x, that are discussed in the text.
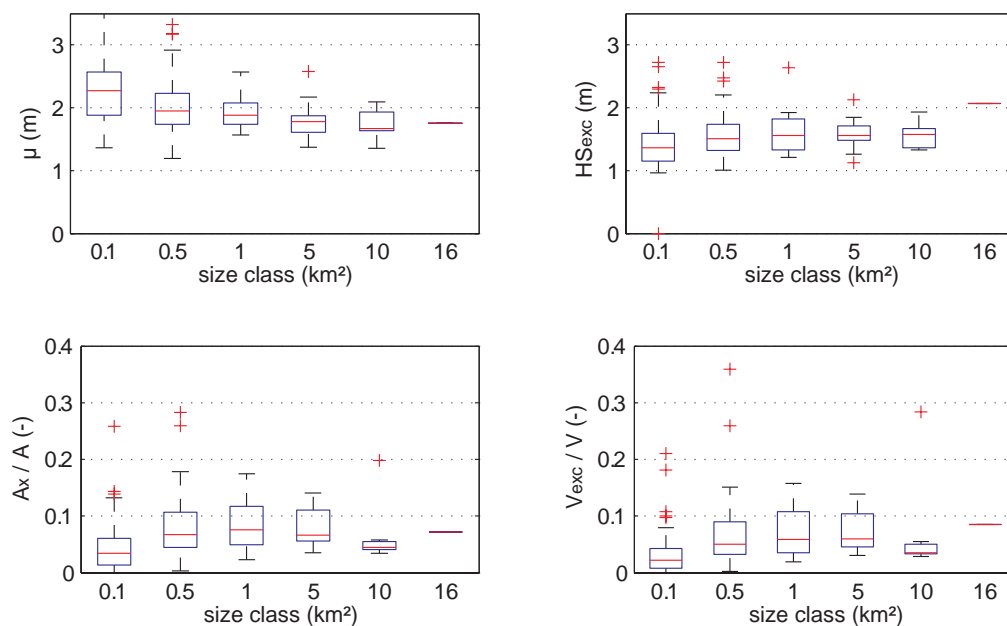
Figure 5.5: Boxplots of mean snow depth μ, snow depth exceeding mean snow depth HS_{exc}, the ratio of A_x to the total glacier area and the ratio of V_{exc} to the total snow cover volume calculated with $HS_r > 1.5$ for all glaciers subdivided into size classes. Note that the label of the size classes show the maximum glacier size and the corresponding minimum glacier size is given by the size class to the left. The number of glaciers in a size class is presented in Table 5.2. At each box-plot, the central mark is the median, the edges of the box are the 25th and 75th percentiles, the whiskers extend to extreme data points within 1.5 times the inter-quantile range and outliers are shown as red crosses.

snow depth μ compared to μ on larger glaciers.

At glaciers of a size between 0.1 and 5 km^2 (53 % of all investigated glaciers, 45 % of the total glacierized area), snow depths of 1.5 times the μ of approx. 2 m were exceeded at a mean A_x of less than 10 % of the total area. The median of V_{exc} on the glaciers of this size was about 5 %. The seven glaciers of a size between 5 and 10 km^2 show mean HS_{exc} similar to smaller glaciers, but the relative area affected by HS_x and V_{exc} is comparatively low. The outlier in the area- and volume-ratio can be assigned to Taschachferner, where the emergence flow at the glacier tongue can be assumed to cause overestimation of actual HS by Δz_{ALS}. Likewise, the only glacier of a size larger than 10 km^2, namely Gepatschferner, shows comparatively high HS_{exc}, A_x and V_{exc}, which is very likely caused by the contribution of snow covered crevasses and ice dynamics on Δz_{ALS}. In general, A_x as well as V_x are less than 10 % of the total glacier area and volume at more than 75 % of all glaciers. The area fraction of A_x considering all investigated glaciers is 7.1 % with a σ of 4.9 %. Mean volume fraction of V_{exc} is 6.6 % with a σ of 5.0 %.

5.3 Discussion

The area with extreme snow depth (A_x) has been analyzed as a function of the threshold used for HS_x (Fig. 5.1). By definition, HS_x with a certain threshold of HS_r increases with increasing mean snow depth μ. However, high μ do not necessarily increase avalanche activity (e.g. Haegeli and McClung 2003; Schweizer et al. 2008). In Chapter 4, two slopes in the investigated area are shown, where large snow amounts remained on the slopes at the end of the accumulation season with highest μ in 2009, whereas avalanches distributed almost the entire snow from these slopes to the glacier surface in 2002. It can be assumed that some of this snow load was redistributed to glacier surface in the following melt season and, thus, additional snow was accumulated in the typical avalanche deposition areas also in 2009. However, this shows that high avalanche activity is more caused by the formations of critical layering of the snow pack than by snow depth only. In addition, the progress of the melt season has some influence on the occurrence of wet snow avalanches from steep slopes prior the 'snow-on' ALS surveys.

In general, using a inter-annually consistent threshold of absolute HS is not applicable, because mean snow depths varied by a factor of two within the investigated years (Chap. 4). In case of avalanche release in years of high μ, typical accumulation areas of avalanches are assumed to show higher HS compared to avalanche deposition in years of lower μ such that these areas are captured by $HS_r \geq 1.5$ as well. Distinct accumulation areas of gravitational snow transport were found in a narrow zone along the foot of steep slopes and sheer rock walls in a terrain inclined more than $20\,°$. However, the areas with extreme snow depths vary considerably from year to year and this is in contradiction to known persistent snow patterns from snow transport and preferential deposition. Formally, this lack of interannual persistency is expressed by the fact that A_x determined for one year is on average twice as high as with the condition that extreme snow depth must be reached in at least two years.

On large glaciers, the analysis of HS_x from ALS data is influenced by firn densification and ice dynamics (e.g. Sold et al. 2013; Helfricht et al. 2014a). Annual emergence velocities of up to $5\,\text{m}\,\text{a}^{-1}$ were measured in the last years at the tongues of the glaciers Taschachferner and Gepatschferner (data not published yet). These areas of emergent ice flow are obvious in Fig. 5.4 box A and box B and cause an overestimation of A_x and V_{exc} of the glaciers (Fig. 5.5). A considerable underestimation of HS derived from ALS is very likely in the firn areas of the same glaciers because of ice flowing towards the ablation zone (Chap. 3). However, large deviations between actual HS and Δz_{ALS} are expected along the central flow line of the glaciers, but to be small along the glacier margins. In general, most of the glaciers

in the investigated region slowed down after a last advance in the 1980's (e.g. Span and Kuhn 2003; Abermann and Lambrecht 2007; Mayer et al. 2013). The influence of ice dynamics at small glaciers and at most of the tongues of larger glaciers ($A < 5\,km^2$) are assumed to be less than $0.5\,m$. For large glaciers like Taschachferner and Gepatschferner, corrections have to be considered in the calculation of HS from Δz_{ALS} as shown by e.g., Sold et al. (2013). However, these corrections require measurements and calculations of mass balance, which both are not available for the two mentioned glaciers. In contrast, actual ice dynamics of Hintereisferner allow to analyze Δz_{ALS} in terms of HS in a large part of the glacier (Chap. 3).

Open crevasses at the time of the ALS survey in fall, which are covered with snow at the end of the accumulation season contribute to overestimation of A_x. Although the crevassed area is small relative to the total glacier area and more frequent on the larger glaciers, HS_x might be large with respect to the penetration depth of the laser signal into crevasses. In this study, HS were analyzed in a raster resolution of $10\,m$. Thus, the influence of crevasses is smoothed. Some influence of crevassed areas on A_x is obvious on Hintereisferner (Fig. 5.2).

Some avalanches are released in steep ice covered slopes of the glaciers. Although these avalanches redistribute snow from steep slopes to flat glacier surfaces, no mass gain in terms of additional snow contributing to glacier mass balance is achieved. Hence, V_{exc} on glaciers is overestimated. For instance avalanches at the southern margin of Hintereisferner were released at a partly ice covered slope. However, with respect to the flat glacier surfaces, this contribution is assumed to be lower than $1\,\%$ of V_{exc}.

Extreme snow depths are assumed to be a result of both: the wind-induced preferential deposition first and the subsequent gravitational snow transport. The transport of snow by wind was found to contribute to the glacier mass balance and to cause increased accumulation in general (e.g. Kuhn 2003) and distinct areas of preferential snow deposition (e.g. Plattner et al. 2006; Dadic et al. 2010a,b; Mott et al. 2011b; Bernhardt et al. 2010). Downward wind in the lee side of ridges causes increased deposition, which in general is more homogeneous in distribution compared to locally limited avalanche accumulation. In contrast, the gravitational mass flow shows limited persistence within the five years. Inter-annually persistent depositions of gravitational snow transport are restricted to very small areas. Thus, the relative importance of gravitational mass flow can be seen less compared to the redistribution by wind. μ on small glaciers in wind sheltered cirques is higher compared to μ on larger glaciers. This results from the increased preferential deposition in the cirques caused by wind and avalanches (e.g. Kuhn 1995). Thus, with respect to the high μ, H_{exc}, are small and the relative area fraction of A_x might be underesti-

mated (Fig. 5.5). However, very small glaciers were found to show high variability of multi-annual volume change in the Austrian Alps (Abermann et al. 2009; Kuhn et al. 2012).

Two types of gravitational snow transport were determined to produce the observed patterns of HS_x. Avalanches with a occurrence of 1 or 2 times in the five investigated years are accumulated in slopes between 10 and 30°. Temporally more persistent snow sloughs accumulated in steeper slopes between 30 and 40°. These findings are consistence with the results of Gruber (2007), who found most avalanches at slopes toes inclined by 30 to 35° and few in flat terrain. (Sovilla et al. 2010) found most avalanches deposited on steep slopes in the range of 21 to 34°. They reported, that the depth of avalanche accumulation is strongly negatively correlated with the slope angle with shallow deposits at steep slopes. We found that the HS of avalanche accumulation patches increased with a increasing number of years of occurrence, whereas the area of the patches decreases to small areas of persistent snow sloughing, respectively.

In snow hydrology, accumulation is defined in terms of snow water equivalent (SWE). In this study, only HS was considered. To transform HS and snow cover volume into the mass of SWE, the bulk density of snow has to be known. Bulk density of snow shows only small variability at the start of melting season in high mountain catchments (e.g. Jonas et al. 2009; Schöber et al. 2014). With a variability of snow density in the order of $10\,\%$ and a mean bulk density of approx. $400\,\mathrm{kg\,m^{-3}}$, variability of V_{exc} is not higher than $0.5\,\%$ of the total snow cover volume. Typical densities of avalanches are found to be somewhat higher than the bulk density of snow at the end of the accumulation season with deposition densities of up to $560\,\mathrm{kg\,m^{-3}}$ (e.g. Sovilla et al. 2001, 2006). However, the accumulation of snow sloughs can be assumed to be less dense. Hence the contribution of the additional mass from gravitational mass transport to seasonal glacier mass balance might be somewhat higher than the fraction of V_{exc} to the total volume.

(Benn and Lehmkuhl 2000) described the influence of avalanches on the distribution of the equilibrium line altitude of glaciers in the Khumbu Himal. They discussed the importance of avalanches for the total accumulation on glaciers of different size, hypsometry and the existence of typical firn areas. Inter-annual variability of the mass balance of the investigated glaciers in the Ötztal Alps can be assumed to be less affected by avalanche deposition with respect to the different precipitation regimes and smaller elevation range of the glaciers and the adjacent mountain slopes.

The observed persistence of snow sloughs show that simple parameterizations of continuous gravitational snow transport like e.g. developed by Gruber (2007) or Bernhardt and Schulz (2010), are a valuable tool to consider typical areas of HS_x

in hydrological models. The application of such slope-dependent approaches were successfully integrated in spatially distributed hydrological models (e.g. Machguth et al. 2006b; Dadic et al. 2008; Strasser 2008; Warscher et al. 2013). However, the spatial model resolution has to be in accordance to the narrow areas of increased snow depth along steep slopes. Thus, spatial resolutions of 50 m or less need to be used in snow-hydrological models adapted to complex mountain terrain.

5.4   Conclusions

We show a method to locate areas of extreme snow depths at the end of the accumulation season. Multi-temporal ALS data with a high spatial resolution of seasonal snow depths are analyzed to investigate the contribution of locally extreme snow depths to seasonal snow volume on glaciers in a large part of the Ötztal Alps and for several glaciers in a partly glacierized subcatchment. Snow transport from ice-free terrain to glacier surface in terms of snow sloughs and avalanches contributes to seasonal mass balance at an area of 5 to 10 % of the total area of individual glaciers. The snow volume, which is redistributed by wind and gravitational transport to glacier surface and, thus, increases snow cover volume in addition to the accumulation by solid precipitation and wind drift, was found to be in the same magnitude. Large areas of avalanche deposits on flat surfaces were only found in one or two years of the five investigated seasons. Temporally more persistent snow sloughs increase snow in narrow zones along the glacier margins at slopes up to 40 °. These areas of typically extreme snow depths can be considered in snow-hydrological models using slope-dependent approaches. The data presented in this study show that parameterizations of mass transport to the foot of the slopes are in good agreement with multi-annual observations. However, affected area, additional volume and exceeding snow depths shown in this study are a reliable basis to validate model results for gravitational snow transport. The extension of this data set and the application of ALS to obtain snow cover distribution in different mountain regions can give more insights in avalanche distribution in mountain catchments and their contribution to glacier mass balance.

Chapter 6

Assimilating ALS data in hydrological models

At the *alpS - Centre for climate change adaptation technologies* (Innsbruck, Austria), two spatially distributed energy balance models, namely SES and AMUNDSEN, are used for hydrological simulations of partly glacierized catchments in the Ötztal Alps (Tyrol, Austria). Even though the models are designed for different purposes in terms of flood forecasting (SES) and simulation of reservoir inflow (AMUNDSEN), model performance of both models was improved by assimilation of ALS derived snow depths into model calibration and validation. In this Chapter, already published results and recent work are presented to emphasize the value of ALS derived snow depth data for hydro-meteorological simulations.

6.1 The snow and ice melt model SES

In the frame of the project HoPI (Hochwasser-Prognose Inn) a flood forecasting system of the Tyrolean river Inn was developed (Kirnbauer et al. 2009; Achleitner et al. 2012). Whereas runoff of most areas is calculated using an HRU based model, glacierized catchments at the Alpine main ridge are simulated using the fully-distributed energy balance model SES (Asztalos 2004). The model is based on the work of Blöschl et al. (1991a) and was designed for flood prognosis in hourly resolution. SES calculates the snow water equivalent (SWE) of the snow cover in the total catchment and the firn layer on glaciers. Melt is simulated for snow, firn and the ice at glacier surface. A linear reservoir approach model is used to rout meltwater and precipitation runoff (Nash 1960; Asztalos et al. 2006). Besides a digital elevation model for the derivation of topographic information, SES requires the meteorological input data of precipitation, temperature, global

radiation, relative humidity and wind speed. For more information on model equations and model performance the reader is referred to the original publication of Kirnbauer et al. (2009) and Schöber et al. (2014). In the following some findings of the study of Schöber et al. (2014) are presented. They are linked to the results of the publications in Chapter 3 and 4 and emphasize the value of using ALS derived snow depth distributions to calibrate and validate simulated SWE.

6.1.1   Publication in Journal of Hydrology

HYDROL 19326
Schöber, J., Schneider, K., Helfricht, K., Schattan, P., Achleitner, S., Schöberl F. and Kirnbauer, R. (2014): Snow cover characteristics in a glacierized catchment in the Tyrolean Alps - Improved spatially distributed modelling by usage of Lidar data, *Journal of Hydrology*, Available online 16 January 2014, ISSN 0022-1694, http://dx.doi.org/10.1016/j.jhydrol.2013.12.054.

Schöber et al. (2014) investigated accumulation characteristics at the end of winter in a partly glacierized catchment in the Austrian Alps. Remotely sensed snow covered area (SCA) and SWE derived from ALS data were assimilated in an extensive calibration and validation scheme for the Vent catchment. The study focused on the validation of modeled SWE with SWE maps calculated from ALS data. The SWE maps were produced from ALS derived snow depths applying a linear regression between snow depth and snow density developed on the basis of a large data set of complementary measurements.

ALS derived accumulation patterns were related to elevation, slope and curvature to simulate the variability of the snow cover. Both, modeled SCA and volume of the snow cover were in good agreement with observed values on the watershed scale. Spatial variability of the snow cover, expressed by subpixel variability of the 1 m original ALS derived snow depths HS_{ALS} within 50 m grid cells in terms of the CV (e.g. Marchand and Killingtveit 2005), appeared to be low on glaciers and on northerly exposed ice-free slopes in higher elevations (Fig. 6.1). This is caused not only from a more homogeneous snow cover, but also from high HS_{ALS} in these areas. Pixels on south facing slopes, areas with shallow snow cover, and in more general pixel in ice-free areas show large sub-pixel variability up to 100 % or even more. ALS data were successfully assimilated in a Monte Carlo calibration scheme. Results of spatially distributed snow water equivalent modeled with SES (SWE_{SES}) of the best model run were compared to ALS derived snow water equivalent (SWE_{ALS}).
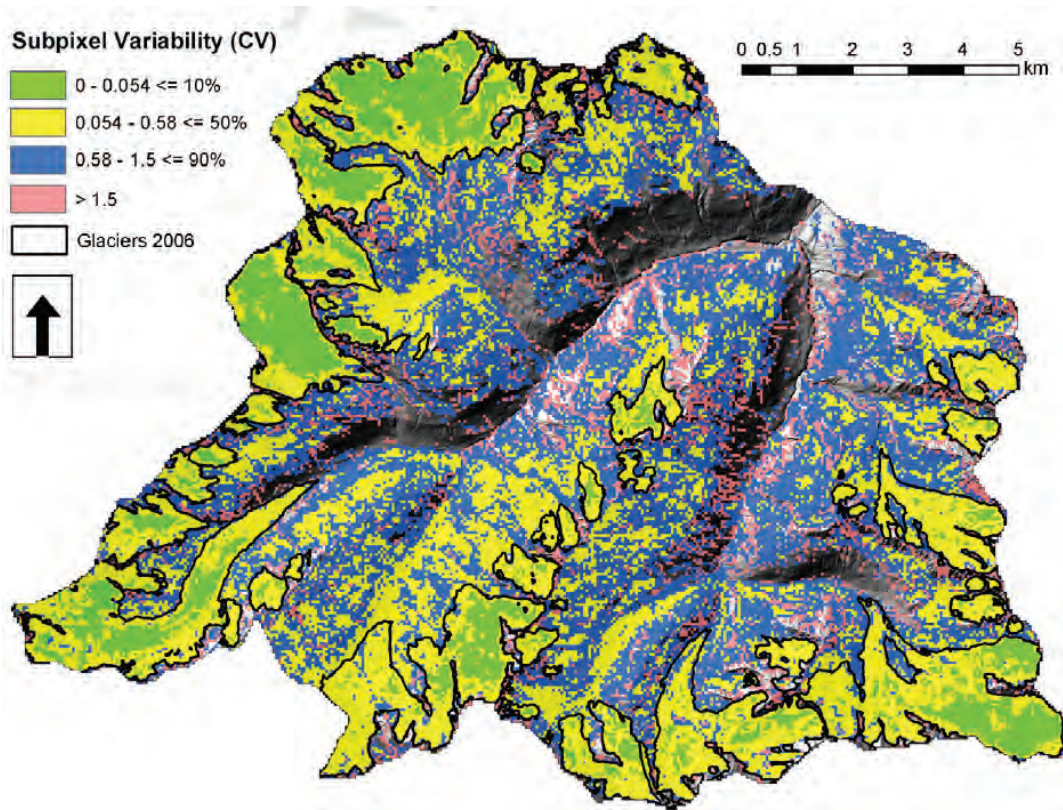
Figure 6.1: Analysis of the sub-pixel variability of HS_{ALS} in the Vent catchment on 20 April 2011: coefficient of variation (CV) of all HS_{ALS} pixels with $1\,\text{m}$ resolution within one $50\,\text{m}$ SES-pixel (Schöber et al. 2014).

$72\,\%$ of all pixels have a deviation between the ALS derived accumulation SWE_{ALS} and the simulated snow water equivalent SWE_{SES} that is lower than 200 mm. The Mean Pearson correlation between SWE_{ALS} and SWE_{SES} is 0.72. Thus, SES satisfyingly reproduce the observed variability of SWE, although the snow cover simulated using SES is apparently smoother compared to ALS derived snow distribution (Fig. 6.2 a and b). The SWE residuals (i.e. the difference of SWE_{ALS} minus SWE_{SES}) are shown for the total catchment (Fig. 6.2 c) and a subregion in the Upper Rofental (Fig. 6.3). In general, modelled residuals are positive (i.e. SWE_{ALS} exceeds SWE_{SES}) on Hintereisferner, whereas negative residuals are obvious on e.g. Kesselwandferner and Vernagtferner.

To analyse the distribution of the residuals in more detail, firn areas and ice areas were delimited using a Landsat image from 31 August 2009 (according to Chap. 3). Most of the negative residuals are located in the firn areas of the glaciers (Fig. 6.2 d, red outline). The median of the residuals is -137 mm SWE in the firn area of Kesselwandferner, whereas the median of the residual in the ice area is -29 mm SWE. The mean relative deviation between SWE_{ALS} and SWE_{SES} in the firn areas of all glaciers in the catchment (Fig. 6.3, GV-firn) is -13 % (-19 % without Hintereisferner)
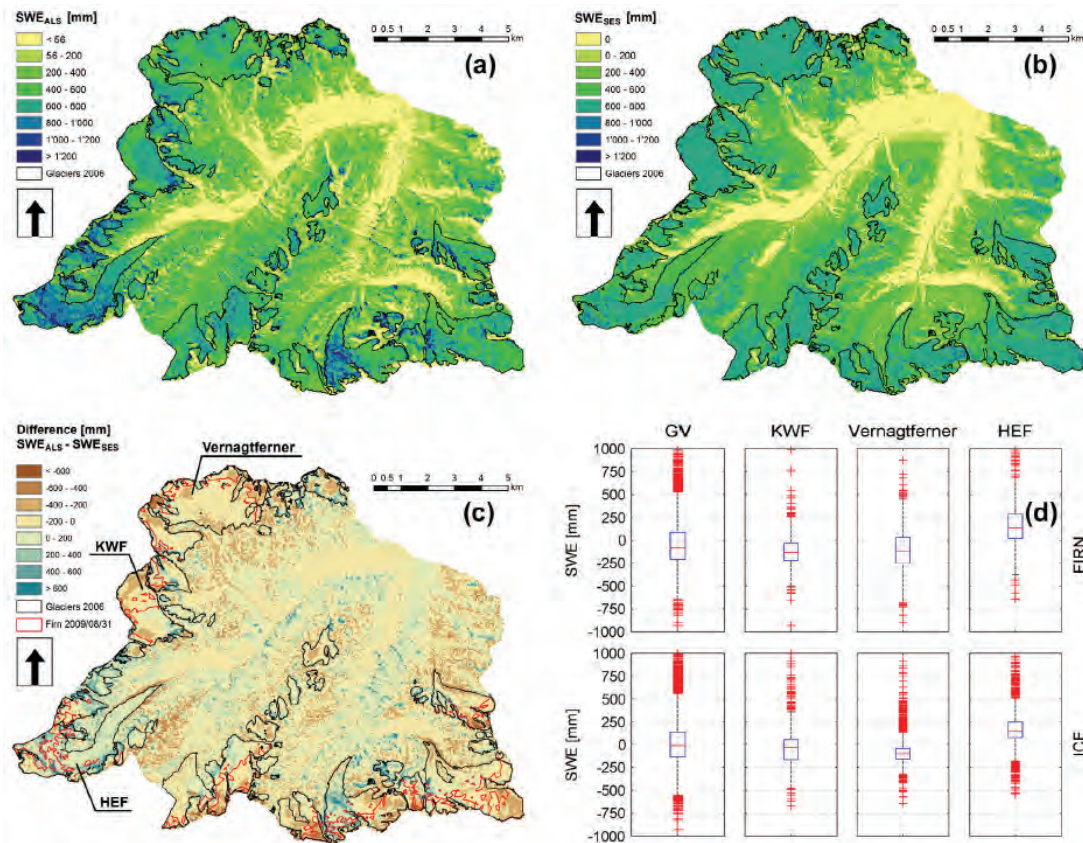
Figure 6.2: The distribution of (a) SWE_{ALS} and (b) SWE_{SES} in the Vent catchment on 20 April 2011. In (c) the distribution of the pixel-wise residuals is plotted. Besides the glacier boundaries outlines of firn areas are given. The boxplots in (d) show the statistical distribution of residuals for the glaciers Hintereisferner (HEF), Kesselwandferner (KWF), Vernagtferner and all glaciers of Vent catchment (GV) subdivided in firn and ice areas (Schöber et al. 2014).

and hence close to the detected deviations between HS_{ALS} and HS_{GPR} measured on glaciers in this catchment (Chap. 3). Higher values of SWE_{SES} compared to SWE_{ALS} are seen as uncritical in the firn areas, where HS_{ALS}, and hence SWE_{ALS}, is influenced by submergence and firn densification. Median residuals close to zero for the ice areas of the entire catchment (GV-ice) are in agreement with the results for HS_{ALS} presented in Chap. 3. Hence, differences between HS_{ALS} and HS_{GPR} found in Chap. 3 on three glaciers of the study region are transferable to the glaciers of the Vent catchment. However, SWE_{SES} is generally lower than SWE_{ALS} on Hintereisferner, either on firn or on ice (Fig. 6.3). This is not related to glacier dynamics. The most likely reason is that the available meteorological data does not reflect the conditions on Hintereisferner (e.g. Hoinkes and Steinacker 1975; Kuhn et al. 1999). Redistribution of snow towards this low elevated glacier tongue is assumed to increase accumulation (Kuhn 2003).
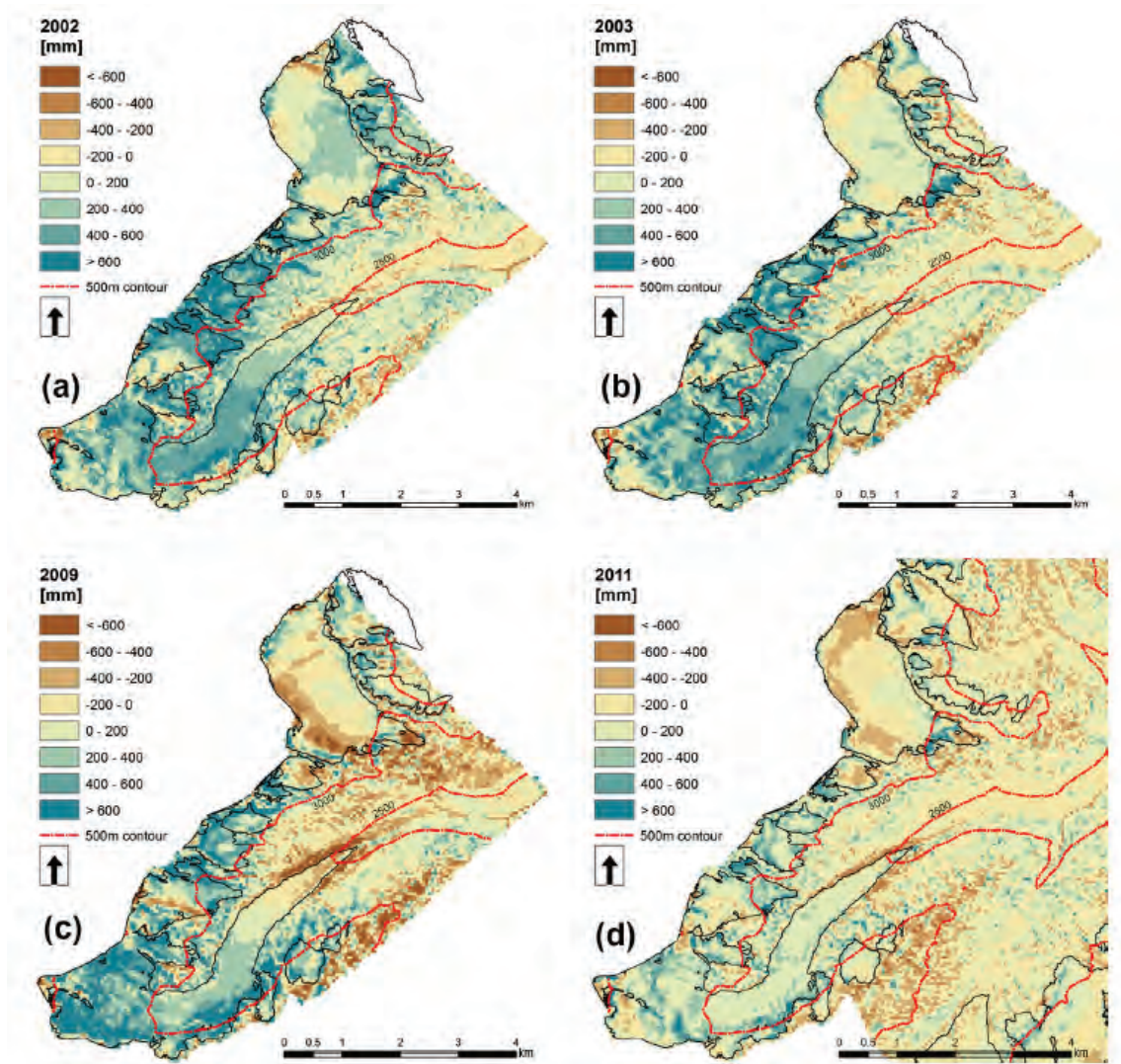
Figure 6.3: Maps of residuals between SWE_{ALS} and SWE_{SES} in the HEF catchment for the available ALS datasets; (a) 7 May 2002, (b) 4 May 2003, (c) 7 May 2009, (d) 20 April 2011. Brownish colors show higher SWE_{SES} compared to SWE_{ALS} (Schöber et al. 2014).

In Schöber et al. (2014), the ability of ALS data to improve the hydrological simulations is shown. In contrast to uncertainties of winter precipitation measurements in mountain catchments of up to 50 % (e.g. Sevruk and Nespor 1998), the assessed uncertainty range for mean SWE_{ALS} in the order of 15 % is comparatively low. Schöber et al. (2014) emphasize the vital importance of including basin-wide SWE measurements in hydrological model applications at the watershed scale. These findings are beneficial for improvements in water resources management.

6.2 Adaptation of AMUNDSEN to the Ötztal Alps

The *A*lpine *MU*ltiscale *N*umerical *D*istributed *S*imulation *EN*gine AMUNDSEN was developed by Strasser (2008) to simulate the snow cover in mountain regions with a high spatial and temporal resolution. Based on a digital elevation model, AMUNDSEN calculates the surface energy balance considering spatially varying shortwave and longwave radiation fluxes caused by topographic effects. Evapotranspiration and snow-canopy interaction are calculated and gravitational snow transport is implemented using the approach of Gruber (2007). Different layers of snow, firn and ice are treated separately in terms of albedo parameterizations and water storage characteristics. AMUNDSEN requires the meteorological input of precipitation, temperature, global radiation, relative humidity and wind speed.

In the frame of the alpS-project MUSICALS (*MU*ltiscale *S*now/*IC*e melt simulation into *AL*pine reservoir*S*), AMUNDSEN was adapted to a large part of the mountain region of the Ötztal Alps (Tyrol, Austria). The aim of the project was to simulate the contribution of discharge from approx. $560\,\text{km}^2$ partly glacierized catchments to inflow of the Gepatsch reservoir (46° 56' N, 10° 44' 30" E) more realistically with respect to the contribution of snow and ice melt. Initial ice thickness distribution of all glaciers in the Ötztal Alps was calculated using the method of Huss and Farinotti (2012) (Seiser et al. 2012). Required glacier surface elevations and glacier outlines of the year 1997 exist from the Second Austrian Glacier Inventory (Lambrecht and Kuhn 2007). The linear reservoir approach used by Asztalos et al. (2006), which is based on Nash-cascades (Nash 1960), was included in AMUNDSEN to transfer surface melt and precipitation discharge to hourly runoff. Warscher et al. (2013) developed a module to simulate snow redistribution. It considers the sky view with respect to the main wind direction. Using this approach, reasonable snow patterns were simulated in the complex terrain of the Berchtesgaden Alps (Bavaria, Germany). However, test runs for the Ötztal Alps showed that increased snow depths on glacier tongues compared to ice-free terrain could not be reproduced.

In AMUNDSEN, snow accumulation on slopes inclined more than 35° is consistently redistributed to the base of the hillsides using the fast and mass-conserving algorithm to parameterize mass transport and deposition developed by Gruber (2007). However, initialization of this gravitational transport with uncorrected snow accumulation on steep slopes results in unrealistically high snow depths in small areas in the transition zone from flat to steep terrain at the end of accumulation season. When summer melt is less than the accumulation in these zones, extreme snow

depths potentially accumulate to high snow walls in long-term simulations.

One objective of the project was to analyze ALS derived snow depths and develop a more reasonable method to redistribute solid precipitation within the catchments prior applying parameterizations of processes adding small-scale spatial variability to snow cover distribution (i.e. redistribution by wind, gravitational snow transport). To account for this preferential deposition, topographic derivatives of the local terrain were tested.

6.2.1 Topographic correction of snow depths

Several empirical models correlate snow cover distribution in mountain catchments to topographic parameters such as elevation, slope and northing (Chap. 1.2.2). Additionally, curvature was found to be useful to simulate small scale variability in snow distribution (e.g. Blöschl and Kirnbauer 1992; Huss et al. 2008; Sold et al. 2013; Schöber et al. 2014). However, modeling the increased snow depth on low elevated glacier tongues is still challenging (e.g. Dadic et al. 2008, 2010a; Schöber et al. 2014).

In this study, the descriptive power of topographic openness was investigated for the simulation of spatial snow cover variability. Originally, topographic openness was developed to visualize topographic character and features in images (Yokoyama et al. 2002). It expresses the degree of dominance or enclosure of a location on an irregular surface. Topographic openness is a measure for the viewshed and calculated from multiple zenith and nadir angles along multiple azimuths. It has two viewer perspectives in terms of positive and negative openness. The latter describes the attribute below the surface (Fig. 6.4) and has low values for convex and high values for concave forms (Fig. 6.5). For detailed explanations of fundamental equations the reader is referred to the work of Yokoyama et al. (2002).

Negative openness turned out to have a higher descriptive power compared to positive openness, which is more similar to the sky view factor. Negative openness values depend on the maximum distance (calculation radius) L which is considered for calculation. Short L result in a high spatial variability of negative openness. Large L values include large scale topography of ridges and valley floors and hence highlight the over-deepening of e.g. the surface elevations of glacier tongues compared to the surrounding ridges and peaks. Maps of the spatial distribution of negative openness calculated with $L = 10\,m$ (Fig. 6.6c) and $L = 5000\,m$ (Fig. 6.6d) for surface topography in the Hintereisferner region are shown in Fig. 6.6b. In general, the potential of negative openness to reproduce spatial variability of HS_r (Fig. 6.6a, Chap. 5.1,
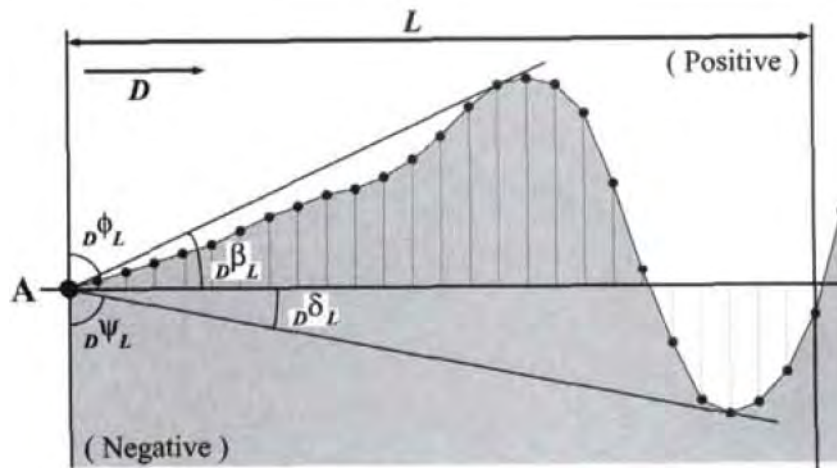
Figure 6.4: Positive and negative surface openness defined in terms of zenith and nadir angles (from Yokoyama et al. (2002)). Different results (black dots) for different calculation radius L are shown.
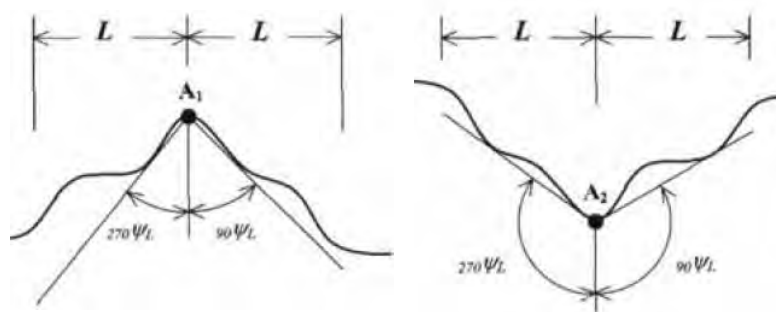

Figure 6.5: Low and high values of negative surface openness at illustrated profile of a hilltop along azimuth for convex and concave surfaces, respectively (from Yokoyama et al. (2002)). The calculation radius L is shown.

Eq. 5.1) on scales of some meters (e.g. at ridges, deep channels) to scales tens to hundreds of meters (glacier surfaces) is obvious. A stepwise forward multiple regression analysis was applied to highlight the descriptive power of negative openness for the spatial distribution of relative snow depths HS_r. Three statistical model setups were compared:

- (i) a model including standard parameters of elevation, northing, slope and curvature

- (ii) a model including elevation and negative openness with ranges L of 10 and 5000 m

- (iii) a model including all six parameters.

A spatial resolution of 10 m was used for the calculation of the parameters elevation, slope, northing and curvature. The regession analysis was based on a very high number of points (n = 361302). Thus, the coefficient of determination r^2 was similar to the adjusted r^2 up to the fifth decimal precision.

Table 6.1 shows the derived multiple regression equations, r^2 and the mean of the squared residuals (MSE) for the multiple linear regressions (i)-(iii). The model (i) has a lower r^2 and a higher MSE compared to model (ii). Thus, the model (ii) including negative openness explains more of the spatial variability of HS_r. The extension of the model (ii) with the parameters of model (i) does not result in a higher model efficiency. The stepwise selection scheme of model (iii) is presented in Table 6.2. After step 3, when both negative openness and elevation are included, model performance does not increase considerably with additional parameters.

Spatially distributed HS_r calculated with the regression model (ii) and (i) are shown in Fig. 6.6 e and f, respectively. Whereas both look similar and are in good agreement with the spatial distribution of ALS derived HS_r, differences can be obtained from the direct comparison of these two model results (Fig. 6.7). The model (ii) shows less HS_r compared to model (i) at exposed ridges. Model (ii) results in higher HS_r in the cirques of typical glacier accumulation areas. Two areas are marked in Fig. 6.7, which both were found to show increased snow depths (Chap. 4). Area A is influenced by snow which is redistributed from the glacier plateau of Gepatschferner to sheltered cirques. High avalanche activity observed in area B (Chap. 5) may result from increased snow accumulation caused by topographic shelter of this particular slope.
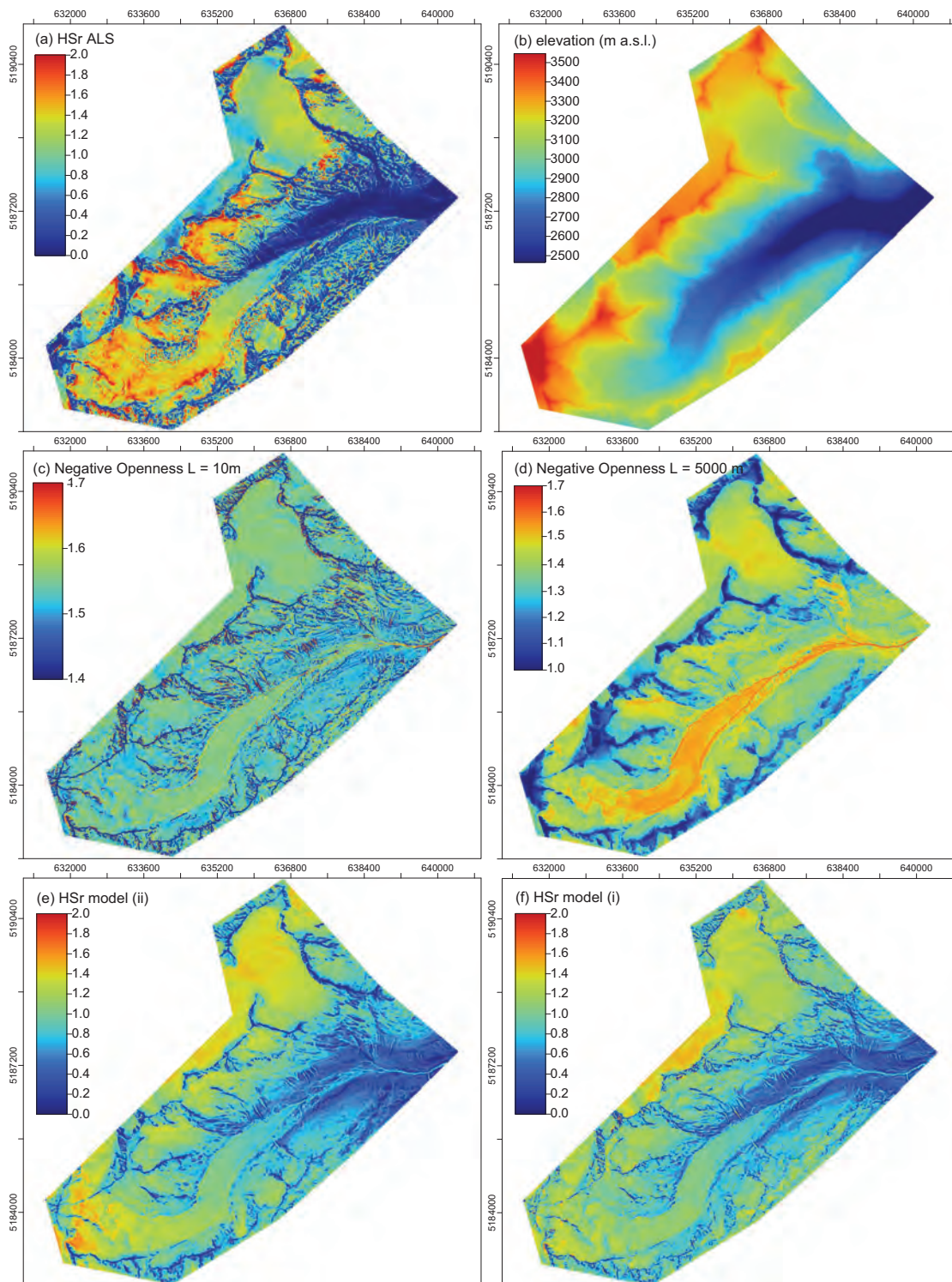
Figure 6.6: Maps of (a) multi-annual mean relative snow depth HS_r, (b) elevation, (c) negative openness with $L = 10\,m$, (d) negative openness with $L = 5000\,m$, (e) the regression result of model (ii) (including elevation, negative openness with $L = 10\,m$ and negative openness with $L = 5000\,m$) and (f) the regression result of model (i) (including elevation, slope, northing and curvature).

Table 6.1: Results for a stepwise forward linear regression including the shown parameters elevation z, negative openness with a range of $10\,\mathrm{m}$ no_{10}, negative openness with a range of $5000\,\mathrm{m}$ no_{5000}, northing n, curvature c and the slope α in a spatial resolution of $10\,\mathrm{m}$.

ID		model parameters							r^2	r^2_{adj}	MSE
(i)	HSr =	$0.000685\,z$			$-0.00073\,n$	$-8.3765\,c$	$-0.01476\,a$	-0.7413	0.32	0.32	0.21
(ii)	HSr =	$0.001098\,z$	$+1.9608\,no_{5000}$	$+1.6534\,no_{10}$				-7.5807	0.39	0.39	0.19
(iii)	HSr =	$0.001177\,z$	$+2.3165\,no_{5000}$	$-0.2822\,no_{10}$	$-0.00085\,n$	$-4.8132\,c$	$-0.00025\,a$	-5.2823	0.40	0.40	0.19

Table 6.2: Results of the stepwise forward selection scheme adding the parameters presented in the second column.

Model Step	variable	r^2	r^2_{adj}	MSE
1	neg. openness $L = 10\,m$	0.18	0.18	0.25
2	elevation z	0.29	0.29	0.22
3	neg. openness $L = 5000\,m$	0.39	0.39	0.19
4	northing n	0.39	0.39	0.19
5	curvature c	0.40	0.40	0.19
6	slope α	0.40	0.40	0.19

Model (ii) can reproduce $39\,\%$ of snow cover variability in a spatial resolution of $10\,\mathrm{m}$. A r^2 of 0.45 resulted using the setup of model (ii) in a spatial resolution of $50\,\mathrm{m}$. Compared to Grünewald et al. (2013), who derived adjusted r^2 of 0.5 for the same region but a rather coarse raster resolution of $400\,\mathrm{m}$, these values satisfyingly confirm the application of the terrain openness in simple relations between topography and snow cover distribution even for spatial resolutions of some tens of meters. However, elevation is required to reproduce spatial variability of the snow cover in statistical models, because it aggregates the effects of melt in lower elevations, varying snow line elevations during precipitation events and the increasing precipitation with elevation.

6.2.2 Simulating the snow cover in the Ötztal Alps

The findings of Chapter 6.2.1 were used to model snow distribution and runoff from the Ötztal Alps. Negative openness was calculated for the entire Ötztal mountain range based on a $50\,\mathrm{m}$ DEM with $L = 50\,m$ and $L = 5000\,m$. The average of both openness calculations was calculated for each raster cell. A linear relation was applied between the minimum and the maximum threshold of negative openness and a correction factor for solid precipitation. At least $10\,\%$ of the initial solid precipitation can be stored even in almost vertical slopes and in very exposed areas. Wind-sheltered areas can aggregate a maximum of 1.6 times the initial solid precipitation. This is a value similar to the redistribution factor derived by Kuhn (2003)
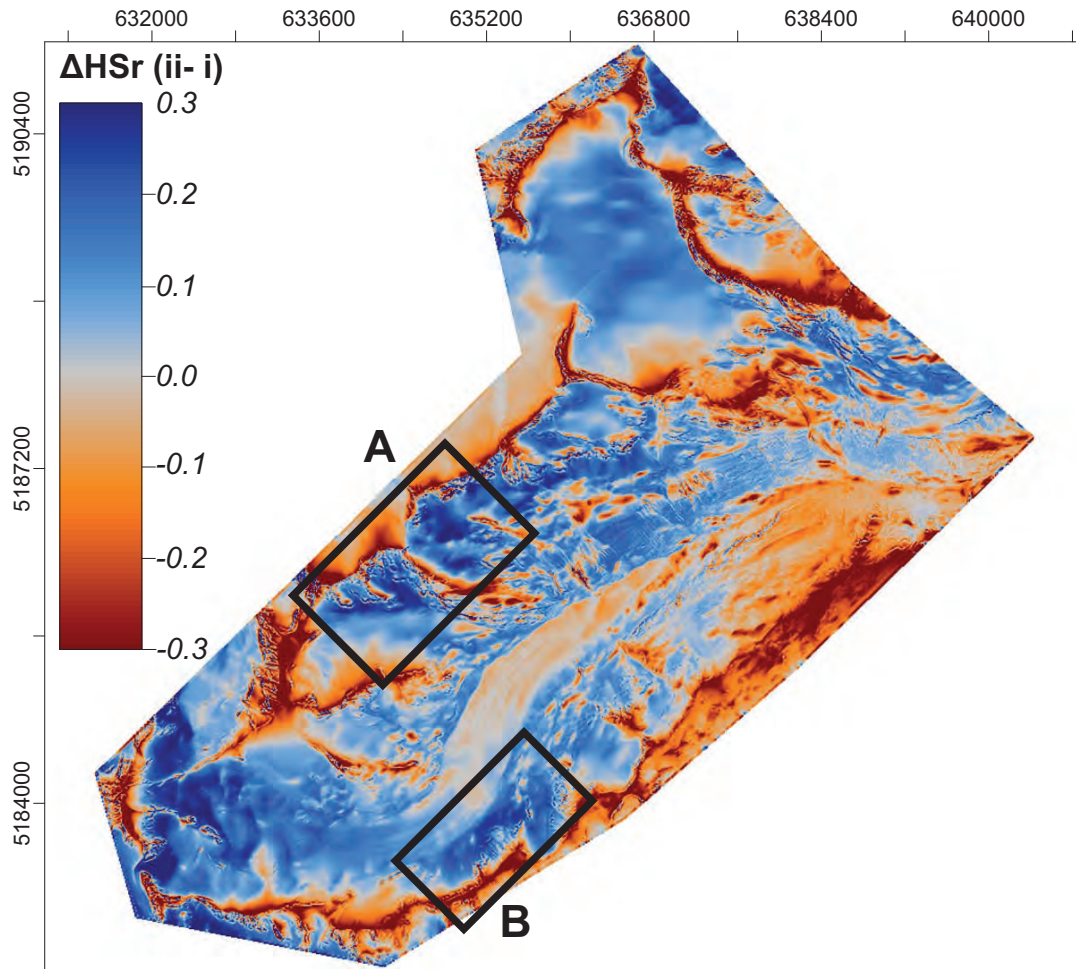
Figure 6.7: Differences in HS_r between the regression result (ii) (including elevation, negative openness with $L = 10\,m$ and negative openness with $L = 5000\,m$) and the regression result (i) (including elevation, slope, northing and curvature).

for basins in the Ötztal Alps. At each time step, solid precipitation of each raster cell is multiplied with the corresponding correction factor. The new total amount of solid precipitation over the entire area is related to the initial precipitation amount to keep the total precipitation volume constant. This ratio, again, is applied to each raster cell. Consequently, simulated accumulation is reduced in areas of low negative openness (i.e. exposed ridges, sheer rock faces) and increased in flat and sheltered areas (i.e. cirques and low elevated valley floors). However, the value range of calculated negative openness and the final relation to precipitation correction are site-specific and have to be calibrated for study regions individually.

Model results of spatially distributed snow water equivalent (SWE_{sim}) at the end of accumulation season were compared to the SWE_{ALS} derived for the winter 2010/2011 (Chap. 6.1.1). SWE_{ALS} was calculated from Δz_{ALS} using the statistical regression between HS and snow density according to Schöber et al. (2014).
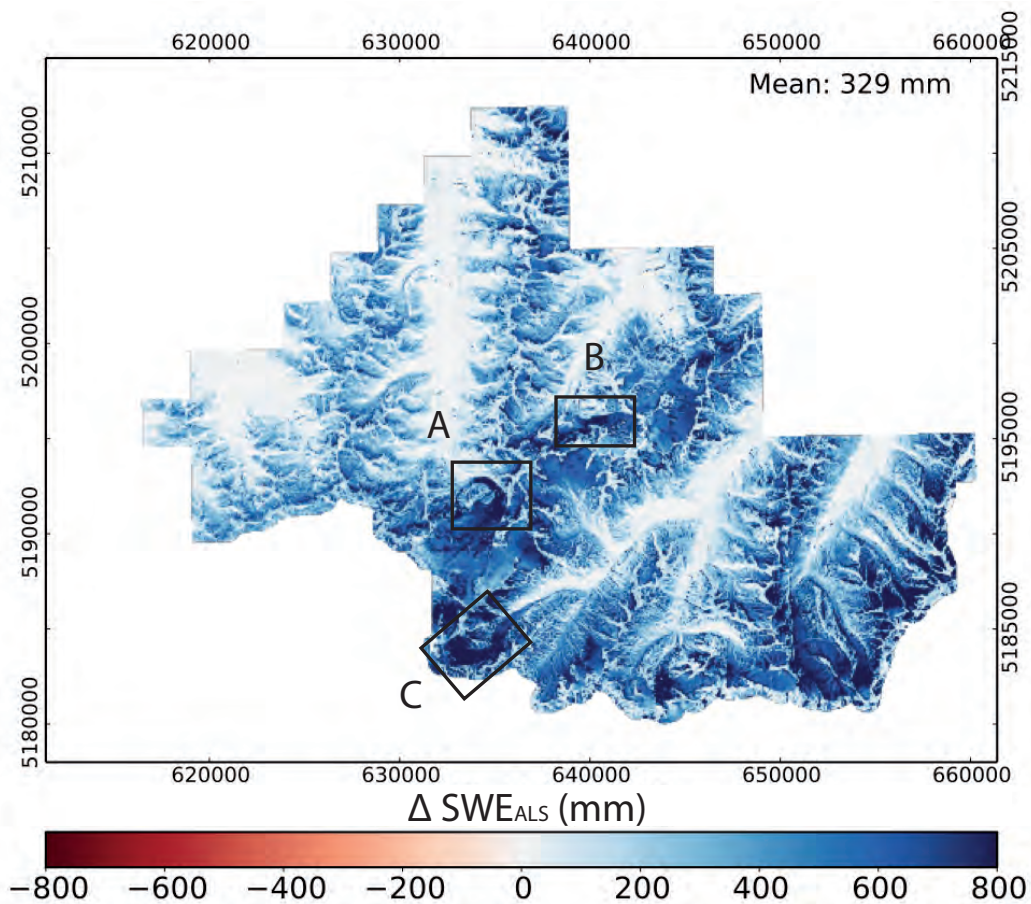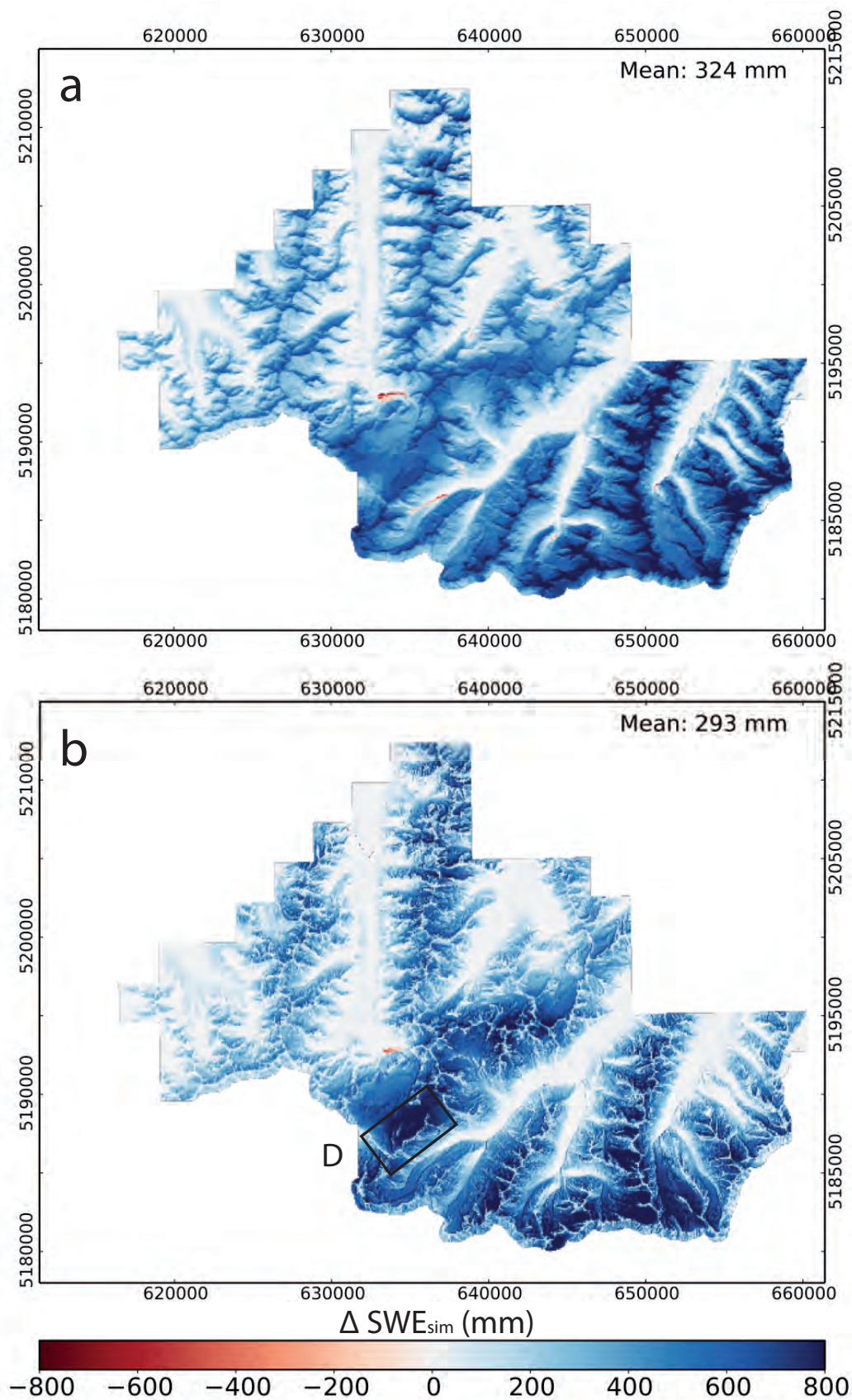
Figure 6.8: Difference in SWE distribution in the Ötztal Alps between the 8 October 2010 and 20 April 2011 calculated from ALS measurements. The boxes A, B and C highlight areas of high surface elevation changes that are discussed in the text.

Fig. 6.9 shows the SWE_{ALS} and SWE_{sim} simulated with elevation correction of precipitation only and with additional topographic correction using the redistribution scheme including negative openness. Areas of high SWE_{ALS} can be found at the glacier tongues of Gepatschferner (Fig. 6.8, box A) and Taschachferner (box B). At these two glaciers tongues Δz_{ALS} and hence SWE_{ALS} is highly influenced by emergence of the ice flow. Recent measurements of the ice flow at the glacier tongues of Gepatschferner and Taschachferner show annual vertical velocities in the magnitude of up to $5\,\mathrm{ma}^{-1}$ (unpublished data). These values are assumed to show locally limited maximum of vertical ice flow in the investigated area. Most of the glaciers in the Ötztal Alps slowed down dramatically after an glacier advance in the 1980's and show only small horizontal and even less vertical ice flow (e.g. Span 1999; Span and Kuhn 2003; Abermann and Lambrecht 2007; Blumthaler 2011).

Figure 6.9: Difference in SWE distribution in the Ötztal Alps between the 8 October 2010 and 20 April 2011 a) simulated with an elevation gradient of precipitation only and b) simulated with topographic correction. The box D highlights an area of high accumulation that is discussed in the text.

Fig. 6.9a shows (SWE_{sim}) applying only a precipitation gradient without topographic correction of the solid fraction. In comparison to SWE_{ALS}, higher SWE_{sim} is simulated at the mountain crests and less SWE_{sim} is simulated for the valley floors and on the glaciers. The application of the redistribution scheme including negative openness resulted in more realistic simulation of snow distribution with almost no snow on ridges and higher SWE_{sim} on glaciers compared to SWE_{sim} at the adjacent slopes (Fig. 6.9 b). As discussed in Chap. 6.1.1, high accumulation on Hintereisferner in 2011 (Fig. 6.8, box C) can not be simulated using standard precipitation input in hydrological models adapted to the entire mountain region. In contrast, SWE_{sim} at the highest elevations of the glaciers is constantly higher than SWE_{ALS} (Fig. 6.9 b, box D). In these typical accumulation areas of the glaciers, Δz_{ALS} underestimates actual HS and thus actual SWE_{sim} of the snow cover due to ice flow and densification of the firn layer. In Chapter 3, it is shown that typical values of underestimation of HS by Δz_{ALS} in firn areas of the glaciers in this region is 0.4 m on average. This corresponds to a SWE_{sim} of approx. 160 mm assuming a typical bulk snow density of $400\,\mathrm{kg\,m^{-3}}$ for snow at the end of accumulation season.

In general, it is obvious that the topographic correction using negative openness shifts reliable amounts of simulated accumulation from the mountain crests to the flat valley floors and to glacier surfaces. These results are promising, even that a large part of the Ötztal Alps (approx. $560\,\mathrm{km^2}$) was simulated at once.

6.2.3   Results of the runoff simulations

Runoff was modeled for the total investigated mountain range of the Ötztal Alps using the spatially distributed model AMUNDSEN in a spatial raster resolution of 50 m and in hourly time steps from 1997 to 2010. The model was calibrated on runoff data of the years 1997 to 2006 and simulated runoff was validated for the years 2007 to 2010. An example of the simulated and the observed runoff is given in Fig. 6.10 for the Gepatsch catchment, which drains directly into the reservoir (Chap. 1.3.1, Fig. 1.4). In general the fit between observed and simulated runoff is promising with respect to the objective of simulating the short-term reservoir inflow. Daily cycles of runoff are captured and timing of runoff contributions from snow, firn and ice are reasonable. For instance, after the cold period in mid of July 2000 associated with solid precipitation in high elevations, runoff is again generated from snow melt before ice melt starts. Observed peaks of runoff caused by heavy rain events are not captured by the simulated runoff. Often, locally limited orographic precipitation is not measured at the rain gauges and, thus, the resulting peak runoff can not be simulated.

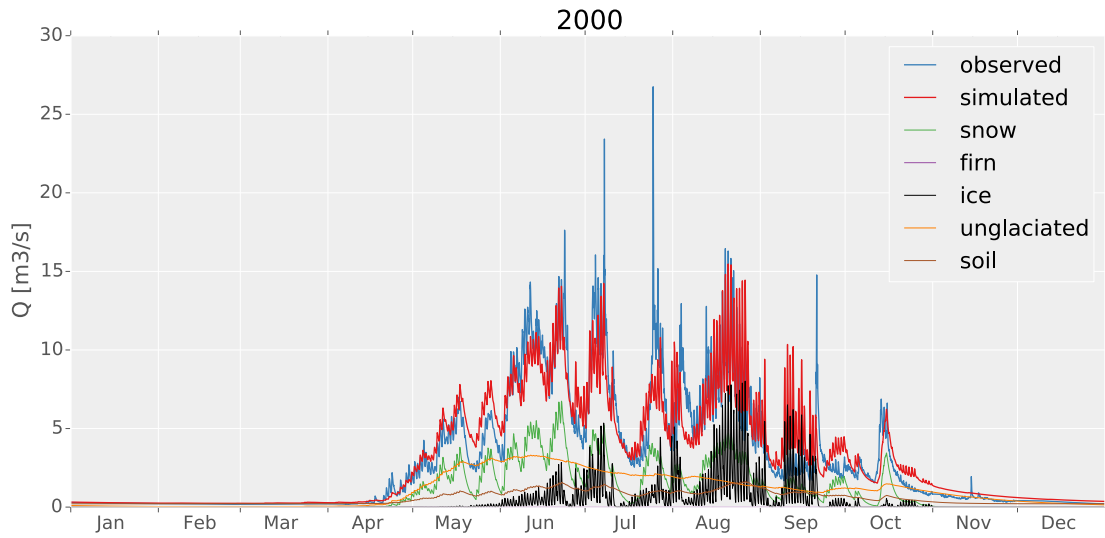Simulated runoff is compared to runoff measurements at 8 gauge stations. In total

Figure 6.10: Example of hourly runoff simulation with AMUNDSEN at the gauge station Gepatschalm in the year 2000. The outflow of each linear reservoirs which contributes to total runoff is plotted separately.

the catchment area contributing to measured runoff is $415 \, \text{km}^2$, which corresponds to $74 \, \%$ of the total investigated area. Size and the ice covered fraction of the catchments are given in Table 6.3. The Nash-Sutcliff-Efficiency NSE (Nash and Sutcliffe 1970) and the volume bias, calculated using observed runoff q_{obs} and the simulated runoff q_{sim} with

$$bias = \frac{\sum(q_{obs} - q_{sim})}{\sum q_{obs}} \qquad (6.1)$$

are used to evaluate the model performance.

Table 6.3: Calibration (cp) and validation (vp) results for runoff simulation with AMUNDSEN in the given partly glacierized catchments.

catchment			cp 1998 - 2006		vp 2007 - 2010	
name	size (km^2)	ice cover 1997 (%)	NSE	bias	NSE	bias
Vent - Rofenache	98.6	38.3	0.84	0	0.82	-0.1
Obergurgl - Gurgler Ache	72.4	31.8	0.82	-0.02	0.79	-0.06
Vent - Niedertal	66.7	31.1	0.79	-0.02	0.68	0.15
Taschachbach	60.5	24.0	0.84	-0.01	0.81	0.05
Gepatschalm	53.9	39.7	0.86	-0.01	0.82	0
Pitze	27.0	48.2	0.88	0	0.85	0
Radurschlbach	24.0	1.5	0.64	0.07	0.62	-0.12
Fissladbach	11.4	2.1	0.66	-0.01	0.74	-0.13

For the six largest catchments, the high mean NSE of 0.84 for simulated hourly runoff in the calibration period and 0.8 for the validation period, respectively, shows that the annual and daily cycle in runoff are well captured. However, NSE is lower for small catchments with almost no glacier surfaces. In these catchments, overall runoff amount is small and errors in precipitation measurements, which are used as model input, have a strong influence on model efficiency. The volume bias is rather small in the calibration period, but shows some higher values in the validation period.

6.2.4 Evaluation of simulated surface elevation changes of glaciers

The application of hydro-meteorological models for long-term runoff-simulations in partly glacierzed mountain catchments requires not only evaluation of simulated runoff, but also information on snow cover and the storage of water in the glaciers (e.g. Blöschl and Kirnbauer 1992; Kuhn 2000; Huss et al. 2014). Whereas modeled SWE was already evaluated by SWE_{ALS}, a realistic snow and ice ablation would secure a realistic simulation of the contribution of the cryosphere to total runoff.

Kuhn et al. (2009) and Huss (2012) showed that the transfer of mass balance from measured to unmeasured glaciers is challenging with respect to meteorological conditions and different glacier types. The simulation of a large part of the total Ötztal Alps with AMUNDSEN is not assumed to reproduce single glacier mass balances. It rather should be able to simulate long term changes of the storage and release of water from the cryosphere. Glacier volume changes can be derived from the glacier inventory of the Ötztal Alps for the period between 1997 and 2006 (Abermann et al. 2009, 2012). These observed surface elevation changes (Δh_{obs}) correspond to a period of nine years and were used to validate surface elevation changes simulated with AMUNDSEN (Δh_{sim}) for the same period. SWE_{sim} was converted into Δh_{sim} using different bulk densities for ice ($900\,kg\,m^{-3}$), firn ($750\,kg\,m^{-3}$) and old snow ($500\,kg\,m^{-3}$).

The mean surface elevation change over this period derived from the glacier inventory was -5.47 m (Fig. 6.11 a). Surface elevation change simulated with AMUNDSEN is -6.06 m (Fig. 6.11b). Thus, the mean value of simulated multi-annual volume loss of the cryosphere is approx. 11 % more negative compared to the observed value.
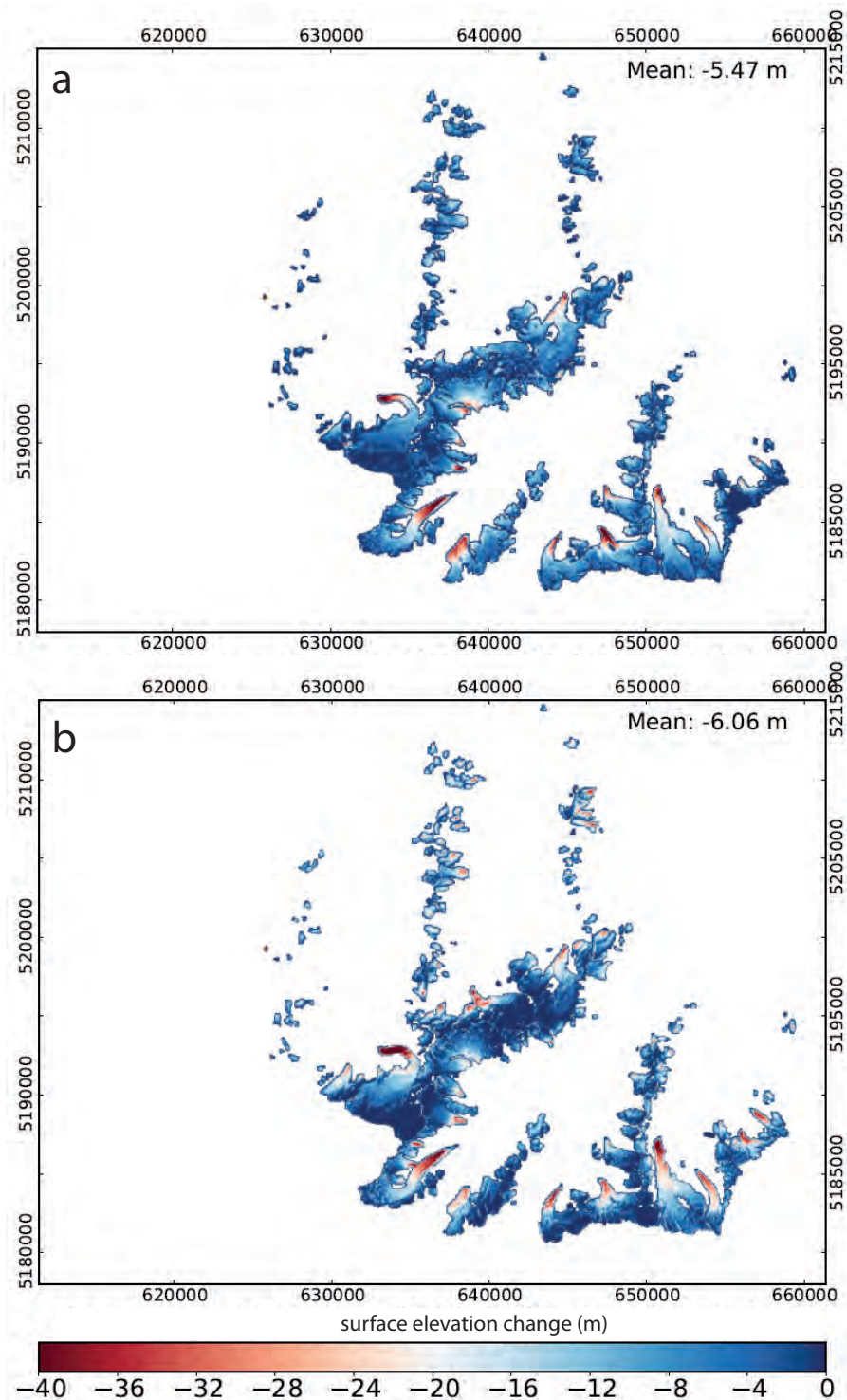
Figure 6.11: Surface elevation changes a) observed on glaciers in the Ötztal Alps between 1997 and 2006 (Δh_{obs}, Austrian glacier inventory,Abermann et al. (2009, 2012) and b) simulated with AMUNDSEN (Δh_{sim}).

However, surface elevation changes of the glacier inventory are calculated from geodetic surveys and, thus, include the contribution of ice flow. Also basal and englacial melt processes contribute to geodetic volume changes. These processes have to be considered when comparing geodetic and direct glaciological mass balance (e.g. Zemp et al. 2010; Fischer 2011). Figure 6.11 shows the two maps of spatially distributed Δh_{obs} and Δh_{sim}. In the higher elevated areas of the glaciers, Δh_{sim} are higher compared to Δh_{obs}. In contrast, at the low elevated glacier tongues, Δh_{sim} were more negative compared to Δh_{obs}. The statistical distributions of the residuals between Δh_{sim} and Δh_{obs} are shown for individual elevation zones in Fig. 6.12. In the elevation of the largest glacier area at about 3050 m a.s.l., the median of the residuals is close to zero. Δh_{sim} is higher than Δh_{obs} at glacier surfaces above 3200 m a.s.l. Maximum of mean residuals is 2.4 m at an elevation of about 3450 m a.s.l.. Residuals of up to $2\,\text{ma}^{-1}$ were found, which is similar to observed ice submergence velocities (Chap. 3). Towards the glacier tongues, the residuals between Δh_{sim} and Δh_{obs} are negative. However, processes as increased ablation caused by layers of dust or thin debris cover on glacier surface, basal and englacial melt and the soil and debris budget at the glacier bed can reduce the difference between simulated ablation and observed surface lowering at the glacier tongues. Negative residuals below 2400 m a.s.l. can be assigned to the glacier tongue of Gepatschferner, which features increased vertical ice flow. However, residuals between Δh_{sim} and Δh_{obs} are small at the very front of this glacier tongue. This can be related to the very rapid downwasting of the partly debris covered glacier tongue of up to $8\,\text{ma}^{-1}$ (unpublished measurements). Additionally, residuals are small if ice thickness is low at the glacier tongue and disappeared in both, simulation and observation, within the investigated period.

However, areas of large differences between Δh_{sim} and Δh_{obs} are restricted to a small number of glaciers. Additionally, high rates of submergence and emergence can be expected at the central flow line, but are assumed to be small towards the glacier margins.

In general, these findings are in good agreement with the educated guess of the difference between geodetic and surface mass balance. Up to now, glacier dynamics are not considered in the model setup of AMUNDSEN. This is also due to the complex topography and very variable ice dynamics of the individual mountain glaciers (Chap 3). Modeling the dynamical response of glaciers in this region needs further investigation and measurements at glaciers which still show distinct ice flow. Nevertheless, simulated surface mass balances have to be corrected for glacier dynamics especially in long-term simulations of glacierized mountain catchments (e.g. Huss et al. 2008, 2010; Sold et al. 2013). This is not relevant for the operational application of AMUNDSEN in short-term runoff forecast as long as the glacier area
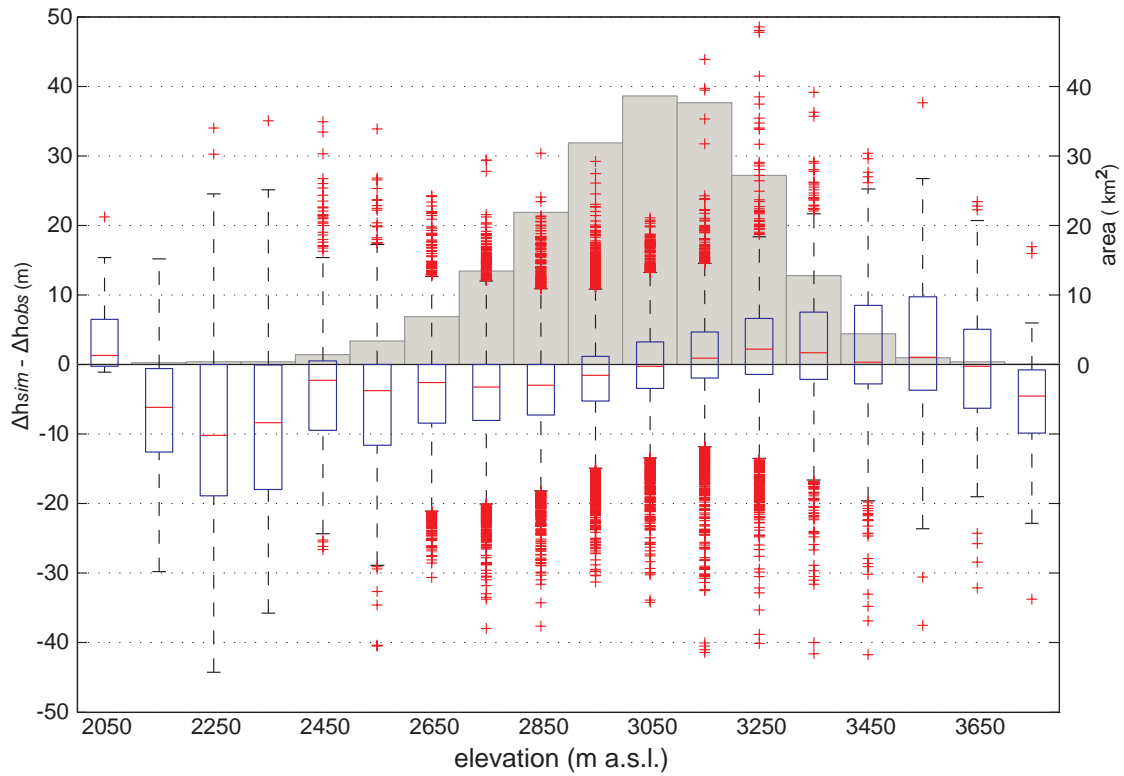
Figure 6.12: Residuals between simulated surface elevation change on glacier surfaces Δh_{sim} and observed glacier thickness changes Δh_{obs} (Austrian Glacier Inventory, Abermann et al. (2009, 2012)) for the period 1997 to 2006. Statistical distributions are shown for all 50 m grid cells in 100 m elevation zones. Note that the red line shows the median, the edges of the box are the 25th and 75th percentiles, the whiskers extend to extreme data points within 1.5 times the inter-quantile range and outliers are shown as red crosses.

distribution used in the model corresponds to actual glacierization in the catchments.

Chapter 7

Conclusions and Outlook

In this thesis, airborne laser scanning (ALS) data of five accumulation seasons were analyzed with the aim to gain information on seasonal snow patterns for the adaptation of hydro-meteorological models to partly glacierized mountain catchments.

ALS data and in-situ measurements of snow depths were compared to detect areas on glacier surfaces, where deviations between ALS-derived snow and actual snow depths are of such a magnitude, that they have to be considered in snow hydrological studies. A systematic approach is presented to analyze deviations between ALS derived snow depths and snow depths calculated from GPR measurements. It was shown that actual snow depths are underestimated when interpreting seasonal surface elevation changes from ALS in terms of snow depths in the accumulation areas of large glaciers. Landsat images were successfully used to delineate areas of increased deviations caused by submergent ice flow and the densification of the firn layer. A distinct overestimation of actual snow depths by ALS data was observed at the glacier tongues of the two largest glaciers in the Austrian part of the Ötztal Alps, namely Taschachferner and Gepatschferner (Chap. 5.3 and 6.2.2), and at the front of Kesselwandferner (Chap. 3). However, most of the glaciers in the investigated mountain region show only small firn areas and low velocities of vertical ice flow. This is caused by the present state of the ice cover in the Ötztal Alps, which is characterized by high annual mass loss and distinctly reduced ice flow within the last decades. Thus, spatially distributed snow depths derived from ALS data at the glacier surface provide information on the minimum snow depths, which must be simulated by hydro-meteorological models particularly in the higher elevated parts of the glaciers in this region. Additional information and assumptions on ice flow are required for the analysis of seasonal surface elevation changes in glacierized mountain regions where higher ice flow velocities can be expected (e.g. Huss et al. 2008, 2010; Sold et al. 2013). The comparison of ALS derived snow depths and ground truth measurements showed that ALS surveys are an important and reliable data source

for the spatial distribution of snow depths for most parts of the here investigated glaciers (Chap. 6).

A high inter-annual persistence of the snow patterns was found on glacier surfaces. These areas contribute to an high fraction of inter-annual persistent snow distribution in the partly glacierized catchment of the Upper Rofental valley (Chap. 4). 75 % of total area in this catchment present a low inter-annual standard deviation of standardized snow depths and, thus, can be interpreted as the standard snow pattern representing highly valuable information for the snow cover modelling of this region. The high inter-annual variability of snow depths in the remaining area is caused by occasional avalanches, wind transport and changes in the surface topography within the investigated 10 year period. Especially areas associated with changes of the ice cover were found to cause inter-annual snow depth variability. With respect to the proceeding changes in climate and ice cover, this fact keeps the modeling of the runoff from snow melt in partly glacierized basins challenging.

Persistent areas of increased snow depths deposited by snow sloughs from steep slopes and rock walls were found along the glacier margins at slopes up to $40°$ (Chap. 5). These areas of extreme snow depths can be considered in hydro-meteorological models using slope-dependent approaches to simulate gravitational snow transport. However, the contribution of the additional volume corresponding to extreme snow depths on glacier surfaces to the total volume of the seasonal snow cover is rather small ($< 5 \%$).

Catchment specific characteristics like the elevation of the maximum specific accumulation, the aspect of the largest accumulation and the relation between slope and snow depths can be determined from ALS-derived snow patterns (Chap. 2). Accumulation gradients were calculated and yield a basic information for the calibration of precipitation gradients in hydro-meteorological models. The geostatistical analysis shows inter-annually persistent scale breaks in snow depth variability at 20 m in ice-free terrain. Thus, a spatial resolution of equal or less than 50 m turned out to be demanded to simulate the major snow cover variability in high mountain terrain. On smooth glacier surfaces, a break in autocorrelation of spatially distributed snow depths can not be inferred easily indicating a scale invariant behavior of snow depths in such areas.

For the first time, the persistence and variability of the snow pattern are presented for five accumulation seasons in a comparatively large catchment with a complex topography of ice-free terrain and glaciers. Although 5 years of analyzed data do not make a climatic mean, the presented dataset - including one season of comparatively low HS and one season of extremely high HS - provide a more reasonable base for statistical analysis and simulation of the snow depth distribution than data of one-

year acquisitions. With respect to their high spatial resolution, ALS derived snow depths are a useful basis to test statistical approaches for the simulation of the spatial snow cover variability. Such empirical relations were used to show the high descriptive power of the topographic derivative Negative Openness for simulations of the spatial snow distribution in mountain catchments.

Using the ALS derived snow depth distributions for the calibration and validation of hydro-meteorological models shows promising results. In general, basin-wide SWE calculated from ALS derived snow depths is better suited than the snow covered area to constrain parameters for hydro-meteorological models (Chap. 6.1.1). The assimilation of SWE maps calculated from ALS data in the calibration and validation of hydro-meteorological models improved the results not only for the runoff, but also for the simulated snow cover distribution and mass balance of the glaciers.

Long time monitoring of SWE stored in the snow cover of alpine catchments can lead to valuable conclusions about inter-annual variability and possible trends in volume and duration of snow cover as an impact of climate change. However, the application of basin-wide ALS surveys is limited by the high costs including the airborne data acquisition and the management of the huge data amounts. Thus, the use of Terrestrial Laser Scanning (TLS) might be of more advantage, although this technique is restricted to smaller basins or subareas with respect to the limited reach of the laser signal and topographic shading. Extensive field surveys simultaneously with the ALS flights enable the quantification of single processes causing deviations between ALS derived and actual snow depths on glacier surfaces. Therefor further investigations and measurements have to be performed at glaciers which still show distinct ice flow (e.g. Sold et al. 2013). Combined measurements of actual snow depths and lidar-derived surface elevation changes will be beneficial to investigate seasonal dynamics of large valley glaciers in the investigated region (e.g. Taschachferner, Gepatschferner, Chap. 6.2.3) and in mountain ranges worldwide.

Revealing both, information about the spatial distribution of snow depths and the volume of the snow pack in entire mountain catchments, ALS data are a valuable source of extensive snow accumulation measurements in high alpine catchments. The information on the spatial snow distribution is beneficial for the adaptation of hydrological models to mountain regions in order to compute the runoff from snow and ice melt more realistically. The results of this study improved the adaptation of hydrological models to partly glacierized mountain catchments. Thus, they will also have a major impact on the reduction of errors of future runoff scenarios as well as on the adaptation of strategies to e.g. run hydropower production in high mountain regions economically more efficient and more sustainable with respect to climate change.

Appendix A

Glaciers and fieldwork impressions

Figure A.1: View from the top of Weissseepitze over the large plateau of Gepatschferner in easterly direction.(photo: Markus Keuschnig, 46°50'47"N, 10°43'02"E, 28. April 2011).

Figure A.2: View from the LIA moraine of Gepatschferner towards the glacier tongue (photo: Martin Stocker-Waldhuber, 46°52'42"N, 10°45'42"E, 27. August 2012).

Figure A.3: View from Gepatschferner towards the Gepatsch reservoir (46°51'23"N, 10°44'41"E, 13. October 2010).

Figure A.4: Next to the tongue of Taschachferner (46°54'10"N, 10°49'30"E, 26. Juli 2013).

Figure A.5: View from the LIA moraine of Kesselwandferner towards the tongue of Hintereisferner (46°49'50"N, 10°49'10"E, 28. April 2011).

Figure A.6: Supportive friends and fieldwork essentials.

Bibliography

Abermann, J., Lambrecht, A., F. A., and Kuhn, M.: Quantifying changes and trends in glacier area and volume in the Austrian Ötztal Alps (1969-1997-2006), The Cryosphere, 3, 205–215, doi:10.5194/tc-3-205-2009, 2009.

Abermann, J., Fischer, A., Lambrecht, A., and Geist, T.: On the potential of very high-resolution repeat DEMs in glacial and periglacial environments, The Cryosphere, 4, 53–65, doi:10.5194/tc-4-53-2010, 2010.

Abermann, J., Seiser, B., Meran, I., Stocker-Waldhuber, M., Goller, M., and Fischer, A.: A new ALS glacier inventory of North Tyrol, Austria, for 2006 AD, Zeitschrift für Gletscherkunde und Glazialgeologie, 43/44, 109–119, 2012.

Abermann, J., S. H. and Lambrecht, A.: Analysis of surface elevation changes on Kesselwand glacier - comparison of different methods, Zeitschrift für Gletscherkunde und Glazialgeologie, 41, 147 – 167, 2007.

Achleitner, S., Schöber, J., Rinderer, M., Leonhardt, G., Schöberl, F., Kirnbauer, R., and Schönlaub, H.: Analyzing the operational performance of the hydrological models in an alpine flood forecasting system, Journal of Hydrology, 412/413, 90 – 100, doi:http://dx.doi.org/10.1016/j.jhydrol.2011.07.047, 2012.

Anderton, S. P., White, S. M., and Alvera, B.: Evaluation of spatial variability in snow water equivalent for a high mountain catchment, Hydrological Processes, 18, 435–453, doi:10.1002/hyp.1319, 2004.

Aschwanden, H., Weingartner, R., and Leibundgut, C.: Zur regionalen Übertragung von Mittelwerten des Abflusses - Teil 1: Raumtypisierung der Abflussregime der Schweiz, Deutsche Gewässerkundliche Mitteilungen, 30 (2/3), 52–61, 1986.

Asztalos, J.: Ein Schnee und Eisschmelzmodell für vergletscherte Einzugsgebiete, Master's thesis, Vienna University of Technology, Austria, 2004.

Asztalos, J., Kirnbauer, R., Escher-Vetter, H., and Braun, L.: A distributed energy balance snow and glacier melt model as a component of a flood forecasting system

for the Inn river, Proceedings of the Alpine Snow Workshop, Munich, October 5-6, Germany, 2006.

Baltsavias, E.: Airborne laser scanning: basic relations and formulas, ISPRS Journal of Photogrammetry and Remote Sensing, 54, 199 – 214, doi:10.1016/S0924-2716(99)00015-5, 1999a.

Baltsavias, E.: Airborne laser scanning: existing systems and firms and other resources, ISPRS Journal of Photogrammetry and Remote Sensing, 54, 164 – 198, doi:10.1016/S0924-2716(99)00016-7, 1999b.

Barnett, T. P., Adam, J. C., and Lettenmaier, D. P.: Potential impacts of a warming climate on water availability in snow-dominated regions, Nature, 438, 303–309, 2005.

Bartelt, P. and Lehning, M.: A physical SNOWPACK model for the Swiss avalanche warning: Part I: numerical model, Cold Regions Science and Technology, 35, 123 – 145, doi:http://dx.doi.org/10.1016/S0165-232X(02)00074-5, 2002.

Bavay, M., Grünewald, T., and Lehning, M.: Response of snow cover and runoff to climate change in high Alpine catchments of Eastern Switzerland, Advances in Water Resources, 55, 4 – 16, doi:10.1016/j.advwatres.2012.12.009, 2013.

Beniston, M.: Climatic Change in Mountain Regions: A Review of Possible Impacts, in: Climate Variability and Change in High Elevation Regions: Past, Present & Future, edited by Diaz, H., vol. 15 of *Advances in Global Change Research*, pp. 5–31, Springer Netherlands, doi:10.1007/978-94-015-1252-7_2, 2003.

Benn, D. I. and Lehmkuhl, F.: Mass balance and equilibrium-line altitudes of glaciers in high-mountain environments, Quaternary International, 65, 15 – 29, doi:http://dx.doi.org/10.1016/S1040-6182(99)00034-8, 2000.

Bergström, S.: The HBV-model - its structure and applications, Tech. Rep. SMHI Hydrology Report No. 4, Swedish Meteorological and Hydrological Institute Narrkoping, Sweden, 1992.

Bernhardt, M. and Schulz, K.: SnowSlide: A simple routine for calculating gravitational snow transport, Geophysical Research Letters, 37, L11 502, doi:10.1029/2010GL043086, 2010.

Bernhardt, M., Liston, G. E., Strasser, U., Zängl, G., and Schultz, K.: High resolution modelling of snow transport in complex terrain using downscaled MM5 wind fields, The Cryosphere, 4, 99 – 113, doi:10.5194/tc-4-99-2010, 2010.

Blöschl, G.: Scaling issues in snow hydrology, Hydrological Processes, 13, 2149–2175, doi:10.1002/(SICI)1099-1085(199910)13:14/15⟨2149::AID-HYP847⟩3.0.CO;2-8, 1999.

Blöschl, G. and Kirnbauer, R.: An analysis of snow cover patterns in a small alpine catchment, Hydrological Processes, 6, 99–109, doi:10.1002/hyp.3360060109, 1992.

Blöschl, G., Gutknecht, D., and Kirnbauer, R.: Distributed Snowmelt Simulations in an Alpine Catchment: 2. Parameter Study and Model Predictions, Water Resources Research, 27, 3181–3188, doi:10.1029/91WR02251, 1991a.

Blöschl, G., Gutknecht, D., and Kirnbauer, R.: Distributed Snowmelt Simulations in an Alpine Catchment: 1. Model Evaluation on the Basis of Snow Cover Patterns, Water Resources Research, 27, 3171–3179, doi:10.1029/91WR02251, 1991b.

Blumthaler, U.: Reproduction of the dynamical behaviour of Vernagtferner, Ötztal Alps, with numerical methods, Master's thesis, Institute of Meteorology and Geophysics, University of Innsbruck, 2011.

Bolch, T., Pieczonka, T., and Benn, D. I.: Multi-decadal mass loss of glaciers in the Everest area (Nepal Himalaya) derived from stereo imagery, The Cryosphere, 5, 349–358, doi:10.5194/tc-5-349-2011, 2011.

Bolch, T., Kulkarni, A., Kääb, A., Huggel, C., Paul, F., Cogley, J. G., Frey, H., Kargel, J. S., Fujita, K., Scheel, M., Bajracharya, S., and Stoffel, M.: The State and Fate of Himalayan Glaciers, Science, 336, 310–314, doi:10.1126/science.1215828, 2012.

Bollmann, E., Sailer, R., Briese, C., Stötter, J., and Fritzmann, P.: Potential of airborne laser scanning for geomorphologic feature and process detection and quantifications in high alpine mountains, Zeitschrift für Geomorphologie, Supplementary Issues, 55, 83–104, doi:10.1127/0372-8854/2011/0055S2-0047, 2011.

Braithwaite, R. and Olesen, O.: Glacier Fluctuations and Climatic Change, chap. Calculation of glacier ablation from air temperature, West Greenland, p. 219233, Glaciology and Quaternary Geology, Dordrecht, 1989.

Braun, L., Weber, M., and Schulz, M.: Consequences of climate change for runoff from Alpine regions, Annals of Glaciology, 31, 19–25, doi:10.3189/172756400781820165, 2000.

Chang, A. T. C., Foster, J. L., and Hall, D. K.: SMMR derived global snow cover parameters, Annals of Glaciology, 9, 39 – 44, 1987.

Chang, K. T. and Li, Z. X.: Modelling snow accumulation with a geographic information system, Int. J. Geogr. Inf. Sci., 14, 693707, 2000.

Clark, M. P., Hendrikx, J., Slater, A. G., Kavetski, D., Anderson, B., Cullen, N. J., Kerr, T., Orn Hreinsson, E., and Woods, R. A.: Representing spatial variability of snow water equivalent in hydrologic and land-surface models: A review, Water Resour. Res., 47, W07 539, 2011.

Cline, D., Elder, K., and Bales, R.: Scale effects in a distributed snow water equivalence and snowmelt model for mountain basins, Hydrological Processes, 12, 1527–1536, doi:10.1002/(SICI)1099-1085(199808/09)12:10/11⟨1527::AID-HYP678⟩3.0.CO;2-E, 1998.

Corps of Engineers, U. A.: Snow Hydrology: Summary Report of the Snow Investigations, North Pacific Division, Portland, Oregon, 1956.

Corripio, J., Durand, Y., Guyomarch, G., Mérindol, L., Lecorps, D., and Pugliése, P.: Land-based remote sensing of snow for the validation of a snow transport model, Cold Regions Science and Technology, 39, 93 – 104, doi:http://dx.doi.org/10.1016/j.coldregions.2004.03.007, 2004.

Cuffey, K. and Paterson, W.: The Physics of Glaciers, Academic Press, 4th edn., 2010.

Dadic, R., Corripio, J. G., and Burlando, P.: Mass-balance estimates for Haut Glacier d'Arolla, Switzerland, from 2000 to 2006 using DEMs and distributed mass-balance modeling, Annals of Glaciology, 49, 22–26, doi:doi:10.3189/172756408787814816, 2008.

Dadic, R., Mott, R., Lehning, M., and Burlando, P.: Wind influence on snow depth distribution and accumulation over glaciers, J. Geophys. Res., 115, F01 012, doi:10.1029/2009JF001261, 2010a.

Dadic, R., Mott, R., Lehning, M., and Burlando, P.: Parameterization for windinduced preferential deposition of snow, Hydrological Processes, 24, 1994–2006, doi:10.1002/hyp.7776, 2010b.

Daniels, D. J.: Ground Penetrating Radar, John Wiley & Sons, Inc., doi:10.1002/0471654507.eme152, 2005.

DeBeer, C. M. and Pomeroy, J. W.: Simulation of the snowmelt runoff contributing area in a small alpine basin, Hydrology and Earth System Sciences, 14, 1205–1219, doi:10.5194/hess-14-1205-2010, 2010.

Deems, J., Paintner, T., and Finnegan, D.: Lidar measurement of snow depth: a review, Journal of Glaciology, 59, 467–479, doi:10.3189/2013JoG12J154, 2013.

Deems, J. S., Fassnacht, S. R., and Elder, K. J.: Fractal Distribution of Snow Depth from Lidar Data, J. Hydrometeor, 7, 285–297, doi:10.1175/JHM487.1, 2006.

Deems, J. S., Fassnacht, S. R., and Elder, K. J.: Interannual consistency in fractal snow depth patterns at two Colorado mountain sites, J. Hydrometeor, 9, 977–988, doi:10.1175/2008JHM901.1, 2008.

Dozier, J.: Spectral signature of alpine snow cover from the landsat thematic mapper, Remote Sensing of Environment, 28, 9 – 22, doi:10.1016/0034-4257(89)90101-6, 1989.

Dyurgerov, M. B. and Meier, M. F.: Glaciers and the changing Earth system: A 2004 snapshot., Inst. of Arctic and Alpine Res., Univ. of Colorado, Boulder, Colorado., 2005.

Egli, L., Jonas, T., Grünewald, T., Schirmer, M., and Burlando, P.: Dynamics of snow ablation in a small Alpine catchment observed by repeated terrestrial laser scans, Hydrological Processes, 26, 1574 – 1585, doi:10.1002/hyp.8244, 2012.

Eisen, O., Nixdorf, U., Keck, L., and Wagenbach, D.: Alpine ice cores and ground penetrating radar: combined investigations for glaciological and climatic interpretations of a cold Alpine ice body, Tellus, 55B, 1007–101, 2003.

Elder, K., Dozier, J., and Michaelsen, J.: Snow accumulation and distribution in an Alpine Watershed, Water Resour. Res., 27, 1541–1552, 1991.

Elder, K., Rosenthal, W., and Davis, R. E.: Estimating the spatial distribution of snow water equivalence in a montane watershed, Hydrological Processes, 12, 1793–1808, doi:10.1002/(SICI)1099-1085(199808/09)12:10/11⟨1793::AID-HYP695⟩3.0.CO;2-K, 1998.

Erxleben, J., Elder, K., and Davis, R.: Comparison of spatial interpolation methods for estimating snow distribution in the Colorado Rocky Mountains, Hydrological Processes, 16, 3627–3649, doi:10.1002/hyp.1239, 2002.

Escher-Vetter, H., Kuhn, M., and Weber, M.: Four decades of winter mass balance of Vernagtferner and Hintereisferner, Austria: methodology and results, Annals of Glaciology, 50, 87–95, doi:10.3189/172756409787769672, 2009.

Essery, R., Morin, S., Lejeune, Y., and Mnard, C. B.: A comparison of 1701 snow models using observations from an alpine site, Advances in Water Resources, 55, 131 – 148, doi:10.1016/j.advwatres.2012.07.013, 2013.

Farinotti, D., Magnusson, J., Huss, M., and Bauder, A.: Snow accumulation distribution inferred from time-lapse photography and simple modelling, Hydrological Processes, 24, 2087–2097, doi:10.1002/hyp.7629, 2010.

Favey, E.: Investigation and improvement of airborne laser scanning technique for monitoring surface elevation changes of glaciers, Ph.D. thesis, ETH Zrich, 2001.

Fischer, A.: Glaciers and climate change: Interpretation of 50 years of direct mass balance of Hintereisferner, Global and Planetary Change, 71, 13 – 26, doi:10.1016/j.gloplacha.2009.11.014, 2010.

Fischer, A.: Comparison of direct and geodetic mass balances on a multi-annual time scale, The Cryosphere, 5, 107–124, doi:10.5194/tc-5-107-2011, 2011.

Fliri, F.: Das Klima der Alpen im Raume von Tirol., Innsbruck-Mnchen, Universittsverlag Wagner. (Monographien zur Landeskunde Tirols, Vol. 1), 1975.

Frei, C. and Schär, C.: A Precipitation Climatology ot the Alps from High-Resolution Rain-Gauge Observations, International Journal of Climatology, 18, 873–900, 1998.

Frolov, A. D. and Macheret, Y. Y.: On dielectric properties of dry and wet snow, Hydrological Processes, 13, 1755–1760, doi:10.1002/(SICI)1099-1085(199909)13:12/13⟨1755::AID-HYP854⟩3.0.CO;2-T, 1999.

Geist, T. and Stötter, J.: Documentation of glacier surface elevation change with multi-temporal airborne laser scanner data - case study: Hintereisferner and Kesselwandferner, Tyrol, Austria, Zeitschrift für Gletscherkunde und Glazialgeologie, 41, 77 – 106, 2007.

Geist, T., Elvehoy, H., Jackson, M., and Stötter, J.: Investigations on intra-annual elevation changes using multi-temporal airborne laser scanning data: case study Engabreen, Norway, Annals of Glaciology, 42, 195–201, doi:doi:10.3189/172756405781812592, 2005.

Goodison, B., Louie, P., and Yang, D.: WMO solid precipitation measurement intercomparison. Final Report, Tech. Rep. 67, World Meteorological Organization, 1998.

Gray, D. M. and Male, D. H.: Handbook of Snow. Principles, Processes, Management and Use, Pergamon Press: Toronto/Oxford/New York/Sydney/Paris/Frankfurt, 1981.

Gruber, S.: A mass-conserving fast algorithm to parameterize gravitational transport and deposition using digital elevation models, Water Resources Research, 43, n/a–n/a, doi:10.1029/2006WR004868, 2007.

Gruber, S. and Hoelzle, M.: Statistical modelling of mountain permafrost distribution: local calibration and incorporation of remotely sensed data, Permafrost and Periglacial Processes, 12, 69–77, doi:10.1002/ppp.374, 2001.

Grünewald, T. and Lehning, M.: Altitudinal dependency of snow amounts in two small alpine catchments: can catchment-wide snow amounts be estimated via single snow or precipitation stations?, Annals of Glaciology, 52, 153–158, doi: doi:10.3189/172756411797252248, 2011.

Grünewald, T., Schirmer, M., Mott, R., and Lehning, M.: Spatial and temporal variability of snow depth and ablation rates in a small mountain catchment, The Cryosphere, 4, 215–225, doi:10.5194/tc-4-215-2010, 2010.

Grünewald, T., Stötter, J., Pomeroy, J. W., Dadic, R., Moreno Baños, I., Marturià, J., Spross, M., Hopkinson, C., Burlando, P., and Lehning, M.: Statistical modelling of the snow depth distribution in open alpine terrain, Hydrology and Earth System Sciences, 17, 3005–3021, doi:10.5194/hess-17-3005-2013, 2013.

Haegeli, P. and McClung, D. M.: Avalanche characteristics of a transitional snow climate - Columbia Mountains, British Columbia, Canada, Cold Regions Science and Technology, 37, 255 – 276, doi:http://dx.doi.org/10.1016/S0165-232X(03)00069-7, 2003.

Hall, D. K., Riggs, G. A., Salomonson, V. V., DiGirolamo, N. E., and Bayr, K. J.: MODIS snow-cover products, Remote Sensing of Environment, 83, 181 – 194, doi:10.1016/S0034-4257(02)00095-0, 2002.

Heilig, A., Schneebeli, M., and Eisen, O.: Upward-looking ground-penetrating radar for monitoring snowpack stratigraphy, Cold Regions Science and Technology, 59, 152 – 162, doi:10.1016/j.coldregions.2009.07.008, 2009.

Helfricht, K., Kuhn, M., Keuschnig, M., and Heilig, A.: Lidar snow cover studies on glaciers in the Ötztal Alps (Austria): comparison with snow depths calculated from GPR measurements, The Cryosphere, 8, 41–57, doi:10.5194/tc-8-41-2014, 2014a.

Helfricht, K., Schöber, J., Schneider, K., Sailer, R., and Kuhn, M.: Inter-annual persistence of the seasonal snow cover in a glacierized catchment, Journal of Glaciology, 60, in press, doi:10.5194/tc-8-41-2014, 2014b.

Hock, R.: A distributed temperature-index ice- and snowmelt model including potential direct solar radiation, Journal of Glaciology, 45, 101111, 1999.

Hock, R.: Temperature index melt modelling in mountain areas, Journal of Hydrology, 282, 104 – 115, doi:http://dx.doi.org/10.1016/S0022-1694(03)00257-9, 2003.

Hock, R.: Glacier melt: a review of processes and their modelling., Progress in Physical Geography, 29, 362–391, doi:10.1191/0309133305pp453ra, 2005.

Höfle, B. and Pfeifer, N.: Correction of laser scanning intensity data: Data and model-driven approaches, ISPRS Journal of Photogrammetry and Remote Sensing, 62, 415 – 433, doi:http://dx.doi.org/10.1016/j.isprsjprs.2007.05.008, 2007.

Hoinkes, H.: Methoden und Möglichkeiten von Massenhaushaltsstudien auf Gletschern, Zeitschrift für Gletscherkunde und Glazialgeologie, 6, 37 – 90, 1970.

Hoinkes, H. and Steinacker, R.: Zur Parametrisierung der Beziehung Klima - Gletscher., Revista Italiana di Geofisica e Scienze affini, 1, 97104, 1975.

Hopkinson, C., Sitar, M., Chasmer, L., Gynan, C., Agro, D., Enter, R., Foster, J., Heels, N., Hoffman, C., Nillson, J., and Pierre, R. S.: Mapping the Spatial Distribution of Snowpack Depth Beneath a Variable Forest Canopy Using Airborne Laser Altimetry, Proccedings of the 58th Annual Eastern Snow Conference, Ottawa, Canada, 2001.

Hopkinson, C., Sitar, M., Chasmer, L., and Treitz, P.: Mapping snowpack depth beneath forest canopies using airborne Lidar, Photogram. Eng. Remote Sens., 70, 323330, 2004.

Huss, M.and Farinotti, D., Bauder, A., and Funk, M.: Modelling runoff from highly glacierized alpine drainage basins in a changing climate, Hydrological Processes, 22, 3888–3902, doi:10.1002/hyp.7055, 2008.

Huss, M.: Present and future contribution of glacier storage change to runoff from macroscale drainage basins in Europe, Water Resources Research, 47, W07 511, doi:10.1029/2010WR010299, 2011.

Huss, M.: Extrapolating glacier mass balance to the mountain-range scale: the European Alps 1900 - 2100, The Cryosphere, 6, 713–727, doi:10.5194/tc-6-713-2012, 2012.

Huss, M. and Farinotti, D.: Distributed ice thickness and volume of all glaciers around the globe, Journal of Geophysical Research: Earth Surface, 117, F04 010, doi:10.1029/2012JF002523, 2012.

Huss, M., Jouvet, G., Farinotti, D., and Bauder, A.: Future high-mountain hydrology: a new parameterization of glacier retreat, Hydrology and Earth System Sciences, 14, 815–829, doi:10.5194/hess-14-815-2010, 2010.

Huss, M., Sold, L., Hoelzle, M., Stokvis, M., Salzmann, N., Farinotti, D., and Zemp, M.: Towards remote monitoring of sub-seasonal glacier mass balance, Annals of Glaciology, 54, 75–83, doi:doi:10.3189/2013AoG63A427, 2013.

Huss, M., Zemp, M., Joerg, P., and Salzmann, N.: High uncertainty in 21st century runoff projections from glacierized basins, Journal of Hydrology, 510, 35 – 48, doi:http://dx.doi.org/10.1016/j.jhydrol.2013.12.017, 2014.

Jansson, P. and Pettersson, R.: Spatial and Temporal Characteristics of a Long Mass Balance Record, Storglaciren, Sweden, Arctic, Antarctic, and Alpine Research, 39, pp. 432–437, 2007.

Jansson, P., Hock, R., and Schneider, T.: The concept of glacier storage: a review, Journal of Hydrology, 282, 116 – 129, doi:http://dx.doi.org/10.1016/S0022-1694(03)00258-0, 2003.

Jepsen, S. M., Molotch, N. P., Williams, M. W., Rittger, K. E., and Sickman, J. O.: Interannual variability of snowmelt in the Sierra Nevada and Rocky Mountains, United States: Examples from two alpine watersheds, Water Resources Research, 48, W02 529, doi:10.1029/2011WR011006, 2012.

Joerg, P., Morsdorf, F., and Zemp, M.: Uncertainty assessment of multi-temporal airborne laser scanning data: A case study on an Alpine glacier, Remote Sensing of Environment, 127, 118 – 129, doi:10.1016/j.rse.2012.08.012, 2012.

Jonas, T., Marty, C., and Magnusson, J.: Estimating the snow water equivalent from snow depth measurements in the Swiss Alps, Journal of Hydrology, 378, 161 – 167, doi:10.1016/j.jhydrol.2009.09.021, 2009.

Kaser, G., Fountain, A., and Jansson, P.: A manual for monitoring the mass balance of mountain glaciers., International Hydrological Programme. (IHP-VI. Technical Documents in Hydrology 59.), UNESCO, Paris, 2003.

Kaser, G., Großhauser, M., and Marzeion, B.: Contribution potential of glaciers to water availability in different climate regimes, Proceedings of the National Academy of Sciences, 107, 20 223–20 227, doi:10.1073/pnas.1008162107, 2010.

Kirnbauer, R., Achleitner, S., Schöber, J., Asztalos, J., and Schönlaub, H.: Hochwasservorhersage Inn: Modellierung der Gletscherabflüsse, Mitteilungsblatt des Hydrographischen Dienstes in Österreich, Nr. 86, 109130, 2009.

Kleindienst, H.: Erweiterung und Erprobung eines anwendungsorientierten hydrologischen Modells zur Gangliniensimulation in kleinen Wildbacheinzugsgebieten, Ph.D. thesis, Institute of Geography, Ludwig Maximilian University Munich, 1996.

Koboltschnig, G. R., Schner, W., Zappa, M., Kroisleitner, C., and Holzmann, H.: Runoff modelling of the glacierized Alpine Upper Salzach basin (Austria): multi-criteria result validation, Hydrological Processes, 22, 3950–3964, doi:10.1002/hyp.7112, 2008.

Kodde, M., Pfeifer, N., Gorte, B., Geist, T., and Höfle, B.: Automatic glacier surface analysis from airborne laser scanning, Int. Arch. Photogramm. Remote Sens. Spatial Inform. Sci., pp. 221–226, 2007.

König, M., Winther, J., and Isaksson, E.: Measuring snow and glacier ice properties from satellite, Reviews of Geophysics, 39 (1), 1–27, doi:10.1029/1999RG000076, 2001.

Kraus, K.: Geometrische Informationen aus Photographien und Laserscanaufnahmen, Band 1, Walter de Gruyter, Berlin - New York, 2004.

Kuhn, M.: The mass balance of very small glaciers., Zeitschrift für Gletscherkunde und Glazialgeologie, 31, 171 – 179, 1995.

Kuhn, M.: Verification of a hydrometeorological model of glacierized basins, Annals of Glaciology, 31, 15–18, doi:doi:10.3189/172756400781820228, 2000.

Kuhn, M.: Redistribution of snow and glacier mass balance from a hydrometeorological model, Journal of Hydrology, 282, 95 – 103, doi:10.1016/S0022-1694(03)00256-7, 2003.

Kuhn, M. and Batlogg, N.: Glacier runoff in Alpine headwaters in a changing climate, Hydrology, Water Resources and Ecology in Headwaters (Proceedings of the HeadWater'98 Conference held at Meran/Merano, Italy, April 1998), IAHS Publication, 248, 79–88, 1998.

Kuhn, M., Dreiseitl, E., Hofinger, S., Markl, G., Span, N., and Kaser, G.: Measurements and models of the mass balance of Hintereisferner, Geografiska Annaler: Series A, Physical Geography, 81, 659–670, doi:10.1111/1468-0459.00094, 1999.

Kuhn, M., Abermann, J., Bacher, M., and Olefs, M.: The transfer of mass-balance profiles to unmeasured glaciers, Annals of Glaciology, 50, 185–190, doi:doi:10.3189/172756409787769618, 2009.

Kuhn, M., Lambrecht, A., Abermann, J., Patzelt, G., and Gross, G.: Austrian Glaciers 1998 and 1969: Area and volume changes, Zeitschrift für Gletscherkunde und Glazialgeologie, Bd. 43/44 (2009/10), 3 – 107, 2012.

Lambrecht, A. and Kuhn, M.: Glacier changes in the Austrian Alps during the last three decades, derived from the new Austrian glacier inventory, Annals of Glaciology, 46, 177–184, doi:doi:10.3189/172756407782871341, 2007.

Lehning, M., Bartelt, P., Brown, B., and Fierz, C.: A physical SNOWPACK model for the Swiss avalanche warning: Part III: meteorological forcing, thin layer formation and evaluation, Cold Regions Science and Technology, 35, 169 – 184, doi:10.1016/S0165-232X(02)00072-1, 2002.

Lehning, M., Völksch, I., Gustafsson, D., Nguyen, T. A., Stähli, M., and Zappa, M.: ALPINE3D: a detailed model of mountain surface processes and its application to snow hydrology, Hydrological Processes, 20, 2111–2128, doi:10.1002/hyp.6204, 2006.

Lehning, M., Löwe, H., Ryser, M., and Raderschall, N.: Inhomogeneous precipitation distribution and snow transport in steep terrain, Water Resources Research, 44, W07 404, doi:10.1029/2007WR006545, 2008.

Lehning, M., Grünewald, T., and Schirmer, M.: Mountain snow distribution governed by an altitudinal gradient and terrain roughness, Geophys. Res. Lett., 38, L19 504, doi:10.1029/2011GL048927, 2011.

Lemke, P., Ren, J., Alley, R., Allison, I., Carrasco, J., Flato, G., Fujii, Y., Kaser, G., Mote, P., Thomas, R., and Zhang, T.: Climate Change 2007: The Physical Science Basis. Contribution of Working Group I to the Fourth Assessment Report of the Intergovernmental Panel on Climate Change, chap. Observations: Changes in Snow, Ice and Frozen Ground., Cambridge University Press, Cambridge, United Kingdom and New York, NY, USA., 2007.

Liston, G. E., Haehnel, R. B., Sturm, M., Hiemstra, C. A., Berezovskaya, S., and Tabler, R. D.: Instruments and Methods: Simulating complex snow distributions in windy environments using SnowTran-3D, Journal of Glaciology, 53, 241–256, doi:doi:10.3189/172756507782202865, 2007.

López-Moreno, J. I. and Nogués-Bravo, D.: Interpolating local snow depth data: an evaluation of methods, Hydrological Processes, 20, 2217–2232, doi:10.1002/hyp. 6199, 2006.

Lui, X.: Airborne LiDAR for DEM generation: some critical issues, Progress in Physical Geography, 32 (1), 31 – 49, doi:10.1177/0309133308089496, 2008.

Lundberg, A., Richardson-Näslund, C., and Andersson, C.: Snow density variations: consequences for ground-penetrating radar, Hydrological Processes, 20, 1483–1495, doi:10.1002/hyp.5944, 2006.

Lundberg, A., Granlund, N., and Gustafsson, D.: Towards automated "Ground truth" snow measurements: a review of operational and new measurement methods for Sweden, Norway, and Finland, Hydrological Processes, 24, 1955–1970, doi:10.1002/hyp.7658, 2010.

Lundquist, J. D. and Dettinger, M. D.: How snowpack heterogeneity affects diurnal streamflow timing, Water Resources Research, 41, W05 007, doi:10.1029/2004WR003649, 2005.

Machguth, H., Eisen, O., Paul, F., and Hoelzle, M.: Strong spatial variability of accumulation observed with helicopter-borne GPR on two adjacent Alpine glaciers., Geophysical Research Letters, 33, L13 503, doi:10.1029/2006GL026576, 2006a.

Machguth, H., Paul, F., Hoelzle, M., and Haeberli, W.: Distributed glacier mass-balance modelling as an important component of modern multi-level glacier monitoring, Annals of Glaciology, 43, 335–343, doi:doi:10.3189/172756406781812285, 2006b.

Magnusson, J., Jonas, T., López-Moreno, I., and Lehning, M.: Snow cover response to climate change in a high alpine and half-glacierized basin in Switzerland, Hydrological Research, 41, 230–240, doi:10.2166/nh.2010.115, 2010.

Marchand, W. and Killingtveit, A.: Statistical probability distribution of snow depth at the model sub-grid cell spatial scale, Hydrological Processes, 19, 355–369, doi:10.1002/hyp.5543, 2005.

Marsh, P.: Snowcover formation and melt: recent advances and future prospects, Hydrological Processes, 13, 2117–2134, doi:10.1002/(SICI)1099-1085(199910)13:14/15⟨2117::AID-HYP869⟩3.0.CO;2-9, 1999.

Martinec, J.: Interpretation and utilization of areal snow-cover data from satellites., Annals of Glaciology, 9, 166 – 169, 1987.

Mayer, C., Lambrecht, A., Blumthaler, U., and Eisen, O.: Vermessung und Eisdynamik des Vernagtferners, Ötztaler Alpen, Zeitschrift für Gletscherkunde und Glazialgeologie, 45/46, 259 – 280, 2013.

McCullagh, M. J.: Terrain and Surface Modelleing Systems: Theory and Practice, The Photogrammetric Record, 12, 747–779, doi:10.1111/j.1477-9730.1988.tb00627.x, 1988.

McKay, G. A. and Gray, D. M.: Handbook of Snow, chap. The distribution of the snow cover, p. 153190, Pergamon Press Canada Ltd, 1981.

Melvold, K. and Skaugen, T.: Multiscale spatial variability of lidar-derived and modeled snow depth on Hardangervidda, Norway, Annals of Glaciology, 54(62), 273–281, doi:10.3189/2013AoG62A161, 2013.

Michlmayr, G., Lehning, M., Koboltschnig, G., Holzmann, H., Zappa, M., Mott, R., and Schner, W.: Application of the Alpine 3D model for glacier mass balance and glacier runoff studies at Goldbergkees, Austria, Hydrological Processes, 22, 3941–3949, doi:10.1002/hyp.7102, 2008.

Molotch, N. P., Colee, M. T., Bales, R. C., and Dozier, J.: Estimating the spatial distribution of snow water equivalent in an alpine basin using binary regression tree models: the impact of digital elevation data and independent variable selection, Hydrological Processes, 19, 1459–1479, doi:10.1002/hyp.5586, 2005.

Mott, R., Schirmer, M., Bavay, M., Grünewald, T., and Lehning, M.: Understanding snow-transport processes shaping the mountain snow-cover, The Cryosphere, 4, 545–559, doi:10.5194/tc-4-545-2010, 2010.

Mott, R., Egli, L., Grünewald, T., Dawes, N., Manes, C., Bavay, M., and Lehning, M.: Micrometeorological processes driving snow ablation in an Alpine catchment, The Cryosphere, 5, 1083–1098, doi:10.5194/tc-5-1083-2011, 2011a.

Mott, R., Schirmer, M., and Lehning, M.: Scaling properties of wind and snow depth distribution in an Alpine catchment, Journal of Geophysical Research: Atmospheres, 116, doi:10.1029/2010JD014886, 2011b.

Nagler, T., Rott, H., Malcher, P., and Müller, F.: Assimilation of meteorological and remote sensing data for snowmelt runoff forecasting, Remote Sensing of Environment, 112, 1408 – 1420, doi:http://dx.doi.org/10.1016/j.rse.2007.07.006, 2008.

Nash, J.: A unit hydrograph study with particular reference to British catchments, Proceedings of Institution of Civil Engineers, 17, 249282, 1960.

Nash, J. and Sutcliffe, J.: River flow forecasting through conceptual models. Part I a discussion of principles., Journal of Hydrology, 10, 282290, 1970.

Nolin, A. W.: Recent advances in remote sensing of seasonal snow, Journal of Glaciology, 56, 1141–1150, doi:10.3189/002214311796406077, 2011.

Ohmura, A.: Physical Basis for the Temperature-Based Melt-Index Method, J. Appl. Meteor., 40, 753–761, 2001.

Painter, T., Rittger, K., McKenzie, C., Slaughter, P., Davis, R., and Dozier, J.: Retrieval of subpixel snow covered area, grain size, and albedo from MODIS, Remote Sensing of Environment, 113, 868 – 879, doi:http://dx.doi.org/10.1016/j.rse.2009.01.001, 2009.

Pellicciotti, F., Brock, B., Strasser, U., Burlando, P., Funk, M., and Corripio, J.: An enhanced temperature-index glacier melt model including the shortwave radiation balance: development and testing for Haut Glacier d'Arolla, Switzerland, Journal of Glaciology, 51, 573–587, doi:doi:10.3189/172756505781829124, 2005.

Pfeffer, W. T., Arendt, A., Bliss, A., Bolch, T., Cogley, J. G., Gardner, A. S., Hagen, J., Hock, R., Kaser, G., Kienholz, C., Miles, E. S., Moholdt, G., Mlg, N., Paul, F., Radic, V., Rastner, P., Raup, B. H., Rich, J., Sharp, M. J., and The Randolph Consortium: The Randolph Glacier Inventory: a globally complete inventory of glaciers., Journal of Glaciology, 60, 537 – 552, doi:10.3189/2014JoG13J176, 2014.

Plattner, C., Braun, L., and Brenning, A.: Spatial variability of snow accumulation on Vernagtferner, Austrian Alps, in Winter 2003/04, Zeitschrift für Gletscherkunde und Glazialgeologie, 39, 4357, 2006.

Pomeroy, J. W., Gray, D. M., Shook, K. R., Toth, B., Essery, R. L. H., Pietroniro, A., and Hedstrom, N.: An evaluation of snow accumulation and ablation processes for land surface modelling, Hydrological Processes, 12, 2339–2367, doi:10.1002/(SICI)1099-1085(199812)12:15⟨2339::AID-HYP800⟩3.0.CO;2-L, 1998.

Pomeroy, J. W., Gray, D. M., Hedstrom, N. R., and Janowicz, J. R.: Prediction of seasonal snow accumulation in cold climate forests, Hydrological Processes, 16, 3543–3558, doi:10.1002/hyp.1228, 2002.

Prokop, A.: Assessing the applicability of terrestrial laser scanning for spatial snow depth measurements, Cold Regions Science and Technology, 54, 155 – 163, doi:http://dx.doi.org/10.1016/j.coldregions.2008.07.002, 2008.

Prokop, A., Schirmer, M., Rub, M., Lehning, M., and Stocker, M.: A comparison of measurement methods: terrestrial laser scanning, tachymetry and snow probing for the determination of the spatial snow-depth distribution on slopes, Annals of Glaciology, 49, 210–216, doi:10.3189/172756408787814726, 2008.

Rees, W. G.: Remote sensing of snow and ice, CRC Press, 2006.

Revuelto, J., López-Moreno, J. I., Azorin-Molina, C., and Vicente-Serrano, S. M.: Topographic control of snowpack distribution in a small catchment in the central Spanish Pyrenees: intra- and inter-annual persistence, The Cryosphere Discussions, 8, 1937–1972, doi:10.5194/tcd-8-1937-2014, 2014.

Rittger, K., Painter, T. H., and Dozier, J.: Assessment of methods for mapping snow cover from MODIS, Advances in Water Resources, 51, 367 – 380, doi:http://dx.doi.org/10.1016/j.advwatres.2012.03.002, 2013.

Rott, H., Yueh, S., Cline, D., Duguay, C., Essery, R., Haas, C., Heliere, F., Kern, M., Macelloni, G., Malnes, E., Nagler, T., Pulliainen, J., Rebhan, H., and Thompson, A.: Cold Regions Hydrology High-Resolution Observatory for Snow and Cold Land Processes, Proceedings of the IEEE, 98, 752–765, doi:10.1109/JPROC.2009.2038947, 2010.

Sailer, R., Fromm, R., Joerg, P., Schaffhauser, A., and Adams, M.: Ground based remote Sensing of Snow properties and avalanche simulation, in: Proceedings of UNESCO Earth Conference, Lesbos, Greece, 2008.

Sailer, R., Bollmann, E., Hoinkes, S., Rieg, L., Spross, M., and Stötter, J.: Quantification of geomorphodynamics in glaciated and recently deglaciated terrain based on airborne laser scanning data, Geografiska Annaler: Series A, Physical Geography, 94, 17–32, doi:10.1111/j.1468-0459.2012.00456.x, 2012.

Salomonson, V. and Appel, I.: Estimating fractional snow cover from MODIS using the normalized difference snow index, Remote Sensing of Environment, 89, 351 – 360, doi:10.1016/j.rse.2003.10.016, 2004.

Schaffhauser, A., Adams, M., Fromm, R., Jörg, P., Luzi, G., Noferini, L., and Sailer, R.: Remote sensing based retrieval of snow cover properties, Cold Regions Science and Technology, 54, 164 – 175, doi:http://dx.doi.org/10.1016/j.coldregions.2008.07.007, 2008.

Schirmer, M. and Lehning, M.: Persistence in intra-annual snow depth distribution: 2. Fractal analysis of snow depth development, Water Resources Research, 47, W09 517, doi:10.1029/2010WR009429, 2011.

Schirmer, M., Wirz, V., Clifton, A., and Lehning, M.: Persistence in intra-annual snow depth distribution: 1. Measurements and topographic control, Water Resour. Res., 47, W09 516, doi:10.1029/2010WR009426, 2011.

Schneiderbauer, S. and Prokop, A.: The atmospheric snow-transport model: Snow-Drift3D, Journal of Glaciology, 52, 526, 2011.

Schöber, J., Achleitner, S., Kirnbauer, R., Schöberl, F., and Schönlaub, H.: Hydrological modelling of glacierized catchments focussing on the validation of simulated snow patterns - applications within the flood forecasting system of the Tyrolean river Inn, Advances in Geosciences, 27, 99–109, doi:10.5194/adgeo-27-99-2010, 2010.

Schöber, J., Schneider, K., Helfricht, K., Schattan, P., Achleitner, S., Schöberl, F.,
    and Kirnbauer, R.: Snow cover characteristics in a glacierized catchment in the
    Tyrolean Alps - Improved spatially distributed modelling by usage of Lidar data,
    Journal of Hydrology, in press, –, doi:http://dx.doi.org/10.1016/j.jhydrol.2013.
    12.054, 2014.

Schulla, J. and Jasper, K.: Model Description WaSiM-ETH, $< http$:
    $//www.wasim.ch/downloads/doku/wasim/wasim_2007_e n.pdf >$, p. 181, 2007.

Schweizer, J., Kronholm, K., Jamieson, J. B., and Birkeland, K. W.: Review of spa-
    tial variability of snowpack properties and its importance for avalanche formation,
    Cold Regions Science and Technology, 51, 253 – 272, doi:10.1016/j.coldregions.
    2007.04.009, 2008.

Seiser, B., Helfricht, K., Huss, M., Fischer, A., Veulliet, E., Schnlaub, H., Kuhn, M.,
    and Strasser, U.: MUSICALS - (Multiscale Snow/ICemelt Discharge Simulation
    into ALpine ReservoirS): Validation of a method to estimate ice volume and ice
    thickness distribution in the Ötztal Alps, Tyrol, Austria, in: Geophysical Research
    Abstracts, EGU General Assambly, vol. 14, EGU2012-11324, 2012.

Sevruk, B.: Correction of precipitation measurements: Swiss experience, WMO/TD,
    104, 187 – 196, 1985.

Sevruk, B. and Nespor, V.: Empirical and theoretical assessment of the wind induced
    error of rain measurements, Water Sci. Technol., 37, 171178, 1998.

Shook, K. and Gray, D. M.: Small-Scale Spatial Structure of Shallow Snowcovers,
    Hydrological Processes, 10, 1283–1292, doi:10.1002/(SICI)1099-1085(199610)10:
    10⟨1283::AID-HYP460⟩3.0.CO;2-M, 1996.

Sithole, G. and Vosselman, G.: Experimental comparison of filter algorithms for
    bare-Earth extraction from airborne laser scanning point clouds, ISPRS Journal
    of Photogrammetry and Remote Sensing, 59, 85 –101, 2004.

Sold, L., Huss, M., Hoelzle, M., Andereggen, H., Joerg, P. C., and Zemp, M.:
    Methodological approaches to infer end-of-winter snow distribution on alpine
    glaciers, Journal of Glaciology, 59, 1047–1059, doi:10.3189/2013JoG13J015, 2013.

Sovilla, B., Sommavilla, F., and Tomaselli, A.: Measurements of mass balance in
    dense snow avalanche events, Annals of Glaciology, 32, 230–236, doi:doi:10.3189/
    172756401781819058, 2001.

Sovilla, B., Burlando, P., and Bartelt, P.: Field experiments and numerical modeling of mass entrainment in snow avalanches, Journal of Geophysical Research: Earth Surface, 111, F03 007, doi:10.1029/2005JF000391, 2006.

Sovilla, B., McElwaine, J. N., Schaer, M., and Vallet, J.: Variation of deposition depth with slope angle in snow avalanches: Measurements from Valle de la Sionne, Journal of Geophysical Research: Earth Surface, 115, n/a–n/a, doi: 10.1029/2009JF001390, 2010.

Span, N.: Zur Dynamik des Kesselwandferners, Ph.D. thesis, Institute of Meteorology and Geophysics, University of Innsbruck, 1999.

Span, N. and Kuhn, M.: Simulating annual glacier flow with a linear reservoir model, Journal of Geophysical Research: Atmospheres, 108, 4313, doi:10.1029/2002JD002828, 2003.

Strasser, U.: Modelling of the mountain snow cover in the Berchtesgaden National Park, Berchtegaden National Park research report, 55, 2008.

Sturm, M. and Wagner, A. M.: Using repeated patterns in snow distribution modeling: An Arctic example, Water Resources Research, 46, W12 549, doi: 10.1029/2010WR009434, 2010.

Sundström, N., Kruglyak, A., and Friborg, J.: Modeling and simulation of GPR wave propagation through wet snowpacks: Testing the sensitivity of a method for snow water equivalent estimation, Cold Regions Science and Technology, 7475, 11 – 20, doi:10.1016/j.coldregions.2012.01.006, 2012.

Tappeiner, U., Tappeiner, G., Aschenwald, J., Tasser, E., and Ostendorf, B.: GIS-based modelling of spatial pattern of snow cover duration in an alpine area, Ecological Modelling, 138, 265 – 275, doi:10.1016/S0304-3800(00)00407-5, 2001.

Trujillo, E., Ramrez, J. A., and Elder, K. J.: Topographic, meteorologic, and canopy controls on the scaling characteristics of the spatial distribution of snow depth fields, Water Resour. Res., 43, W07 409, 2007.

Vaughan, D., Comiso, J., Allison, I., Carrasco, J., Kaser, G., Kwok, R., Mote, P., Murray, T., Paul, F., Ren, J., Rignot, E., Solomina, O., Steffen, K., and Zhang, T.: Climate Change 2013: The Physical Science Basis. Contribution of Working Group I to the Fifth Assessment Report of the Intergovernmental Panel on Climate Change, chap. Observations: Cryosphere, Cambridge University Press, Cambridge, United Kingdom and New York, NY, USA., 2013.

Vetter, M.: Airborne laser scanning terrain and land cover models as basis for hydrological and hydraulic studies, Ph.D. thesis, Vienna University of Technology, Faculty of Mathematics and Geoinformation, 2013.

Viviroli, D., Drr, H., Messerli, B., Meybeck, M., and Weingartner, R.: Mountains of the world water towers for humanity: typology, mapping and global significance, Water Resources Research, 43, W07 447, doi:10.1029/2006WR005653, 2007.

Viviroli, D., Zappa, M., Gurtz, J., and Weingartner, R.: An introduction to the hydrological modelling system PREVAH and its pre- and post-processing-tools, Environmental Modelling & Software, 24, 1209 – 1222, doi:http://dx.doi.org/10.1016/j.envsoft.2009.04.001, 2009.

Wagner, W., Ullrich, A., Ducic, V., Melzer, T., and Studnicka, N.: Gaussian decomposition and calibration of a novel small-footprint full-waveform digitising airborne laser scanner, ISPRS Journal of Photogrammetry and Remote Sensing, 60, 100 – 112, doi:http://dx.doi.org/10.1016/j.isprsjprs.2005.12.001, 2006.

Warscher, M., Strasser, U., Kraller, G., Marke, T., Franz, H., and Kunstmann, H.: Performance of complex snow cover descriptions in a distributed hydrological model system: A case study for the high Alpine terrain of the Berchtesgaden Alps, Water Resources Research, 49, 2619–2637, doi:10.1002/wrcr.20219, 2013.

Wehr, A. and Lohr, U.: Airborne laser scanning - an introduction and overview, ISPRS Journal of Photogrammetry and Remote Sensing, 54, 68 – 82, doi:10.1016/S0924-2716(99)00011-8, 1999.

WGMS: Fluctuations of Glaciers 19952000, vol. VIII, IUGG (CCS) UNEP UNESCO, World Glacier Monitoring Service, Zurich, Switzerland, 2005.

WGMS: Fluctuations of Glaciers 20002005, vol. IX, ICSU(WDS)/IUGG(IACS)/UNEP/UNESCO/WMO, World Glacier Monitoring Service, Zurich, Switzerland, 2008.

WGMS: Fluctuations of Glaciers 20052010, vol. X, ICSU(WDS)/IUGG(IACS)/UNEP/UNESCO/WMO, World Glacier Monitoring Service, Zurich, Switzerland, doi:10.5904/wgms-fog-2012-11, 2012.

Winstral, A. and Marks, D.: Long-term snow distribution observations in a mountain catchment: Assessing variability, time stability, and the representativeness of an index site, Water Resources Research, 50, 293305, doi:10.1002/2012WR013038, 2014.

Winstral, A., Elder, K. J., and Davis, R. E.: Spatial Snow Modeling of Wind-Redistributed Snow Using Terrain-Based Parameters, J. Hydrometeor, 3, 524–538, doi:10.1175/1525-7541(2002)003⟨0524:SSMOWR⟩2.0.CO;2, 2002.

Wirz, V., Schirmer, M., Gruber, S., and Lehning, M.: Spatio-temporal measurements and analysis of snow depth in a rock face, The Cryosphere, 5, 893–905, doi:10.5194/tc-5-893-2011, 2011.

WMO: Snow Cover Measurements and Areal Assessment of Precipitation and Soil Moisture, WMO report 748, WMO, Geneva, 1992.

Yokoyama, R., Shlrasawa, M., and Pike, R.: Visualizing Topography by Openness: A New Application of Image Processing to Digital Elevation Models, PHOTOGRAMMETRIC ENGINEERING & REMOTE SENSING, pp. 157 –265, 2002.

Zemp, M., Hoelzle, M., and Haeberli, W.: Six decades of glacier mass-balance observations: a review of the worldwide monitoring network, Annals of Glaciology, 50, 101–111, doi:10.3189/172756409787769591, 2009.

Zemp, M., Jansson, P., Holmlund, P., Gärtner-Roer, I., Koblet, T., Thee, P., and Haeberli, W.: Reanalysis of multi-temporal aerial images of Storglaciären, Sweden (1959 - 1999) - Part 2: Comparison of glaciological and volumetric mass balances, The Cryosphere, 4, 345–357, doi:10.5194/tc-4-345-2010, 2010.

List of Symbols and Abbreviations

γ_h	Semivariance of snow depths for a given lag distance h
Δh_{GPR}	Snow depth calculated from GPR measurements
Δh_{obs}	Observed multi-annual surface elevation change on glacier sufaces
Δh_{sim}	Simulated multi-annual surface elevation change on glacier sufaces
Δz_{ALS}	Surface elevation change derived from ALS data
ALS	Airborne Laser Scanning
$AMUNDSEN$	Alpine MUltiscale Numerical Distributed Simulation ENgine (Strasser 2008)
A_x	Area where HS excesses $\bar{H}S$
CV	Coefficient of Variation
$dGPS$	Differenttial Global Positioning System
D_l	Long range fractal Dimension
D_s	Short range fractal Dimension
DEM	Digital Elevation Model
DSM	Digital Surface Model
DTM	Digital Terrain Model
GF	Gepatschferner (glacier)
GPR	Ground penetrating Radar
GPS	Global Positioning System
HEF	Hintereisferner (glacier)
HS	Snow Depth
$\bar{H}S$	Spatial mean snow depth
HS_r	Relative Snow Depth
HS_s	Standardized Snow Depth
HS_x	Snow Depth where HS excesses $\bar{H}S$
HS_{exc}	Snow Depth where HS excesses $\bar{H}S$ reduced by the mean snow depth
IMU	Inertial Measurement Unit
KWF	Kesselwandferner (glacier)
$lidar\,/\,LiDAR$	Light Detection And Ranging
MSE_s	Mean Squared Error of standardized snow depths

r_{HS}	Residuals of Snow Depths to their vicinity
SCA	Snow Covered Area
SE_s	Squared Error of standardized snow depths
SES	Snow and ice melt model (Kirnbauer et al. 2009)
SWE	Snow Water Equivalent
TLS	Terrestrial Laser Scanning
TWT	Two Way Travel time of the radar signal
V_{exc}	Volume of the snow cover that correspnds to HS_{exc}
VF	Vernagtferner (glacier)

Acknowledgments

Curriculum Vitae

Mag. rer. nat. Kay Helfricht

Lohbachufer 7, A-6020 Innsbruck
Tel: +43 650 2016396
mail: kay.helfricht@oeaw.ac.at

Date of Birth: 5 September 1981
Place of Birth: Dresden
Citizenship: German

RESEARCH INTERESTS
mountain hydrology - snow cover distribution in mountain catchments
- glacier mass balance -
glacier dynamics - remote sensing of the cryosphere - applied geophysics

RESEARCH EXPERIENCE AND EDUCATION:

since 2014   Junior Researcher at the Institute of Interdisciplinary Mountain Research of the Austrian Academy of Sciences, Innsbruck, Austria.

2010–2014   Junior Researcher at the alpS - Centre for Climate Change Adaptation, Innsbruck, Austria

2010–2014   Ph.D. student in the Ice and Climate group at the Institute of Meteorology and Geophysics, University of Innsbruck.

2007–2013   Research assistant in the Ice and Climate group at the Institute of Meteorology and Geophysics, University of Innsbruck.

2009   Diploma thesis supervised by Dr. Andrea Fischer, Institute of Meteorology and Geophysics, University of Innsbruck: *"Veränderungen des Massenhaushaltes am Hallstätter Gletscher seit 1856"*.

2004–2009   Diploma study at the University of Innsbruck. *Master of Natural Science (Magister rer. nat.)* in Meteorology.

RESEARCH PROJECTS:

2013–2014   StartClim2013-C: Runoff scenarios in the Ötztal valley (Tyrol, Austria) considering climate change driven changes of the cryosphere

2010–2014   Comet-Project H03 MUSICALS (Multiscale Snow - Ice Melt Discharge Simulations into Alpine Reservoirs), alpS - Centre for Climate Change Adaptation

2007–2010   Glacier mass balance measurements and analysis on Hallstätter Glacier (Austria)

2007   Georeferencing and digitizing of ice thickness measurements on Austrian glaciers

TRAINING COURSES:

Regular Student at the AG 325 Arctic Glaciology Course 2012 at the University Centre in Svalbard (UNIS, Longyearbyen).

List of Publications and Presentations

REFEREED PUBLICATIONS:

Helfricht, K., Kuhn, M., Keuschnig, M. and Heilig, A. (2014). Lidar snow cover studies on glaciers in the Ötztal Alps (Austria): comparison with snow depths calculated from GPR measurements. The Cryosphere, 8(1), 41-57, doi:10.5194/tc-8-41-2014.

Schöber, J., Schneider, K., Helfricht, K., Schattan, P., Achleitner, S., Schöberl, F., and Kirnbauer, R. (2014): Snow cover characteristics in a glacierized catchment in the Tyrolean Alps - Improved spatially distributed modelling by usage of Lidar data, Journal of Hydrology, in press, doi:http://dx.doi.org/10.1016/j.jhydrol.2013.12.054.

Helfricht, K., Schöber, J., Seiser, B., Fischer, A., Stötter, J. and Kuhn, M. (2012). Snow accumulation of a high alpine catchment derived from LiDAR measurements. Advances in Geoscience, 32, 31-39, doi: 10.5194/adgeo-32-31-2012.

DATA PUBLICATIONS:

Helfricht, K. and Fischer, A. (2009a). Glacier bed of Hallstätter Gletscher calculated from ice thickness measurements 2009 and airborne laser scan DEM 2007. , In Supplement to: Helfricht, Kay (2009): Veränderungen des Massenhaushaltes am Hallstätter Gletscher seit 1856. Magister Thesis, Institute of Meteorology and Geophysics, University of Innsbruck, Austria, 153 pp, PANGAEA. doi:10.1594/PANGAEA.809691

Helfricht, K. and Fischer, A. (2009b). Ice thickness distribution of Hallstätter Gletscher calculated from GPR measurements in 2009, In Supplement to: Helfricht, Kay (2009): Veränderungen des Massenhaushaltes am Hallstätter Gletscher seit 1856. Magister Thesis, Institute of Meteorology and Geophysics, University of

Innsbruck, Austria, 153 pp, PANGAEA. doi:10.1594/PANGAEA.809692

Fischer, A., Stocker-Waldhuber, M., Helfricht, K. and Reingruber, K. (2011): Glacier Mass Balance of Hallstaetter Glacier, Dachstein, Austria, from 2006/07-2009/10.PANGAEA. doi:10.1594/WDCC/MB HSG 2007 2010

POSTER PRESENTATIONS:

Helfricht, K., Schneeberger, K., Welebil, I., Schöber, J., Huss, M. Formayer, H., Huttenlau, M., Schneider, K.: Runoff scenarios of the river Ötztaler Ache (Tyrol, Austria) considering climate change driven changes of the cryosphere European Geosciences Union (EGU) General Assembly 2014, Vienna, 30.04.2014.

Helfricht, K., Lehning, M., Sailer, R., Kuhn, M.: The influence of gravitational snow transport on the winter mass balance of Alpine glaciers in the Ötztal Alps. 18. Alpine Glaciology Meeting, Innsbruck, 27.02.2014.

Helfricht, K., Schneider, K.; Sailer, R.; Kuhn, M.: Lidar snow cover studies in the Ötztal Alps. 11th Swiss Geoscience Meeting 2013, Lausanne, 16.11.2013.

Helfricht, K., Kuhn, M., Keuschnig, M., Heilig, A., Schneider, K.: Combination of Lidar and GPR measurements to derive snow and ice dynamics at glacier surfaces. European Geosciences Union (EGU) General Assembly 2013, Vienna, 09.04.2013.

Helfricht, K.,Keuschnig, M., Heilig, A., Mayer, C., Kuhn, M.: Evaluation of airborne laser scan measurements of winter snow accumulation at glacier surface. 16th Alpine Glaciology Meeting (AGM 2012), Zürich, 02.02.2012.

ORAL PRESENTATIONS:

Helfricht, K., Kuhn, M., Keuschnig, M., Heilig, A.: Experiences with velocity assumptions for GPR measurements of snow depth. Workshop: Liquid water in snow - Measurement techniques and modeling approaches, Davos, 02.04.2014.

Helfricht, K., Hanzer, F., Schneider, K., Marke, T., Kuhn, M., Strasser, U.: Using Lidar data for enhanced simulation of snow accumulation distribution in hydrological modelling of Alpine glacierized catchments. Davos Atmosphere and Cryosphere Assembly (DACA 2013), Davos, 10.07.2013.

Helfricht, K., Schneider, K., Schöber, J., Sailer, R. and Kuhn, M.: Analysis of

multi-annual end-of-season snow accumulation patterns from Lidar data. Davos Atmosphere and Cryosphere Assembly (DACA 2013), Davos, 08.07.2013.

Helfricht, K., Kuhn, M.: Application of airborne laser scanning for hydrological investigations in alpine catchments. One Decade of Airborne Laser Scanning at Hintereisferner 2012, Obergurgl, 04.10.2012.

Helfricht, K., Seiser, B.; Strasser, U., Kuhn, M., Sailer, R., Stötter, J., Veulliet, E., Schönlaub, H.: Multiscale Snow/Icemelt Discharge Simulation into Alpine Reservoirs - the alpS MUSICALS project. 15th Alpine Glaciology Meeting (AGM 2011), Munich, 25.02.2011

Leopold-Franzens-Universität Innsbruck

Eidesstattliche Erklärung

Ich erkläre hiermit an Eides statt durch meine eigenhändige Unterschrift, dass ich die vorliegende Arbeit selbständig verfasst und keine anderen als die angegebenen Quellen und Hilfsmittel verwendet habe. Alle Stellen, die wörtlich oder inhaltlich den angegebenen Quellen entnommen wurden, sind als solche kenntlich gemacht.

Die vorliegende Arbeit wurde bisher in gleicher oder ähnlicher Form noch nicht als Magister-/Master-/Diplomarbeit/Dissertation eingereicht.

Datum	Unterschrift